UNIVERSITY OF CALIFORNIA
Santa Barbara

# Surprises at the edge: theoretical investigations at the boundaries of quantum Hall systems

A Dissertation submitted in partial satisfaction
of the requirements for the degree of

Doctor of Philosophy

in

Physics

by

Jennifer Ann Cano

Committee in Charge:

Professor Chetan Nayak, Chair

Professor Matthew Fisher

Professor John Martinis

June 2015

The Dissertation of
Jennifer Ann Cano is approved:

---

Professor Matthew Fisher

---

Professor John Martinis

---

Professor Chetan Nayak, Committee Chairperson

May 2015

Surprises at the edge: theoretical investigations

at the boundaries of quantum Hall systems



by

Jennifer Ann Cano

*To my parents, for their never-ending love and support.*

# Acknowledgements

The six years that I have spent at UCSB have been both enjoyable and productive. For this, there are many people to whom I am grateful.

I would first and foremost like to thank my advisor, Chetan Nayak, for his seemingly infinite supply of patience and wisdom. He has given me the tools, connections, and confidence necessary to be a successful scientist. He taught me how to write a paper and give a talk, and, by example, showed me how to mentor students, maintain collaborations and host a conference. His influence will persist throughout my academic career.

The other members of my committee, Matthew Fisher and John Martinis, have also been valuable mentors. Matthew has come to all of my practice talks, armed with insightful questions and constructive criticism, which has made me a better scientist and speaker. His deep understanding of physics, as well as his accompanying anecdotes, make him someone that I look for an excuse to talk to. During my first year at UCSB, John impressed me with his thoughtful approach to designing lectures and exams, which changed my perspective on teaching. In subsequent years, collaborative meetings with John's group exposed me to the experimental side of condensed matter physics, which gave me a knowledge base that I continue to draw from.

I would also like to acknowledge my undergraduate advisor, Paul Fendley, whose creativity sparked my interest in condensed matter physics and made me a strong can-

didate for UCSB. Although his responsibility could have ended there, I am grateful that he has continued to answer my emails, whether picking his brain about non-equilibrium calculations or where to go for a post doc.

It has been a pleasure to work at Station Q. I am thankful to all researchers at Station Q, past and present, that I have interacted with: Bela Bauer, Maissam Barkeshli, Parsa Bonderson, Meng Cheng, Bryan Clark, David Clarke, Lukasz Fidkowski, Michael Freedman, Dong Liu, Roman Lutchyn, Mike Mulligan, Kirill Shtengel, Zhenghan Wang, Jon Yard and Mike Zaletel. In particular, while in Santa Barbara, Mike Mulligan was like a second advisor. I am grateful for many conversations about Luttinger liquids, as well as running and cycling. Of course, Station Q would not be the same without Sean Fraer, who not only keeps the printer stocked and the coffee flowing, but makes the days better with his friendly demeanor and occasional stories about Isla Vista history.

I have been lucky to have wonderful officemates in Elings Hall: Eugeniu, Younghyun, Brayden, Kaushal, Dominic, Christina and Claire have been my friends, teachers, challengers and collaborators. I have learned as much from our group meetings as from our whiteboard arguments and conversations en route to a seminar.

I have benefitted from the entire CMT group at UCSB through the Hardtimes Seminar and Many Body Journal Club, which have led to stimulating conversations and given me a broader knowledge of the field. I have also benefitted from collaborators outside of

UCSB: Andrew Doherty, David Reilly, and Taylor Hughes have been a pleasure to work with and learn from.

My classmates, with whom I suffered through E&M, studied late while unknowingly inhaling asbestos in the now-demolished trailer, and celebrated the weekends in San Clemente, were an integral part of my happiness during my first year at UCSB. I am thankful for many conversations with Jim Garrison on physics and on life. I am especially grateful to my original WiP group, Karina, Genevieve and Anna, who first helped me feel adjusted at UCSB and then became my mentors and best friends.

Outside of the physics department, the UCSB Triathlon Team has kept me both sane and young. My teammates have been a fountain of inspiration and amusement. I will forever be a better person and athlete because of this experience.

I am indebted to my family, who has always had 100% confidence in me and provided unconditional love. Together, my parents gave me a passion for math and science that has shaped my life. My sister Ali has been my best friend and cheerleader for as long as I can remember. I am so grateful for their support and friendship.

Last, my time in Santa Barbara has been shaped by having Cyrus by my side. He has kept me calm when my mind is crazy and celebrated the little successes of every day of this journey.

# Curriculum Vitæ

## Jennifer Ann Cano

### Education

| | |
|---|---|
| 2015 | Ph.D. in Physics, University of California, Santa Barbara.<br>Advisor: Chetan Nayak |
| 2009 | B.S. in Physics, B.A. in Mathematics, University of Virginia.<br>Advisor: Paul Fendley |

### Awards

| | |
|---|---|
| 2005 | University of Virginia Jefferson Scholar |
| 2007 | Goldwater Scholar |
| 2008 | University of Virginia E. E. Floyd Prize in Mathematics |
| 2009 | University of Virginia E. J. McShane Prize in Mathematics |
| 2009 | University of Virginia Most Outstanding Undergraduate Major in Physics |
| 2009 | NSF Graduate Research Fellowship |
| 2009 | University of California, Santa Barbara GAANN Fellowship |

### Publications

1. Jennifer Cano and Paul Fendley, "Spin Hamiltonians with Resonating-Valence-Bond Ground States," *Phys. Rev. Lett.* **105**, 067205 (2010).

2. Younghyun Kim, Jennifer Cano and Chetan Nayak, "Majorana zero modes in semiconductor nanowires in contact with higher-Tc superconductors," *Phys. Rev. B* **86**, 235429 (2012).

3. Jennifer Cano, Andrew C. Doherty, Chetan Nayak and David J. Reilly, "Microwave absorption by a mesoscopic quantum Hall droplet," *Phys. Rev. B* **88**, 165305 (2013). *Editor's Suggestion.*

4. Jennifer Cano, Meng Cheng, Michael Mulligan, Chetan Nayak, Eugeniu Plamadeala and Jon Yard, "Bulk-Edge Correspondence in 2+1-Dimensional Abelian Topological Phases," *Phys. Rev. B* **89**, 115116 (2014).

5. Jennifer Cano and Chetan Nayak, "Unexpected tunneling from downstream neutral modes," *Phys. Rev. B* **90**, 235109 (2014).

# Abstract

## Surprises at the edge: theoretical investigations at the boundaries of quantum Hall systems

Jennifer Ann Cano

The quantum Hall effect is recognized as one of the earliest examples of a topological phase of matter. Yet, thirty-five years after its initial discovery, there remain many open questions, especially surrounding states that may host fractional excitations and exotic statistics. Through the bulk-edge correspondence, many questions can be answered by studying the low-energy edge excitations. In this thesis, we investigate analytically certain aspects of the edge excitations using Chern-Simons-Landau-Ginzburg theory. The results include some surprises: our microwave absorption proposal leads to an interferometer whose read-out is first order in the tunneling amplitude; tunneling current across a quantum point contact is affected by the presence of a neutral mode; and the bulk-edge correspondence for chiral Abelian phases can be one-to-many. We now describe these investigations in more detail.

We start by proposing an experiment to measure the microwave absorption spectrum of a quantum Hall droplet. We show that the number and velocities of charged edge modes can be directly measured from a droplet of known shape. In contrast to standard transport measurements, different edge equilibration regimes can be accessed in the same

device. If there is a quantum point contact, then quasiparticle properties, including braiding statistics, can be observed. Their effects are manifested as modulations of the spectrum that are, notably, first-order in the tunneling amplitude at the point contact.

We next consider transport through a quantum point contact in states with counter-propagating neutral edge modes. We show that both the noise and the average transmitted current are affected by downstream perturbations within the standard edge state model. We argue that the change in transmitted current should be observable in experiments that have observed increased noise.

Finally, we investigate the bulk-edge correspondence for chiral Abelian quantum Hall phases. We show that the same bulk two-dimensional topological phase can have multiple distinct, fully-chiral edge phases. This can happen at the integer quantum Hall states at $\nu = 8$ and 12 and the fractional states at $\nu = 8/7, 12/11, 8/15, 16/5$. We give a general criterion for the existence of multiple distinct chiral edge phases for the same bulk phase and discuss experimental consequences. We find that edge phases correspond to lattices while bulk phases correspond to genera of lattices. Since there are typically multiple lattices in a genus, the bulk-edge correspondence is typically one-to-many.

---

Professor Chetan Nayak
Dissertation Committee Chair

# Contents

# List of Figures

# Chapter 1

# Introduction

## 1.1 Overview of the quantum Hall effect

A two-dimensional electron gas (2DEG) subject to a strong magnetic field perpendicular to the plane of the 2DEG will display quantized plateaus in its off-diagonal conductance,

$$\sigma_{xy} = \nu \frac{e^2}{h} \tag{1.1}$$

where $\nu$ is either an integer or a rational fraction. At the same time, its diagonal conductance vanishes:

$$\sigma_{xx} = 0 \tag{1.2}$$

This effect is remarkable for a number of reasons: first, the quantization is so precise – within a few parts in a billion – that it prompted a new standard for resistance, the

von Klitzing constant, $R_K = h/e^2 \approx 25.8\text{k}\Omega$.[1] Second, the fractions that are observed are very particular: as the temperature is decreased, first the thirds appear, then the fifths, then the sevenths, etc, while even-denominator fractions are much more rare; this is an intriguing display of number theory in a real physical system. Third, theory has predicted that fractional conductance implies the existence of fractional charge and statistics; more exotic statistics might also be possible. For these reasons, the quantum Hall effect has remained an active area of research since its discovery in 1980.[2]

In this chapter, we overview the basic details of the quantum Hall effect and then develop the theoretical formalism that is the starting point for later chapters. For more details related to the earlier sections, we refer the reader to the thorough pedagogical reviews by Girvin[3] and MacDonald[4] and the classic text of Prange and Girvin.[5]

## 1.2 Experimental basics

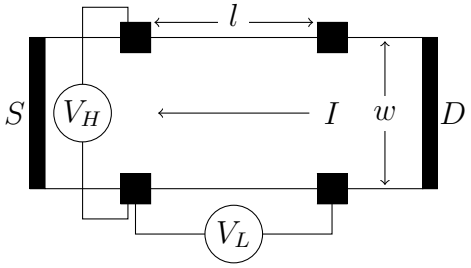


Figure 1.1: **Hall measurement.** Current is driven horizontally. Voltages are measured parallel and perpendicular to the current. The black regions represent Ohmic contacts.

The basic experiment consists of a two-dimension electron gas in a rectangular sample. A current is applied along one direction. The current, $I$, between the source, $S$, and drain, $D$, and the voltages, $V_H$ and $V_L$ are measured, as indicated in Fig 1.1. The current density is $j = I/w$. Assuming a constant electric field, the longitudinal electric field (parallel to the current) is $E_L = V_L/l$. Thus, the longitudinal resistance is $R_L = V_L/I = E_L l/(jw) = \rho_{xx} l/w$. The transverse electric field is $E = V_H/w$. Thus, the Hall resistance is $R_H = V_H/I = Ew/(jw) = \rho_{xy}$, independent of sample dimensions. It is a special feature of two dimensions that the resistance and resistivity have the same dimensions; because the size factors drop out in the Hall resistance, an extremely precise measurement is possible.

The integer quantum Hall effect was first measured in 1980 by von Klitzing, Dorda and Pepper,[2] for which von Klitzing was awarded the Nobel Prize in 1985. Two years later, the $\nu = 1/3$ fractional quantum Hall effect was reported by Tsui, Störmer and Gossard.[6] Laughlin, Störmer and Tsui were awarded the 1998 Nobel Prize for their theoretical and experimental contributions. In 1987, Willett, et al, observed the first even-denominator Hall states at $\nu = 5/2$.[7] A recent Hall trace from a GaAs/AlGaAs sample at 20mK is shown in Fig 1.2. Extremely precise integer plateaus from $\nu = 1$ up to $\nu > 10$ are visible, as well as many fractions.

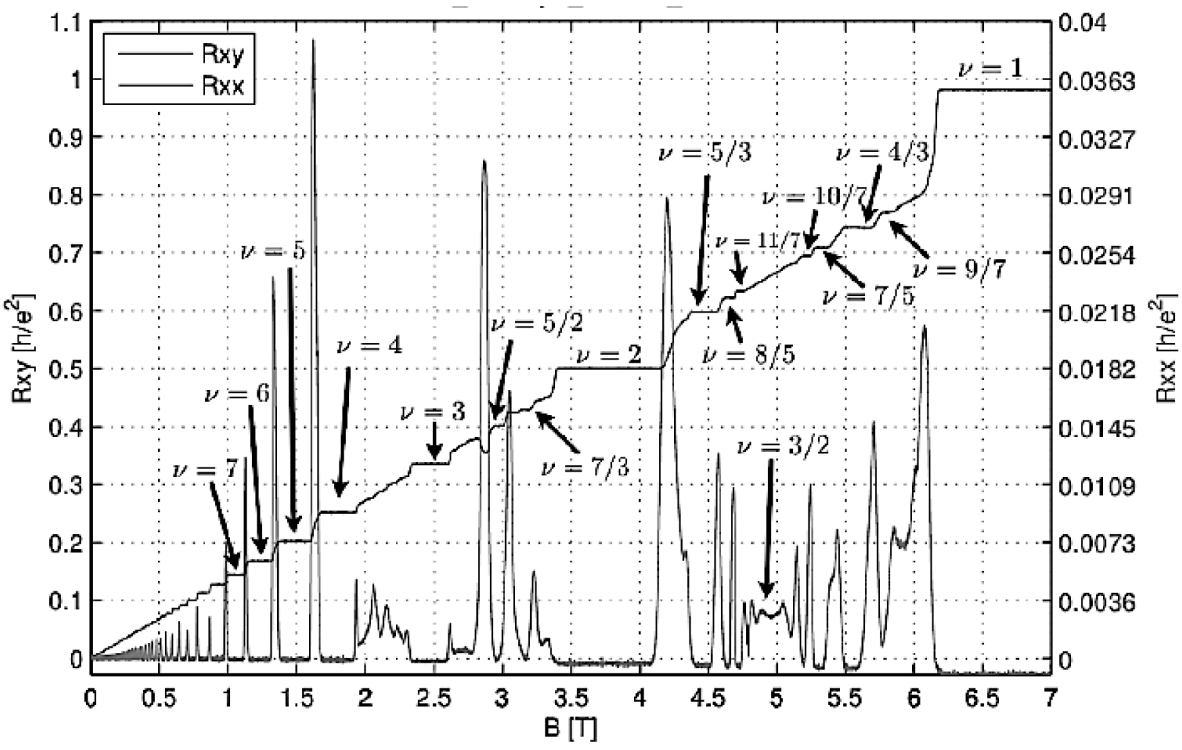


Figure 1.2: **Quantum Hall Trace.** Reprinted with permission from Ref 8.

## 1.3 Theory of the integer quantum Hall effect

### 1.3.1 Exact solution in a translationally invariant system

The IQH effect can be explained by considering a single electron in a strong magnetic field, $\mathbf{B} = B\hat{z}$, restricted to move in the $x - y$ plane. Such an electron is described by the Hamiltonian,

$$H = \frac{1}{2m}\left(\mathbf{p} + e\mathbf{A}\right)^2 \tag{1.3}$$

where $m$ is the electron mass and $-e$ is the electron charge. Choosing the Landau gauge, $\mathbf{A} = xB\hat{y}$, the Hamiltonian can be rewritten,

$$H_0 = \frac{1}{2m}\left(p_x^2 + \left(p_y + exB\right)^2\right) \tag{1.4}$$

The Hamiltonian is translationally invariant in the $y$ direction. Hence, eigenstates take the form $\psi_{k,n}(x,y) = e^{iky} f_{k,n}(x)$, where $n$ is a to-be-determined label, and the functions $f$ satisfy:

$$\left(\frac{p_x^2}{2m} + \frac{m\omega_c^2}{2}\left(x - x_k\right)^2\right) f_{k,n}(x) = E_{k,n} f_{k,n}(x) \tag{1.5}$$

where $x_k = -k\ell^2$, $\ell = \sqrt{\hbar/(eB)}$ is the magnetic length, and $\omega_c = \frac{eB}{m}$ is the cyclotron energy. This is the familiar harmonic oscillator with a $k$-dependent shift. Thus,

$$\psi_{k,n}(x,y) = \frac{e^{iky}}{N_{k,n}} e^{-(x-x_k)^2/(2\ell^2)} H_n\left((x - x_k)/\ell\right) \tag{1.6}$$

where $n$ is a non-negative integer, $N_{k,n}$ is a normalization constant, $H_n$ is the $n^{\text{th}}$ Hermite polynomial, and the energy corresponding to $\psi_{k,n}$ is

$$E_{k,n} \equiv E_n = \hbar\omega_c \left(n + \frac{1}{2}\right) \tag{1.7}$$

All of the states with the same $n$ are said to comprise the $n^{\text{th}}$ Landau level and share the same energy, independent of their wavenumber in the $y$ direction! Thus the Landau levels are massively degenerate. The degeneracy can be estimated for a sample with dimensions $L_x, L_y$: if each wave function is centered at $x_k$, then $0 \leq |x_k| \leq L_x$, so that the degeneracy is given by

$$N_\Phi \equiv \frac{L_y}{2\pi} \int_0^{eBL_x/\hbar} dk = \frac{BL_yL_x}{\Phi_0} \tag{1.8}$$

where here the flux quantum is $\Phi_0 = h/e$. We see that there is exactly one state in each Landau level for each unit of flux piercing the sample.

In the presence of a uniform electric field, $\mathbf{E} = E\hat{x}$, the Hamiltonian (1.3) has an extra term, $H_E = eEx$. Because the Hamiltonian remains translationally invariant in the $y$ direction, Eqs (1.5) and (1.6) are valid, with $x_k \to x_k + \frac{v}{\omega_c}$ and $E_{k,n} \to E_{k,n} - \frac{m}{2}v^2 + \hbar kv$; we have defined the drift velocity, $\mathbf{v} \equiv \frac{\mathbf{E}\times\mathbf{B}}{B^2} = -\frac{E}{B}\hat{y} \equiv v\hat{y}$. The energy of each Landau level increases as a function of $k$ in the presence of an electric field. We can verify that the expectation value of the velocity operator is exactly the drift velocity:

$$\langle\psi_{k,n}|v_y|\psi_{k,n}\rangle = \frac{1}{m}\langle\psi_{k,n}|p_y + exB|\psi_{k,n}\rangle$$

$$= \frac{eB}{mN_{k,n}^2}\int dx\,(x-x_k)e^{-\left(x-x_k-\frac{v}{\omega_c}\right)^2/\ell^2}\left[H_n\left(\left(x-x_k-\frac{v}{\omega_c}\right)/\ell\right)\right]^2 = v, \tag{1.9}$$

where the last equality comes from the fact that the squared Hermite polynomials and the exponential are even in $x - x_k - \frac{v}{\omega_c}$. A similar calculation shows that $\langle\psi_{k,n}|v_x|\psi_{k,n}\rangle = 0$. Thus, when $N$ Landau levels are filled, Eq (1.8) tells us that there are $NN_\Phi$ electrons, and the total current is $I = -NN_\Phi ev/L_y$. Since the voltage across the sample is $EL_x$, the Hall conductance is given by $\sigma_{xy} = -\frac{NN_\Phi ev}{EL_yL_x} = N\frac{e^2}{h}$, exactly Eq (1.1) with $\nu \in \mathbb{Z}$.

Thus, for the translationally invariant system, we have exactly computed the eigenstates and the Hall conductance. However, it is not obvious that this computation applies to a real system, which has both disorder and edges. Furthermore, it is impossible to continuously tune the chemical potential, since it always costs either no energy or $\hbar\omega_c$ to add an electron to the system. Thus, in the rest of this section, we demonstrate why the plateaus in conductance do appear while tuning either the magnetic field or the chemical potential in a real system.

### 1.3.2 Edge effects

Following Halperin,[9] consider a system periodic in the $y$ direction with a confining potential dictating boundaries at $x = x_1$ and $x = x_2$. Away from the edges of the sample, when $x_1 < x_k < x_2$ and $|x_{1,2} - x_k| \gg \ell$, Eq (1.5) is a good approximation and eigenstates

are described by Eq (1.6). When there is no applied electric field, such states carry no current, according to Eq (1.9) with $E = 0$. However, near the boundary, the constraint that the wave function must vanish as $x \to x_{1,2}$ increases its energy. In particular, when $x_k = x_2$, the system is described by a half harmonic oscillator (the potential is $V(x) = x^2 m\omega_c^2/2$ when $x < 0$ and $V(x) = \infty$ when $x > 0$), for which the energy levels are exactly the odd harmonic oscillator energies, $E_{2n+1} = \hbar\omega_c(2n + \frac{3}{2})$. When $x \lesssim x_2$, the energy should be between $E_n$ and $E_{2n+1}$. When $x_k > x_2$, the energy increases like $(x_2 - x_k)^2 m\omega_c^2/2$, the minimum value of the confining potential in this case. Similar phenomena occur when $x_k$ is near $x_1$. Thus, the Landau levels bend upwards near the edge of the sample, as illustrated in Fig 1.3b. Since the current density is not symmetric in the states near the edge of the sample, these states carry current. The group velocity is given by $v_{k,n} = \partial_k E_{k,n}/\hbar$, which, since $k$ increases with $x$, has the opposite sign on either side of the sample. Thus, when there is no applied electric field, current still flows along the edges of the sample, in opposite directions, but there is no net current.

When a voltage is applied, one edge will be at a lower chemical potential then the other, causing its edge modes to be more populated. This imbalance causes a net current flow across the sample. Consider a chemical potential of $\mu_1$ on the left edge and $\mu_2$ on the right edge, where $(N + \frac{1}{2})\hbar\omega_c < \mu_{1,2} < (N + \frac{3}{2})\hbar\omega_c$ for some $N$. The current can be

computed by integrating over the velocities, $v_{k,n}$:

$$I = -e\frac{L_y}{2\pi}\sum_{n=0}^{\infty}\int dk\frac{\partial E_{k,n}}{\hbar\partial_k}\frac{\rho_{k,n}}{L_y} = -\frac{e}{h}\sum_{n=0}^{\infty}\int_{\mu_1}^{\mu_2} dE\rho_{E,n} = -\frac{e}{h}N(\mu_2-\mu_1) = \frac{e^2}{h}NV \quad (1.10)$$

where $\rho_{k,n}(\rho_E)$ is the probability the state $\psi_{k,n}$(states at energy $E$, Landau level $n$) are occupied and we have taken $T = 0$. By definition, the Hall conductance is $\sigma_{xy} = I/V = \frac{e^2}{h}N$. Thus, in a clean sample, the conductance remains quantized as long as the difference in chemical potential is smaller than the spacing between Landau levels. If the difference in chemical potential between the edges is accompanied by an electric field in the bulk, some of the current contributing to Eq (1.10) will come from bulk modes, as shown in Eq (1.9), but the result is unchanged.

### 1.3.3 Effect of disorder

When disorder is present, one might fear that it would cause backscattering that would ruin the quantized current. In the case where all of the current is carried at the edges of the sample and the edges are far apart, it is clear that this is not the case: channels on the same edge are parallel-propagating, so that any scattering between them will not alter the current, and channels on opposite edges, although oppositely-propagating, are too far apart for any scattering to occur. Thus, the current remains perfectly quantized according to Eq (1.1) with $\nu \in \mathbb{Z}$.

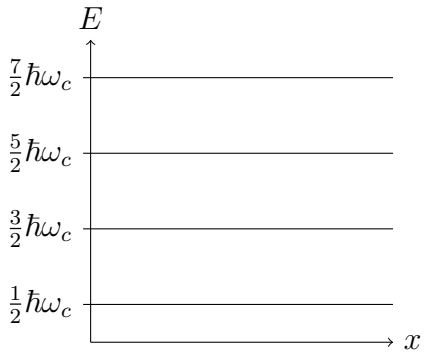


(a) Translationally invariant system

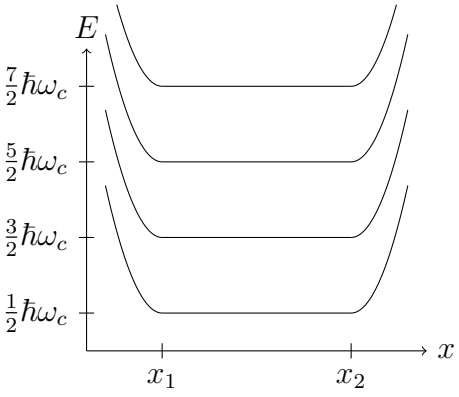


(b) Clean system with edges

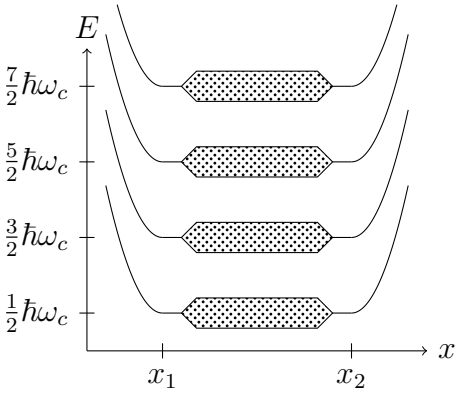


(c) Disorder broadening

Figure 1.3: **Landau Levels.**

In the case where some current is carried in the bulk, it is less obvious that backscattering does not occur. To address this case, we follow the famous gauge argument of Laughlin in Ref 10, refined by Halperin.[9] Because the quantum Hall effect exists in a variety of geometries, Laughlin chooses a convenient geometry, the Corbino disk, for his thought experiment. As shown in Figure 1.4, the impurities in the sample are confined to an inner region, separated from the edges of the disk, and a flux, $\Phi$, can be threaded through the center of the disk. The magnetic field, $B$, penetrates the entire plane. For small disorder, the energy spectrum will resemble that in Fig 1.3c. Suppose that the Fermi energy is between two Landau levels – above the top of the smeared disorder band corresponding to level $N$ and below the bottom of the smeared band of $N+1$ – and that $\Phi$ is adiabatically changing in time from zero to $\Phi_0$. The change in flux generates an emf around the disk. In the clean region, because there is a voltage around the disk, there is a precise Hall conductance, $\sigma_{xy} = Ne^2/h$, which pushes electrons from the inner to the outer edge of the disk. Precisely: let $C$ be a curve in the outer clean region and $A$ the area it bounds; then the charge transferred across $C$ is given by

$$\begin{aligned}\int dt \int_A \partial_t \rho &= -\int dt \int_A \nabla \cdot \mathbf{j} = -\int dt \oint_C \mathbf{j} \cdot d\mathbf{n} \\ &= -\int dt \oint_C \boldsymbol{\sigma}\mathbf{E} \cdot d\mathbf{n} = -N\frac{e^2}{h}\int dt \oint_C \mathbf{E} \cdot d\mathbf{l} \\ &= N\frac{e^2}{h}\int dt \partial_t \Phi = Ne \end{aligned} \tag{1.11}$$

where $d\mathbf{n}$ denotes the outward pointing unit vector normal to $C$, $d\mathbf{l}$ denotes the unit tangent vector to $C$, and $\boldsymbol{\sigma}$ denotes the conductivity tensor. Thus, threading one unit of flux through the disk has transferred one electron for each filled Landau level across the imaginary curve $C$. By hypothesis, because there are no states at the Fermi energy in the bulk, the occupation of the bulk states could not have changed during this process. Thus, the charge that passed through $C$ to the outer edge must have come from the inner edge, where there are states at the Fermi level. This implies that the conductance in the bulk is identical to the conductance in the clean regions and Eq (1.1) with $\nu \in \mathbb{Z}$ is satisfied everywhere.

We can be even less rigid than the picture shown in Fig 1.3c: there can be states at the Fermi level as long as they are localized. Such localized states are immune to the change in flux because they do not wind around the center. Thus, the density of states for a quantum Hall system can have bands of extended states near the center of the Landau levels and bands of localized states between the Landau levels, as shown in Fig 1.5. This configuration allows the chemical potential to be continuously tuned; as it moves across a band of localized states, the conductance will be on a plateau, and as it moves across the extended states, the conductance will jump to the next plateau. Thus, the width of the bands of extended states dictates the width of the regions between plateaus. If the disorder is too strong, the transition regions will overcome the plateaus and the quantized plateaus will disappear.

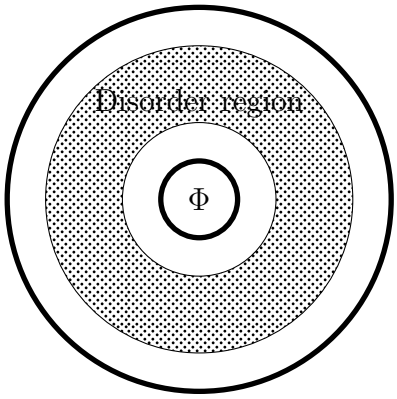


Figure 1.4: **Corbino disk.** The thick lines indicate the inner and outer edges of the disk. The hatching shows where disorder is present. A magnetic field, $B$, penetrates the entire plane and an additional variable flux, $\Phi$, is threaded through the center.

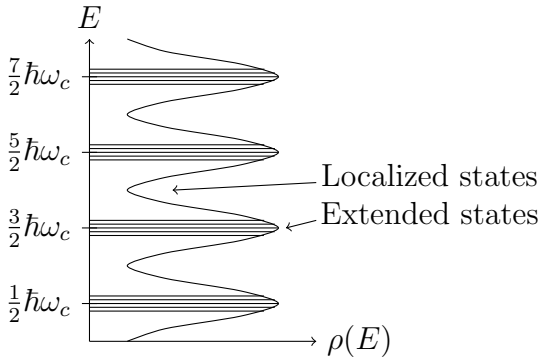


Figure 1.5: **Density of States for a quantum Hall System.** The extended states form a band near the center of the Landau level, while the remaining states are localized.

## 1.4 Theory of the fractional quantum Hall effect

In clean enough systems, plateaus in conductance at fractional values of $e^2/h$ appear. This effect cannot be explained by the free-electron theory from which we derived the integer effect. In contrast, interactions are crucial to the fractional quantum Hall effect, which will appear when the Coulomb energy scale exceeds the energy scale set by disorder. In this section, we review the strongly correlated electron states that display a quantized conductance in a clean system and then modify Laughlin's flux-threading argument of Sec 1.3.3 to show that this conductance remains quantized in the presence of disorder.

### 1.4.1 Laughlin wave functions

Angular momentum will play an important role in understanding the fractional quantum Hall effect. Thus, we return to Eq (1.3), rewriting the Hamiltonian in the symmetric gauge, $\mathbf{A} = -\frac{1}{2}\mathbf{r} \times \mathbf{B}$, which preserves rotational symmetry:

$$\begin{aligned} H_0 &= \frac{\hbar\omega_c}{2}\left(\left(-i\ell\partial_x + \frac{y}{2\ell}\right)^2 + \left(-i\ell\partial_y - \frac{x}{2\ell}\right)^2\right) \\ &= \frac{\hbar\omega_c}{2}\left(-\partial_z\partial_{\bar{z}} - \frac{x+iy}{2}(\partial_x - i\partial_y) + \frac{x-iy}{2}(\partial_x + i\partial_y) + \frac{z\bar{z}}{4}\right) \\ &= \frac{\hbar\omega_c}{2}\left(-4\partial_z\partial_{\bar{z}} - z\partial_z + \bar{z}\partial_{\bar{z}} + \frac{z\bar{z}}{4}\right) \\ &= \frac{\hbar\omega_c}{2}\left[1 + \left(-2\partial_z + \frac{\bar{z}}{2}\right)\left(2\partial_{\bar{z}} + \frac{z}{2}\right)\right] \end{aligned} \tag{1.12}$$

where $z = (x + iy)/\ell, \bar{z} = (x - iy)/\ell$ and, to be consistent with conventional notation, we have taken $\mathbf{B} = -B\hat{z}$. Since this is exactly the same Hamiltonian as analyzed in Sec 1.3.1, ground states have energy $\frac{1}{2}\hbar\omega_c$. Thus, the ground state sector consists of exactly the (unnormalized) wave functions, $\psi_m(z, \bar{z}) = z^m e^{-z\bar{z}/4}$, which are eigenstates of the angular momentum operator, $L_z = \hbar\left(z\partial_z - \bar{z}\partial_{\bar{z}}\right)$, with angular momentum $\hbar m$. These states are localized to a radius $r_m \equiv \left(\langle r^2\rangle\right)^{1/2} = \sqrt{2m\ell^2}$. For a system with $N$ electrons, whose positions are described by $z_i$, $i = 1, ..., N$, we can generalize $\psi_m$ to an anti-symmetric wave function,

$$\Psi_m(\{z_i\}) = \prod_{i<j}(z_i - z_j)^m e^{-\sum_i |z_i|^2/4}, \tag{1.13}$$

known as the $m^{\text{th}}$ Laughlin wave function.[11,12] Anti-symmetry under exchanging two electrons requires $m$ odd. It is evident that functions that are symmetric under exchanging two electrons can be multiplied by $\Psi_m$ to yield another ground state of Eq (1.12); these wavefunctions, which are less spatially compact than $\Psi_m$, represent excitations; we come back to them in Sec 1.4.4.

The highest power of any $z_i$ that appears in $\Psi_m$ is $m(N-1)$. Thus, $\Psi_m$ occupies an area $A = \pi r^2_{m(N-1)} = 2\pi m(N-1)\ell^2$. The filling fraction for $\nu = \Psi_m$ is $N\Phi_0/(BA) = N/(m(N-1))$. Hence, in the large $N$ limit, the wavefunction $\Psi_m$ describes a state at filling fraction $1/m$.

So far, we have found the ground state sector of Eq (1.3), within which the kinetic energy has disappeared, leaving us a highly degenerate set of states spanned by the $\Psi_m$. Interactions break this degeneracy. In the next section, we describe a set of interacting Hamiltonians for which a particular $\Psi_m$ is the exact ground state.

### 1.4.2 Haldane pseudopotentials

Interactions can be included in Eq (1.3) with the term,

$$H_{\text{int}} = \sum_{i<j} V_{ij} \equiv \sum_{i<j} V(|z_i - z_j|), \tag{1.14}$$

where $V_{ij} = \frac{1}{4\pi\epsilon}\frac{e^2}{|z_i - z_j|}$ describes the Coulomb interaction. Since $V_{ij}$ is a function only of the magnitude of $|z_i - z_j|$, it is diagonal in the relative angular momentum basis, i.e.,

$$\frac{\langle \Psi_m(z_i, z_j)|V_{ij}|\Psi_{m'}(z_i, z_j)\rangle}{\langle \Psi_m(z_i, z_j)|\Psi_m(z_i, z_j)\rangle} = V_m \delta_{mm'} \tag{1.15}$$

The $V_m$ are called the Haldane pseudopotentials, introduced in Ref 13, which completely specify the interaction potential. For the Coulomb potential, it is easy to check that $V_m = \frac{e^2}{4\pi\epsilon\ell}\frac{\Gamma(m+1/2)}{2\Gamma(m+1)}$. Here, we consider an arbitrary potential and rewrite the interaction terms in terms of the pseudopotentials as:

$$V_{ij} = \sum_{mm'} P_{ij}^m V_{ij} P_{ij}^{m'} = \sum_m V_m P_{ij}^m, \tag{1.16}$$

where we have defined $P_{ij}^m$, which projects the $i^{\text{th}}$ and $j^{\text{th}}$ electrons onto a state of relative angular momentum $\hbar m$.

Pairs of electrons in the Laughlin wave functions $\Psi_m(\{z_i\})$ have at least relative angular momentum $\hbar m$.[1] Thus, the states $\Psi_{m>1}$ are exact ground states of the fictional potential $V_{ij} = V_1 P^1_{ij}$. $\Psi_3(\{z_i\})$ is the most spatially compact. It follows that for a system with a confining potential, $\Psi_3(\{z_i\})$ would be the lowest-energy state. Generalizing, $\Psi_{2k+1}(\{z_i\})$ is the exact ground state of the fictional interaction described by the Haldane pseudopotentials $V_1, ..., V_{2k-1} > 0$, $V_{m>2k+1} = 0$. This state has a finite excitation gap to bulk excitations: a more compact state has at least one pair of electrons with angular momentum $m < 2k+1$, which costs energy $V_m$, while a less compact state is penalized by the confining potential.[2] The gap makes the state stable to perturbations in the Hamiltonian. Thus, we might expect that $\Psi_{2k+1}$ can be smoothly deformed into the exact ground state of the Coulomb potential without changing any quantized properties. For skeptics, Laughlin verified that his wavefunctions have an extremely high overlap with the exact ground states of the Coulomb potential, as well as with $-\ln(r)$ and $e^{-r^2/2}$ potentials, for systems with three electrons.[11] It is remarkable that such a straight-forward wave function, easily expressed in closed form, and derived from non-interacting electrons, can so successfully describe the ground state.

Combining the results of this and the previous section, the Laughlin wave functions are the exact ground states of an interacting Hamiltonian, sit at filling $\nu = 1/m$, lie in the lowest Landau level, and have a finite gap to excitations. For such a state, we

[1] In the two electron wave function, the two electrons have exactly relative angular momentum $\hbar m$.
[2] As discussed in Sec 1.4.4, density waves at the edge are gapless.

would expect a quantized Hall conductance following the logic of Sec 1.3.2. Furthermore, Laughlin's gauge argument, as described in Sec 1.3.3, predicts fractional excitations with charge $e/m$!

### 1.4.3 Laughlin quasiholes

Wavefunctions for excited states with a quasihole at some position $z_0$ are given by[11]

$$\Psi_m^{\rm qh}(\{z_i\}, z_0) = \prod_i (z_i - z_0)\Psi_m(\{z_i\}) \tag{1.17}$$

where $\Psi_m$ is defined in Eq (1.13). Notice that if we add $m$ quasiholes to the Laughlin state, the resulting wavefunction, $\prod_i (z_i - z_0)^m \Psi_m(\{z_i\})$, looks like the $m^{\rm th}$ Laughlin wavefunction for $N+1$ electrons, but with only the charge of $N$ electrons. We conclude that a single quasihole has charge $e/m$. The effect of the quasihole is identical to threading a flux through the Hall system at $z_0$.

To determine the statistics of the quasiholes, we compute the phase acquired by the wavefunction when one quasihole encircles another, following Ref 14: consider the wavefunction for electrons at positions $z_i$ and some number of quasiholes at positions $w_j$: $\psi(\{z_i(t), w_j(t)\}) \equiv \prod_{i,j}(z_i - w_j)\Psi_m(\{z_i\})$. Fix the positions of the electrons and all of the quasiholes except for $w_1$, which moves adiabatically to enclose an area $A_1$. The Berry phase is given by[15]

$$\gamma_m = i \int dt \langle \psi(\{z_i(t), w_j(t)\}) | \frac{d}{dt} | \psi(\{z_i(t), w_j(t)\}) \rangle$$

$$
\begin{aligned}
&= i \int dt \langle \psi(\{z_i(t), w_j(t)\}) | \sum_i \left( \frac{-\partial_t w_1(t)}{z_i - w_1(t)} \right) | \psi(\{z_i(t), w_j(t)\}) \rangle \\
&= i \int dt (-\partial_t w_1(t)) \int \frac{d^2 z}{z - w_1(t)} \langle \psi(\{z_i(t), w_j(t)\}) | \rho(z) | \psi(\{z_i(t), w_j(t)\}) \rangle \\
&= -i \oint dw_1 \int d^2 z \frac{\langle \rho(z) \rangle}{z - w_1} = -2\pi \int_{A_1} d^2 z \langle \rho(z) \rangle = -\frac{2\pi}{m} \left( \frac{\Phi_1}{\Phi_0} - N_{\mathrm{qh}} \right) \qquad (1.18)
\end{aligned}
$$

where $\rho(z) \equiv \sum_i \delta(z - z_i)$ and $N_{\mathrm{qh}}$ is the number of quasiholes in $A_1$. To obtain the last equality, recall that if none of the quasiholes $w_{j>1}$ are in the region $A_1$, then the total charge in $A_1$ is given by $\rho A_1 = \nu \Phi_1 / \Phi_0$, where $\Phi_1$ is the magnetic flux through $A_1$; for every quasihole in $A_1$, the charge is reduced by $1/m$.

The first term on the right hand side of the last line of Eq (1.18) is the phase acquired by the wavefunction when a charge $e/m$ quasiparticle encircles flux $\Phi_1$. The second term tells us that the wavefunction acquires an additional phase $2\pi/m$ when one quasihole circles another. The calculation reminds us of the intimate connection between charge and statistics.

There is no quasiparticle wavefunction that is an exact eigenstate of Eq (1.12). Laughlin proposed a trial wavefunction $\psi^{\mathrm{qp}} = \prod_i (\partial/\partial_{z_i} - z_0) \, \Psi_m$ and showed that it had a high overlap with the ground state found by exact diagonalization of a system with four quasiparticles.[11] Here, we will infer the properties of quasiparticles from those of the quasiparticles and not discuss their wavefunction.

Fractional quantum Hall systems are one of the few experimentally realizable systems predicted to display fractional charge and statistics. Hence, this prediction should not be taken lightly. In Sec 1.6 we discuss experiments that can probe these effects.

### 1.4.4 Edge excitations

We saw in Sec 1.3.2 that gapless edge excitations exist at the edge of integer quantum Hall states. The same is true for Laughlin states: while bulk excitations must be gapped because they require compressing the ground state, density waves can exist at the edge of the system at arbitrarily low energies. To understand this better, we follow Ref 16.

Given a Laughlin wavefunction, $\Psi_m$, which is a ground state of $H_0 + H_{\text{int}}$, where $H_0$ is defined by Eq (1.12) and $H_{\text{int}}$ is described by the Haldane pseudopotentials $V_{k<m} > 0, V_{k\geq m} = 0$, as described in Sec 1.4.2, the function $S(\{z_i\})\Psi_m$ is also a ground state, where $S$ is a polynomial symmetric in its arguments. However, when $S \neq 1$, the wavefunction will have an energy penalty in the presence of a confining potential. Lets enforce the energy penalty by adding a term $\lambda M$ to the Hamiltonian, where $M = \hbar \sum_i (z_i \partial_{z_i} - \bar{z}_i \partial_{\bar{z}_i})$ is the total angular momentum about the origin. Then $S$ can be expressed as $S = \sum_n s_n^{p_n}$, where $s_n \equiv \sum_i z_i^n$ and $p_n$ is a non-negative integer. Computing $\lambda M s_n = \lambda \hbar n s_n$, the state $S\Psi_m$ has excitation energy

$$\Delta E = \lambda \hbar \sum_n n p_n, \tag{1.19}$$

linearly proportional to angular momentum. Hence, we have found modes which are gapless in the infinite system limit. Since gapless excitations cannot exist in the bulk, we conclude that they are edge excitations.

Notice that a quasihole at $z_0$, as described by Eq (1.17), also takes the form $S(\{z_i\})\Psi_m$. However, when $z_0$ is far away from the edge (i.e., at least a magnetic length), $S$ requires a macroscopic number of $s_n$ and hence defines a finite-energy excitation; in particular, when $z_0 = 0$, $M\Psi_m^{\rm qh} = (\hbar N + M_0)\,\Psi_m^{\rm qh}$, where $N$ is the total number of electrons and $M_0$ the eigenvalue of $M$ in the ground state. As $z_0$ approaches the edge, it becomes less of a disturbance in density, until at $z_0 \to \infty$, it costs zero energy and effectively becomes an edge excitation. Thus, edge and bulk excitations can be considered together as a continuum of all excitations. This logic also tells us that a quasihole of charge $e/m$ added to the center of the system adds a compensating charge $-e/m$ to the edge of the system; as the hole approaches the edge, the charges cancel.

Finally, the excitation energy computed in Eq (1.19) describes a system of harmonic oscillators each with energy $\omega = n$ and occupation number $p_n$. In Sec 1.5.5, we will derive this result from the field theory approach.

### 1.4.5 Hierarchy states

The Laughlin wave functions help us understand the odd-denominator $\nu = 1/m$ states. However, many other fractions have been observed. We can understand the

other fractions through hierarchy constructions. In this section, we consider the Haldane-Halperin hierarchy[13,17] and Jain's composite fermion picture.[18] These two theories differ in their microscopic construction but describe the same universal physics.[19] The hierarchy procedure described in this section can only generate odd-denominator fractions. Hence, a new framework is necessary to describe even-denominator states, which we describe in Sec 1.4.6.

**Haldane-Halperin hierarchy**

The construction begins with a Laughlin state $\nu = 1/m$. As magnetic flux pierces this state and charged quasiparticles proliferate, eventually we would expect the quasiparticles themselves to form a Laughlin state. Recall that the pre-factor $\prod_{i<j}(z_i - z_j)^m$ in Eq (1.13) requires $m$ odd to accommodate the statistics of the electrons. Thus, the pre-factor for a quasiparticle wavefunction should take the form $\prod_{i<j}(z_i - z_j)^{2p-\frac{1}{m}}$, for some integers $k$ (a quasihole wavefunction would have a similar pre-factor, with exponent $2p + \frac{1}{m}$.) It follows that generalized quasiparticle(hole) wavefunctions will be at quasiparticle(hole) filling $\nu_{\text{qp/qh}} = 1/(2p \mp \frac{1}{m})$, where the $-$ sign is for quasiparticles and the $+$ sign is for quasiholes. The electron filling fraction is related to the quasiparticle(hole) filling fraction by $\nu_{\text{el}} = \pm\frac{1}{m^2}\nu_{\text{qp/qh}}$; one can see this by rederiving Eq (1.8) for fractionally charged particles, for which that are only $\Phi/(m\Phi_0)$ states, compared to $\Phi/\Phi_0$ states for electrons. Hence, the total electron filling fraction is $\nu = \frac{1}{m} \pm \frac{1}{m^2(2p\mp\frac{1}{m})} = \frac{1}{m\mp\frac{1}{2p}}$.

Iterating this process yields a family of states with filling fractions:

$$\nu = \frac{1}{m \mp \frac{1}{2p_1 \mp \frac{1}{2p_2 \mp \ldots}}} \tag{1.20}$$

However, it is not expected that all of these states will be observed in experiment: each layer of the hierarchy is increasingly fragile and a state whose gap to excitations is less than the energy scale set by disorder will not be observed.

### Jain's composite fermion hierarchy

Another tool to understand fractions that fall outside the Laughlin paradigm is Jain's composite fermion construction, in which fractional states are understood as integer states of "composite fermions," particles consisting of an even number of flux quanta bound to an electron.[18] The number of flux quanta must be even to preserve the fermionic statistics of the electrons; one expects statistics to be important in considering fractional states because of their key role in the Laughlin wavefunctions – interactions explain why $\nu = 1/m$ with $m$ an odd integer. If $2p$ quanta of flux are attached to each electron and the composite particles are filled to the integer state at (composite) filling $N$, then for $N_{\rm el}$ electrons, $N = N_{\rm el}/(\Phi/\Phi_0 - 2pN_{\rm el})$, so that the electron filling fraction is $\nu = N_{\rm el}\Phi_0/\Phi = N/(1 + 2pN)$. Thus, the Jain sequence also generates filling fractions with odd denominators.

If this picture is to describe a real system, the binding of flux to electrons would not be exact, causing a decrease in stability as more flux quanta were added. At large enough $p$, the state will be destroyed by disorder. Consequently, both the Jain hierarchy and the Haldane-Halperin hierarchy predict an ordering for the strength of particular fractions.

### 1.4.6 Even denominator states

The hierarchy states described in Sec 1.4.5 offer explanations for odd-denominator fractions. However, these do not offer an explanation for the observed[7] state at $\nu = 5/2$. Much attention has been paid to the $\nu = 5/2$ state, which we will discuss specifically in Sec 1.7.2. Here, we show more generally how exchanging flux and statistics leads to a family of even-denominator states.

Before the experimental observation of any even-denominator fractions, Halperin noticed that if electrons formed tightly-bound pairs, then applying Laughlin's theory to these charge-$2e$, bosonic pairs would yield the fractions $\nu = 4/m$, where here $m$ is an even integer.[20] (This can be generalized to bound states of $n$ electrons, which yield the series $\nu = n^2/m$ for any $m$ and $n$ with the same parity.) Taking $m = 8$ yields $\nu = 1/2$, the first attempt to explain an even-denominator fraction, but Halperin had no explanation for why a strong attractive pairing would occur. Greiter, Wen and Wilczek offered an explanation by relating the $\nu = 1/2$ state to a state of electrons in zero magnetic field,

which has a BCS pairing instability, and proposed a new wavefunction, which we now motivate.[21,22]

Following Ref 23, consider electrons of density $\rho$ in a magnetic field $B_i$ and adiabatically increase the magnetic field by threading flux at the location of each electron, until a total field $B_f$ is reached and each electron has $\alpha$ (possibly fractional) flux quanta attached to it. The initial and final magnetic fields are related by $B_f/\Phi_0 = B_i/\Phi_0 + \alpha\rho$, and thus the initial and final filling fractions are related by

$$\frac{1}{\nu_f} = \frac{1}{\nu_i} + \alpha \tag{1.21}$$

Since the final composite particles have exchange statistics $\pi\alpha$, Eq (1.21) says that the change in inverse filling fraction is equal to the change in statistics, or, $\Delta(1/\nu) = \Delta(\theta/\pi)$. When $\alpha$ is an even integer and $\nu_i$ is an integer, Eq (1.21) reduces to the composite fermions of Jain, described in Sec 1.4.5. Instead, Refs 21 and 22 consider the case where $B_i = 0$ and $\alpha = 2$, yielding $\nu_f = 1/2$. Thus, the $\nu = 1/2$ state is adiabatically connected to a free fermion system in zero magnetic field, known to be unstable to BCS pairing. At small values of $\alpha$, where one can perturb away from $B = 0$, the superconducting instability was found to have a large $p$-wave component.[22] While the perturbation theory does not apply at $\alpha = 2$, it motivates a trial wavefunction, namely, a paired wavefunction with $p$-wave correlations:

$$\Psi_{\rm BCS}(\{z_i\}) = \mathrm{Pf}\left(\frac{1}{z_i - z_j}\right) \equiv \mathcal{A} \prod_{i \text{ even}}^{N} \frac{1}{z_i - z_{i-1}}, \tag{1.22}$$

where the $\mathcal{A}$ indicates anti-symmetrization over all possible ways of pairing the $N$ electrons. In Sec 1.4.1, we showed that wavefunctions in the lowest Landau level must be analytic functions of $z_i$. Thus, a potential wavefunction based on $\Psi_{\rm BCS}$ that describes a state at $\nu = 1/2$ is

$$\Psi_{\rm Pf} = {\rm Pf}\left(\frac{1}{z_i - z_j}\right)\prod_{k<l}(z_k - z_l)^2 \prod_m e^{-|z_m|^2/4} \tag{1.23}$$

a generalization of the Laughlin wavefunctions in Eq (1.13). The factors of $(z_k - z_l)^2$ ensure both that $\Psi_{\rm Pf}$ is analytic in the $z_i$ and that the electrons are at filling fraction $1/2$; the filling fraction is computed the same way as in the Laughlin case, following the text after Eq (1.13). It is evident that the wavefunction can be modified to describe any filling fraction $\nu = 1/(2m)$ by taking $2 \to 2m$. The wavefunction $\Psi_{\rm Pf}$ is an exact ground state of a local Hamiltonian with repulsive 3-body interactions (while $\Psi_{\rm BCS}$ is the exact ground state of a Hamiltonian with 2-body delta-function interactions).[22]

Independently, and motivated by conformal field theory, $\Psi_{\rm Pf}$ was also proposed by Moore and Read, who showed that the excitations have non-Abelian statistics;[24] we postpone the discussion of statistics until Sec 1.7.2. However, in the strong-pairing limit proposed by Halperin, the $m = 8$ Laughlin state has quasiparticles with charge $1/8$ that of the pair, i.e., charge $e/4$, and (Abelian) exchange statistics $\pi/8$. Thus, although pairing is the crux of both theories, they describe different phases of matter.

## 1.5 Chern-Simons-Landau-Ginzburg Theory

Despite the descriptive and predictive success of Laughlin's wavefunction approach, it is desirable to have a field theory description of the fractional quantum Hall effect, which would capture the universal aspects of the phase, independent of the particular wavefunction. The history and a clear pedagogical account of this approach is given in Ref 25, which we draw on extensively in this section. Many of the ideas originate from Ref 26.

### 1.5.1 Flux Attachment

In this section, we develop the mathematical formalism behind the flux-statistics transmutation discussed in Sec 1.4.6. Statistically, an electron is equivalent to a boson with an odd number of flux quanta attached to it. The flux-attachment can be implemented via the gauge field $\mathbf{a}(x)$, which satisfies

$$\mathbf{b} \equiv \nabla \times \mathbf{a}(x) = (2k+1)\phi_0 \rho(x)\hat{z}, \tag{1.24}$$

where $\rho(x)$ is the electron density. If the external field is oriented opposite to $\mathbf{b}$, i.e., $\mathbf{B} = -B\hat{z}$, with $B > 0$, then when $(2k+1)\phi_0\langle\rho(x)\rangle = B$, the net field $\mathbf{b} + \mathbf{B}$ seen by each boson will exactly cancel. Hence, the fractional fillings $\nu = 1/(2k+1)$ are special points where Bose-condensation can occur. The Meissner effect then tells us that the

condensate is incompressible: because magnetic flux cannot penetrate the condensate, there is an energy gap to adding electrons.

### 1.5.2 Consequences of superfluid analogy

Heuristically, we can derive the Hall resistance from this picture: each composite particle contributes to the charge current, $I_c = edN/dt$, and the vortex (flux) current, $I_v = (2k+1)\phi_0 dN/dt$. The latter induces a transverse voltage drop, $V_H = I_v$, and hence the Hall resistance is given by $R_H = V_H/I_c = (2k+1)h/e^2$.

Taking the analogy further, a charged superfluid has vortices that contain integer units of flux. In our Hall fluid, since $2k+1$ flux quanta are bound to a single electron, a vortex consisting of a single flux quantum carries charge $e/(2k+1)$. It follows that the exchange statistics between two composites consisting of a single flux quantum and charge $e/(2k+1)$ will be $\pi/(2k+1)$. Thus, we have reproduced the Laughlin quasiparticles and their statistics. These quasiholes are responsible for the quantized Hall conductance: as in a Type II superconductor, where current can flow without dissipation as long as the vortices are pinned by impurities, Hall current can flow without dissipation as long as the quasiholes are pinned. These are exactly the localized states described in Sec 1.3.3.

### 1.5.3 Derivation of Chern-Simons action

The Lagrangian for bosons with the flux attachment described in Sec 1.5.1 is[3]

$$\mathcal{L}_\phi = \phi^\dagger \left(i\hbar\partial_t - ec(A_0 + a_0)\right)\phi - \frac{1}{2m}\left|(i\hbar\nabla - e\mathbf{A} - e\mathbf{a})\,\phi\right|^2 - \frac{1}{2}\int d^2\mathbf{r}'\delta\rho(\mathbf{r})V(\mathbf{r}-\mathbf{r}')\delta\rho(\mathbf{r}') \tag{1.25}$$

where $\phi$ is the quantized bosonic field operator, satisfying $\left[\phi(\mathbf{r}), \phi^\dagger(\mathbf{r}')\right] = \delta^2(\mathbf{r}-\mathbf{r}')$, $\rho(\mathbf{r}) = \phi^\dagger(\mathbf{r})\phi(\mathbf{r})$ and $\delta\rho(\mathbf{r}) \equiv \rho(\mathbf{r}) - \bar{\rho}$ is the deviation from average density, $\bar{\rho}$. The components of $\mathbf{a}$ can be expressed as

$$a_i(\mathbf{r}) = -\frac{\phi_0}{2\pi}\frac{\theta}{\pi}\epsilon^{ij}\int d^2\mathbf{r}'\frac{r_j - r_j'}{|\mathbf{r}-\mathbf{r}'|^2}\rho(\mathbf{r}'), \tag{1.26}$$

where $\theta = (2k+1)\pi$ and $\epsilon^{\alpha\beta}$ is the antisymmetric tensor. We can check that Eq (1.26) satisfies Eq (1.24):

$$b^z(x) \equiv \epsilon^{ij}\partial_{r_i}a_j(\mathbf{r}) = \frac{\phi_0}{2\pi}\frac{\theta}{\pi}\nabla_{\mathbf{r}}\cdot\left(\int d^2\mathbf{r}'\frac{\mathbf{r}-\mathbf{r}'}{|\mathbf{r}-\mathbf{r}'|^2}\rho(\mathbf{r}')\right) = \phi_0(2k+1)\rho(\mathbf{r}) \tag{1.27}$$

We have used the two-dimensional identity $\nabla\cdot(\hat{\mathbf{r}}/r) = 2\pi\delta^2(\mathbf{r})$.[4] At any fixed time, the gauge field $\mathbf{a}$ is completely determined. Its dynamics are given by the continuity equation, $\partial_t\rho(\mathbf{r},t) + \partial_i j_i(\mathbf{r},t) = 0$, which yields

$$\epsilon^{ij}\dot{a}_i(\mathbf{r},t) = \phi_0(2k+1)j_j(\mathbf{r},t), \tag{1.28}$$

[3]The Lagrangian in Eq (1.25) is chosen such that the spectrum of its corresponding Hamiltonian is identical to that of the electrons with no flux attachment, as verified in Ref 25.

[4]We derive this by noting that when $r \neq 0$, $\nabla\cdot(\hat{\mathbf{r}}/r) = 1/r\partial_r(r/r) = 0$, but the divergence theorem tells us $\int d^2\mathbf{r}\nabla\cdot(\hat{\mathbf{r}}/r) = \oint(\hat{\mathbf{r}}/r)\cdot\hat{r}rd\theta = 2\pi$, where the integral is over any circle centered at the origin. We conclude $\nabla\cdot(\hat{\mathbf{r}}/r) = 2\pi\delta^2(\mathbf{r})$.

up to a constant. Thus, $\mathbf{a}$ is completely determined in terms of the fields $\phi$ by Eqs (1.27) and (1.28).

We now seek a Lagrangian for $\mathbf{a}$, which will produce Eqs (1.27) and (1.28) after applying the Euler-Lagrange equation. This is exactly the Chern-Simons action,

$$\mathcal{L}_{\mathrm{CS}} = \frac{1}{2}\frac{\pi}{\theta}\frac{ec}{\phi_0}\epsilon^{\mu\nu\rho}a_\mu\partial_\nu a_\rho, \tag{1.29}$$

where the Greek indices run over $0, 1, 2$. We have introduced $a_\mu = (a_0, \mathbf{a})$. To reproduce Eqs (1.27) and (1.28), we add a current term, $-ea_\mu j^\mu$ to $\mathcal{L}_{\mathrm{CS}}$, vary with respect to $a_0$ and $\mathbf{a}$, respectively, and then choose the gauge $a_0 = 0$. Notice that $\mathcal{L}_{\mathrm{CS}}$ is gauge invariant up to a surface term: if $\delta a_\mu = \partial_\mu \Lambda$, then $\delta\mathcal{L}_{\mathrm{CS}} = \frac{1}{2}\frac{\pi}{\theta}\frac{ec}{\phi_0}\epsilon^{\mu\nu\rho}\partial_\mu\left(\Lambda\partial_\nu a_\rho\right)$. The mean field theory solution to the combined Lagrangian, $\mathcal{L} = \mathcal{L}_\phi + \mathcal{L}_{\mathrm{CS}}$, is $\phi(x) = \sqrt{\bar{\rho}}, \mathbf{a} = -\mathbf{A}, a_0 = -A_0$. Plugging this solution into the equations of motion gives the filling fraction $\nu = 1/(2k+1)$ and the Hall conductance, $\sigma_{xy} = \frac{1}{2k+1}\frac{e^2}{h}$. Because there is a gap to excitations, we would expect this solution to be robust to small fluctuations, which is verified in Ref 25.

As described in the previous section, when the magnetic field is moved away from the idea filling fraction, vortices are created to compensate. In terms of the field theory, a vortex at the origin takes the form

$$\phi(r,\theta) = f(r/\ell)\sqrt{\bar{\rho}}e^{\pm i\theta}, \quad \delta\mathbf{a}(r,\theta) = \pm\frac{\phi_0}{2\pi}\frac{\hat{\theta}}{r}, \quad a_0 = 0 \tag{1.30}$$

where the dimensionless function $f$ satisfies $f(0) = 0, f(x \to \infty) = 1$; the former constraint comes from requiring $\phi$ to be continuous. Such a vortex carries unit flux

$\oint \delta\mathbf{a} \cdot \mathbf{dl} = \pm\phi_0$, and, applying Eq (1.27), fractional charge $\frac{\pm 1}{2k+1}$. As is the case in a charged superconductor, the energy cost of a vortex is finite, consistent with an excitation gap.[5]

### 1.5.4 Derivation of dual action

Two dimensional superconductors exhibit a flux-charge duality. In our two-dimensional quantum Hall system, because each flux quantum is bound to a quasiparticle, the duality is between quasiparticles and electrons. Writing the Lagrangian, $\mathcal{L} = \mathcal{L}_\phi + \mathcal{L}_{\text{CS}}$, in its dual form, we find a theory with quasiparticles as the fundamental object. In the next section, we will integrate out the gapped bulk theory to find the low-energy theory of the edge, which will be the starting point for upcoming chapters.

Writing $\phi(\mathbf{r}) = \sqrt{\rho(\mathbf{r})}e^{i\chi(\mathbf{r})}$, we define the vortex current

$$j^{\text{v}}_\mu(\mathbf{r}) \equiv \frac{c}{2\pi}\epsilon^{\mu\nu\rho}\partial_\nu\partial_\sigma\chi(\mathbf{r}) \tag{1.31}$$

Naively, $j^{\text{v}} = 0$, but, crucially, because $\chi$ is not continuous when vortices are present, $j^{\text{v}}$ is non-zero at the vortices. In particular, if there is a vortex at the origin, according to (1.30), $\chi(r,\theta) = \theta$ and the vortex density computed from Eq (1.31) is exactly unity:

$$\int d^2x\rho^{\text{v}} \equiv \int d^2x\frac{j^{\text{v}}_0}{c} = \frac{1}{2\pi}\int d^2x\epsilon^{ij}\partial_i\partial_j\chi(\mathbf{r}) = \frac{1}{2\pi}\oint \nabla\chi(\mathbf{r}) = 1 \tag{1.32}$$

[5] In Eq (1.25), the change in $\mathbf{a}$ exactly cancels the $\hat{\theta}$ contribution to $\nabla\phi$, so that $\delta E \propto \int_0^\infty xdx\,(f'(x))^2$, where $f$ is defined by Eq (1.30). In contrast, a neutral superfluid does not couple to the electromagnetic gauge field and $\delta E \propto \int_0^\infty xdx\left((f'(x))^2 + (f(x))^2\,\frac{1}{x^2}\right)$, which yields the familiar result that vortex energy diverges logarithmically with system size.

Substituting this form of $\phi$ into the sum of the Lagrangian (1.25) and taking $\rho$ constant except for vortex configurations,

$$\mathcal{L}_\chi = \rho\left(-\hbar\partial_t\chi - ec\delta a_0\right) - \frac{\rho}{2m}\left(-\hbar\nabla\chi - e\delta\mathbf{a}\right)^2 - \frac{1}{2}\int d^2\mathbf{r}'\delta\rho(\mathbf{r})V(\mathbf{r}-\mathbf{r}')\delta\rho(\mathbf{r}'), \quad (1.33)$$

where we have defined $\delta\mathbf{a} = \mathbf{a} - \mathbf{A}$. The action is linearized by introducing a Hubbard-Stratonovich field, $j$, which yields

$$\mathcal{L}'_\chi = \rho\left(-\hbar\partial_t\chi - ec\delta a_0\right) + j_i\left(-\hbar\nabla\chi - e\delta\mathbf{a}\right)_i + \frac{m}{2\bar{\rho}}j_i j_i - \frac{1}{2}\int d^2\mathbf{r}'\delta\rho(\mathbf{r})V(\mathbf{r}-\mathbf{r}')\delta\rho(\mathbf{r}') \quad (1.34)$$

Varying with respect to $\chi$ yields the equation of motion, $\partial_t\rho + \nabla\cdot j = 0$, which motivates us to introduce the dual gauge field $a^{\mathrm{v}}$, defined by

$$\rho = \frac{1}{\phi_0}\epsilon_{ij}\partial_i a^{\mathrm{v}}_j, \quad j_i = \frac{c}{\phi_0}\epsilon_{ij}(\partial_j a^{\mathrm{v}}_0 - \partial_0 a^{\mathrm{v}}_j), \quad (1.35)$$

up to a gauge transformation, $a^{\mathrm{v}}_\mu \to a^{\mathrm{v}}_\mu + \partial_\mu\Lambda$. Comparing Eq (1.35) to Eqs (1.27) and (1.28) shows that each quantum of vortex flux is attached to an electron, while previously a quantum of the original flux $\mathbf{a}$ was bound to each quasiparticle. Substituting Eq (1.35) into $\mathcal{L}'_\chi$ yields

$$\begin{aligned}\mathcal{L}'_\chi = &-ea^{\mathrm{v}}_\mu j^{\mathrm{v}}_\mu - \frac{e^2c}{h}\epsilon^{\mu\nu\rho}\delta a_\mu\partial_\nu a^{\mathrm{v}}_\rho + \frac{m}{2\bar{\rho}}\left(\frac{c}{\phi_0}\right)^2(\partial_j a^{\mathrm{v}}_0 - \partial_0 a^{\mathrm{v}}_j)^2 \\ &- \frac{1}{2\phi_0^2}\int d^2\mathbf{r}'\epsilon^{ij}\partial_i\delta a^{\mathrm{v}}_j(\mathbf{r})V(\mathbf{r}-\mathbf{r}')\epsilon^{kl}\partial_k\delta a^{\mathrm{v}}_l(\mathbf{r}') \end{aligned} \quad (1.36)$$

We will now drop the third and fourth terms, which have more derivatives in $a^{\mathrm{v}}$, and integrate out the gauge fields $\mathbf{a}$ in $\mathcal{L}'_\chi + \mathcal{L}_{\mathrm{CS}}$ to find the dual Lagrangian,

$$\mathcal{L}_{\mathrm{dual}} = -e a^{\mathrm{v}}_\mu j^{\mathrm{v}}_\mu - \frac{e^2 c}{\hbar}\frac{(2k+1)}{4\pi}\epsilon^{\mu\nu\rho} a^{\mathrm{v}}_\mu \partial_\nu a^{\mathrm{v}}_\rho - \frac{1}{2\pi}\frac{e^2 c}{\hbar}\epsilon^{\mu\nu\rho} A_\mu \partial_\nu a^{\mathrm{v}}_\rho, \tag{1.37}$$

which is entirely in terms of the vortex fields and currents – or, equivalently, the quasi-particles. We could add a kinetic term for the vortex creation/annihilation operator, but this term is not important if there are only a few vortices and they are pinned (which also justifies dropping the interaction term in $\mathcal{L}'_\chi$.)

We can check that Eq (1.37) yields the correct observables: integrating out the gauge field, $a^{\mathrm{v}}$, yields

$$\mathcal{L}[A] = \frac{e^2 c}{h}\epsilon^{\mu\nu\rho}\frac{1}{2}\frac{1}{2k+1} A_\mu \partial_\nu A_\rho \tag{1.38}$$

After including a current $J_\mu A^\mu$, the equations of motion are $\frac{e^2 c}{h}\epsilon^{\mu\nu\rho}\frac{1}{2k+1}\partial_\nu A_\rho = J^\mu$, which gives the correct Hall conductance, $\sigma_{xy} = \frac{1}{2k+1}\frac{e^2}{h}$, and filling fraction, $\nu = \frac{1}{2k+1}$.

### 1.5.5 Effective theory on a manifold with a boundary

Consider the Hamiltonian derived from $\mathcal{L}_{\mathrm{dual}}$, taking $j^{\mathrm{v}} = 0$: if we choose the gauge $a_0 = A_0 = 0$, the Hamiltonian disappears, because every term has either $a_0, A_0$ or $\partial_0 a_\mu$. This is because bulk Chern-Simons theory only captures the ground state properties of the system; by definition, all ground states are degenerate. Notice that when the magnetic field deviates from a perfect filling fraction, the ground state contains quasi-

particles, so the theory does capture information about quasiparticles and statistics. Because $\mathcal{L}_{\text{dual}}$ is gauge-invariant up to a surface term, $\mathcal{H}_{\text{dual}} = 0$ on any closed manifold; this is not an artifact of our gauge choice.

On a manifold with a boundary, we know from Sec 1.4.4 that there are low energy excitations at the edge. Thus, on a manifold with a boundary, we do not have the gauge freedom to choose $a_0 = A_0 = 0$. Instead, the gauge freedom becomes a physical degree of freedom, whose equation of motion includes the velocity of the edge excitations. Because the velocity is determined by the microscopic details of the edge, it is not included in the Chern-Simons theory.

To input this information, we follow Wen:[27] choose coordinates $\tilde{x} = x + vt, \tilde{y} = y, \tilde{t} = t$, where the coordinate $x$ is parallel to the boundary. The components of any vector $w$ in these coordinates satisfy, $w_{\tilde{\mu}}\hat{x}_{\tilde{\mu}} = w_\mu \hat{x}_\mu$, so that, $w_{\tilde{t}} = w_t - v w_x, w_{\tilde{x},\tilde{y}} = w_{x,y}$. Then define the field $\alpha_\mu \equiv a^{\text{v}}_\mu + A_\mu/(2k+1)$ and choose the gauge $\alpha_{\tilde{0}} = 0$. The equation of motion from $\alpha_{\tilde{0}}$ is then a constraint, $\epsilon^{\tilde{i}\tilde{j}}\partial_{\tilde{i}}\alpha_{\tilde{j}} = 0$, which is satisfied by writing $\alpha_{\tilde{i}} = \partial_{\tilde{i}}\varphi$, for some continuous field $\varphi$. Inserting this gauge choice into $\mathcal{L}_{\text{dual}}$ with $j^{\text{v}}_\mu = 0$ yields,

$$\begin{aligned}
\mathcal{S}_{\text{dual}}\big|_{\alpha_{\tilde{0}}=0} &= \frac{e^2 c}{\hbar}\int d^2\tilde{x}d\tilde{t}\frac{\epsilon^{\tilde{i}\tilde{j}}}{4\pi}\left(-(2k+1)\partial_{\tilde{i}}\varphi\partial_{\tilde{0}}\partial_{\tilde{j}}\varphi - A_{\tilde{i}}\partial_{\tilde{0}}\partial_{\tilde{j}}\varphi + \partial_{\tilde{i}}\varphi\partial_{\tilde{0}}A_{\tilde{j}} - \partial_{\tilde{i}}\varphi\partial_{\tilde{j}}A_{\tilde{0}}\right) + \mathcal{S}[A] \\
&= \frac{e^2 c}{\hbar}\int d^2\tilde{x}d\tilde{t}\frac{\epsilon^{\tilde{i}\tilde{j}}}{4\pi}\partial_{\tilde{j}}\left(-(2k+1)\partial_{\tilde{i}}\varphi\partial_{\tilde{0}}\varphi - \partial_{\tilde{i}}\varphi A_{\tilde{0}}\right) + \frac{\epsilon^{\tilde{i}\tilde{j}}}{4\pi}\partial_{\tilde{0}}\left(\partial_{\tilde{i}}\varphi A_{\tilde{j}}\right) + \mathcal{S}[A] \\
&= -\frac{e^2 c}{\hbar}\int d\tilde{x}d\tilde{t}\frac{1}{4\pi}\left((2k+1)\partial_{\tilde{x}}\varphi\partial_{\tilde{0}}\varphi + \partial_{\tilde{x}}\varphi A_{\tilde{0}}\right) + \mathcal{S}[A] \\
&= \frac{e^2}{\hbar}\int dxdt\frac{1}{4\pi}\left((2k+1)\partial_x\varphi\left(\partial_t - v\partial_x\right)\varphi - \partial_x\varphi(A_t - vA_x)\right) + \mathcal{S}[A] \qquad (1.39)
\end{aligned}$$

where $\mathcal{S}[A]$ is the action from the Lagrangian (1.38) and we have used the fact that the boundary is parallel to the $x$ direction. If we require the Hamiltonian to be bounded from below, then $v$ and $2k+1$ must have the same signs; we take them to be positive. Substituting the equation of motion for $\varphi$ into the second term yields the more symmetric form $A_\mu \epsilon_{\mu\nu} \partial_\nu \varphi$.

Now consider the effect of a vortex in the bulk, so that $j_0 = c\delta(\mathbf{x})$. The equation of motion from $\alpha_{\tilde{0}}$ becomes $\epsilon^{\tilde{i}\tilde{j}} \partial_{\tilde{i}} \alpha_{\tilde{j}} = -\frac{h}{e} \frac{1}{2k+1} \delta(\mathbf{x})$. This equation is satisfied if $\varphi \to \varphi - \frac{1}{2k+1}\theta$, where $\theta$ is the angular coordinate. Alternately, a branch cut could be drawn originating at the vortex and extending to the edge of the sample, so that $\varphi \to \varphi + \frac{2\pi}{2k+1}$ upon crossing the branch cut. Either way, the field $\varphi$ will acquire a phase $2\pi/(2k+1)$ upon encircling the vortex.

### 1.5.6 Edge operators

In Sec 1.5.5, the bulk action was reduced to one that exists only on the edge of the manifold. It describes a $(1+1)$-dimensional chiral boson: the equation of motion (neglecting $A$) is $\partial_x \left(\partial_t - v\partial_x\right) \varphi = 0$, which implies $\varphi(x,t) = \varphi(x+vt)$. The conjugate momentum is $\pi = \frac{2k+1}{4\pi} \partial_x \varphi$, which yields the equal time commutation relation,[6]

$$[\varphi(x), \partial_y \varphi(y)] = i \frac{2\pi}{2k+1} \delta(x-y) \tag{1.40}$$

[6]The commutation relation for chiral fields differs by a factor of two from that of non-chiral fields, $[\phi(x), \pi(y)] = i\delta(x-y)$, because two chiral fields can be mapped to a single non-chiral field.

Here, we are using natural units, and will continue to do so for the rest of this section. The coupling between $\varphi$ and $A$ yields the charge density and current operators:

$$\begin{aligned} \rho &= \frac{1}{2\pi}\partial_x\varphi \\ j &= \frac{1}{2\pi}\partial_t\varphi \end{aligned} \tag{1.41}$$

Eqs (1.40) and (1.41) allow us to compute, using the Baker-Campbell-Hausdorff formula,

$$e^{i\alpha\varphi}(x)\rho(y) = \left(\rho(y) + [i\alpha\varphi(x), \rho(y)]\right) e^{i\alpha\varphi(x)} = \left(\rho(y) - \frac{\alpha}{2k+1}\delta(x-y)\right) e^{i\alpha\varphi(x)} \tag{1.42}$$

Hence, $e^{i\varphi}$ and $e^{i(2k+1)\varphi}$ are creation operators for quasiparticles and electrons, respectively. Integrating (1.40) over $y$ yields, $[\varphi(x), \varphi(y)] = i\frac{\pi}{2k+1}\mathrm{sgn}(x-y)$. Apparently, $\varphi$ does not commute with itself in different places! This is a peculiar property of chiral fields. We can then compute the fractional statistics of the quasiparticle operators,

$$e^{i\alpha\varphi(x)}e^{i\beta\varphi(y)} = e^{i\beta\varphi(y)}e^{i\alpha\varphi(x)}e^{-\alpha\beta[\varphi(x),\varphi(y)]} = e^{i\beta\varphi(y)}e^{i\alpha\varphi(x)}e^{-i\frac{\alpha\beta\pi}{2k+1}\mathrm{sgn}(x-y)} \tag{1.43}$$

All operators, $e^{i\alpha\varphi}$, allowed in the theory should be local with respect to the electron, $e^{i(2k+1)\varphi}$; i.e., under two exchanges, the phase acquired should be trivial. Taking $\beta = 2k+1$ in Eq (1.43), we see that this is equivalent to requiring $\alpha \in \mathbb{Z}$. Hence, physical operators take the form $e^{in\varphi}$, with $n$ an integer.

We would like to compute the correlators of the quasiparticle operators. First, we compute the $\langle\varphi\varphi\rangle$ correlator at $A = 0$ in imaginary time, $\tau = it$,

$$\langle\varphi(x,\tau)\varphi(0,0)\rangle - \langle\varphi(0,0)\varphi(0,0)\rangle = \int \frac{dq}{2\pi}\frac{d\omega}{2\pi}\left(e^{iqx+i\omega\tau} - 1\right)\langle\varphi(q,\omega)\varphi(-q,-\omega)\rangle$$

$$
\begin{aligned}
&= \frac{2\pi}{2k+1}\int \frac{dq}{2\pi}\frac{d\omega}{2\pi}\frac{(e^{iqx+i\omega\tau}-1)}{iq(\omega+iqv)} \\
&= \frac{2\pi}{2k+1}\mathrm{sgn}(\tau)\int \frac{dq}{2\pi}\frac{\Theta(q\tau)}{q}\left(e^{iq(x-iv\tau)}-1\right) \\
&= \frac{2\pi}{2k+1}\int_0^\infty \frac{dq}{2\pi}\frac{\left(e^{iq(x-iv\tau)}-1\right)}{q} \\
&= -\frac{1}{2k+1}\ln\left((v\tau+ix)/a\right) \qquad (1.44)
\end{aligned}
$$

where we assumed the integral only had finite contribution when $q(x-iv\tau) > 1$ and introduced $a$, a short distance scale inversely proportional to the high-energy cut-off. From (1.44), we can have the quasiparticle and electron correlators:

$$
\langle e^{in\phi(x,\tau)}e^{-in\phi(0,0)}\rangle = e^{n^2(\langle\phi(x,\tau)\phi(0,0)\rangle-\langle\phi(0,0)\phi(0,0)\rangle)} \propto \frac{1}{(v\tau+ix)^{\frac{n^2}{2k+1}}} \qquad (1.45)
$$

Thus, the scaling dimension of the single quasiparticle operator is $\frac{1}{2(2k+1)}$, while the electron operator has scaling dimension $\frac{2k+1}{2}$. The unusual scaling dimension (compared to the Fermi-liquid scaling dimension of $\frac{1}{2}$) is due to the highly-correlated nature of the state and tells us that we are dealing with a (chiral) Luttinger liquid. The scaling dimension can also be used as an experimental signature of a particular Hall state through tunneling experiments, as described in Sec 1.6.1.

To connect with the discussion of edge excitations in Sec 1.4.4, we derive the Hamiltonian corresponding to Eq (1.39) (now dropping $A$),

$$
\mathcal{H}_{\mathrm{dual}} = \frac{m}{4\pi}\int dx v\partial_x\varphi\partial_x\varphi = \frac{m}{4\pi}vL\sum_k k^2\varphi_k\varphi_{-k} \qquad (1.46)
$$

where we have now defined $m = 2k + 1$ to prevent confusion with the momentum and defined the Fourier transformed fields, $\varphi_k = \frac{1}{L}\int dx e^{ikx}\phi(x)$, for $k = 2\pi n/L, n \in \mathbb{Z}$. To determine the spectrum of this Hamiltonian, define the creation/annihilation operators $a_k^\dagger \equiv \sqrt{\frac{kmL}{2\pi}}\varphi_k, a_k \equiv \sqrt{\frac{kmL}{2\pi}}\varphi_{-k}$, for $k > 0$, which satisfy, using (1.40), $[a_k, a_{k'}^\dagger] = \delta(k-k')$. Then

$$\mathcal{H}_{\text{dual}} = v\sum_{k>0} k a_k^\dagger a_k \tag{1.47}$$

The edge behaves like a harmonic oscillator, consistent with the energy spectrum in Eq (1.19). When $L$ is finite, the edge excitations cost finite energy $vk$; as $L \to \infty$, they become gapless.

### 1.5.7 $K$-matrices

The edge theory derived in Sec 1.5.5 can be generalized to the case where there are multiple gauge fields, which can occur in a layered system or in the hierarchy states described in Sec 1.4.5. Starting from Eq (1.25) with multiple gauge fields, the derivation of the past few sections yields a generalization of Eq (1.39),

$$S = \int dxdt \frac{1}{4\pi}\left(K_{IJ}\partial_t - V_{IJ}\partial_x\right)\varphi_I\partial_x\varphi_I - \frac{1}{2\pi}\epsilon^{\mu\nu}A_\mu\partial_\nu\varphi_I t_I, \tag{1.48}$$

where $K_{IJ}$ is a symmetric, integer matrix, $V$ is a symmetric positive-definite matrix, and $t$ is an integer vector. The signs of the eigenvalues of $K$ dictate the direction of propagation of each edge mode; we say that $K$ is chiral if all eigenvalues share the same

sign. The commutation relation that generalizes Eq (1.40) is

$$[\varphi_I, \partial_y \varphi_J(y)] = 2\pi i K^{-1}_{IJ} \delta(x-y) \tag{1.49}$$

The charge density is generalized from Eq (1.41) by $\rho = \sum_J \frac{t_I \partial_x \phi_I}{2\pi}$, and similarly for the current operator. The quasiparticle whose creation operator is $e^{in_J\phi_J}$ is labelled by the integer vector $n_J$. It carries charge $n_I K^{-1}_{IJ} t_J$ and its mutual statistics with the particle $n'_J$ is $2\pi n_I K^{-1}_{IJ} n'_J$. Trivial quasiparticles are labelled by $n_J = l_I K_{IJ}$, where $l_I$ is an integer vector; evidently they have trivial statistics with all other quasiparticles in the theory. If the edge theory is chiral, then the generalization of Eq (1.45) is that the operator $e^{in_I\phi_I}$ has scaling dimension $2\Delta_n = n_I K^{-1}_{IJ} n_J$. If $K$ is not chiral, which can happen, for example, if holes condense out of a filled Landau level, then the scaling dimensions depend on the $V$ matrix.[7] Furthermore, the structure of the edge can be significantly more complicated: backscattering between different edge modes could drive the edge into a new phase, potentially even a phase where the edge is gapped. We explore this situation further in Sec 1.7.1.

The classification of edge states by their $K$-matrices and $t$-vectors was pioneered by Wen[27] and represents a complete classification of Abelian quantum Hall states, unifying the microscopic theories for fractional states discussed in Sec 1.4.5.

[7] Following Ref 28, it is straight-forward to compute $\Delta_m = \frac{1}{2} m_I \Lambda_{IJ} \Lambda^T_{JK} m_K$, where $\Lambda \equiv \Lambda_1 \Lambda_2 \Lambda_3$. $\Lambda_1$ is an orthogonal matrix that diagonalizes $K$: $\left(\Lambda_1^T K \Lambda_1\right)_{IJ} = \delta_{IJ}\lambda_I$; $\Lambda_2$ rescales $K$: $(\Lambda_2)_{IJ} = \delta_{IJ}/\sqrt{|\lambda_I|}$; and $\Lambda_3$ (combined with $\Lambda_{1,2}$) diagonalizes $V$, while preserving the signature of $K$: $\left(\Lambda^T V \Lambda\right)_{IJ} = \delta_{IJ} v_I$, $\Lambda_3^T \eta \Lambda_3 = \eta$, where $\eta_{IJ} = \delta_{IJ}\mathrm{sgn}(\lambda_I)$. For the chiral edge, $\eta = \mathbb{I}$, from which it follows $\Lambda\Lambda^T = K^{-1}$; hence, $\Delta_m$ is independent of $V$ in this case.

Eq (1.48) will be the starting point for Chapters 2, 3, 4.

## 1.6 Experimental probes of the edge

In the earliest theoretical papers describing the fractional quantum Hall effect, Laughlin proposed the existence of quasiparticles with fractional charge and statistics.[11] In this section, we describe two experiments that can probe these attributes – shot noise measurements and interferometry – which will be central to later chapters. The theoretical predictions rely on the field theory developed in Sec 1.5.

### 1.6.1 Theory of the quantum point contact

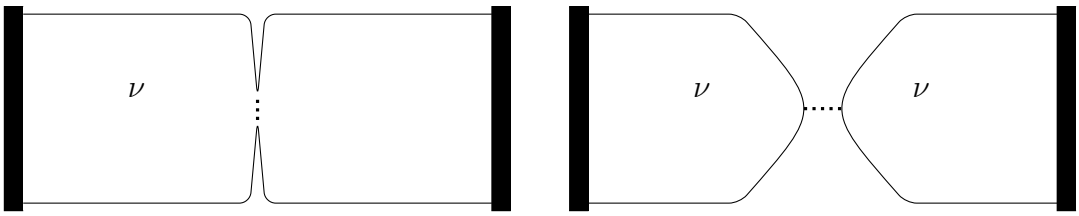


(a) QPC across Hall bar (b) QPC between two Hall bars

Figure 1.6: **Quantum point contact.** Dotted lines indicate where backscattering can occur between oppositely-propagating edges. The dark rectangles are Ohmic contacts. In (a), all quasiparticles can tunneling across the quantum point contact, while in (b), only electrons can tunnel.

The quantum point contact (QPC) is arguably the most fundamental tool in fractional quantum Hall experiments. In the ideal case, it consists of a single point where tunneling can occur between two oppositely propagating quantum Hall edges, as depicted in Fig 1.6, or between a Hall bar and a normal lead. When the tunneling occurs within a quantum Hall fluid, as shown in Fig 1.6a, all quasiparticles in the fluid will have an amplitude for tunneling across the QPC. On the other hand, if tunneling requires traversing the vacuum, as shown in Fig 1.6b, the only quasiparticles that can tunnel are those which can exist in the vacuum, i.e., electrons and multiples of the electron.

Using the edge theory developed in Secs 1.5.5 – 1.5.7, tunneling within the Hall fluid can be incorporated into the Lagrangian by adding a term,[8]

$$\mathcal{L}_{\text{tun}} = \sum_{n\in\mathbb{Z}^N}{}' \left(\lambda_n e^{-iq_n Vt} e^{in_I\varphi_I^R} e^{-in_J\varphi_J^L} + h.c.\right)\delta(x) \tag{1.50}$$

where $\varphi^{R/L}$ denote the right- and left- moving fields on opposite edges of the Hall bar, $q_n = n_I K_{IJ}^{-1} t_J$ is the charge of the quasiparticle labelled by $n$, $V$ is the voltage difference across the QPC, and the QPC is at $x = 0$. The first term creates a quasiparticle on the right-moving edge, while the second term annihilates the same species on the left-moving edge. The prime on the sum indicates that first non-zero entry of $n$ should be positive; this is to prevent double counting $n$ and $-n$. If the tunneling is in the vacuum, only trivial quasiparticles can tunnel and the sum is restricted to $n_I = K_{IJ} l_J, l_J \in \mathbb{Z}$. Usually, we will only be concerned with the most relevant such operator. In the case

[8]For a detailed description of tunneling, see Ref 29.

where tunneling is weak ($\lambda_n \ll 1$), we compute the tunneling current across the QPC perturbatively.

The operator that measures current across the QPC is given by

$$I_{\text{tun}} = \sum_{n\in\mathbb{Z}^N}{}' \left( iq_n\lambda_n e^{-iq_nVt} e^{in_I\varphi_I^R} e^{-in_J\varphi_J^L} + h.c \right) \delta(x) \tag{1.51}$$

For a theory with a single edge mode, we can compute the contribution to the tunneling current from a quasiparticle $\chi = e^{in\phi}$ that has charge $e^*$ and scaling dimension is $\delta$ to lowest order in perturbation theory, when $\lambda \ll 1$:

$$\begin{aligned}
\langle I_{\text{tun}}\rangle &= \langle I_{\text{tun}} i\int dt\mathcal{L}_{\text{tun}}\rangle \\
&= -\frac{|\lambda|^2}{m}\int dt e^{ie^*Vt}\langle \left(\chi^L\right)^\dagger(0,0)\chi^R(0,0)\chi^L(0,t)\left(\chi^R\right)^\dagger(0,t)\rangle + h.c \\
&= -e^*|\lambda|^2\int dt\frac{2i\sin(Vte^*)}{(ivt)^{4\delta}} \\
&= -|V|^{4\delta-1}\left(\frac{e^*}{v}\right)^{4\delta}\text{sgn}(V)\int dy\frac{2i\sin(y)}{(iy)^{4\delta}} \\
&= -|V|^{4\delta-1}\left(\frac{e^*}{v}\right)^{4\delta}\text{sgn}(V)\frac{2\pi}{\Gamma(4\delta)}
\end{aligned} \tag{1.52}$$

We have used the correlator (1.45). The important point is the scaling of the tunneling current, $I_{\text{tun}} \propto V^{4\delta-1}$, a significant departure from Ohmic scaling. This is a universal prediction of the field theory that could, in principle, be verified in experiment.

In a similar vein, we can compute the contribution to the shot noise from $\chi$,

$$S(\omega) \equiv \int dt e^{i\omega t}\langle I_{\text{tun}}(0)I_{\text{tun}}(t) + I_{\text{tun}}(t)I_{\text{tun}}(0)\rangle$$

$$= (e^*)^2|\lambda|^2 \int dt e^{i\omega t} \Big( e^{ie^*Vt} \langle \left(\chi^L\right)^\dagger (0,0) \chi^R(0,0) \chi^L(0,t) \left(\chi^R\right)^\dagger (0,t) \rangle +$$

$$+ e^{-ie^*Vt} \langle \left(\chi^L\right)^\dagger (0,t) \chi^R(0,t) \chi^L(0,0) \left(\chi^R\right)^\dagger (0,0) \rangle \Big)$$

$$= (e^*)^2|\lambda|^2 \int dt e^{i\omega t} \frac{2\cos(Vte^*)}{(ivt)^{4\delta}} \tag{1.53}$$

In the zero-frequency limit,

$$S(\omega = 0) = e^*|\lambda|^2|V|^{4\delta-1} \left(\frac{e^*}{v}\right)^{4\delta} \frac{2\pi}{\Gamma(4\delta)} = e^*|I_{\text{tun}}| \tag{1.54}$$

Thus, the ratio of zero-frequency shot noise to tunneling current gives a measurement of the charge of the quasiparticle whose tunneling across the QPC is most relevant. This was originally proposed in Ref 30 and was experimentally verified in the $\nu = 1/3$ state in Refs 31 and 32.

### 1.6.2 Interferometry

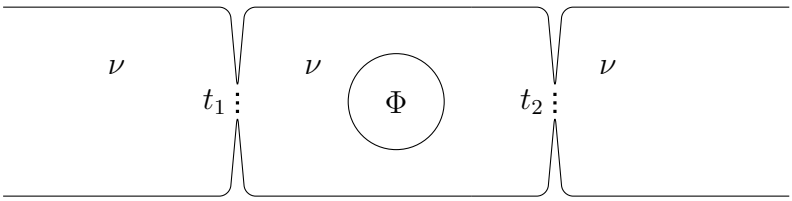


Figure 1.7: **Two point contact interferometer.** The two QPCs have tunneling amplitudes $t_1$ and $t_2$. A hole in the center can have a variable amount of flux, $\Phi$.

A key attribute of quantum Hall quasiparticles is their mutual statistics. To measure statistics, the interferometer was proposed in Ref 33, which we follow here. Depicted in

Fig 1.7, the interferometer consists of a Hall bar with two QPCs, creating two paths for quasiparticles to traverse the edge. Thus, tunneling conductance displays an interference pattern, which varies periodically as magnetic flux is inserted through the center region. The period reveals the charge of the quasiparticle. In particular, at fixed filling fraction, the phase a quasiparticle acquires from circling the central flux is $e^*\Phi/\hbar$, thus the period is $\Delta B = h/(Ae^*)$.[9]

To measure the mutual statistics between quasiparticles, the number of quasiparticles in the central region must be varied. If two quasiparticles have mutual statistics $2\pi\theta$, introducing a quasiparticle increases the interference phase by exactly this amount, creating a phase shift in the interference pattern. Currently, there is no experimental procedure for directly manipulating the positions of quasiparticles in a quantum Hall sample. However, as the area of the device is varied, quasiparticles can indirectly be introduced.

Interferometry experiments are difficult to interpret because many variables are changing at once. The earliest experiments on the $\nu = 1/3$ state,[34,35] performed a decade ago, are still open to interpretation. More recent work has focused on disentan-

[9]There is a subtle complication: if instead of the filling fraction being fixed, the particle number is fixed, then as the magnetic field is increased by one flux quantum, a quasihole will be created to exactly compensate for the additional flux, and the period will be $\Phi_0/A$. Thus, the system must have a backgate to vary the chemical potential and reservoir of electrons that can flow in, so that filling fraction, and not particle number, is kept constant. This situation is discussed in more detail in Ref 33.

gling the effects of changing area, flux and particle density, as well as of interactions, in the central region.[36–38]

## 1.7 Particular quantum Hall states of interest

Here we discuss the edge structure of two quantum Hall states that will be relevant to later chapters.

### 1.7.1 $\nu = 2/3$: a non-chiral edge

Quantum Hall theories with edge modes propagating in both directions have an additional complication: interactions between oppositely-propagating modes can cause the Hall conductance to deviate from its quantized valued, contradictory to experimental observation. This problem was first investigated in the context of the $\nu = 2/3$ state, which was originally predicted to have a forwards-propagating $\nu = 1$ edge mode and a backwards propagating $\nu = 1/3$ edge.[39–41] However, the backwards propagating mode was never detected in experiment and the conductance plateau was consistently observed to be quantized.[42]

Kane, Fisher and Polchinski (KFP)[43] resolved this contradiction by showing that random backscattering between the modes would drive the edge to a new fixed point with quantized conductance. The eigenmodes of the edge would then be a single foward-

propagating charged mode and a backwards propagating neutral mode. This theory generalizes to the filling fractions $\nu = n/(2np+1)$, which have backwards-moving modes when $p < 0$.[28]

Experiments that probe the edge can distinguish the equilibrated and non-equilibrated edge phases. In Ref 44, shot noise experiments, like those described in Sec 1.6.1, show evidence consistent with the equilibrated edge. Refs 45 and 46 present strong evidence for the existence of an upstream neutral mode; we consider Ref 46 in detail in Chapter 3. In Chapter 2, we consider probing the $\nu = 2/3$ edge with microwaves as a novel way to distinguish the two edge phases.

However, the story is not so simple: more recently, upstream modes have been observed at filling fractions predicted to be fully chiral.[47] Edge reconstruction is more ubiquitous than fits into the simplest theoretical models. This fact must be kept in mind when designing experiments and interpreting results.

### 1.7.2 $\nu = 5/2$: a candidate for non-Abelian statistics

The possibility that non-Abelian statistics could be realized in a fractional quantum Hall system spurred an intense research effort to understand the $\nu = 5/2$ state, which is the most experimentally accessible candidate state. Before discussing the edge structure of this state, we take a brief detour to explain non-Abelian statistics.

**Statistics in 2D**

In dimensions greater than two, there is not a well-defined notion of one particle making a loop around another particle because any loop can be continuously deformed to a point. Since exchange of two identical particles is equivalent to half a loop, the wavefunction can acquire a phase of 0 or $\pi$ under exchange ($2\pi$ upon completing the loop); these phases correspond to bosons and fermions, respectively, and these are the only point-like particles that can exist in dimensions greater than two. In two dimensions, there is a well-defined notion of one particle circling another. If one particle adiabatically circles another, the wavefunction can acquire a nontrivial phase.[48] If the phase is not a multiple of $2\pi$, the quasiparticles are called anyons.[49]

This is not the full story: consider a system of $N$ identical particles at spatial positions $R_i, i = 1, ..., N$. Now consider all paths in space-time that return these particles to the positions $R_i$ after time $T$, where particles are allowed to swap positions. The equivalence classes of paths that are adiabatically connected, while keeping the endpoints fixed, are exactly the elements of the braid group, $B_N$. The one-dimensional representations of the braid group are the phases acquired by a wavefunction after two particles are exchanged. (This can be extended to include distinguishable particles if each particle is restricted to return to its endpoint after time $T$.) Higher dimensional representations are unitary matrices: if there is a degenerate set of ground states, adiabatic winding of one particle

around another can transform one ground state into a linear combination of the other ground states according to such a matrix. If the matrices do not commute, the particles are said to display non-Abelian statistics. For more details on non-Abelian statistics – and especially their application to quantum computing – we refer the reader to Ref 50 and references therein.

**Non-Abelian statistics at $\nu = 5/2$**

Eq (1.23) gives the Pfaffian wavefunction, a candidate wavefunction to describe the bulk state at $\nu = 5/2$. The paired nature of the wavefunction requires that quasiholes also come in pairs.[24] As the positions of two quasiholes approach each other, they are equivalent to a single Laughlin-type quasihole – that is, they correspond to insertion of a single flux quantum. Hence, a single quasihole is equivalent to half a flux quantum; this gives a hint that something more exotic than an Aharonov-Bohm phase could occur. Mapping the problem to a known one in conformal field theory reveals that the state with four quasiholes is two-fold degenerate and the two ground states transform into each other when one quasiparticle circles another.[24,51] Heuristically, the two-fold degeneracy results from the two ways the four quasiparticles can be grouped into pairs.

**Edge structure**

The edge excitations can be counted in a manner similar to that described in Sec 1.4.4 for the Laughlin states; the counting shows that the edge is described by a gapless chiral fermion, in addition to the gapless boson common to all Abelian states.[16,52]

The half-filled state has particle-hole symmetry. Thus, the anti-Pfaffian state, which is the particle-hole conjugate to the Pfaffian, is an equally viable candidate to describe the phase at $\nu = 5/2$.[53,54] The edge structure of the anti-Pfaffian state is found by reversing the boundary between the Pfaffian and the $\nu = 1$ state. This interface is non-chiral; analogous to the $\nu = 2/3$ edge described in Sec 1.7.1, random backscattering between oppositely-propagating modes drives the edge to an equilibrated phase which has one chiral boson propagating parallel to the edge modes of the two filled Landau levels and three counter-propagating chiral fermions.

There are also other candidate states that we will not discuss here.

Many experiments probing the edge physics have attempted to determine the phase of the $\nu = 5/2$ state. Both the Pfaffian and the anti-Pfaffian have charge-$e/4$ quasiparticles (corresponding to a half flux quantum), but differ in the minimum scaling dimension of a tunneling operator and in their chirality. The $e/4$ quasiparticle charge was measured in Ref 55 and 56 by measuring the shot noise across a QPC, as described in Sec 1.6.1, and in Ref 57 using local thermometry in the bulk. The minimum scaling

dimension was also measured in Ref 55 and was shown to be more consistent with the anti-Pfaffian state than the Pfaffian. An experiment with two quantum point contacts[46] revealed a non-chiral edge, also consistent with the anti-Pfaffian state; this experiment is the focus of Chapter 3. There is also experimental evidence of non-Abelian statistics (present in both the Pfaffian and anti-Pfaffian), using a more elaborate version[58,59] of the interferometry described in Sec 1.6.2.[60] We propose an interferometry experiment using microwave absorption that would provide complementary evidence of non-Abelian statistics in Chapter 2.

Numerical investigations have examined the effect of Landau level mixing, which breaks particle-hole symmetry; we refer the reader to Ref 50 for these references. Ref 61 includes Landau level mixing perturbatively and shows that the Pfaffian phase is favored when Landau level mixing is below a critical value that is a function of the well-width; above this threshold the perturbation theory is less reliable and the results inconclusive. It is not clear which regime describes the experimental results.

In summary, determining the universality class of the $\nu = 5/2$ plateaus achieved in experiments remains an active area of research.

## 1.8 Surprises at the edge

We now motivate the three papers that comprise this thesis.

### 1.8.1 Microwave absorption of quantum Hall edges

The experiments that we have discussed to probe quantum Hall edges are all transport measurements. However, transport measurements rely on Ohmic contacts, which introduce a host of non-universal physics. Furthermore, they average over the edge modes, so cannot directly distinguish equilibrated from non-equilibrated edges. In Chapter 2, we consider probing quantum Hall devices with microwaves. The device we are imagining is contact-free and the absorption spectrum has a peak corresponding to each charged edge mode. In addition, if a quantum point contact is introduced, the device becomes an interferometer, where the period of oscillations in the absorption spectrum corresponds to the statistics of quasiparticles in the bulk. The amplitude of oscillations is first-order in the tunneling amplitude – this is in contrast to the interferometer discussed in Sec 1.6.2, where the correction is second-order.

In Sec 1.7.1, we explained that the $\nu = 2/3$ edge can either be in the non-equilibrated or equilibrated edge phase. One might expect a phase transition between these two regions: in small systems, where the edge does not have a chance to equilibrate, two counter-propagating charged modes should be present, while in larger systems, the system has a chance to reach an equilibrated edge with one charged mode and a counter-propagating neutral mode. The microwave experiment could distinguish between these phases by counting the number of charged edge modes.

### 1.8.2 Upstream neutral modes

In Sec 1.7.1, we explained why a counter-propagating neutral mode must be present to explain the quantized conductance at $\nu = 2/3$. Since that prediction, it has been an experimental challenge to observe the neutral mode. This challenge was finally overcome by observing that neutral modes can influence the shot noise across a QPC, as demonstrated in Ref 46. This experiment can also distinguish between the Pfaffian and anti-Pfaffian states described in Sec 1.7.2. In Chapter 3, using the field theory developed in Sec 1.5.5, we analyze this experiment. From our analysis, we make the unexpected prediction that neutral modes can also affect charged tunneling current.

### 1.8.3 Bulk-edge correspondence

In systems with a shallow edge confining potential, the electron density might not drop off sharply from filling fraction $\nu$ to filling fraction 0. Instead, it might be energetically favorable for the electrons to form one or more incompressible strips at the edge.[62–65] This effect is known as edge reconstruction. Since the incompressible strips also have edge modes, the result is an extra set of counter-propagating modes at the edge.

In Chapter 4, we show that interactions between these modes and the original edge modes can change the phase of the edge, implying that the edge-bulk correspondence

is many-to-one. If the original edge was non-chiral, it is not a surprise that multiple edge phases can exist; for example, the $\nu = 2/3$ state has two possible edge phases. However, for chiral edges, where backscattering cannot occur, it was assumed that the bulk-edge correspondence was unique. Thus, our result is unexpected. We classify the chiral Abelian phases where this can occur and provide experimental signatures of the two distinct edge phases. We find that edge phases correspond to lattices, while bulk phases correspond to genera of lattices.

# Chapter 2

# Microwave absorption of quantum Hall droplets

In this chapter, we consider the absorption of microwaves by a quantum Hall droplet. We show that the number and velocities of charged edge modes can be directly measured from a droplet of known shape. In contrast to standard transport measurements, different edge equilibration regimes can be accessed in the same device. If there is a quantum point contact in the droplet, then quasiparticle properties, including braiding statistics, can be observed. Their effects are manifested as modulations of the microwave absorption spectrum that are, notably, first-order in the tunneling amplitude at the point contact.

## 2.1 Introduction

A classic problem in mathematical physics asks "can you hear the shape of a drum?" [66,67] In this chapter, we address the natural generalization: "can you hear an anyon in a drum?" For the sake of concreteness, we consider a 'drum' that is a mesoscopic quantum Hall device of circumference $L \approx 10 - 100\mu$m. The excitations of the edge of a quantum Hall droplet, which are gapless in the limit of a large droplet, have a minimum energy $2\pi\hbar v/L$, where $v$ is the velocity of edge modes and $L$ is the circumference of the droplet. Therefore, for $v = 10^4 - 10^5$ m/s, the edge modes of such a drum can be 'heard' in the frequency range $\approx 1 - 100$ GHz or, in other words, with microwaves. Such modes have already been observed using spectroscopy [68–76] in samples on the millimeter scale and analyzed using semiclassical models, [77,78] and have also been observed through time resolved measurements. [42,79–82] Here, we focus exclusively on the absorption spectrum of micron-scale samples tuned to quantum Hall plateaus.

As we show in this chapter, microwave absorption gives a window into edge excitations that is different from and complementary to transport.[39,82] Moreover, it provides a probe that can enable one to observe a key feature of the theory of fractional quantum Hall states – the exotic braiding statistics of its excitations – that has, thus far, remained somewhat elusive experimentally. The fractional charge and statistics of quasiparticles are the lynchpins of the theory of the fractional quantum Hall effect. According to Laughlin's gauge argument, fractional quantized Hall conductance can only occur if there are quasiparticles with fractional charge.[10] There is strong experimental support for fractional charge $e^* = e/3$[31,32,83–86] at $\nu = 1/3, 7/3$ and for $e^* = e/4$[56,57,87] at $\nu = 5/2$. But fractionally-charged quasiparticles must have fractional braiding statistics,[88] and both microscopic wavefunctions[14,17] and long-wavelength effective field theories[26,89] predict that quasiparticles in the fractional quantum Hall effect are anyons. However, the braiding properties of quasiparticles are not directly manifested in bulk transport experiments or even in transport through a quantum point contact. A two point contact interferometer device is, until now, the only proposed way to directly observe them. Although there is a measurement[87] that is consistent with non-Abelian anyon quasiparticles at $\nu = 5/2$, it is not definitive since it has not been reproduced and other interpretations are conceivable. The setup described in this chapter would enable a truly distinct and independent measurement of quasiparticle braiding properties. Moreover, it can enable the measurement of some aspects of the physics of quantum Hall edge excitations, such

as the number of edge modes and their velocities, that are difficult to directly observe in transport experiments.

Our proposed setup consists of a quantum Hall droplet or circular disk coupled to a broadband microwave co-planar waveguide and used as a microwave spectrometer, as shown in Fig. 2.1. The electric field between the central track and ground of the waveguide couples to the charged edge modes of the droplet and allows a non-invasive means of probing the system, without contacting the electron gas. The absorption spectrum, determined by measuring the amount of transmitted microwave power through the waveguide, will be one or more series of peaks corresponding to the allowed edge modes of the droplet.

For a circular droplet, there will be one peak for each charged edge mode and the positions of the peaks in frequency provide a direct measurement of the velocity of the mode. This is particularly interesting for certain fractions that are predicted to have counter propagating edge modes on a completely clean edge but one charged and one oppositely propagating neutral mode on a disordered edge large enough for modes to equilibrate.[28,43] The most notable example is at $\nu = 2/3$, where such neutral modes were recently observed.[45,46] In our setup, we would expect to see one charged mode in a device that is larger than the equilibration length, and multiple modes in smaller devices. The latter possibility has not yet been observed. Furthermore, a surprising result in Ref. 45 is the observation of an upstream mode at $\nu = 1$ and, simultaneously, a local Hall

resistivity of $\frac{3}{2}\frac{h}{e^2}$. This observation indicates that a local measurement between points 20 $\mu$m apart is at a distance less than the equilibration length and in this region, the edge supports both $\nu = 1$ and $\nu = 2/3$ edges. Hence, in a droplet smaller than this length, one would detect multiple charged modes. At $\nu = 5/2$, one of the candidate states, the anti-Pfaffian state[53,54] similarly has two phases of edge excitations, one with a single charged mode and one with two, one upstream and one downstream.

A quantum point contact (QPC) can be produced by fabricating standard surface gates that overlap the droplet to create an interferometer: the heights of the peaks oscillate as a function of magnetic field and the oscillations experience a phase slip when the number of quasiparticles changes. However, unlike in a two-point contact interferometer, the oscillations are *first-order in the tunneling amplitude*.

In what follows, we first compute the absorption spectrum of a quantum Hall droplet in an integer or Laughlin state with no QPC. Next, we consider filling fractions with more complicated edges and show how the absorption spectrum reveals the number of current carrying modes. Then, we add the QPC and show how the spectrum acts as an interferometry measurement. We then repeat the calculation for filling fraction $\nu = 5/2$ and predict the non-Abelian interference pattern.

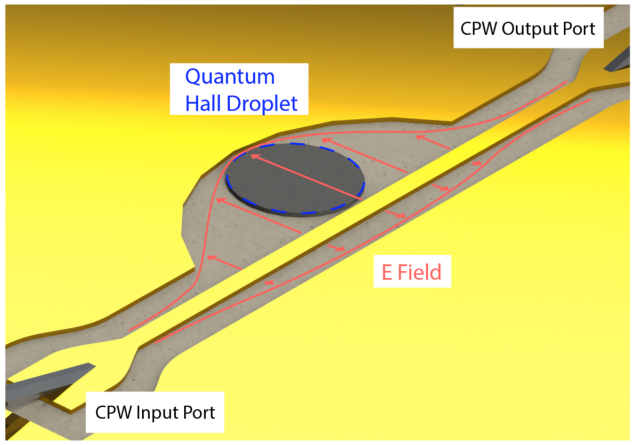


Figure 2.1: **Quantum Hall droplet in a microwave waveguide.** Note that the droplet and microwave wavelength are not drawn to scale. The latter is much larger, and the electric field is approximately constant on the scale of the droplet.

## 2.2 General Considerations

### 2.2.1 Experimental Setup

We consider a single mesoscopic disk or droplet of electron gas in the quantum Hall regime and capacitively coupled to a broadband, coplanar waveguide or narrow band resonator (see Fig. 2.1). The droplet is not in ohmic contact with any leads, allowing continuous edge states around its circumference, and is probed purely through its microwave absorption spectrum. When the frequency of incident microwaves is tuned so that they are resonant with one of the excited states of the quantum Hall device, there will be absorption and a corresponding change in the amplitude and phase of the mi-

crowave power transmitted through the coplanar waveguide. Small changes in microwave power and phase are readily measured with cryogenic amplification and standard homodyne detection techniques. We envision devices that also include an adjacent Hall bar, fabricated on-chip but sufficiently far away to be decoupled from the droplet. This Hall bar enables simultaneous transport measurement for comparison with microwave data.

In addition to the microwave response from the edge magnetoplasmons, there will be a background signal from the bulk. We estimate the dipole matrix element of a localized bulk excitation to be $\sim e\ell_0$, where $l_0$ is the magnetic length. Between Landau levels (where the transverse Hall conductance shows plateaus in transport), such an excitation will give a weak background contribution $\sim \omega^2(e\ell_0)^2$ to the absorption spectrum $R(\omega)$ of the edge magnetoplasmons. When the number of occupied Landau levels is changing, however, the bulk excitations can lead to significant absorption $R(\omega) \sim \Gamma/(\omega^2 + \Gamma^2)$ characteristic of a metallic state (where the DC conductivity is $\sim 1/\Gamma$). In this regime the contribution from edge magnetoplasmons will merge with the spectrum of bulk excitations. However, it can be easily separated by measuring the microwave response as a function of frequency and magnetic field.

There will also be non-local bulk excitations, which are the edge channels that circumnavigate domains of a different filling fractions. For example, when the droplet is at filling $\nu = 1$, there are puddles of $\nu = 0$ and $\nu = 2$ in the bulk. Surrounding these puddles are bulk magnetoplasmons that are identical to the edge magnetoplasmons (but do not

traverse the entire sample) and couple to the electric field in the same way. Depending on their size and the local steepness of the confining potential, some bulk modes might be in the same frequency range as the edge modes, but if this is so, the signal of bulk modes should be weaker than that of the edge because of their small dipole moment. In addition, scanning the magnetic field should distinguish a bulk magnetoplasmon because it will exist across several filling fractions until it either disappears or merges with the edge spectrum as a bulk state percolates across the system to drive a transition between plateaus.

Another consideration is that, even on a plateau, if the microwave frequency is higher than the mobility gap, then there will be absorption characteristic of a metal in the bulk. Therefore, in order to be resonant with an edge excitation of energy $\omega = 2\pi v/L$ (where $L$ is the circumference of the droplet) but still below the bulk mobility gap (or, operationally, the gap deduced from transport, $\Delta_{\mathrm{tr}}$), we need $2\pi v/L < \Delta_{\mathrm{tr}}$. Thus, relatively large devices and smaller velocities are advantageous. Large devices are also expected to couple more strongly to the electric field from the waveguide and hence show a larger response. On the other hand, in order to probe different equilibration regimes and to observe quantum interference effects, it is advantageous to have smaller devices. Thus, there is an intermediate regime $L \approx 10\mu$m and velocity $v \approx 10^4\,$m/s in which we expect to be able to isolate the physics of edge excitations if the system lies on a quantum Hall plateau. Note that some experimental observations[42,79,90] are

consistent with a larger velocity $\sim 10^5\,\mathrm{m/s}$; it may be necessary to tune gate potentials and the magnetic field in order to have a smaller velocity in which the aforementioned intermediate regime of frequencies exists.[76,80]

### 2.2.2 Kohn's Theorem

As mentioned in the introduction, for a very clean quantum Hall device at a filling fraction with multiple edge modes, we expect to see one peak in the absorption spectrum for every charged edge mode with a distinct velocity. This is of particular interest for fractions predicted to have a disorder driven (equilibrated) fixed point, because the clean and disordered systems would have different numbers of charged modes, and hence different signatures in the absorption spectrum.

On the other hand, since the electric field is nearly constant on the scale of the the quantum Hall device, it couples to the dipole moment of the system as follows:

$$\begin{aligned} H &= \sum_i \frac{\mathbf{p}_i^2}{2m} + \sum_{i>j} V(\mathbf{r}_i - \mathbf{r}_j) + \sum_i U(\mathbf{r}_i) + e\sum_i \mathbf{r}_i \cdot \mathbf{E} \\ &= \frac{\mathbf{P}_{\text{c.m.}}^2}{2Nm} + Ne\mathbf{R}_{\text{c.m.}} \cdot \mathbf{E} \\ &\quad + \tilde{U}(\mathbf{R}_{\text{c.m.}}, \mathbf{r}_{\text{rel},1}, \ldots, \mathbf{r}_{\text{rel},N-1}) + H_{\text{rel}} \end{aligned} \tag{2.1}$$

where $\mathbf{R}_{\text{c.m.}}$ and $\mathbf{P}_{\text{c.m.}}$ are the center-of-mass coordinate and momentum; $\mathbf{r}_{\text{rel},1}, \ldots, \mathbf{r}_{\text{rel},N-1}$ are the relative coordinates; $\tilde{U}(\mathbf{R}_{\text{c.m.}}, \mathbf{r}_{\text{rel},1}, \ldots, \mathbf{r}_{\text{rel},N-1}) \equiv \sum_i U(\mathbf{r}_i)$; and $H_{\text{rel}}$ is the Hamiltonian for the relative motion of the electrons. Kohn's theorem stems from the

observation that the electric field is only coupled directly to the center-of-mass motion and the center-of-mass motion is only coupled to the relative motion through $\tilde{U}$. If $\tilde{U}(\mathbf{R}_{\text{c.m.}}, \mathbf{r}_{\text{rel},1}, \ldots, \mathbf{r}_{\text{rel},N-1}) = \tilde{U}_{\text{c.m.}}(\mathbf{R}_{\text{c.m.}}) + \tilde{U}_{\text{rel}}(\mathbf{r}_{\text{rel},1}, \ldots, \mathbf{r}_{\text{rel},N-1})$, as is the case for a quadratic confining potential (and for a translationally-invariant system), the center-of-mass motion decouples from the relative motion. In such a case, the response to an electric field is determined entirely by the center-of-mass motion.

In a system in its ground state in a quadratic potential, the electric field can only cause a transition to the first excited state, so there will be only a single peak in the absorption spectrum. Hence, we must conclude that in our effective theory of the edge, the edge mode velocities and inter-mode interactions are such that the there is only a single charged mode (of a type that we discuss in the next section). But, if $U$ is not quadratic, the center-of-mass coordinate is coupled to the relative coordinates, and there will be peaks corresponding to excitations of the relative motion of the electrons. Thus, we will be able to learn more about the details of the edge structure electromagnetically.

Generically, we do not know the coupling strength between the center-of-mass coordinate and the relative coordinates and the confining potential might have to be tuned in order to see multiple peaks. We expect this coupling to be tunable by changing the shape of the droplet or the steepness of the edge.

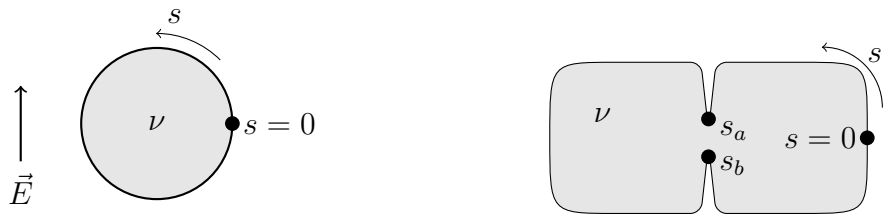


(a) Circular droplet, no QPC (b) Generic droplet with QPC

Figure 2.2: **Quantum Hall droplets.**

## 2.3 Circular droplet

### 2.3.1 Laughlin states and $\nu = 1$

We first consider the simple set-up depicted in Fig 2.2a, a circular quantum Hall droplet in a uniform electric field at filling fraction $\nu = 1/m$, for $m \geq 1$ an odd integer. For these fractions, there is a single edge mode that will couple to the electric field when the frequency of the field matches that of an excitation at the edge. We compute the absorption spectrum using a framework that is generalized in subsequent sections.

The edge modes are described by the chiral Luttinger liquid action[29,91,92]

$$\mathcal{S}_0 = \frac{m}{4\pi} \int dt\, ds\, (\partial_t - v\partial_s)\phi(s,t)\partial_s\phi(s,t) \tag{2.2}$$

where $s$ parametrizes the distance along the edge of the droplet, and $v$ is the velocity of the edge mode. The field $\phi$ satisfies the equal-time commutation relation $[\phi(x,t), \partial_s\phi(y,t)] = \frac{2\pi}{m} i\delta(x-y)$. The charge density at a point $s$ along the edge is given by $\rho = \partial_s\phi/(2\pi)$. The electric field of the microwaves $\vec{E} = E\cos(\omega t)\hat{y}$ couples to the

charge density of the droplet according to

$$\mathcal{L}_E = E\cos(\omega t)y(s)\rho(s,t) \tag{2.3}$$

where $y(s)$ gives the $y$-component of the edge of a droplet; $\rho$ is the charge density at the edge, given by $\rho = \partial_s\phi/(2\pi)$, where $\phi$ is governed by the action (2.2). For a circular droplet of circumference $L$, $y(s) = \frac{L}{2\pi}\sin(2\pi s/L)$.

This is the minimal edge theory dictated by the bulk qantum Hall state. There can be additional non-chiral pairs of edge modes, depending on how soft the edge potential is. We will focus here on the case in which there are only the minimal edge modes dictated by the bulk. The more general case can be analyzed by a straightforward extension of the present discussion.

The spectrum $R(\omega)$ including both absorption and emission components is found by Fermi's Golden Rule:

$$R(\omega) = \frac{E^2}{2}\int ds_1 ds_2 y(s_1)y(s_2)S^{\rho\rho}(s_1,s_2,\omega) \tag{2.4}$$

where,

$$S^{\rho\rho}(s_1,s_2,\omega) = \int dt\cos(\omega t)\langle\rho(s_1,t)\rho(s_2,0)\rangle \tag{2.5}$$

There is a subtlety in computing the $\langle\rho\rho\rangle$ correlation function: because electrons acquire a phase upon circling the droplet, the field $\phi$ is not periodic. However, this phase drops out of all calculations until we include a QPC, so we defer discussion of this phase to

Appendix B.1 and here compute the density-density function using the form of $y(s)$ given above and the action (2.2). The result is a spectrum with a single pair of peaks at $\omega = \pm 2\pi v/L$:

$$R(\omega) = \nu \frac{E^2 L^2}{32\pi} \delta(\omega \pm 2\pi v/L) \tag{2.6}$$

Fortunately, these peaks are expected to be in an experimentally accessible regime: using the value $v = 10^4$ m/s extrapolated from measurements in Ref 90, for a large Hall droplet with $L = 50$ $\mu$m the peaks are at frequency $\omega/2\pi = 200$ MHz. The frequency increases inversely with $L$ as the droplet gets smaller in size; for $L = 10$ $\mu$m, $\omega/2\pi \approx 1$ GHz.

The delta-function shape of the peaks in the absorption spectrum comes from the isolated poles of the density-density propagator, which correspond to an infinite lifetime for edge excitations. Realistically, the edge excitations will have a finite lifetime due to physics that is neglected in the action of Eq 2.2, such as losses in the waveguide, finite longitudinal resistance, and phonon coupling. In a lossless waveguide, phonon coupling will be the dominant contribution to the width and we consider it in detail in Appendix A. The result is that the spectrum of Eq 2.6 is modified to

$$R(\omega) = \nu \frac{E^2 L^2}{32\pi^2} \frac{\eta(\omega)}{(\omega - 2\pi v/L)^2 + \eta(\omega)^2} \tag{2.7}$$

where $\eta(\omega) = \mathrm{Im}\left[\Sigma(k, \omega)\right]$ in Appendix A. When the piezoelectric contribution dominates that of the deformation potential, as for GaAs, $\eta \propto 1/L$ and the Q-factor of the device is independent of its circumference. For a GaAs device with $v = 10^5$m/s, we find

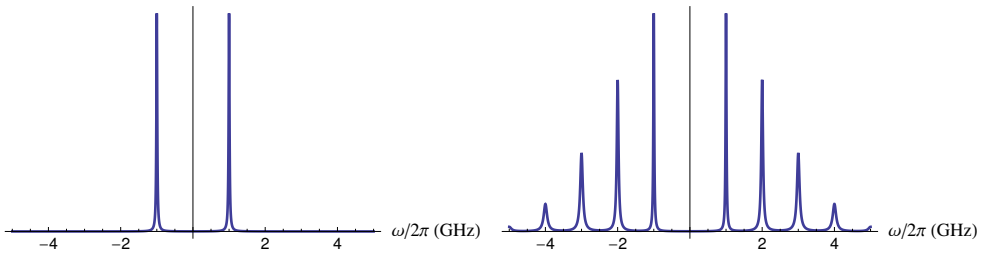


(a) Circular droplet (b) Droplet with QPC

Figure 2.3: **Absorption spectra for a $10\mu$m droplet with $v = 10^4$m/s and peak width determined by phonon coupling.** The circular droplet (a) permits only one set of peaks, while the non-circular droplet (b) allows a series of peaks.

$Q \approx 350$. For droplets with circumference $10 - 50$ $\mu$m, $\eta(\omega) \approx \frac{n}{m} \times 10$MHz for the $n$th peak at filling fraction $\nu = 1/m$. The absorption spectrum for the circular droplet is shown in Fig 2.3a.

Having only a single peak is specific to the circular droplet. Generically, there are peaks at $\omega = 2\pi nv/L$ for all integers $n$ with width given by $\eta(\omega)$, and the spectrum is generalized for a droplet of arbitrary shape to

$$R(\omega) = \frac{\nu E^2}{4\pi L} \sum_k \frac{k\eta(\omega)}{(\omega - kv)^2 + \eta(\omega)^2} y(k)y(-k) \tag{2.8}$$

This is consistent with the discussion of Kohn's theorem in Sec 2.2.2. Because a quadratic confining potential can only result in a circular (or elliptical) droplet, these shapes must only have one peak in the absorption spectrum. Other shapes result from non-quadratic terms in the confining potential and are not violating Kohn's theorem by having multiple

peaks. For most circle-like shapes, the additional peaks are very small, but for the double-lobed droplet depicted schematically in Fig 2.2b, several peaks should be visible, as shown in Fig 2.3b.

At finite temperature there is a prefactor $\coth(\beta\omega/2)$ to Eqs 2.7 and 2.8. We do not consider the temperature dependence of $\eta(\omega)$.

For a droplet of any shape, the absorption spectrum provides a direct measurement of the edge mode velocity. The edge excitation velocity has been deduced in several experiments at specific filling fractions[42,79,93] but there is only one reported measurement that studies its evolution with magnetic field.[90] Measuring the edge velocity from the absorption spectrum would provide a more direct measurement than Ref 90 and confirm their estimate of when the velocity switches from a 'skipping orbit model' to the $\vec{E} \times \vec{B}$ drift velocity.

### 2.3.2 Probing the structure of the edge

When $\nu \neq 1/m$, the edge structure is more complicated. There are expected to be multiple edge modes, which have distinct velocities and mix via density-density interactions and impurity scattering. Here we consider the absorption spectrum of a droplet at a filling fraction with multiple edge modes, first in the clean limit, and then with disorder.

A perfectly clean edge with $n$ edge modes may be described by the Lagrangian

$$\mathcal{L}_K = \frac{1}{4\pi} \sum_{ij} \partial_s \tilde{\phi}_i \left( K_{ij} \partial_t + \tilde{v}_{ij} \partial_s \right) \tilde{\phi}_j \tag{2.9}$$

where the $n$-by-$n$ matrix $K$ determines the filling fraction by $\nu = \sum_{ij} K^{-1}_{ij}$ and $v$ is a matrix of non-universal velocities and density-density interactions. The charge density is given by

$$\rho = \sum_i \tilde{\rho}_i \equiv \frac{1}{2\pi} \sum_i \partial_s \tilde{\phi}_i \tag{2.10}$$

Following Ref 28, we simultaneously diagonalize $K$ and $v$ by conjugation with a matrix $M$: $\left(M^T \tilde{v} M\right)_{ij} = v_i \delta_{ij}$ and $\left(M^T K M\right)_{ij} = \eta_i \delta_{ij}$ with $\eta_i \in \{\pm 1\}$. Then Eq 2.9 can be rewritten as a sum of non-interacting chiral edge modes $\phi_i = M^{-1}_{ij} \tilde{\phi}_j$ with respective velocities $v_i \eta_i$, which might be positive or negative:

$$\mathcal{L}_{many} = \frac{1}{4\pi} \sum_i \partial_s \phi_i \left( \eta_i \partial_t + v_i \partial_s \right) \phi_i \tag{2.11}$$

Then Eqs (2.3)-(2.5) can be used, and the absorption spectrum is given by Eq 2.4 with

$$S^{\rho\rho}_K(s_1, s_2, \omega) = \int dt \cos(\omega t) \sum_{ijk} M_{ij} M^T_{jk} \langle \rho_j(s_1, t) \rho_j(s_2, 0) \rangle \tag{2.12}$$

where $\rho_j = \partial_s \phi_j / (2\pi)$. For a circular droplet, we find:

$$R_K(\omega) = \frac{E^2 L^2}{32\pi} \sum_{ijm} M_{ij} M^T_{jm} \delta(\omega \pm 2\pi v_j / L) \tag{2.13}$$

We check this result in two simplifying cases:

1. When there is only one edge mode, $K = 1/\nu$, $M = \sqrt{\nu}$ and Eq 2.13 is exactly Eq 2.6.

2. For integer quantum Hall states $\nu = n$ without any inter-mode density-density interactions, $K = M = \mathbf{I}_n$ and $\tilde{v}$ is diagonal, but generically not proportional to $\mathbf{I}_n$. Then Eq 2.13 simplifies to

$$R_{\nu=n}(\omega) = \frac{E^2 L^2}{32\pi} \sum_{j=1}^{n} \delta(\omega \pm 2\pi v_j / L) \tag{2.14}$$

   The spectrum consists of $n$ peaks corresponding to the $n$ different velocities of the edge modes. However, as discussed in Section 2.2.2, if the confining potential is quadratic, then there will be a single peak, corresponding to the center-of-mass motion of the entire electron system and all of the edge mode velocities must be the same.

For generic filling fractions with $n$ edge modes and inter-mode interactions, we expect to see $n$ peaks with a non-universal pre-factor $\sum_{im} M_{ij} M_{mj}$ in front of the $j^{\text{th}}$ peak. Hence, in the clean limit, the absorption spectrum counts the number of distinct edge modes. If this limit could be observed, it would be direct evidence of the physical reality of the edge mode theory.

For a droplet of arbitrary shape, Eq 2.13 generalizes to

$$R_{many}(\omega) = \frac{E^2}{4L} \sum_{ijm} M_{ij} M^T_{jm} \sum_k k\, y(k) y(-k) \delta(\omega - k v_j) \tag{2.15}$$

which is the many-mode equivalent of Eq 2.8. In this case, we see $n$ series of peaks for which the spacing between peaks in each series is proportional to the velocity of the corresponding edge mode.

The presence of disorder allows equilibration between edge modes, which can dramatically change the edge structure. In Ref 28, it is shown that tunneling between edge modes due to scattering off random impurities can drive the system to a random fixed point. For a certain hierarchy of states with $n$ edge modes, the fixed point is stable and has one charged mode and $n-1$ neutral modes. Since the neutral modes do not couple to the electric field, the absorption spectrum in this limit will be exactly that of Sec 2.3.1: a single peak for a circular droplet or a single series of peaks for a droplet of arbitrary shape. Specifically, at integer fillings $\nu = n$, arbitrarily weak disorder is a relevant term that will drive the edge modes to equilibrate and the absorption spectrum will consist of only one peak corresponding to the equilibrated charged mode. For filling fractions with counter propagating edge modes, such as $\nu = 2/3$, it takes a critical amount of disorder to drive the system into the equilibrated state with only one charged mode. Hence, for weak disorder or for a droplet smaller than the equilibration length, we would expect to see $n$ peaks in the absorption spectrum, as in the clean limit, but when the size of the droplet exceeds the equilibration length, we expect to see only one peak. Recent experiments detecting neutral upstream modes at expected fractions[45,46] are presumably in the equilibrated regime. By considering droplets of multiple sizes (perhaps tuned by

gating) in our setup, both regimes could be observed. Note that, unlike in transport experiments, we would not have to change the locations of contacts in order to access different regimes – there are no contacts in our device.

## 2.4 Interferometry

When probed through microwave absorption, a quantum Hall droplet with a *single* QPC acts an interferometer whose interference pattern appears as a correction to the height of the absorption peaks that oscillates with magnetic field. We will calculate this correction to first-order in the tunneling amplitude and find its dependence on the magnetic field and the number of quasiparticles in the droplet. It is notable that the result is non-zero already at first-order in the tunneling amplitude, since transport through a Fabry-Perot interferometer would only see oscillations at second-order in the tunneling amplitude.[33,36,58,85,90,94–98]

In this section, we consider the cases $\nu = n$ and $\nu = n + 1/m$. We model the QPC by adding a tunneling term to the Lagrangian,

$$\mathcal{L}_{tun} = \lambda e^{i\phi(s_a,t)} e^{-i\phi(s_b,t)} + h.c. \tag{2.16}$$

where in the integer case Eq 2.16 represents the tunneling of electrons across the QPC while, in the Laughlin case, the term represents the tunneling of charge $e/m$ quasiparticles across the QPC. In the latter case, we could also add a term to represent the

tunneling of electrons across the QPC, but such a term is less relevant. The position of the QPC is given by $s_a$ and $s_b$, as shown schematically in Fig 2.2b.

We want to find $\delta R(\omega)$, the leading order correction to the absorption spectrum in the presence of tunneling. We calculate $\delta R(\omega)$ in Appendix B.1 for a droplet of arbitrary shape. Here we consider a simplified, but realistic, case in which the droplet is symmetrical over the x-axis, so that $y(s) = -y(L-s)$ and $s_b = L - s_a$, yielding

$$\delta R(\omega) = 4|\lambda|\left[\frac{E^2}{m^2}\coth\frac{\beta\omega}{2}H(\omega)G(\beta)\right]\cos(\varphi) \tag{2.17}$$

where $H$ and $G$ are given by,

$$H(\omega) = \frac{1}{L^2}\sum_{\substack{k_{1,2}=2\pi n/L \\ k_1\neq -k_2}} y(k_1)y(k_2)\frac{\sin(k_1 s_a)\sin(k_2 s_a)}{v(k_1+k_2)} \times\left(\frac{\eta(\omega)}{\eta(\omega)^2+(\omega+k_1 v)^2}-\frac{\eta(\omega)}{\eta(\omega)^2+(\omega-k_2 v)^2}\right) \tag{2.18}$$

$$G(\beta) = \exp\left[\frac{\pi}{mL}\sum_{k>0}\frac{2}{k}(\cos(2ks_a)-1)\coth\frac{\beta v k}{2}\right] \tag{2.19}$$

$H$ determines the size of the corrections as a function of frequency and $G(\beta)\coth(\beta\omega/2)$ contains all the temperature dependence of the corrections. Both $H$ and $G$ depend on the placement of the QPC. The phase $\varphi$ is given by

$$\varphi = \frac{2\pi}{m}\left(\frac{\Phi_R}{\Phi_0}+n_R-\frac{2s_a}{L}\left(\frac{\Phi}{\Phi_0}+n_{tot}\right)\right)+\alpha \tag{2.20}$$

where $m = 1$ for integer states and $m = 1/(\nu - \lfloor\nu\rfloor)$ for Laughlin states, $\Phi$ is the flux penetrating the bulk, $\Phi_R$ is the flux penetrating the right lobe, $n_{tot}$ is the number of

quasiparticles in the bulk, $n_R$ is the number of quasiparticles in the right lobe, and $\alpha$ is a phase that is independent of magnetic field. Eq 2.20 shows that for a droplet of fixed shape, the correction $\delta R(\omega)$ varies sinusoidally with magnetic field and its phase is determined by the number of quasiparticles in each lobe. The basic physical picture is the following. The density-density correlation function involves the creation and annihilation of a quasiparticle-quasihole pair. Since the density is integrated over the edge of the droplet, this pair can be created anywhere. At first-order in the tunneling, the pair can encircle either lobe (which involves a single tunneling event at the point contact). These different processes will interfere with each other, and the interference will essentially be controlled by the *difference* between the phases associated with encircling either droplet. However, the sizes of the lobes matter: it is easier for the pair to encircle a smaller lobe, so a quasiparticle in a smaller lobe gives a larger contribution to the interference phase than a quasiparticle in a larger lobe. In the next subsections, we will analyze the oscillations and phase shifts; determine the optimal placement of the QPC to see maximum oscillations; and calculate the decay of oscillations at finite temperature.

### 2.4.1 Oscillations and phase shifts

We now consider the oscillations coming from the phase $\varphi$ in Eq 2.20. There are two predictions: first, if we fix the number of quasiparticles and vary the magnetic field, we

expect oscillations with period proportional to the charge of the quasiparticles:

$$\Delta B = m\Phi_0 \left( A_R - \frac{2s_a}{L} A \right)^{-1} \tag{2.21}$$

where $A$ and $A_R$ denote the areas of the total droplet and the right lobe, respectively. The factor of two comes directly from Eq 2.20. We consider this expression in a few limiting cases: first when $s_a \to 0$, the right side of the droplet disappears so that $A_R \to 0$. Hence, $\Delta B \to \infty$ and there are no oscillations; this is what we would expect because the QPC effectively disappears into the right side. Similarly, when $s_a = L/2$, the left side disappears and $A = A_R$; again there are no oscillations and $\Delta B \to \infty$. The third case is when $s_a = L/4$ and the right and left lobes have equal area $A_R = A_L = A/2$. Then, the left and right lobes enter symmetrically into Eq 2.20, except for a negative sign. The sign results from the fact that when a particle tunnels, it skips the right lobe but traverses the left lobe one extra time (or vice versa), causing the phases of each lobe enter oppositely. In this case, Eq 2.21 shows that again, oscillations disappear.

The second prediction is that phase shifts occur for the Laughlin states when the quasiparticle number in either lobe changes, and the phase shift might differ for each lobe. When a quasiparticle is added to the left lobe, the phase shift is $\Delta\varphi = \frac{4\pi}{m}\frac{s_a}{L}$, but when a quasiparticle is added to the right lobe, the phase shift is $\Delta\varphi = \frac{2\pi}{m}\left(1 - \frac{2s_a}{L}\right)$. There will also be a phase shift $\Delta\varphi = \frac{2\pi}{m}$ if a quasiparticle moves from the left to the right lobe. One simplifying case is when the droplet has symmetry about the $y$-axis

and $s_a = L/4$: in this case both phase shifts are $\pi/m$ and the oscillations in magnetic field disappear. Without oscillations in magnetic field, it might be easier to observe the statistical phase shift.

This interferometer has the same basic features as the scheme proposed in Ref 33 and executed in Refs 36,85,90,97,98, where $\Delta B = mA/\Phi_0$ and $\Delta\varphi = 2\pi/m$ always. However, our scheme has the additional feature that there is a different phase shift when a quasiparticle is added to the right lobe compared to when one is added to the left lobe, which makes it possible to see where quasiparticles are added when magnetic flux is varied. Moreover, it is possible to disentangle the electromagnetic Aharonov-Bohm effect due to the magnetic flux from the effect of quasiparticle braiding statistics. For instance, when $A_R = A_L$ (which also means that $s_a = L/4$), changing the magnetic field has no effect whatsoever on the electromagnetic Aharonov-Bohm phase difference between trajectories encircling the left and right lobes. However, a change in the magnetic field may result in the creation of a quasiparticle which will be in either the right lobe or the left lobe (unless the electrostatics of the device causes us to be in the unlucky situation in which the quasiparticle sites right at the point contact), which will lead to a change in the interference phase $\varphi$ of, respectively $\pi/m$ or $-\pi/m$. The complication is that the phase shifts are non-universal and depend on the ratio $s_a/L$.

### 2.4.2 Amplitude of oscillations at low temperature

Next we want to determine where to place the QPC to maximize the amplitude of oscillations. Both $H$ and $G$ depend on $s_a$; we first consider $H$. If we assume $\eta \ll 2\pi v/L$, then $H$ takes the simplified form when evaluated at the center of a peak,

$$H(\omega = 2\pi n v/L) = \frac{2y(k)\sin(ks_a)}{L^2\eta(\omega)v} \sum_{k' \neq k} \frac{y(k')\sin(k's_a)}{k' - k} \tag{2.22}$$

where $k = \omega/v$. For simplicity, we consider a droplet whose lobes are perfect circles of radius $R_1$ and $R_2$, and assume that the qualitative features of any droplet with two rounded lobes are captured by this double-circle shape. We then define the ratio $f = s_a/L = R_1/(R_1 + R_2)$, which specifies the position of the QPC. To find the optimal position of $s_a$, we evaluate numerically the dimensionless function $H_n(f) \equiv (\eta(\omega)v(2\pi)^5/L^3)\, H(2\pi n v/L)$, shown in Fig 2.4a for the first few peaks. For the $n = 1$ peak, the oscillations are largest for circles of differing radii, but remain sizable throughout the region $.1 < f < .4$.

We now consider $G$ in the low temperature limit:

$$G(\beta \gg L/v\pi) = \frac{e^{-\gamma/m}}{\left(\frac{2L}{a}\sin(2\pi f)\right)^{1/m}} \tag{2.23}$$

where we have introduced a short-distance cutoff $a$, and $\gamma$ is the Euler-Mascheroni constant. In Fig 2.4b, we plot the ratio $G(f)/G(f = .25)$ for $\nu = 1, 1/3, 1/5, 1/7$. $G$ is at minimum for the symmetrical droplet and diverges as the droplet reaches maximum

asymmetry. Hence, barring the ability to know precisely the shape of the droplet and evaluate Eq 2.17 explicitly, an experiment would have to test a variety of asymmetric droplets to find the optimal shape that maximizes the product of $H$ and $G$.

### 2.4.3 Decay of oscillations with temperature

In the previous section, we estimated the magnitude of oscillations in the limit $\pi\beta v/L \gg 1$, when the temperature dependence dropped out. This is the correct limit for a very small droplet with $L = 2\mu$m, for which the inequality is satisfied for $T \ll 120$mK, but for intermediate droplets $L = 10 - 50\mu$m, we are not likely to be in this regime. Here we consider the opposite limit when $\beta v\pi/L \ll 1$. In this case, the temperature will define a length scale $L_T$ above which the magnitude of oscillations decays exponentially through the function $G \propto e^{-L/L_T}$. We can roughly estimate the scale of decay by taking only the first term in the sum over $k$ in Eq 2.19, yielding

$$L_T = \frac{\beta\pi vm}{1-\cos(4\pi f)} \geq \beta\pi vm/2 \equiv L_T^{min} \tag{2.24}$$

The symmetric droplet ($f = \frac{1}{4}$) achieves the minimum limit $L_T = L_T^{min}$. The length scale diverges for the maximally asymmetric droplets with $f = 0$ or $f = .5$. Taking $v = 10^4$m/s and $\nu = 1/3$, $L_T^{min} = 7\mu$m at 50mK and $L_T^{min} = 18\mu$m at 20mK. This temperature dependence is shown in Fig 2.4c at $\nu = 1/3$ for the symmetric droplet with $f = .25$. For asymmetric shapes, the droplet could be larger.

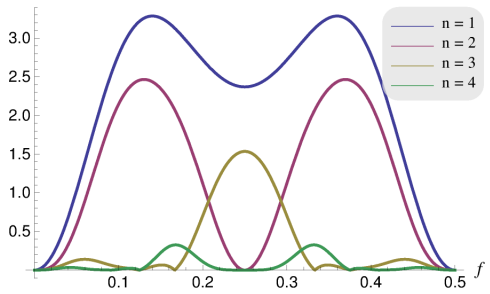


(a) $H_n(f)$ for various peaks

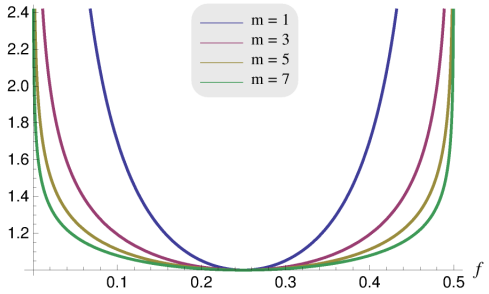


(b) $\frac{G(f)}{G(f=.25)}$ in the low temperature limit

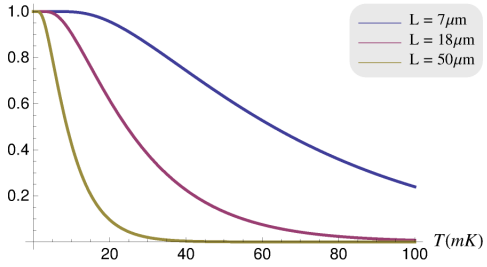


(c) Ratio $\frac{G(\beta)}{G(\beta\to\infty)}$ for $f = .25$ at $\nu = 1/3$

Figure 2.4: **Dependence of $H$ and $G$ on $f$ and $T$.**

## 2.5 Non-Abelian interferometry at $\nu = 5/2$

Recent experiments[46,55,60,87,99] suggest that the wavefunction of a quantum Hall state at filling fraction $\nu = 5/2$ is in the same universality class as the Moore-Read Pfaffian state[22,24,51] or the anti-Pfaffian state.[53,54] Both states have non-Abelian quasiparticles of Ising type.[100] Here we will determine the absorption spectrum for the Pfaffian and anti-Pfaffian states, first without and then with a QPC. We show that the latter system acts as a non-Abelian interferometer.

### 2.5.1 Droplet with no QPC

The edge theories of the Pfaffian and anti-Pfaffian states consist of a charged sector and a neutral sector. The charged sector consists of a free chiral boson $\phi$. The neutral sector consists of a chiral Majorana fermion, $\psi$ and its accompanying twist field $\sigma$. The neutral sector is related to the critical point of the 1+1-D transverse Ising model: at its critical point, the Ising model in the continuum limit is described by a massless Majorana fermion. Because the mapping from the original spin field of the model to the fermion field is non-local, the spin field introduces a branch cut to the fermion. In the same way, the twist field $\sigma$ introduces a branch cut for the fermion $\psi$ in the Pfaffian and anti-Pfaffian edge theories.

In the Pfaffian state, the charged and neutral modes have the same chirality, while in the anti-Pfaffian state, the charged and neutral modes have opposite chirality, which can be seen from deriving the anti-Pfaffian as the particle-hole conjugate to the Pfaffian.[53,54] However, this difference will not affect the absorption spectrum. The same derivation shows that the anti-Pfaffian state actually has three chiral Majorana modes, but since they are uncoupled in our model, we need only consider one of them.

In both theories, the bosonic edge modes are described by the Lagrangian of Eq 2.2 with $m = 2$, which couple to the electric field through Eq 2.3. The neutral fermions do not couple to the electric field and, consequently, do not affect the spectrum of a droplet

without a QPC. Hence, the analysis of a droplet without a QPC is identical to that of the integer and Laughlin states. The absorption spectrum for an arbitrary shape is the same as in Sec 2.3.1, where it is given in Eq. 2.8. There will be peaks at all frequencies that are multiples of $2\pi v/L$ and the peak placement is a direct measurement of the bosonic edge velocity. At non-zero temperature, there is a pre-factor $\coth(\beta\omega/2)$.

Another leading candidate to describe filling fraction $\nu = 5/2$ is the Abelian (3,3,1) state.[20] In the limit of a clean edge, this state has a different interferometric signature: following Sec 2.3.2, we would expect to see two series of peaks in the absorption spectrum corresponding to the two edge modes, in contrast to the single series for the Pfaffian and anti-Pfaffian. However, the states will be indistinguishable if there is disorder on the edge that drives the edge modes to equilibrate. Henceforth, we will focus on the Pfaffian and anti-Pfaffian states.

### 2.5.2 Non-Abelian interferometry with a QPC

We see new effects when a QPC is introduced. There are several types of quasiparticles, all of which could tunnel across the QPC, but the most relevant tunneling term is that for charge $e/4$ quasiparticles, given by

$$\mathcal{L}_{tun}^{5/2} = \lambda \Phi_{1/4}(s_a, t)\Phi_{1/4}^{\dagger}(s_b, t) + h.c. \tag{2.25}$$

where $\Phi_{1/4} = \sigma e^{i\phi/2}$ is the annihilation operator for a charge $e/4$ quasiparticle. In Appendix B.2, we detail the method to compute the correction to the absorption spectrum to order $\lambda$. The result for a droplet symmetrical over the x-axis is

$$\delta R(\omega) = 4|\lambda| \left[ \frac{E^2}{16} \coth \frac{\beta\omega}{2} H(\omega) G(\beta) \right] |\mathcal{G}(s_a)| \cos(\varphi_{5/2}) \tag{2.26}$$

where $H$ and $G$ are the same as for the integer and Laughlin fractions and are given by Eq 2.18-2.19 with $m = 2$. The phase $\varphi_{5/2}$ is given by

$$\varphi_{5/2} = \frac{\pi}{2} \left( \frac{\Phi_R}{\Phi_0} + \frac{n_R}{2} - \frac{2s_a}{L} \left( \frac{\Phi}{\Phi_0} + \frac{n_{tot}}{2} \right) \right) + \frac{\pi}{16} + \alpha \tag{2.27}$$

As in the Abelian case, the interference phase is essentially controlled by the difference in the phase associated with encircling the right droplet and the left droplet. The glaring difference between the Abelian and non-Abelian case is the presence of the function

$$\mathcal{G}(s_a) \equiv \langle \sigma(s_a) \sigma(L - s_a) \rangle \tag{2.28}$$

in Eq 2.26, which is the topological contribution to the phase and will be the focus of the rest of the discussion in this section. $\mathcal{G}$ depends on the total topological charges in the right and left lobes, which we denote by $F_{R/L} \in \{I, \psi, \sigma\}$. When there are no quasiparticles in the bulk,

$$\mathcal{G}(s_a)_{\text{no qp}} = \mathcal{G}_0(s_a) \equiv e^{i\pi/16} \left( \frac{L}{\pi} \sin(2\pi s_a / L) \right)^{-1/8} \tag{2.29}$$

For other topological charges, the result is proportional to $\mathcal{G}_0(s_a)$, as shown in Table 2.5.

| $F_L$ | $F_R$ | $\mathcal{G}(s_a)/\mathcal{G}_0(s_a)$ |
|---|---|---|
| $I$ | $\psi$ | $-\cos(2\pi s_a/L)$ |
| $I$ | $\sigma$ | $(\sin(\pi s_a/L))^{1/2}$ |
| $\psi$ | $\psi$ | 1 |
| $\psi$ | $\sigma$ | $(\sin(\pi s_a/L))^{1/2}$ |
| $\sigma$ | $\sigma$ | 0 |

Figure 2.5: **Ratio of topological pre-factor to peak height.**

Table 2.5 shows that having quasiparticles in the bulk can reduce the amplitude of oscillations. In particular, when there is an odd number of $\sigma$ quasiparticles in each lobe, oscillations disappear completely. The disappearance is a direct consequence of non-Abelian statistics: if the two bulk quasiparticles are fused to $I$ (or $\psi$), the tunneling quasiparticles will flip their fused state from $I$ to $\psi$ (or vice versa), causing the first order term to disappear. This term will re-appear to second-order from virtual tunneling processes (and might be visible as smaller oscillations). Hence, if the number of quasiparticles is varied, either explicitly or by changing the area of the droplet or the magnetic flux penetrating it, we would expect to see oscillations that disappear when there are an odd number of quasiparticles in each lobe. This effect was predicted for an interferometer with two QPCs in Ref 58,96, has been analyzed in great detail in Ref 96,101–104 and has been seen experimentally in Ref 60,87,99. The experiment we propose would be complementary to existing experiments and has the advantage that oscillations are first-order in the tunneling amplitude.

Finally, we note that there is a simple statistical mechanical interpretation of this table. The correlation function $\mathcal{G}(s_a)$ is the expectation value of the spin $\langle\sigma\rangle$ in the critical Ising model (either the critical classical $2D$ Ising model or the critical transverse field quantum Ising model) on a strip of length $L/2$ with specified boundary conditions. If there are no quasiparticles in the bulk, the Ising model has fixed + boundary conditions at both ends, and $\langle\sigma\rangle$ is given by the power-law decay from the ends characteristic of the critical point. If the total charge (of both lobes combined) is $\psi$, then the two ends have opposite fixed boundary conditions, + at one end and − at the other. Then $\langle\sigma\rangle$ vanishes at the midpoint of the strip and is either positive or negative to the left or right of the midpoint (i.e. if the left or right lobe is larger, $s_a < L/4$ or $s_a > L/4$). If the total topological charge is $\sigma$, then one end of the Ising model has fixed boundary conditions and the other free boundary conditions, and $\langle\sigma\rangle$ is given by the power-law decay from one end characteristic of the critical point. Finally, if there is topological charge $\sigma$ in each lobe, then the Ising model has free boundary conditions at both ends and $\langle\sigma\rangle$ is simply zero.

## 2.6 Discussion

In this chapter we propose a new method to probe the edge of a quantum Hall droplet by measuring its microwave absorption spectrum. For a simple, circular droplet, this

measurement would reveal the number of charged modes and their velocities. For edges with counter propagating edge modes, this information would resolve open questions about how current is carried at the edge. When a QPC is introduced, the droplet can serve as an interferometer. Its capabilities are similar to existing proposals and experiments, but has the advantage that the amplitude of oscillations is first-order in the tunneling amplitude. There are also subtle differences from transport through a two point contact interferometer, such as a dependence on the side of the QPC to which a quasiparticle has been added, which leads to a non-universal phase shift.

At $\nu = 5/2$, such a measurement could determine if the state of the system is non-Abelian: if it is, then oscillations in the absorption spectrum appear when there are an even number of $\sigma$ quasiparticles in each lobe but not when there is an odd number. This experiment would be complementary to existing interferometry experiments[87] at $\nu = 5/2$ and, as in the Abelian case, has the advantage of having oscillations at first-order in the tunneling amplitude.

Thus far, quasiparticle properties of fractional quantum Hall states have been deduced from resistance oscillations in mesoscopic devices. Here, we propose a new approach in which this information is gathered from the absorption spectrum. It could confirm existing experimental results and, in doing so, resolve questions on the fundamental tenets of the theory of the fractional quantum Hall effect.

Moreover, by coupling a quantum Hall device to microwaves, we open the possibility of using photons as a quantum bus to transfer information from a $\nu = 5/2$ qubit[50,95] to superconducting or even semiconductor quantum dot qubits.

# Chapter 3

# Unexpected tunneling current from downstream neutral modes

In this chapter, we analyze transport through a quantum point contact in fractional quantum Hall states with counter-propagating neutral edge modes. We show that both the noise (as expected and previously calculated by other authors) and (perhaps surprisingly) the average transmitted current are affected by downstream perturbations within the standard edge state model. We consider two different scenarios for downstream perturbations. We argue that the change in transmitted current should be observable in experiments that have observed increased noise.

## 3.1 Introduction

The current traversing the edge of a quantum Hall device is elegantly described by chiral Luttinger liquid (CLL) theory.[27] For Laughlin states, the theory has only one edge mode, while for more complicated states, there might be multiple edge modes. Particle-hole conjugate states were originally predicted to have charged edge modes propagating in both directions,[39–41] but such counter-propagating charged modes were never detected.[42] This mystery was resolved when it was shown that in the presence of disorder and interactions, certain edges with counter-propagating charged modes could reconstruct into an edge with a single charged mode and counter-propagating neutral modes.[28,43] The question then remained, how can one detect the elusive neutral mode(s)? The question was answered by Bid, *et al.*,[46] who observed an increase in the noise across a quantum point contact (QPC) caused by a downstream perturbation, which they interpreted as evidence for the existence of neutral excitations.

Measuring the shot noise across a QPC to confirm the $e/3$ charge of Laughlin's predicted quasiparticles was a breakthrough development in quantum Hall physics.[30–32,105]

Since then, significant effort has been devoted to using shot noise measurements to gain insight into more complicated edges.[44,47,56,106–116] The experiment of Ref. 46 consists of a Hall bar with a QPC across which noise and current are measured, as shown in Fig 3.1. Current is then injected into one edge, downstream of the QPC (here downstream always refers to the net direction of charged current), and the change in current and shot noise are measured. Intuitively, if the edge is chiral, then the current injection should not change the shot noise or current across the QPC; if the edge has a non-chiral charged mode, then the shot noise and current across the QPC should both change; if the edge has a non-chiral neutral mode, then shot noise across the QPC should increase but current should remain unchanged. Using this intuition, Ref 46 confirmed the existence of the counter-propagating neutral modes for $\nu = 2/3, 3/5$ and $5/2$, as well as confirmed the pure chirality of the edge at $\nu = 1/3, 2/5$ and 1. This was a breakthrough experiment in understanding quantum Hall edge physics at particle-hole conjugate states.

At that time, a rigorous theoretical model of the experiment using CLL theory was absent. In trying to fill that void, we have found a surprising result that defies the intuitive prediction: a non-chiral neutral mode can change both the current and shot noise across the QPC.

Our model assumes weak coupling between the quantum Hall edge and the external lead that injects current downstream of the QPC, which allows us to treat the effect of the current injection perturbatively. In Sec 3.2.1, we consider a toy model with

fermionic edge modes, which illustrates our unexpected result without the (technical) complication of fractionalization. In Sec 3.2.2, we consider a general model with multiple Luttinger liquid edge modes that allows fractionalization and is expected to describe several Abelian particle-hole conjugate states. In both cases, we observe that injecting current downstream of the QPC changes the charged current across the QPC through the upstream propagation of neutral modes. The sign of the change depends on the scaling dimension of the tunneling quasiparticles.

In Sec 3.3, we consider the model proposed in Refs 117 and 118, which assumes that the effect of injecting current into an edge is to increase the temperature of that edge. We show that the increased temperature also changes the tunneling current across the QPC.

Finally, in Sec 3.4, we compare the theoretical models to experimental results at $\nu = 2/3$. Both models predict a decrease in the magnitude of the tunneling current, which could reach tenths of nanoamps over the parameter regime of the experiment. Given the precision of the experiment, we believe this to be an observable effect. We then discuss directions for future work.

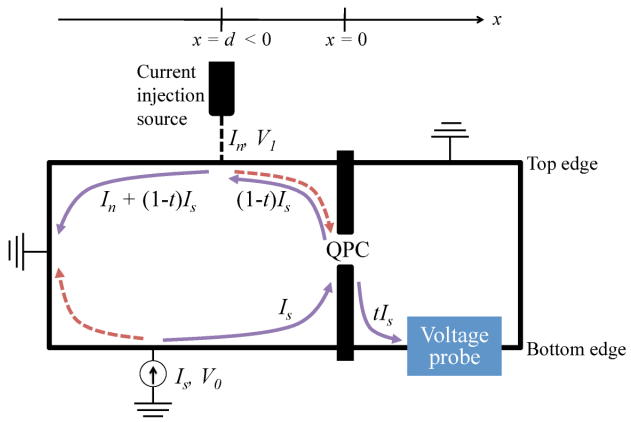


Figure 3.1: **Experimental set-up.** Current $I_n$ is injected into the top edge while current $I_s$ is sourced to the bottom edge. Solid purple lines show the direction of charged current, with magnitude indicated, while dotted red lines show the propagation of counterclockwise neutral modes.

## 3.2 Weak Downstream Perturbations

The experiment has two main features that need to be included in our model: a QPC at $x = 0$, across which current and voltage are measured, and a current source at $x = d$ that injects current into the quantum Hall edge, downstream of the QPC; a schematic of the experimental set-up is shown in Fig 3.1. The QPC is modeled in the usual way, by including terms which tunnel quasiparticles between the edges of the Hall bar.[119,120] We model the downstream current source similarly: we assume the current

source is a metallic lead which is weakly coupled to the quantum Hall edge and tunnels electrons between the two. We first compute the tunneling current and shot noise across the QPC in the absence of the injected current. We then turn on the current injection and compute the change in current and shot noise. If the edge is completely chiral, then the injected current, which enters downstream of the QPC, has no effect on the shot noise and current across the QPC. Here, we are interested in the more interesting case in which the edge consists of a chiral charged mode and an anti-chiral neutral mode; this can result from the equilibration of two counter-propagating charged modes, as in the particle-hole conjugates of the Laughlin states. We warm up by considering a toy model of free fermion edge modes and then generalize to an arbitrary edge, which permits fractionally charged excitations.

### 3.2.1 Free fermion edge

The purpose of this section is to show in a simple free fermion model that the change in noise, as well as the perhaps unexpected change in current, is a general result. This should give the reader confidence that the technical calculations in the next section are correct.

The edge of our free fermion model consists of a counterclockwise-propagating charged mode and a clockwise-propagating neutral mode. We denote the fermion annihilation operators for these modes $\psi_c$ and $\psi_n$, respectively. Since the 'top' (T) and 'bottom' (B)

edges, as indicated in Fig 3.1, are separated by grounded contacts, each annihilation operator has a subscript $T/B$ and the Lagrangian is a sum of separate Lagrangians on each edge $\mathcal{L} = \mathcal{L}_T + \mathcal{L}_B$, where

$$\mathcal{L}_{T/B} = \frac{1}{2\pi}\int dx \Big(\psi^\dagger_{c,T/B}(\pm\partial_t + v_{c,T/B}\partial_x)\psi_{c,T/B} + \psi^\dagger_{n,T/B}(\mp\partial_t + v_{n,T/B}\partial_x)\psi_{n,T/B}\Big) \tag{3.1}$$

The signs $\pm, \mp$ correspond to the $T/B$ edge and $v_{c/n,T/B}$ is the velocity of the indicated mode. The QPC at $x = 0$ is incorporated in the Lagrangian through the tunneling term

$$\mathcal{L}^1_{tun} = -\lambda_1 \psi^\dagger_{c,T}\psi_{c,B}\delta(x) + h.c. \tag{3.2}$$

This term contributes equally to the current whether or not the current injection is present because it does not involve the neutral mode. Hence, the change in current attributed to the presence of the current injection is due to the pair-tunneling term that mixes the charged and neutral modes:

$$\mathcal{L}^2_{tun} = -\lambda_2 \psi^\dagger_{c,T}\psi^\dagger_{n,T}\psi_{c,B}\psi_{n,B}\delta(x) + h.c. \tag{3.3}$$

Similar single- and pair-tunneling terms involving only the neutral modes may also be present, but they do not contribute to the shot noise or current. Terms involving more fields or derivatives might also be present, but we do not need to consider them here. We will usually consider an applied voltage, $V_0$, across the QPC, which is incorporated through the phase of the tunneling coefficients: $\lambda_{1,2} \to \lambda_{1,2}e^{-i\omega_0 t}$, where $\omega_0 = eV_0$.

We model the current injection by a second QPC at $x = d$ that allows tunneling from an external lead, whose fermion annihilation operator we denote by $\Psi$. We will always take $d < 0$, as shown in Fig 3.1. Single electron tunneling across the QPC is included by the term:

$$\mathcal{L}^1_{inj} = -\Lambda_1 \Psi^\dagger \psi_{c,T} \delta(x - d) + h.c. \tag{3.4}$$

Similarly to $\mathcal{L}^1_{tun}$, this term contributes equally to the current whether or not the current injection is present because it does not involve the neutral mode. Hence, the change in current attributed to the current injection is due to the pair tunneling term that mixes the charged and neutral fermion modes:

$$\mathcal{L}^2_{inj} = -\Lambda_2 \Psi^\dagger \Psi^\dagger_n \psi_{c,T} \psi_{n,T} \delta(x - d) + h.c. \tag{3.5}$$

To conserve charge, we have assumed the lead also has a neutral fermion mode, $\Psi^\dagger_n$. The voltage difference $V_1$ between the external lead and the top edge of the Hall bar is incorporated through the tunneling coefficients by $\Lambda_{1,2} \to \Lambda_{1,2} e^{-i\omega_1 t}$, where $\omega_1 = eV_1$.

The charged current operator across the QPC at $x = 0$ is given by $I_{tun} = e\frac{d}{dt}\langle N \rangle = -ie\langle [N, H] \rangle = I_1 + I_2$, where $N = \psi^\dagger_{c,T} \psi_{c,T}$ is the electron number of the charged field and

$$I_1 = -ie\lambda_1 e^{-i\omega_0 t} \psi^\dagger_{c,T} \psi_{c,B} \delta(x) + h.c. \tag{3.6}$$

$$I_2 = -ie\lambda_2 e^{-i\omega_0 t} \psi^\dagger_{c,T} \psi^\dagger_{n,T} \psi_{c,B} \psi_{n,B} \delta(x) + h.c. \tag{3.7}$$

Similarly, the operator that measures current across the QPC at $x = d$ is given by $I_{inj} = I_{\Psi 1} + I_{\Psi 2}$, where

$$I_{\Psi 1} = -ie\Lambda_1 e^{-i\omega_1 t}\Psi^\dagger \psi_{c,T}\delta(x-d) + h.c. \tag{3.8}$$

$$I_{\Psi 2} = -ie\Lambda_2 e^{-i\omega_1 t}\Psi^\dagger \Psi_n^\dagger \psi_{c,T}\psi_{n,T}\delta(x-d) + h.c. \tag{3.9}$$

It is straightforward to compute $\langle I_{tun}\rangle_0$ and $\langle I_{inj}\rangle_0$, where the subscript 0 indicates the lowest order in perturbation theory:

$$\langle I_{tun}\rangle_0 = 2\pi e\omega_0|\lambda_1|^2 + \frac{\pi e}{3}\omega_0^3|\lambda_2|^2 \tag{3.10}$$

$$\langle I_{inj}\rangle_0 = 2\pi e\omega_1|\Lambda_1|^2 + \frac{\pi e}{3}\omega_1^3|\Lambda_2|^2 \tag{3.11}$$

We have absorbed $v_{i,T/B}$ into the tunneling coefficients. We now show that to the next order in perturbation theory, $\langle I_{tun}\rangle$ depends on the injected current at $x = d$, *even though only neutral excitations move the towards the QPC at* $x = 0$. Specifically, we define

$$\Delta I_{tun} \equiv \langle I_{tun}\rangle - \langle I_{tun}\rangle|_{\Lambda_i=0} \tag{3.12}$$

and show that $\Delta I_{tun} \neq 0$. It is not hard to show that $I_1$ is independent of the current injected downstream (and hence independent of $\Lambda_{1,2}$) because it depends only on the charged edge mode, which moves from $x = d$ to the left ground without passing the QPC at $x = 0$. Hence, $\Delta I_{tun} = \langle I_2\rangle - \langle I_2\rangle|_{\Lambda_i=0}$, which can be computed perturbatively

by,

$$\Delta I_{tun} = \langle I_2 \left( i \int dt_1 \mathcal{L}^2_{tun} \right) \left( i \int dt_2 \mathcal{L}^2_{inj} \right) \left( i \int dt_3 \mathcal{L}^2_{inj} \right) \rangle_0 + \mathcal{O}(|\lambda_2|^2 |\Lambda_2|^4, |\lambda_2|^4 |\Lambda_2|^2) \tag{3.13}$$

Because the system is not in equilibrium at non-zero voltage, the correlation function in Eq (3.13) requires careful treatment, which is explained in Appendix C.1. The full calculation is shown in Appendix C.2. Here we state the result:

$$\Delta I_{tun} = \frac{4\pi^3}{3} e |\lambda_2|^2 |\Lambda_2|^2 \omega_0 \omega_1^4 \tag{3.14}$$

We have assumed that the neutral fermions are Majorana fermions, which yields the physically reasonable result that $\Delta I_{tun} = 0$ when $\omega_0 = 0$. If this is not the case, then $\Delta I_{tun}$ will have additional terms which are odd in $\omega_1$. These terms are computed in Appendix C.2.

Eq (3.14) shows the main point of this work and gives an experimental prediction for this fictitious edge: the charged current measured across the QPC at $x = 0$ will change when current is injected at $x = d$, even though it is only carried to $x = 0$ by the neutral mode. Physically, we understand this as the presence of extra neutral fermions enhancing the probability of a pair-tunneling event. Since tunneling events in one direction are favored to begin with, due to the voltage bias, the probability for these events is more enhanced, leading to increased current. That this is realized in such a

simple model hints that it is a general result, which applies to any edge with oppositely propagating neutral and charged modes and tunneling operators that mix the two.

### 3.2.2 Luttinger liquid edge

To generalize the results of the previous section to edges with fractional excitations, we describe the edge by a Luttinger liquid with counter-propagating charged and neutral modes, denoted by the bosonic fields $\phi_c$ and $\phi_n$. We assume the Lagrangian is diagonal in these modes after scattering and interactions have been included. In the set-up shown in Fig 3.1, the Lagrangian is a sum of Lagrangians on the top and bottom edges, $\mathcal{L} = \mathcal{L}_T + \mathcal{L}_B$, where

$$\mathcal{L}_{T/B} = \frac{1}{4\pi}\int dx \left(g_c \left(\pm\partial_t + v_{c,T/B}\partial_x\right)\phi_{c,T/B}\partial_x\phi_{c,T/B} + g_n \left(\mp\partial_t + v_{n,T/B}\partial_x\right)\phi_{n,T/B}\partial_x\phi_{n,T/B}\right) \tag{3.15}$$

where $T/B$ denotes the top or bottom edge, the $v$'s denotes the velocities, and $g_c$ and $g_n$ are integers that determine the scaling dimensions of operators in the theory. A quasiparticle is labelled by an integer pair $q = (q_n, q_c)$, which determines its annihilation operator, $\Phi_q = e^{iq_n\phi_n + iq_c\phi_c}$ and its charge, $q_c e^*$, where $e^*$ is the minimum quasiparticle charge. By convention, we take $q_c > 0$; the hermitian conjugate terms correspond to creation operators. The scaling dimension of $\Phi_q$ is given by $q^2/2$, where we have defined the inner product $q^2 = q \cdot q \equiv q_c^2/g_c + q_n^2/g_n$. For a particular edge theory, not all pairs

are allowed excitations; for example, for the $\nu = 2/3$ edge that we will discuss in more detail in Sec 3.4, $g_c = 6$, $g_n = 2$, $e^* = 1/3$ and allowed excitations have $q_c = q_n \mod 2$.[43]

The QPC at $x = 0$ is included in the Lagrangian through the tunneling term,

$$\mathcal{L}_{tun} = -\sum_{q,q'} \lambda_{qq'} \Phi^\dagger_{q,T} \Phi_{q',B} \delta(x) + h.c. \tag{3.16}$$

For $\lambda_{qq'}$ to be nonzero, the quasiparticles $q$ and $q'$ must have the same charge and statistics, but not necessarily the same neutral component. If there is a voltage $V_0$ across the QPC then $\lambda_q \to \lambda_q e^{-iq_c\omega_0 t}$, where $\omega_0 = e^* V_0$. The current injection is described by a QPC at $x = d$ that tunnels electrons between an external lead and the quantum Hall edge. Let $\Psi$ denote the electron annihilation operator of the lead. Then the current injection is described by the Lagrangian,

$$\mathcal{L}_{inj} = -\sum_{r} \Lambda_R \Psi^\dagger \Phi_{r,T} \delta(x - d) + h.c. \tag{3.17}$$

where $\Lambda_r$ is only nonzero if $r_c e^* = e$, so that the sum is over all electron operators in the theory. If there is a voltage $V_1$ across the QPC at $x = d$ then $\Lambda_r \to \Lambda_r e^{-i\omega_1 t}$, where $\omega_1 = eV_1$. Less relevant terms that tunnel pairs of electrons across the QPC might also be present, but we do not consider them here.

The tunneling current operators are given by $I_{tun} = \sum_{q,q'} I_{qq'}$ and $I_{inj} = \sum_r I_{r\Psi}$, where

$$I_{qq'} = -iq_c e^* \lambda_{qq'} \Phi^\dagger_{q,T} \Phi_{q',B} \delta(x) + h.c. \tag{3.18}$$

$$I_{r\Psi} = -ie\Lambda_r \Psi^\dagger \Phi_{r,T} \delta(x-d) + h.c. \tag{3.19}$$

It is straightforward to compute to lowest order in perturbation theory, absorbing the velocities into the tunneling constants,

$$\langle I_{tun} \rangle_0 = \sum_{q,q'} \frac{2\pi e^* q_c}{\Gamma(q^2+q'^2)} |\lambda_{qq'}|^2 \mathrm{sgn}(\omega_0) |q_c \omega_0|^{q^2+q'^2-1} \tag{3.20}$$

$$\langle I_{inj} \rangle_0 = \sum_{r} \frac{2\pi e}{\Gamma(1+r^2)} |\Lambda_r|^2 \mathrm{sgn}(\omega_1) |\omega_1|^{r^2} \tag{3.21}$$

These results are identical to Eqs (3.10) and (3.11) when the scaling dimensions of the tunneling terms are matched. The zeroth order, zero-frequency shot noise is given by the sum

$$S(\omega = 0) = \sum_{q,q'} q_c e^* \left| \langle I_{qq'} \rangle_0 \right| \tag{3.22}$$

As in the previous section, we want to find the change in tunneling current at $x = 0$ in the presence of the injection at $x = d$, when $d < 0$, so the current moving from the injection to the QPC at $x = 0$ is carried only by the neutral mode. We define the change in current by $\Delta I_{tun}$ in Eq (3.12). To leading order,

$$\Delta I_{tun} = \langle I_{tun} \left( i \int dt_1 \mathcal{L}_{tun} \right) \left( i \int dt_2 \mathcal{L}_{inj} \right) \left( i \int dt_3 \mathcal{L}_{inj} \right) \rangle_0 \tag{3.23}$$

To ensure that $\Delta I_{tun} = 0$ when $\omega_0 = 0$, we assume that the tunneling coefficient $\lambda_{qq'}$ for tunneling a quasiparticle with $q = (q_n, q_c)$ from the top edge is the same as that for a quasiparticle with opposite neutral charge, $q = (-q_n, q_c)$, and similarly for tunneling $q'$

from the bottom edge and $r$ to the external lead $\Lambda_r$.[1] Here we state the result in two limiting cases; the full expression is given in Appendix C.3. In the limit $|\omega_1| \ll |\omega_0|$,

$$\frac{\Delta I_{tun}}{e^* \mathrm{sgn}(\omega_0)} = \sum_{\substack{q,q',r \\ r_n,q_n \neq 0}} b_{qq',r} \frac{|\omega_1|^{r^2+1} |\omega_0 q_c|^{q^2+q'^2-3}}{\Gamma(r^2+2)\Gamma(q^2+q'^2-2)} \tag{3.24}$$

while in the limit $|\omega_1| \gg |\omega_0|$,

$$\frac{\Delta I_{tun}}{e^* \mathrm{sgn}(\omega_0)} = \sum_{\substack{q,q',r \\ r_n,q_n \neq 0 \\ 0<q^2+q'^2<2}} -b_{qq',r} \frac{|\omega_1|^{r^2-1} |\omega_0 q_c|^{q^2+q'^2-1}}{\Gamma(r^2)\Gamma(q^2+q'^2)} + \sum_{\substack{q,q',r \\ r_n,q_n \neq 0 \\ q^2+q'^2>2}} b_{qq',r} \frac{|\omega_1|^{r^2+q^2+q'^2-3} |\omega_0 q_c|}{\Gamma(r^2+q^2+q'^2-2)} \tag{3.25}$$

where $b_{qq',r} \propto q_c |\lambda_{qq'}|^2 |\Lambda_r|^2$ is a positive constant. Eqs (3.24) and (3.25) agree with Eq (3.14) after identifying $r^2 = 3, q'^2 + q^2 = 4$ and show our main result in general form: *electrons injected into the edge at $x = d$ will cause a change in the charged tunneling current at $x = 0$, even though only the neutral part of the injected electrons move from $x = d$ to $x = 0$.* This general formulation is applicable to any bosonized Abelian quantum Hall edge with counter-propagating modes. We expect it could be extended to a non-Abelian edge by matching the scaling dimensions of the tunneling operators. Interestingly, though, the sign of $\Delta I_{tun}$ depends on the magnitude of the scaling dimensions $q$ and $q'$ and the simple picture of enhanced tunneling in the fermionic

[1] This assumption is consistent with the experimental observation[46] that excess shot noise is symmetric under reversing the sign of the source current $I_s$. An observation of excess shot noise not symmetric under $I_s \to -I_s$ would demonstrate that quasiparticles with opposite neutral charge $q_n$ do not have equal tunneling amplitudes.

model is generalized to enhanced or diminished tunneling depending on the scaling dimensions of the tunneling quasiparticles.

When we compare to experimental data we will want the excess zero-frequency shot noise, which is also computed in Appendix C.3. We find that in the limit $|\omega_1| \ll |\omega_0|$,

$$\Delta S_{tun} = (e^*)^2 \sum_{\substack{q,q',r \\ r_n,q_n \neq 0}} q_c b_{qq',r} \frac{|\omega_1|^{r^2+1} |\omega_0 q_c|^{q^2+q'^2-3}}{\Gamma(r^2+2)\Gamma(q^2+q'^2-2)} \tag{3.26}$$

while in the limit $|\omega_1| \gg |\omega_0|$,

$$\Delta S_{tun} = (e^*)^2 \sum_{\substack{q,q',r \\ r_n,q_n \neq 0}} \frac{q_c b_{qq',r} |\omega_1|^{r^2+q^2+q'^2-2}}{\Gamma(r^2+q^2+q'^2-1)} \tag{3.27}$$

## 3.3 Temperature difference model

In the previous section, we modeled the current injection by an external lead weakly coupled to the edge of the Hall bar by a QPC. An alternate approach is used in Refs 117 and 118. There, they assume that the sole effect of the current injection is to increase the temperature of the top edge of the Hall bar, while the temperature of the bottom edge remains constant. The increase in temperature is responsible for an increase in shot noise across the QPC at $x = 0$, which is computed in Refs 117 and 118. However, it does not appear to have been noted that the increase in temperature also changes the magnitude of the tunneling current. Here, we write an expression for $\Delta I_{tun}$ when there

is a temperature difference between the two edges of the Hall bar and describe how it differs qualitatively from our prediction for $\Delta I_{tun}$ in the previous section.

We again describe the edge of the quantum Hall bar using Luttinger liquid theory. We consider an edge with counter-propagating charged and neutral modes, described by the Lagrangian $\mathcal{L} = \mathcal{L}_T + \mathcal{L}_B$, where $\mathcal{L}_{T/B}$ are given by Eq (3.15). Quasiparticles are labelled by integer pairs $q = (q_n, q_c)$, with their charge given by $q_c e^*$ and annihilation operator $\Phi_m$. The QPC at $x = 0$ is described by $\mathcal{L}_{tun}$ in Eq (3.16). When there is a voltage $V_0$ applied across the QPC, $\lambda_q \to \lambda_q e^{-iq_c\omega_0 t}$, where $\omega_0 = e^* V_0$. Following Ref 118, the tunneling current from a particular species of quasiparticle $\Phi_q$ from the top edge of the Hall bar to a species $\Phi_{q'}$ on the bottom edge can be computed when the top edge is at temperature $T_T$ and the bottom edge at $T_B$ using the finite temperature prescription for correlation functions described in Sec C.3.1, yielding

$$\langle I_{tun}\rangle_0 = \mathrm{sgn}(\omega_0) 4 \sum_{q,q'} q_c e^* |\lambda_{qq'}|^2 (\pi T_B)^{q^2+q'^2-1} \sin(\frac{\pi}{2}(q^2+q'^2)) F\left(\frac{q_c|\omega_0|}{\pi T_B}, \frac{T_T}{T_B}\right) \quad (3.28)$$

where $F$ is the integral

$$F(\alpha,\beta) = \int_0^\infty dx \frac{\beta^{q^2}\sin(\alpha x)}{(\sinh(\beta x))^{q^2}(\sinh(x))^{q'^2}} \quad (3.29)$$

We have absorbed the edge mode velocities into the tunneling coefficients. When there are multiple species of quasiparticles, their contributions to the tunneling current add.

Define the excess current $\Delta I_{tun} = \langle I_{tun} \rangle - \langle I_{tun} \rangle_{T_T = T_B}$. The contribution to $\Delta I_{tun}$ from tunneling from $\Phi_q$ to $\Phi_{q'}$, transferring charge $q_c e^*$, is proportional to

$$F\left(\frac{q_c|\omega_0|}{\pi T_B}, \frac{T_T}{T_B}\right) - F\left(\frac{q_c|\omega_0|}{\pi T_B}, 1\right) < 0 \tag{3.30}$$

where the inequality results from imposing the physical constraint $T_T/T_B > 1$. Consequently, when $\sin(\frac{\pi}{2}(q^2 + q'^2)) > 0$, increasing the injected current decreases the magnitude of the tunneling current, while in the opposite case, the magnitude of the tunneling current decreases. As in the previous section, the sign of the change in current depends on the scaling dimensions of the tunneling quasiparticles.

To fit the temperature difference theory to the experimental data in the next section, we will need the expression for zero-frequency noise measured at the voltage probe when $I_n = 0$, which is computed in Ref 118. The contribution to the noise from the process of tunneling $\Phi_q$ on the top edge to $\Phi_{q'}$ on the bottom edge is

$$\begin{aligned} S_{tun}|_{T_T=T_B} = &-\frac{2}{\pi}(2\pi T_B)^{2q^2+2q'^2-1}(q_c e^*)^2 |\lambda_{qq'}|^2 \sinh\left(\frac{1}{2}\pi\alpha_q\right) \\ &\times iB(q^2 + q'^2 + \frac{i\alpha_q}{2}, q^2 + q'^2 - \frac{i\alpha_q}{2})\left(\psi(q^2 + q'^2 + \frac{i\alpha_q}{2}) - \psi(q^2 + q'^2 - \frac{i\alpha_q}{2})\right) \end{aligned} \tag{3.31}$$

where $\alpha_q = q_c\omega_0/(\pi T_B)$, $B$ is the beta function and $\psi$ is the digamma function. The contributions from multiple species of quasiparticles add. Note that there is an important diference between this model and the model of a weak downstream perturbation in Section 3.2. If the two edges are at different temperatures, then all tunneling processes

are affected by the temperature difference. However, in the case of a weak downstream perturbation, only tunneling processes involving counter-propagating neutral modes will be affected. In the case of the $\nu = 2/3$ state, these would be charge-$e/3$ tunneling processes; charge-$2e/3$ tunneling processes, which do not involve the neutral modes, would be independent of the downstream perturbation in the limit of vanishing interaction between charged and neutral modes.

## 3.4 Comparison to experiment at $\nu = 2/3$

We have shown that injecting current downstream from the QPC should produce a change in the tunneling current across the QPC. In this section, we try to estimate the magnitude of this change when the system is at filling fraction $\nu = 2/3$ to determine whether it could be observed in experiment. When we model the current injection by weakly coupling a lead to the edge of the Hall bar, as described in Sec 3.2, we do this by fitting our theoretical expression for $\Delta S_{tun}$ to the measured excess shot noise in Ref 46. The best-fit values of the tunneling amplitudes allow us to estimate $\Delta I_{tun}$. In the temperature difference model of Sec 3.3 we fit the measured shot noise at $I_n = 0$ from Ref 46 and use best-fit parameters from Ref 118 to estimate $\Delta I_{tun}$. Coincidentally, in both models we find that there should be tunneling current on the order of .1 nA, which should be observable in experiment.

### 3.4.1 Theoretical description of the $\nu = 2/3$ edge

The $\nu = 2/3$ edge is expected to be described by the Lagrangian (3.15), with $g_c = 6, g_n = 2$ and $e^* = e/3$.[43] Tunneling across the QPC at $x = 0$, as described by Eq (3.16), is dominated by three equally most-relevant terms. Two of these terms tunnel charge $e/3$ quasiparticles, described by $q_n = \pm 1, q_c = 1$ and the third tunnels a charge $2e/3$ quasiparticle with $q_n = 0, q_c = 2$. Other quasiparticles are less relevant and we will not consider them here. Either species of charge-$e/3$ quasiparticle can tunnel from the top edge of the Hall bar to either species at the bottom edge; let $|\lambda_1|^2$ denote the sum of the squares of the amplitudes corresponding to charge $e/3$ tunneling across the Hall bar and let $|\lambda_2|^2$ denote the square of the amplitude corresponding to tunneling charge $2e/3$ across the Hall bar. Tunneling from the external electron lead, described in Eq (3.17), is dominated by two most-relevant terms, which have $r_n = \pm 1, r_c = 3$. We denote their respective couplings $\Lambda_1, \Lambda_2$. Hence, all of these most-relevant tunneling terms have $q^2 = 2/3$ and $r^2 = 2$.

The experimental data is in terms of the source current, $I_s$, and the injected current, $I_n$, which we need to express in terms of our theoretical parameters $V_0$ and $V_1$ (weakly coupled lead) or $V_0, T_T$ and $T_B$ (temperature difference model). The source current is related to the voltage $V_0$ applied across the Hall bar by the Hall conductance, $I_s = \frac{2}{3}\frac{e^2}{h}V_0$. In the weak coupling case, Eq (3.21) yields $I_n \equiv \langle I_{inj} \rangle_0 \propto \mathrm{sgn}(\omega_1)\omega_1^2$, where $\omega_1 = eV_1$.

In the temperature difference model, we use the fit from Ref 118, which expresses the temperatures in terms of the injected current by $T_T/T_B - 1 \propto |I_n|^p$, where $p$ is determined from the fit.

### 3.4.2 Theoretical prediction of excess current for the $\nu = 2/3$ edge weakly coupled to the current injection

We fit our theoretical expression for $\Delta S_{tun}$ to data in Ref 46 and use the fit to predict $\Delta I_{tun}$. The experimental data includes a measurement of excess shot noise as a function of $I_n$ when $I_s = 0$ and as a function of $I_s$ for several values of $I_n$.

The excess shot noise as a function of $I_n$ when $I_s = \omega_0 = 0$ is shown in Fig 3.2, overlaid with the experimental data for several transmission probabilities $t$ from Fig 2 in Ref 46. Using Eq (3.27), our theory predicts the scaling $\Delta S_{tun} \propto |\omega_1|^{4/3} \propto |I_n|^{2/3}$, which is plotted with only an overall scaling factor for each $t$. We have taken $T = 0$ for simplicity. The theoretical model fits the experimental data well at all transmission probabilities. It is especially good at $t = 99\%$, where perturbation theory is most applicable.

In Fig 3.3 we show the excess shot noise $\Delta S_{tun}$ as a function of the source current $I_s$, for several values of injected current, $I_n$. The dots show the experimental data from Fig 3a in Ref 46, where the noise at $I_n = 0$ has been subtracted from the noise measured

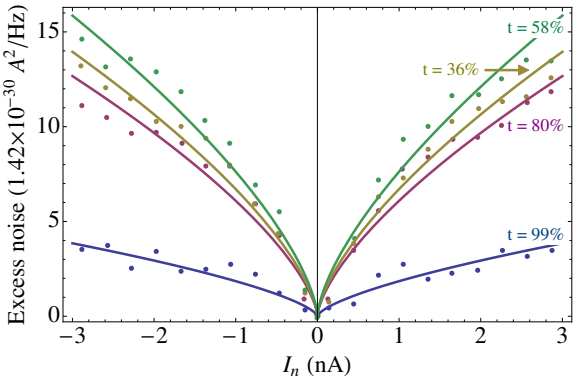


Figure 3.2: **Excess shot noise as a function of $I_n$ at $\nu = 2/3$.** Dots show experimental data at several transmission probabilities $t$ and lines indicate the theoretical prediction $\Delta S_{tun} \propto |I_n|^{2/3}$.

at finite $I_n$. The lines show our theoretical prediction, described in Sec 3.2.2 and shown explicitly in Appendix C.3.5 for the $\nu = 2/3$ edge:

$$\Delta S_{tun} = 2a\left(\frac{1}{3}\right)^2 \mathrm{sgn}(I_n)\left(\mathrm{sgn}(c\sqrt{|I_n|}-\pi I_s)|\pi I_s - c\sqrt{|I_n|}|^{4/3} + \mathrm{sgn}(\pi I_s + c\sqrt{|I_n|})|\pi I_s + c\sqrt{|I_n|}|^{4/3} - \frac{8}{3}c\sqrt{|I_n|}|\pi I_s|^{1/3}\right) \tag{3.32}$$

where $a \propto |\lambda_1|^2|\Lambda_1|^2$ and $c = \mathrm{sgn}(I_n)|\Lambda_1|^{-1}/\sqrt{2\pi}$ . We have taken $|\Lambda_1| = |\Lambda_2|$, consistent with the symmetry of the measured data under $I_s \to -I_s$. From here on, we will take the tunneling amplitudes to be constant for simplicity.[2] The constant $a$ is only known up to proportionality, as described in Appendix C.3. The factor of 2 in front is consistent with the definition of shot noise in Ref 46. Fitting $\Delta S_{tun}$ at $I_n = -.5, -1.0, -1.5,$

[2]Experimental data on transmission, as in Ref 46, is inconsistent with this assumption, but it does not qualitatively affect our point.

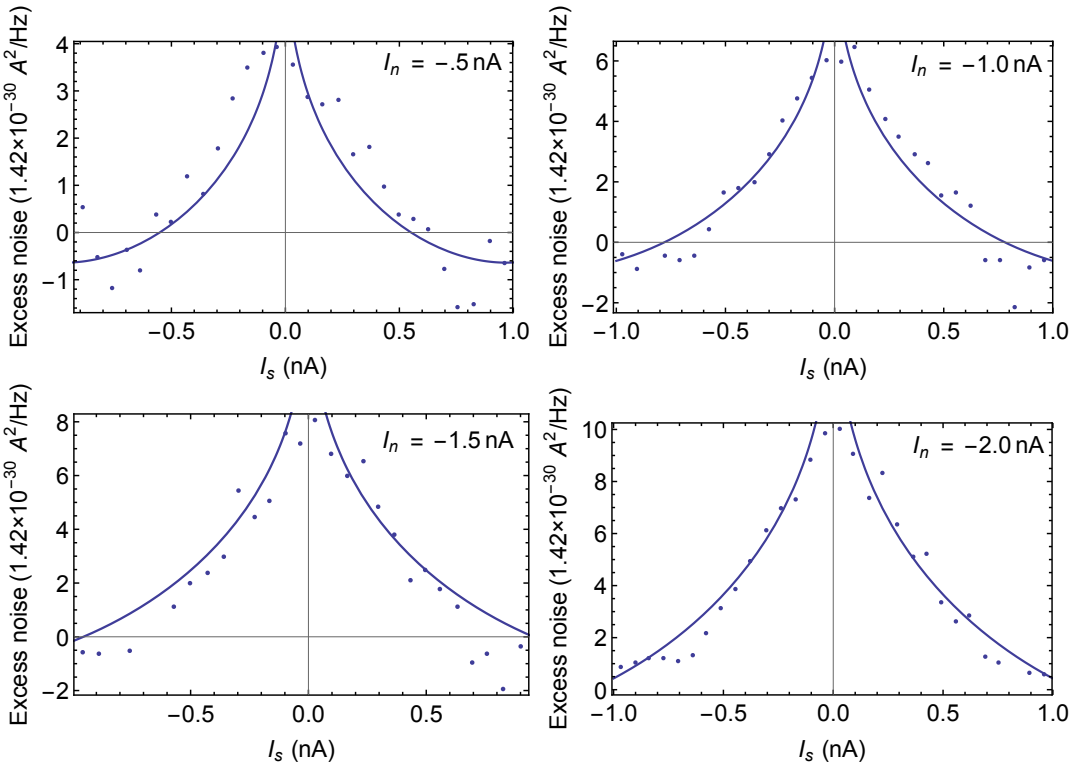


Figure 3.3: **Excess shot noise as a function of source current at finite $I_n$ at $\nu = 2/3$.** Dots show the measured shot noise at the indicated value of $I_n$, where the contribution at $I_n = 0$ has been subtracted. Lines indicate the theoretical prediction.

and $-2.0$ nA and averaging the best fit values yields $a = 4.4 \times 10^{-30}\text{A}^2/\text{Hz}/\text{nA}^{4/3}$ and $c = \text{sgn}(I_n)4.9\ \text{nA}^{1/2}$. Fig 3.3 shows the excess noise at all four values of $I_n$ overlaid with the theoretical prediction using the averaged best fit values. The fits show that a change in temperature is not necessary to fit the excess noise that is measured.

We then use the fit parameters to predict the change in current, $\Delta I_{tun}$, that results from injecting the neutral current, as described in Sec 3.2.2 and computed in Appendix C.3.5:

$$\Delta I_{tun} = \frac{a}{e}\frac{1}{3}\text{sgn}(I_n)\left(-|\pi I_s - c\sqrt{|I_n|}|^{4/3} + |\pi I_s + c\sqrt{|I_n|}|^{4/3} - \frac{8}{3}c\sqrt{|I_n|}\text{sgn}(I_s)|\pi I_s|^{1/3}\right) \tag{3.33}$$

This prediction for excess current is shown in Fig 3.4 using the best-fit values. $\Delta I_{tun}$ has the opposite sign as $I_s$ and a maximum magnitude of .12nA when $I_n = -2$nA. Given that $I_n$ is measured in tenths of nanoamps, we expect $\Delta I_{tun} = .12$nA to be observable. This prediction might explain the slight decrease in transmission in Fig 3a of Ref 46, but it is difficult to discern from the measurement whether the effect is real. It would helpful to increase $I_n$ further and observe whether the change in transmission becomes significant.

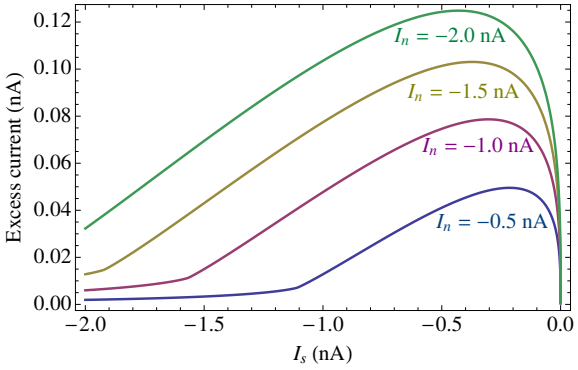


Figure 3.4: **Prediction of excess current when the injection lead is weakly coupled to the edge of the Hall bar at $\nu = 2/3$.** The absolute value in Eq (3.33) causes the kink in each curve, which would be smooth at finite temperature.

### 3.4.3 Theoretical prediction of excess current for the $\nu = 2/3$ system with a temperature difference between the edges

In the temperature difference model, the excess noise at $I_n = 0$ is given by Eq (3.31) applied to the $\nu = 2/3$ edge,

$$S_{tun}|_{T_T=T_B} = -\frac{4}{\pi}(2\pi T_B)^{1/3}|\lambda_1|^2 \left[ \left(\frac{1}{3}\right)^2 \sinh(\frac{\pi\alpha}{2}) B\left(\frac{2}{3}+i\frac{\alpha}{2}, \frac{2}{3}-i\frac{\alpha}{2}\right) i\psi\left(\frac{2}{3}+i\frac{\alpha}{2}\right) + \theta\left(\frac{2}{3}\right)^2 \sinh(\pi\alpha) B\left(\frac{2}{3}+i\alpha, \frac{2}{3}-i\alpha\right) i\psi\left(\frac{2}{3}+i\alpha\right)\right] + h.c. \tag{3.34}$$

where $\alpha = I_s/T_B$ and $\theta = |\lambda_2|^2/|\lambda_1|^2$. There is an extra factor of 2, consistent with the definition of shot noise used in Ref 46. Using the best-fit value of $\theta = .39$ obtained in Ref 118, we fit the shot noise at $I_n = 0$ to find $T_B = 48$mK and $|\lambda_1|^2 = 1.8 \times 10^{-29}\mathrm{K}^{-1/3}\mathrm{A}^2\mathrm{Hz}^{-1}$. These values yield the fit in Fig 3.5 and allow us to predict the

magnitude of excess current using Eqs (3.28) and (3.29):

$$\Delta I_{tun} = \mathrm{sgn}(\omega_0) 4C \left( \int_0^\infty dx \frac{\beta^{2/3} \left( \frac{1}{3}\sin(\alpha x) + \frac{2}{3}\theta \sin(2\alpha x) \right)}{(\sinh(\beta x))^{2/3} (\sinh(x))^{2/3}} - \frac{\frac{1}{3}\sin(\alpha x) + \frac{2}{3}\theta \sin(2\alpha x)}{(\sinh(x))^{4/3}} \right) \tag{3.35}$$

where $C = (\pi T_B)^{1/3} |\lambda_1|^2 \sin(2\pi/3)$ and $\beta = T_T/T_B$. For simplicity we have taken the tunneling amplitudes to be constant. In Ref 118, the authors find the fit $\beta = 1 + 5.05|I_n \text{ nA}^{-1}|^{.54}$, which predicts that $\beta$ increases from 1 to 8 as $I_n$ is turned up to 2 nA. The predicted current is shown in Fig 3.6, where the maximum change in current is seen to be .12 nA. Coincidentally, this is the same magnitude as predicted from the weak tunneling model. We believe this current to be observable in experiment.

The theoretical prediction is a good fit to the data but both the best-fit temperature of $T_B = 48$mK and the best-fit temperature increase by a factor of $\beta \sim 8$ at $I_n = -2$ nA are significantly larger than the increase from 10mK to 25mK estimated in Ref 46. This might be attributed to a discrepancy between the modified free-fermion model used in Ref 46 to fit the data and the Luttinger liquid model used here. An independent measurement in Ref 121 found the temperature of a $\nu = 2/3$ edge to increase from 30mK to 130mK over a similar range of $I_n$, using quantum dot thermometry.[45,122] However, it is not clear whether the measurement in Ref 110 of excess noise that varies with transmission probability at a QPC that has neutral modes impinging from both edges can be explained completely by the temperature difference model: since both edges would be

raised to the same temperature there would no longer be a temperature gradient across the QPC.

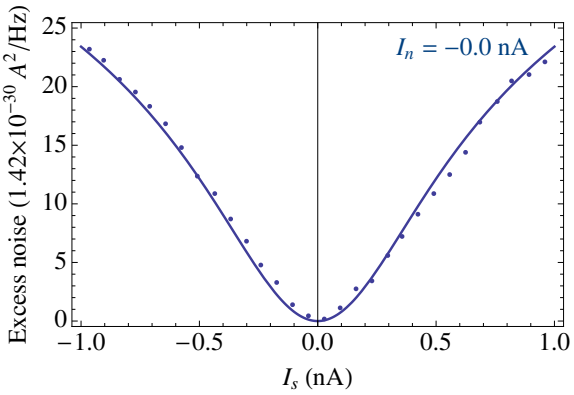


Figure 3.5: **Excess noise when $I_n = 0$ at $\nu = 2/3$.** Dots show the measured noise while lines show the theoretical best fit.

## 3.5 Discussion

We have used a theoretical model to predict that for an edge with counter-propagating neutral modes, current injected downstream of the QPC causes a change in both the shot noise and tunneling current across the QPC. In the specific case of $\nu = 2/3$, we have compared our expression for excess shot noise to the values measured in experiment to determine two fitting parameters. We then used these fitting parameters to predict that the magnitude of the tunneling current could decrease by as much as .1 nA when downstream current is injected. This current should be barely large enough to be observed

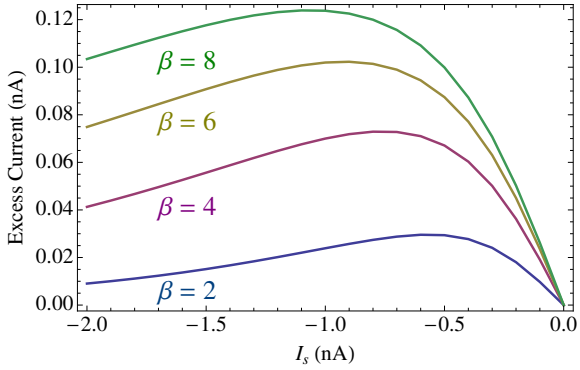


Figure 3.6: **Prediction of excess current in the temperature difference model at $\nu = 2/3$.**

experimentally; it would increase if the injected current increased, which could perhaps be a subject of future work.

In a different model of the system which incorporates the injected current as a temperature difference between the two edges of the Hall bar, fitting the experimental shot noise data also (coincidentally) predicts that the tunneling current should change by approximately .1 nA. This fit yields a ratio of the temperatures $T_T/T_B \approx 8$, which seems high, but is not unreasonable, given the measurements in Ref 121.

It is likely that the physical edge is described by a theory that contains elements from both models. Since both models predict a measurable change in transmission when current is injected downstream of the QPC, we believe this change is a real feature. The prediction runs counter to the intuition that motivated the seminal experiment in Ref 46; hence, it would be interesting to systematically study this effect experimentally.

We expect that our theory could be applied to the $\nu = 5/2$ state by matching the scaling dimensions of the tunneling operators, but the non-Abelian nature of some candidate states might prove to be non-trivial. Another future direction would be to study the dependence of the shot noise and tunneling current on the distance between the current injection site and the QPC at $x = 0$.

# Chapter 4

# Bulk-Edge Correspondence in $(2+1)$-Dimensional Abelian Topological Phases

In this chapter, we show that the same bulk two-dimensional topological phase can have multiple distinct, fully-chiral edge phases. We give examples of this effect in the integer quantum Hall states at $\nu = 8$ and 12 and the Abelian fractional states at $\nu = 8/7, 12/11, 8/15, 16/5$. We give a general criterion for the existence of multiple distinct chiral edge phases for the same bulk phase and discuss experimental consequences. We find that edge phases correspond to lattices while bulk phases correspond to genera of lattices. Since there are typically multiple lattices in a genus, the bulk-

edge correspondence is typically one-to-many. We explain these correspondences using the theory of integral quadratic forms. We show that fermionic systems can have edge phases with only bosonic low-energy excitations and discuss a fermionic generalization of the relation between bulk topological spins and the central charge. The latter follows from our demonstration that every fermionic topological phase can be represented as a bosonic topological phase, together with some number of filled Landau levels. Our analysis shows that every Abelian topological phase can be decomposed into a tensor product of theories associated with prime numbers $p$ in which every quasiparticle has a topological spin that is a $p^n$-th root of unity for some $n$. It also leads to a simple demonstration that all Abelian topological phases can be represented by $U(1)^N$ Chern-Simons theory parameterized by a K-matrix.

This chapter is reprinted with permission from "Bulk-edge correspondence in (2 + 1)-dimensional Abelian topological phases," by Jennifer Cano, Meng Cheng, Michael Mulligan, Chetan Nayak, Eugeniu Plamadeala, and Jon Yard, Phys. Rev. B 89, 115116. 

## 4.1 Introduction

In the limit of vanishing electron-electron interactions, the edge excitations of an integer quantum Hall state form a multi-channel chiral Fermi liquid. These excitations

are stable with respect to weak interactions by their chirality.[123] However, the Coulomb energy in observed integer quantum Hall states is larger than the energy of the lowest gapped edge excitation. Therefore, interactions are not weak in these experiments, and we must consider whether interactions with gapped unprotected non-chiral excitations can alter the nature of the gapless protected chiral edge excitations of an integer quantum Hall state even when the bulk is unaffected.[1]

In this chapter, we show that sufficiently strong interactions can drive the edge of an integer quantum Hall state with $\nu \geq 8$ into a different phase in which the edge excitations form a multi-channel chiral *Luttinger liquid* while the bulk remains adiabatically connected to an integer quantum Hall state of non-interacting electrons. This chiral Luttinger liquid is also stable against all weak perturbations, but it is not adiabatically connected to the edge of an integer quantum Hall state of non-interacting electrons even though the bulk of the system is. For $\nu \geq 12$, there are several possible such stable chiral edge phases corresponding to the same bulk phase. The edge excitations of many fractional quantum Hall states, such as the principal Jain series with $\nu = \frac{n}{2pn+1}$ form a multi-channel chiral Luttinger liquid, which is stable against weak perturbations due to its chirality. We show that such edges can also be subject to reconstruction into a different chiral Luttinger liquid as a result of strong interactions with gapped unprotected

[1] In fact, the Coulomb energy is often larger than the bulk cyclotron energy, too, so it is not a given that the bulk state is in the same universality class as the non-interacting integer quantum Hall state, but we will assume that this is true.

excitations at the edge. The new chiral Luttinger liquid is also stable against all weak perturbations.

A similar phenomenon was recently analyzed in the context of bosonic analogues of integer quantum Hall states.[124] Without symmetry, integer quantum Hall states of bosons that only support bosonic excitations in the bulk, not anyons, occur only when the chiral central charge, $c_- = c_R - c_L$, the difference between the number of right- and left-moving edge modes, is a multiple of eight (or, equivalently, when the thermal Hall conductance is $\kappa_{xy} = c_- \frac{\pi^2 k_B^2 T}{3h}$ with $c_- = 8k$ for integers $k$).[125] There is a unique[126,127] bulk state for each possible value of $c_- = 8k$, but there are many possible chiral edge phases when the chiral central charge is greater than 8: there are two chiral edge phases for $c_- = 16$, twenty-four chiral edge phases for $c_- = 24$, more than one billion for $c_- = 32$, and larger numbers of such edge phases for $c_- > 32$. The transition between the two possible chiral edge phases was studied in detail in the $c_- = 16$ case.[124,128]

These fermionic and bosonic quantum Hall states illustrate the fact that the boundary-bulk correspondence in topological states is not one-to-one. There can be multiple possible edge phases corresponding to the same bulk phase. This can happen in a trivial way: two edge phases may differ by unstable gapless degrees of freedom, so that one of the edge theories is more stable than the other.[30,129–132] (One interesting refinement of this scenario is that the additional gapless degrees of freedom can be protected by a symmetry so that, in the presence of this symmetry, both edge phases are stable.[133])

However, our focus here is the situation in which there are multiple edge phases, each of which is stable to weak perturbations without any symmetry considerations and none of which is more "minimal" than the others. In other words, in the integer and fractional quantum Hall states that we discuss here – which have the additional property that they are all chiral – all of the edge phases are on the same footing. Although they can bound the same bulk, such edge phases generically have different exponents and scaling functions for transport through point contacts and tunneling in from external leads. In some cases, the differences only show up in three-point and higher edge correlation functions.

In Sections 4.7.1, 4.7.2 of this chapter, we discuss fermionic integer quantum Hall states at $\nu = 8$ and $\nu = 12$, their possible stable chiral edge phases, and the experimental signatures that could distinguish these phases. In Section 4.7.3, we discuss the simplest fractional quantum Hall states with multiple chiral edge phases, which occur at $\nu = 8/7, 8/15, 16/5$ (fermions) and $\nu = 12/23$ (bosons). Some of the edge phases that we construct do not support gapless excitations with the quantum numbers of an electron. When the Hall conductance is non-zero, the edge must have gapless excitations; in a system of electrons, there must be a finite-energy excitation everywhere in the system with an electron's quantum numbers. However, it is not necessary that the electron be among the gapless edge excitations of an electronic quantum Hall state; it may be a gapped excitation at the edge, above the gapless excitations that are responsible for carrying the Hall current.

Given the above statement that the same bulk phase can have multiple distinct chiral edge phases, we should ask what breaks down in the usual relation between bulk topological phases and their associated edge spectra. By the usual relationship, we mean the "integration by parts" of a bulk Abelian Chern-Simons action that gives an edge theory of chiral bosons with the same K-matrix.[134,135] The answer is simply that the usual relation focuses only upon the lowest energy excitations of a system and ignores higher-energy excitations. These higher-energy excitations are necessarily adiabatically connected to a topologically-trivial band insulator in the bulk and, generically, gapped excitations at the edge. Surprisingly, interactions between these "trivial" modes and the degrees of freedom responsible for the topologically non-trivial state can drive an edge phase transition that leads to a distinct edge phase without closing the bulk gap. We refer to the relationship between these two distinct edge theories associated with the same bulk as *stable equivalence*. At the level of the gapless edge modes, this manifests itself in the form of an edge reconstruction. While the interpolation at the edge necessarily involves strong interactions, these can be understood using standard Luttinger liquid techniques.

The relationship between the edge and the bulk can also be viewed in the following manner. Each quasiparticle in the bulk has a topological twist factor $\theta_a = e^{2\pi i h_a}$, with $0 < h_a < 1$. If the edge is fully chiral, each such quasiparticle corresponds to a tower of excitations. The minimum scaling dimension for creating an excitation in

this tower is $\min \Delta_a = h_a + n_a$ for some integer $n_a$. The other excitations in the tower are obtained by creating additional bosonic excitations on top of this minimal one; their scaling dimensions are larger than the minimal one by integers. But if the edge has a different phase, the minimal scaling dimension operator in this tower may be $\min \Delta_a = h_a + \tilde{n}_a$. Therefore, the spectrum of edge operators can be different, even though the fractional parts of their scaling dimensions must be the same. (In the case of a fermionic topological phase, we must compare scaling dimensions modulo 1/2, rather than modulo 1. By fermionic topological phase, we mean one which can only occur in a system in which some of the microscopic consitutents are fermions. At a more formal level, this translates into the existence of a fermionic particle which braids trivially with all other particles.)

The purpose of this chapter is to describe the precise conditions under which two different edge phases can terminate the same bulk state, i.e. are stably equivalent. These conditions are intuitive: the braiding statistics of the quasiparticle excitations of the bulk states must be identical and the chiral central charges of the respective states must be equal.

Let us summarize the general relation between bulk Abelian topological states and their associated edge phases in slightly more mathematical terms. Edge phases are described by lattices $\Lambda$ equipped with an integer-valued bilinear symmetric form $B$.[19,136–140] We collectively write this data as $\mathcal{E} = (\Lambda, B)$. The signature of $B$ is simply the chiral

central charge $c_-$ of the edge theory. Given a basis $e_I$ for $\Lambda$, the bilinear form determines a K-matrix $K_{IJ} = B(\vec{e_I}, \vec{e_J})$. In a bosonic system, the lattice $\Lambda$ must be even while in a fermionic system, the lattice $\Lambda$ is odd. (An odd lattice is one in which at least one basis vector has (length)$^2$ equal to an odd integer. The corresponding physical system will have a fermionic particle that braids trivially with all other particles. This particle can be identified with an electron. An even lattice has no such vectors and, therefore, no fermionic particles that braid trivially with all other particles. Hence, it can occur in a system in which none of the microscopic constituents are fermions. Of course, a system, such as the toric code, may have fermionic quasiparticles that braid non-trivially with at least some other particles.) Given the lattice $\Lambda$, vertex operators of the edge theory are associated with elements in the dual lattice $\Lambda^*$. For integer quantum Hall states, $\Lambda^* = \Lambda$, however, for fractional states $\Lambda \subset \Lambda^*$. The operator product expansion of vertex operators is simply given by addition in $\Lambda^*$.

Each bulk phase is characterized by the following data concisely written as $\mathcal{B} = (A, q, c_- \bmod 24)$:[136,138–142] a finite Abelian group $A$ encoding the fusion rules for the distinct quasiparticle types, a finite quadratic form $q$ on $A$ that gives the topological spin to each particle type, and the chiral central charge modulo 24. As we will discuss at length, since the map $\mathcal{E} \to \mathcal{B}$ associating edge data $\mathcal{E}$ to a given bulk $\mathcal{B}$ is *not* one-to-one, several different edge phases may correspond to the same bulk phase. We will provide an in-depth mathematical description of the above formalism in order to

precisely determine when two distinct edge phases correspond to the same bulk phase. To determine all of the edge phases that can bound the same bulk, one can perform a brute force search through all lattices of a given dimension and determinant. (For low-dimensional cases, the results of such enumeration is in tables in Ref. 143 and in, for instance, G. Nebe's online Catalogue of Lattices.) Moreover, one can use a mass formula described in Section 4.5 to check if a list of edge phases is complete.

We will exemplify the many-to-one nature of the map $\mathcal{E} \to \mathcal{B}$ through various examples. The most primitive example occurs for integer quantum Hall states. For such states, the lattice is self-dual, $\Lambda^* = \Lambda$ so there are no non-trivial quasiparticles. For $c_- < 8$, there is a unique edge theory for the fermionic integer quantum Hall state, however, at $c_- = 8$, there are two distinct lattices: the hypercubic latttice $\mathbb{I}_8$ and the $E_8$ root lattice. Therefore, the associated gapless edge theories corresponding to each lattice may bound the same bulk state; there exists an edge reconstruction connecting the two edge phases. Fractional states for which $A$ is non-trivial enrich this general structure.

A rather remarkable corollary of our analysis is the following: all rational Abelian topological phases in 2+1 dimensions can be described by Abelian Chern-Simons theory. By rational, we mean that there is a finite number of bulk quasiparticle types, i.e., the group $A$ has finite order. As may be seen by giving a physical interpretion to a theorem of Nikulin[144] the particle types, fusion rules, and topological twist factors determine a genus of lattices, from which we can define an Abelian Chern-Simons theory. A second

result that follows from a theorem of Nikulin[144] is that any fermionic Abelian topological phase can be mapped to a bosonic topological phase, together with some number of filled Landau levels.

The remainder of this chapter is organized as follows. We begin in Section 4.2 by reviewing the formalism used to describe the bulk and boundary excitations of Abelian Hall states. As a means to both motivate the general mathematical structure and because of their intrinsic interest, we provide two examples of stable equivalence in the fractional quantum Hall setting in Section 4.3 and summarize their physically distinct signatures. In Section 4.4, we abstract from these two examples the general method for understanding how distinct edge phases of a single bulk are related via an edge phase transition. In Section 4.5, we explain the bulk-edge correspondence through the concepts of stable equivalence and genera of lattices. In Section 4.6, we explain how fermionic topological phases can be represented by bosonic topological phases together with some number of filled Landau levels. In Section 4.7, we analyze observed integer and fractional quantum Hall states that admit multiple stable, fully chiral edge phases. In Section 4.8, we explain how a number of theorems due to Nikulin, that we use throughout the text, apply to the description of *all* Abelian topological field theories in (2+1)-D. We conclude in Section 4.9. We have three appendices that collect ideas used within the text.

## 4.2 Preliminaries

### 4.2.1 Edge Theories

In this section, we review the formalism that describes the edges of conventional integer and Abelian fractional quantum Hall states. We begin with the edges of fermionic integer quantum Hall states. We assume that the bulks of these states are the conventional states that are adiabatically connected to the corresponding states of non-interacting fermions. As we will see in later sections, the edge structure is not uniquely determined, even if we focus solely on chiral edge phases that are stable against all weak perturbations.

All integer quantum Hall states have one edge phase that is adiabatically connected to the edge of the corresponding non-interacting fermionic integer quantum Hall state. This edge phase has effective action $S_0 + S_1$, where

$$S_0 = \int dxdt\, \psi_J^\dagger \left(i\partial_t + A_t + v_J(i\partial_x + A_x)\right) \psi_J \tag{4.1}$$

and $J = 1, 2, \ldots, N$. We shall later study two interesting examples that occur when $N = 8$ or $N = 12$. The operator $\psi_J^\dagger$ creates an electron at the edge in the $J^{\text{th}}$ Landau level; $v_J$ is the edge velocity of an electron in the $J^{\text{th}}$ Landau level. Inter-edge interactions take the form

$$S_1 \quad = \quad \int dx\, dt \left(t_{JK}(x)\, e^{i\left(k_F^J - k_F^K\right)x}\, \psi_J^\dagger \psi_K \;+\; \text{h.c.} \;+\; v_{JK}\psi_J^\dagger \psi_J \psi_K^\dagger \psi_K \;+\; \ldots\right). \tag{4.2}$$

The ... in Eq. (4.2) represent higher-order tunneling and interaction terms that are irrelevant by power counting. We neglect these terms and focus on the first two terms. Electrons in different Landau levels will generically have different Fermi momenta. When this is the case, the tunneling term (the first term in Eq. (4.2)) will average to zero in a translationally-invariant system. In the presence of disorder, however, $t_{IJ}(x)$ will be random and relevant (e.g. in a replicated action which is averaged over $t_{IJ}(x)$). Moreover, it is possible for the Fermi momenta to be equal; for instance, in an $N$-layer system in which each layer has a single filled Landau level, the Fermi momenta will be the same if the electron density is the same in each layer. Fortunately, we can make the change of variables:

$$\psi_J(x) \to \left(\overline{\mathcal{P}} \exp\left(i \int_{-\infty}^{x} dx' M(x')\right)\right)_{JK} \psi_K(x),$$

where $M(x)$ is the matrix with entries $M_{JK} = t_{JK}(x')\, e^{i\left(k_F^J - k_F^K\right)x'}/\overline{v}$, $\overline{v} = \sum_J v_J/N$, and $\overline{\mathcal{P}}$ denotes anti-path-ordering. When this is substituted into Eq. (4.1), the first term in Eq. (4.2) is eliminated from the action $S_0 + S_1$. This is essentially a U(N) gauge transformation that gauges away inter-mode scattering. An extra random kinetic term proportional to $(v_J - \overline{v})\delta_{IJ}$ is generated, but this is irrelevant in the infrared when disorder-averaged.

The second term in Eq. (4.2) is an inter-edge density-density interaction; $v_{JK}$ is the interaction between edge electrons in the $J^{\text{th}}$ and $K^{\text{th}}$ Landau levels. This interaction

term can be solved by bosonization. The action $S_0 + S_1$ from Eqs. (4.1) and (4.2) can be equivalently represented by the bosonic action

$$S = \int dx\, dt \left( \frac{1}{4\pi} \delta_{IJ} \partial_t \phi^I \partial_x \phi^J - \frac{1}{4\pi} V_{IJ} \partial_x \phi^I \partial_x \phi^J + \frac{1}{2\pi} \sum_I \epsilon_{\mu\nu} \partial_\mu \phi^I A_\nu \right), \quad (4.3)$$

where $V_{II} \equiv v_I + v_{II}$ (no summation) and $V_{IJ} \equiv v_{IJ}$ for $I \neq J$. The electron annihilation operator is bosonized according to $\psi_J \sim \eta_J e^{i\phi^J}$. Here $\eta_J$ is a "Klein factor" satisfying $\eta_J \eta_K = -\eta_K \eta_J$ for $J \neq K$, which ensures that $\psi_J \psi_K = -\psi_K \psi_J$. Products of even numbers of Klein factors can be diagonalized and set to one of their eigenvalues, $\pm 1$, if all terms in the Hamiltonian commute with them. They can then be safely ignored. This is the case in all of the models studied in this paper. This action can be brought into the following diagonal form (setting the external electromagnetic field to zero for simplicity):

$$S = \int dx\, dt \left( \frac{1}{4\pi} \delta_{IJ} \partial_t \tilde{\phi}^I \partial_x \tilde{\phi}^J - \frac{1}{4\pi} v_I \delta_{IJ} \partial_x \tilde{\phi}^I \partial_x \tilde{\phi}^J \right) \quad (4.4)$$

with an orthogonal transformation $\phi^I = O^I_J \tilde{\phi}^J$ that diagonalizes $V_{IJ}$, $O^I_L V_{IJ} O^J_K = \tilde{v}_L \delta_{LK}$. Two-point correlation functions take the form

$$\left\langle e^{i m_I \phi^I} e^{-i m_K \phi^K} \right\rangle = \prod_{J=1}^{N} \frac{1}{(x - \tilde{v}_J t)^{m_I m_K O^I_J O^K_J}}. \quad (4.5)$$

There is no sum over $J$ in the exponent on the right-hand-side of Eq. (4.5). The electron Green function in the $I^{\text{th}}$ Landau level is a special case of this with $m_K = \delta_{IK}$.

It is now straightforward to generalize the preceding discussion to the case of an arbitrary Abelian integer or fractional quantum Hall state.[27] For simplicity, we will

focus on the case of fully chiral phases in which all edge modes move in the same direction. Such phases do not, in general, have a free fermion representation and can only be described by a chiral Luttinger liquid. They are characterized by equivalence classes of positive-definite symmetric integer *K-matrices* $K$, and integer *charge vectors* $t$ that enter the chiral Luttinger liquid action according to

$$S_{LL} \quad = \quad \int dx\, dt \left( \frac{1}{4\pi} K_{IJ} \partial_t \phi^I \partial_x \phi^J \;-\; \frac{1}{4\pi} V_{IJ} \partial_x \phi^I \partial_x \phi^J \;+\; \frac{1}{2\pi} t_I \epsilon_{\mu\nu} \partial_\mu \phi^I A_\nu \right). \quad (4.6)$$

The fields in this action satisfy the periodicity condition $\phi^I \equiv \phi^I + 2\pi n^I$ for $n^I \in \mathbb{Z}$. Two phases, characterized by the pairs $(K_1, t_1)$ and $(K_2, t_2)$, are equivalent if $K_1 = W^T K_2 W$ and $t_1 = t_2 W$, where $W \in \mathrm{GL}(N, \mathbb{Z})$ since the first and third terms in the two theories can be transformed into each other by the change of variables $\phi^I = W^I{}_J \tilde{\phi}^J$. So long as $W \in \mathrm{GL}(N, \mathbb{Z})$, the periodicity condition satisfied by $\tilde{\phi}^J$ is precisely the same as the periodicity condition satisfied by $\phi^I$. The matrix $V_{IJ}$ consists of marginal deformations that do not change the phase of the edge but affect the propagation velocities. (If we wish, we can think of each phase as a fixed surface under RG flow, and the $V_{IJ}$s are marginal deformations that parametrize the fixed surface.) All such chiral edge theories are stable to all weak perturbations by the same reasoning by which we analyzed integer quantum Hall edges. The simplest fermionic fractional quantum Hall edge theory is that of the Laughlin $\nu = 1/3$ state, for which $K = (3)$ and $t = (1)$ (a $1 \times 1$ matrix and

a 1-component vector, respectively). Integer quantum Hall edges are the special case, $K_{IJ} = \delta_{IJ}$ or, allowing for basis changes, $K = W^T W$ with $W \in \mathrm{GL}(N, \mathbb{Z})$.

It is useful to characterize these phases by lattices $\Lambda$ rather than equivalence classes of K-matrices. Let $e_I^a$ be the eigenvector of $K$ corresponding to eigenvalue $\lambda_a$: $K_{IJ} e_J^a = \lambda^a e_I^a$. We normalize $e_J^a$ so that $e_J^a e_J^b = \delta^{ab}$ and define a metric $g_{ab} = \lambda_a \delta_{ab}$. Then, $K_{IJ} = g_{ab} e_I^a e_J^b$ or, using vector notation, $K_{IJ} = \mathbf{e}_I \cdot \mathbf{e}_J$. We will be focusing mostly on positive-definite lattices, so that $g_{ab}$ has signature $(N, 0)$ but we will occasionally deal with Lorentzian lattices, for which we take $g_{ab}$ has signature $(p, N-p)$. The metric $g_{ab}$ defines a *bilinear form* $B$ on the lattice $\Lambda$ (and its dual $\Lambda^*$) – this just means we can multiply two lattice vectors $\vec{e}_I, \vec{e}_J$ together using the metric, $\vec{e}_I \cdot \vec{e}_J = e_I^a g_{ab} e_J^b = B(\vec{e}_I, \vec{e}_J)$. The $N$ vectors $\mathbf{e}_I$ define a lattice $\Lambda = \{m_I \mathbf{e}_I | m_I \in \mathbb{Z}\}$. The $\mathrm{GL}(N, \mathbb{Z})$ transformations $K \to W^T K W$ are simply basis changes of this lattice, so we can equally well describe edge phases by equivalence classes of $K$-matrices or by lattices $\Lambda$. The conventional edge phases of integer quantum Hall states described above correspond to hypercubic lattices $\mathbb{Z}^N$, which we will often denote by the corresponding $K$ matrix in its canonical basis, $\mathbb{I}_N$. The $\nu = 1/3$ Laughlin state corresponds to the lattice $\Lambda = \mathbb{Z}$ with dual $\Lambda^* = \frac{1}{3}\mathbb{Z}$. [2] The connection of quantum Hall edge phases to lattices can be exploited more easily if we make the following change of variables, $X^a = e_I^a \phi^I$, in terms of which the action

[2] This statement assumes the periodicity convention, $\phi \equiv \phi + 2\pi n$, for $n \in \mathbb{Z}$.

takes the form

$$S = \frac{1}{4\pi}\int dx\, dt\Big(g_{ab}\partial_t X^a \partial_x X^b - v_{ab}\partial_x X^a \partial_x X^b.\Big) \tag{4.7}$$

The variables $X^a$ satisfy the periodicity condition $\mathbf{X} \equiv \mathbf{X} + 2\pi\mathbf{y}$ for $\mathbf{y} \in \Lambda$ and $v_{ab} \equiv V_{IJ} f_a^I f_b^J$, where $f_a^I$ are basis vectors for the dual lattice $\Lambda^*$, satisfying $f_a^I e_J^a = e_{La}(K^{-1})^{LI} e_J^a = \delta_J^I$.

Different edge phases (which may correspond to different bulks or the same bulk; the latter is the focus of this paper) are distinguished by their correlation functions. The periodicity conditions on the fields $X^a$ dictate that the allowed exponential operators are of the form $e^{i\mathbf{v}\cdot\mathbf{X}}$, where $\mathbf{v} \in \Lambda^*$. These operators have scaling dimensions

$$\dim\big[e^{i\mathbf{v}\cdot\mathbf{X}}\big] = \frac{1}{2}|\mathbf{v}|^2. \tag{4.8}$$

They obey the operator algebra

$$: e^{i\mathbf{v_1}\cdot\mathbf{X}} :: e^{i\mathbf{v_2}\cdot\mathbf{X}} :\sim: e^{i(\mathbf{v_1}+\mathbf{v_2})\cdot\mathbf{X}} :, \tag{4.9}$$

where $: \cdot :$ denotes normal ordering. Thus, the operator spectrum and algebra is entirely determined by the underlying dual lattice $\Lambda^*$.

In a quantum Hall state, there are two complementary ways of measuring some of the scaling exponents. The first is a quantum point contact (QPC) at which two edges of a quantum Hall fluid are brought together at a point so that quasiparticles can tunnel across the bulk from one edge to the other. Even though a single edge is completely

stable against all weak perturbations, a pair of oppositely-directed edges will, in general, be coupled by relevant perturbations

$$S = S_T + S_B + \int dt \sum_{\mathbf{v}\in\Lambda^*} v_{\mathbf{v}}\, e^{i\mathbf{v}\cdot[\mathbf{X}_T - \mathbf{X}_B]}. \tag{4.10}$$

Here, $T, B$ are the two edges, e.g., the top and bottom edges of a Hall bar; we will use this notation throughout whenever it is necessary to distinguish the two edges. The renormalization group (RG) equation for $v_{\mathbf{v}}$ is

$$\frac{dv_{\mathbf{v}}}{d\ell} = \left(1 - |\mathbf{v}|^2\right) v_{\mathbf{v}}. \tag{4.11}$$

If $\mathbf{v}\cdot\mathbf{f}^I t_I \neq 0$, the above coupling transfers $\mathbf{v}\cdot\mathbf{f}^I t_I$ units of charge across the junction and this perturbation will contribute to the backscattered current according to

$$I^b \propto |v_{\mathbf{v}}|^2\, V^{2|\mathbf{v}|^2-1}. \tag{4.12}$$

A second probe is the tunneling current from a metallic lead:

$$\begin{aligned} S &= S_{\text{edge}} + S_{\text{lead}} \\ &\quad + \int dt \sum_{\mathbf{v}\in\Lambda} t_{\mathbf{v}} \left[\psi^\dagger_{\text{lead}} \partial\psi^\dagger_{\text{lead}} \partial^2\psi^\dagger_{\text{lead}} \ldots\right] e^{i\mathbf{v}\cdot\mathbf{X}}. \end{aligned}$$

The term in square brackets [...] contains $n$ factors of $\psi^\dagger_{\text{lead}}$ and $n(n-1)/2$ derivatives, where $n = \mathbf{v}\cdot\mathbf{f}^I t_I$ must be an integer. The RG equation for $t_{\mathbf{v}}$

$$\frac{dt_{\mathbf{v}}}{d\ell} = \left(1 - \frac{n^2}{2} - \frac{1}{2}|\mathbf{v}|^2\right) t_{\mathbf{v}}. \tag{4.13}$$

The contribution to the tunneling current from $t_{\mathbf{v}}$ (assuming $n \neq 0$) is

$$I^{\text{tun}} \propto |t_{\mathbf{v}}|^2 \; V^{|\mathbf{v}|^2+n^2-1}. \tag{4.14}$$

Here, we have assumed that the spins at the edge of the quantum Hall state are fully spin-polarized and that tunneling from the lead conserves $S_z$. If, however, either of these conditions is violated, then other terms are possible in the action. For instance, charge-2$e$ tunneling can take the form

$$t_{\text{pair}} \int dt \, \psi^\dagger_{\text{lead},\uparrow} \psi^\dagger_{\text{lead},\downarrow} \; e^{i\mathbf{v}\cdot\mathbf{X}}, \tag{4.15}$$

where $\mathbf{v} \cdot \mathbf{f}^I t_I = 2$. Then, we have tunneling current

$$I^{\text{tun}} \propto |t_{\mathbf{v}}|^2 \; V^{|\mathbf{v}|^2+1}. \tag{4.16}$$

Generically, two lattices $\Lambda_1$ and $\Lambda_2$ can be distinguished by the possible squared lengths $|\mathbf{v}|^2$ for $\mathbf{v} \in \Lambda_1^*$. In many cases of interest, the shortest length, which will dominate the backscattered current discussed above, is enough to distinguish two edge phases of the same bulk. However, sometimes, as in the case of the two bosonic integer quantum Hall states with $c = 16$ discussed in Ref. 124 the spectrum of operator scaling dimensions (not just the shortest length, but all lengths along with degeneracies at each length level) is precisely the same in the two theories, so they could only be distinguished by comparing three-point correlation functions. In either case, different edge phases can be distinguished by their correlation functions.

### 4.2.2 Bulk Theories

In a later section, we will explain how bulk phases correspond to the mathematical notion of a *genus* of lattices, while their associated edge theories are given by lattices within a genus (or in the case of fermionic theories, a pair of genera, one odd and one even). In order to explain the relation between the genus of a lattice and a bulk Abelian phase, we recall some facts about Abelian topological phases.

Suppose that we have a $2+1$d Abelian topological phase associated to a lattice $\Lambda$. Choosing a basis $\mathbf{e}_I$ for the lattice $\Lambda$, we define $K_{IJ} = \mathbf{e}_I \cdot \mathbf{e}_J$ and write a bulk effective action

$$\mathcal{S} = \int d^3x \Big( \frac{1}{4\pi} \epsilon^{\mu\nu\rho} K_{IJ} a^I_\mu \partial_\nu a^J_\rho + \frac{1}{2\pi} j^\mu_I a^I_\mu \Big). \tag{4.17}$$

A particle in this theory carrying charge $m_I$ under the gauge field $a_I$ can be associated with a vector $\mathbf{v} \equiv m_I \mathbf{f}^I$, where $\mathbf{f}_I$ is the basis vector of $\Lambda^*$ dual to $\mathbf{e}_I$ and satisfying $(K^{-1})^{IJ}\mathbf{e}_J = \mathbf{f}^I$. Recall that because $\Lambda \subset \Lambda^*$, any element in $\Lambda$ can be expressed in terms of the basis for $\Lambda^*$, however, the converse is only true for integer Hall states for which $\Lambda = \Lambda^*$. Particles $\mathbf{v}$, $\mathbf{v}' \in \Lambda^*$ satisfy the fusion rule $\mathbf{v} \times \mathbf{v}' = \mathbf{v} + \mathbf{v}'$ and their braiding results in the multiplication of the wave function describing the state by an overall phase $e^{2\pi i \mathbf{v}\cdot\mathbf{v}'}$. Since this phase is invariant under shifts $\mathbf{v} \to \mathbf{v} + \boldsymbol{\lambda}$ for $\boldsymbol{\lambda} \in \Lambda$, the topologically-distinct particles are associated with elements of the so-called discriminant group $A = \Lambda^*/\Lambda$. The many-to-one nature of the edge-bulk correspondence is a reflection

of the many-to-one correspondence between lattices $\Lambda$ and their discriminant groups $A$. Equivalent bulk phases necessarily have identical discriminant groups so our initial choice of lattice is merely a representative in an equivalence class of bulk theories.

We now define a few terms. A *bilinear symmetric form* on a finite Abelian group $A$ is a function $b\colon A \times A \to \mathbb{Q}/\mathbb{Z}$ such that for every $a, a', a'' \in A$,

$$b(a + a', a'') = b(a, a'') + b(a', a'')$$

and $b(a, a') = b(a', a)$. As all bilinear forms considered in this paper will be symmetric, we will simply call them *bilinear forms* with symmetric being understood. A *quadratic form* $q$ on a finite Abelian group $A$ is a function $q : A \to \mathbb{Q}/\mathbb{Z}$ such that $q(na) = n^2 q(a)$ for every $n \in \mathbb{Z}$, and such that

$$q(a + a') - q(a) - q(a') = b(a, a')$$

for some bilinear form $b\colon A \times A \to \mathbb{Q}/\mathbb{Z}$. In this case, we say that $q$ *refines* $b$, or is a *quadratic refinement* of $b$. A bilinear $b$ or quadratic form $q$ is *degenerate* if there exists a non-trivial subgroup $S \subset A$ such that $b(s, s') = 0$ or $q(s) = 0$ for every $s, s' \in S$. Throughout this paper, all bilinear and quadratic forms will be assumed nondegnerate. Each K-matrix $K$ determines a symmetric bilinear form $B$ on $\mathbb{R}^n$ via $B(\mathbf{x}, \mathbf{y}) = \mathbf{x}^T K \mathbf{y}$ that takes integer values on the lattice $\mathbb{Z}^n \subset \mathbb{R}^n$. Every other lattice $\Lambda \subset \mathbb{R}^n$ on which $B$ is integral can be obtained by acting on $\mathbb{Z}^n$ by the orthogonal group $\{g \in \mathrm{GL}(N, \mathbb{R}) : gKg^T = K\}$ of $K$. On the other hand, an integral symmetric bilinear form

is equivalent to a lattice according to the construction before Eq. (4.7) in Section 4.2.1. We are therefore justified in using the terminology "lattice" and "K-matrix" in place of "integral symmetric bilinear form" throughout this paper. Every diagonal entry of a K-matrix $K$ is even iff the (length)$^2$ of every element in the lattice $\mathbb{Z}^N$ is even. We call $K$ *even* if this is the case, and otherwise it is *odd*. Even K-matrices determine integral quadratic forms on $\mathbb{Z}^N$ via $Q(\mathbf{x}) = \frac{1}{2}\mathbf{x}^T K\mathbf{x}$, while for odd K-matrices they are half-integral. When we simply write bilinear or quadratic form or, sometimes, *finite bilinear form* or *finite quadratic form*, we will mean a nondegenerate symmetric bilinear form, or nondegenerate quadratic form, whose domain is a finite Abelian group. Throughout, we abbreviate the ring $\mathbb{Z}/N\mathbb{Z}$ of integers modulo $N$ as $\mathbb{Z}/N$.

The $S$-matrix of the theory can be given in terms of the elements of the discriminant group:

$$S_{[\mathbf{v}],[\mathbf{v}']} = \frac{1}{\sqrt{|A|}} e^{-2\pi i \mathbf{v}\cdot\mathbf{v}'} = \frac{1}{\sqrt{|A|}} e^{-2\pi i m_I (K^{-1})^{IJ} m'_J}, \tag{4.18}$$

where $\mathbf{v} = m_I \mathbf{f}^I, \mathbf{v}' = m'_J \mathbf{f}^J \in \Lambda^*$ and $|A|$ is the dimension of the discriminant group. The bracketed notation $[\vec{v}]$ indicates an equivalence class of elements $[\vec{v}] \in \Lambda^*/\Lambda = A$. Our normalization convention is to represent elements in the dual lattice $\Lambda^*$ with integer vectors $m_I$. The bilinear form $B$ on $\Lambda^*$ reduces modulo $\Lambda$ to define a finite bilinear form on the discriminant group $\Lambda^*/\Lambda$ via

$$b([m_I \mathbf{f}^I], [m'_J \mathbf{f}^J]) = B(m_I \mathbf{f}^I, m'_J \mathbf{f}^J) = m_I (K^{-1})^{IJ} m'_J.$$

The topological twists $\theta_{[\mathbf{v}]}$, which are the eigenvalues of the $T$ matrix, are defined by

$$T_{[\mathbf{v}],[\mathbf{v}']} = e^{-\frac{2\pi i}{24}c_-}\,\theta_{[\mathbf{v}]}\,\delta_{[\mathbf{v}],[\mathbf{v}']} \tag{4.19}$$

where

$$\theta_{[\mathbf{v}]} = e^{\pi i \mathbf{v}\cdot\mathbf{v}}. \tag{4.20}$$

Note that Eq. (4.19) implies that the theory is invariant under shifts of $c_-$ by 24 so long as the topological twists $\theta_{[\mathbf{v}]}$ are invariant, but its modular transformation properties, which determine the partition function on 3-manifolds via surgery,[145] is sensitive to shifts by $c_- \neq 0 \pmod{24}$.

If the topological twists are well-defined on the set of quasiparticles $A$, then they must be invariant under $\mathbf{v} \mapsto \mathbf{v} + \boldsymbol{\lambda}$, where $\boldsymbol{\lambda} \in \Lambda$, under which

$$\theta_{[\mathbf{v}]} \mapsto \theta_{[\mathbf{v}+\lambda]} = \theta_{[\mathbf{v}]}\, e^{\pi i \boldsymbol{\lambda}\cdot\boldsymbol{\lambda}}. \tag{4.21}$$

If the K-matrix is even, so that we are dealing with a bosonic theory, $\boldsymbol{\lambda}\cdot\boldsymbol{\lambda}$ is even for all $\boldsymbol{\lambda} \in \Lambda$. If the K-matrix is odd, however – i.e. if the system is fermionic – then there are some $\boldsymbol{\lambda} \in \Lambda$ for which $\boldsymbol{\lambda}\cdot\boldsymbol{\lambda}$ is odd. In this case, the topological twists are not quite well-defined, and more care must be taken, as we describe in Section 4.6. Given the above definition, only $T^2$ is well-defined.

In a bosonic Abelian topological phase, we can define a finite quadratic form $q$ on the discriminant group, usually called the *discriminant form*, according to

$$q([\vec{v}]) = \frac{1}{2}\vec{v}^2 = \frac{1}{2} m_I (K^{-1})^{IJ} m_J \bmod \mathbb{Z}, \tag{4.22}$$

where $\vec{v} = m_I \mathbf{f}^I$. In a topological phase of fermions, we will have to define $q$ with more care, as we discuss in Section 4.6. Thus, we postpone its definition until then and will only discuss Abelian bosonic topological phases in the remainder of this section. In terms of the discriminant form $q$, the $T$-matrix takes the form

$$\theta_a = e^{2\pi i q(a)}, \tag{4.23}$$

and the $S$-matrix takes the form

$$S_{a,a'} = \frac{1}{\sqrt{|A|}} e^{2\pi i (q(a-a') - q(a) - q(-a'))} \tag{4.24}$$

$$= \frac{1}{\sqrt{|A|}} e^{-2\pi i (q(a+a') - q(a) - q(a'))} \tag{4.25}$$

The equation for the $S$-matrix makes use of the fact that the finite bilinear form $b$ can be recovered from the finite quadratic form according to $b(a, a') = q(a+a') - q(a) - q(a')$. (It is satisfying to observe that the relation between the bilinear form $b$ and the discriminant form $q$ coincides exactly with the phase obtained by a wave function when two particles are twisted about one another.) While the introduction of the discriminant form may appear perverse in the bosonic context, we will find it to be an essential ingredient when discussing fermionic topological phases.

In any bosonic topological phase, the chiral central charge is related to the bulk topological twists by the following relation:[146]

$$\frac{1}{\mathcal{D}} \sum_a d_a^2 \theta_a = e^{2\pi i c_-/8}. \tag{4.26}$$

Here $\mathcal{D} = \sqrt{\sum_a d_a^2}$ is the total quantum dimension, $d_a$ is the quantum dimension of the quasiparticle type $a$, and $\theta_a$ is the corresponding topological twist/spin. $c_- = c - \overline{c}$ is the chiral central charge. In an Abelian bosonic phase described by an even matrix $K$, the formula simplifies to

$$\frac{1}{\sqrt{|A|}} \sum_{a \in A} e^{2\pi i q(a)} = e^{2\pi i c_-/8}, \tag{4.27}$$

since $d_a = 1$ for all quasiparticle types. Here $|A| = \sqrt{|\det K|}$ and $c_- = r_+ - r_-$ is the signature of the matrix, the difference between the number of positive and negative eigenvalues. (We will sometimes, as we have done here, use the term signature to refer to the difference $r_+ - r_-$, rather than the pair $(r_+, r_-)$; the meaning will be clear from context.) Notice that $e^{2\pi i q(a)}$ is just the topological twist of the quasiparticle represented by $a \in \Lambda^*/\Lambda$. This is known as the Gauss-Milgram sum in the theory of integral lattices.

Let us pause momentarily to illustrate these definitions in a simple example: namely, the semion theory described by the K-matrix, $K = (2)$. This theory has discriminant group $A = \mathbb{Z}/2\mathbb{Z} = Z_2$ and, therefore, two particle types, the vacuum denoted by the lattice vector $[0]$ and the semion $s = [1]$. Recall that our normalization convention is to take the bilinear form on $A$ to be $b([\vec{x}], [\vec{y}]) = x \cdot \frac{1}{2} \cdot y$; the associated quadratic form is then $q([\vec{x}]) = \frac{1}{2} b([\vec{x}], [\vec{x}])$. The discriminant form, evaluated on the semion particle, is given by $q([1]) = \frac{1}{2} \cdot \frac{1^2}{2}$. The T matrix equals $\exp(-2\pi i/24)\mathrm{diag}(1, i)$, and the S-matrix, $S = \frac{1}{\sqrt{2}} \left( \begin{smallmatrix} 1 & 1 \\ 1 & -1 \end{smallmatrix} \right)$. Evaluating the Gauss-Milgram sum confirms that $c_- = 1$.

In order to determine the discriminant group from a given $K$-matrix, we can use the following procedure. First, we compute the Gauss-Smith normal form of the $K$-matrix, which can be found using a standard algorithm.[147] Given $K$, this algorithm produces integer matrices $P$, $Q$, $D$ such that

$$K = PDQ. \tag{4.28}$$

Here both $P$ and $Q$ are unimodular $|\det P| = |\det Q| = 1$, and $D$ is diagonal. The diagonal entries of $D$ give the orders of a minimal cyclic decomposition of the discriminant group

$$A \simeq \prod_J \mathbb{Z}/D_{JJ},$$

with the fewest possible cyclic factors, giving yet another set of generators for the quasiparticles. Although more compact, this form does not directly lend itself towards checking the equivalence of discriminant forms.

Now recall that the bases of $\Lambda$ and $\Lambda^*$ are related by $K$:

$$\mathbf{e}_I = K_{IJ}\mathbf{f}^J \tag{4.29}$$

Substituting the Gauss-Smith normal form, this can be rewritten

$$(P^{-1})^{IL}\mathbf{e}_L = D^{IK}Q_{KJ}\mathbf{f}^J. \tag{4.30}$$

The left-hand side is just a basis change of the original lattice. On the right-hand side, the row vectors of $Q$ that correspond to entries of $D$ greater than 1 give the generators

of the cyclic subgroups of the discriminant group. A non-trivial example is given in Appendix D.

## 4.3 Two Illustrative Examples of Bulk Topological Phases with Two Distinct Edge Phases

The chiral Luttinger liquid action is stable against all small perturbations involving only the gapless fields in the action in Eq. (4.6) (or, equivalently in the integer case, the action in Eq. (4.1)). This essentially follows from the chirality of the theory, but it is instructive to see how this plays out explicitly.[123] However, this does not mean that a given bulk will have only a single edge phase.[65] A quantum Hall system will have additional gapped excitations which we can ignore only if the interactions between them and the gapless excitations in Eq. (4.6) are weak. If they are not weak, however, we cannot ignore them and interactions with these degrees of freedom can lead to an edge phase transition.[124]

We will generally describe the gapped excitations with a K-matrix equal to $\sigma_z = \left(\begin{smallmatrix} 1 & 0 \\ 0 & -1 \end{smallmatrix}\right)$. We may imagine this K-matrix arising from a thin strip of $\nu = 1$ fluid living around the perimeter of our starting Hall state.[65] For edge phase transitions between bosonic edges theories, we should instead take the gapped modes to be described by a K-matrix equal to $\sigma_x = \left(\begin{smallmatrix} 0 & 1 \\ 1 & 0 \end{smallmatrix}\right)$. It is important to realize that the existence of the localized

(gapped) edge modes described by either of these K-matrices implies the appropriate modification to the Chern-Simons theory describing the bulk topological order. This addition does not affect the bulk topological order;[145] without symmetry, such a gapped state is adiabatically connected to a trivial band insulator.

We illustrate this with two concrete examples. We begin with the general edge action

$$S = \int dx\, dt \left( \frac{1}{4\pi} K_{IJ} \partial_t \phi^I \partial_x \phi^J - \frac{1}{4\pi} V_{IJ} \partial_x \phi^I \partial_x \phi^J + \frac{1}{2\pi} t_I \epsilon_{\mu\nu} \partial_\mu \phi^I A_\nu \right). \tag{4.31}$$

The first example is described by the K-matrix

$$K_1 = \begin{pmatrix} 1 & 0 \\ 0 & 11 \end{pmatrix}, \tag{4.32}$$

with $t = (1, -1)^T$. This is not an example that is particularly relevant to quantum Hall states observed in experiments – we will discuss several examples of those in Section 4.7 – but it is simple and serves as a paradigm for the more general structure that we discuss in Sections 4.5 and 4.6.

Let us suppose that we have an additional left-moving and additional right-moving fermion which, together, form a gapped unprotected excitation. The action now takes the form

$$S = \int dx\, dt \left( \frac{1}{4\pi} \left( K_1 \oplus \sigma_z \right)_{IJ} \partial_t \phi^I \partial_x \phi^J - \frac{1}{4\pi} V_{IJ} \partial_x \phi^I \partial_x \phi^J + \frac{1}{2\pi} t_I \epsilon_{\mu\nu} \partial_\mu \phi^I A_\nu \right), \tag{4.33}$$

where we have now extended $t = (1, -1, 1, 1)^T$. The K-matrix for the two additional modes is taken to be $\sigma_z$. We will comment on the relation to the $\sigma_x$ case in Sections 4.4 and 4.5.

If the matrix $V_{IJ}$ is such that the perturbation

$$S' = \int dx\, dt\, u' \cos(\phi_3 + \phi_4), \tag{4.34}$$

is relevant, and if this is the only perturbation added to Eq. (4.33), then the two additional modes become gapped and the system is in the phase (4.32). Suppose, instead, that the only perturbation is

$$S'' = \int dx\, dt\, u'' \cos(\phi_1 - 11\phi_2 + 2\phi_3 + 4\phi_4). \tag{4.35}$$

This perturbation is charge-conserving and spin-zero (i.e., its left and right scaling dimensions are equal). If it is relevant, then the edge is in a different phase. To find this phase, it is helpful to make the basis change:

$$W^T(K_1 \oplus \sigma_z)W = K_2 \oplus \sigma_z, \tag{4.36}$$

where

$$K_2 = \begin{pmatrix} 3 & 1 \\ 1 & 4 \end{pmatrix}, \tag{4.37}$$

and

$$W = \begin{pmatrix} 0 & 0 & 1 & 0 \\ 0 & -2 & 0 & 1 \\ -2 & 3 & 0 & -2 \\ 1 & -7 & 0 & 4 \end{pmatrix}. \tag{4.38}$$

Making the basis change $\phi = W\phi'$, we see that

$$\phi_1 - 11\phi_2 + 2\phi_3 + 4\phi_4 = \phi_3' + \phi_4'. \tag{4.39}$$

Therefore, the resulting phase is described by (4.37).

To see that these are, indeed, different phases, we can compute basis-independent quantities, such as the lowest scaling dimension of any operator in the two theories. In the $K_1$ theory, it is 1/22 while in the $K_2$ theory, it is 3/22. Measurements that probe the edge structure in detail can, thereby, distinguish these two phases of the edge. Consider, first, transport through a QPC that allows tunneling between the two edges of the Hall bar, as described in Sec 4.2.1. In the state governed by $K_1$, the most relevant backscattering term is $\cos(\phi_2^T - \phi_2^B)$. Applying Eq (4.12), the backscattered current will depend on the voltage according to

$$I_1^b \propto V^{-9/11}. \tag{4.40}$$

An alternative probe is given by tunneling into the edge from a metallic lead. The most relevant term in the $K_1$ edge phase that tunnels one electron into the lead is $\psi_{\text{lead}}^\dagger e^{i\phi_1^T}$. Applying Eq (4.14) yields the familiar current-voltage relation,

$$I_1^{\text{tun}} \propto V. \tag{4.41}$$

In contrast, in the phase governed by $K_2$, the most relevant backscattering term across a QPC is given by $\cos(\phi_2'^T - \phi_2'^B)$, which from Eq (4.12) yields the current-voltage relation

$$I_2^b \propto V^{-5/11}, \tag{4.42}$$

while the most relevant single-electron tunneling term is given by $\psi^\dagger_{\text{lead}} e^{-3i\phi_1'^T - i\phi_2'^T}$, which yields the scaling from Eq (4.14)

$$I_2^{\text{tun}} \propto V^3. \tag{4.43}$$

Since the two edge theories given by $K_1$ and $K_2$ are connected by a phase transition just on the edge, we may expect they bound the same bulk Chern-Simons theory. Indeed, the bulk quasiparticles can be identified up to ambiguous signs due to their fermionic nature. First, the discriminant group of the $K_1$ theory is $\mathbb{Z}/11$. We define a quasiparticle basis for this theory as $\psi_j \equiv (-j, -6j)^T, j = 0, 1, \ldots, 10$. (While the cyclic nature of the group $\mathbb{Z}/11$ implies the identification $(a, b) \equiv (a', b')$ mod $(1, 11)$ for $a, b, a', b' \in \mathbb{Z}$, we choose the above basis in order to ensure charge conservation.) The $S$ matrix is given by $S_{jj'} = \frac{1}{\sqrt{11}} e^{-\frac{72\pi i}{11} jj'}$. For the other theory given by $K_2$, the discriminant group obviously has the same structure with the generator being $(0, 1)^T$ and the quasiparticles are denoted by $\psi'_j$. The $S$ matrix is given by $S'_{jj'} = \frac{1}{\sqrt{11}} e^{-\frac{6\pi i}{11} jj'}$. Now we make the following identification:

$$\psi'_j \longleftrightarrow \psi_j. \tag{4.44}$$

This identification preserves the U(1) charge carried by each quasiparticle. The $S$ matrices are also identified:

$$S_{j,j'} = \frac{1}{\sqrt{11}} e^{-\frac{72\pi i}{11} jj'} = \frac{1}{\sqrt{11}} e^{-\frac{6\pi i}{11} jj'} = S'_{jj'}. \tag{4.45}$$

Since the diagonal elements of $S$ are basically $T^2$, it follows that the topological spins are also identified up to $\pm 1$.

Our second example is

$$K_1' = \begin{pmatrix} 1 & 0 \\ 0 & 7 \end{pmatrix}, \tag{4.46}$$

with $t = (1, 1)^T$. As before, we suppose that a non-chiral pair of modes comes down in energy and interacts strongly with the two right-moving modes described by (4.46). The action now takes the form

$$S = \int dx\, dt \left( \frac{1}{4\pi} \left(K_1' \oplus \sigma_z\right)_{IJ} \partial_t \phi^I \partial_x \phi^J - \frac{1}{4\pi} V_{IJ} \partial_x \phi^I \partial_x \phi^J + \frac{1}{2\pi} t_I \epsilon_{\mu\nu} \partial_\mu \phi^I A_\nu \right). \tag{4.47}$$

If the matrix $V_{IJ}$ is such that the perturbation

$$S' = \int dx\, dt\, u' \cos(\phi_3 + \phi_4) \tag{4.48}$$

is relevant and this is the only perturbation added to Eq. (4.47), then the two additional modes become gapped and the system is in the phase in Eq. (4.46). Suppose, instead, the only perturbation is the following:

$$S'' = \int dx\, dt\, u'' \cos(\phi_1 + 7\phi_2 + \phi_3 + 3\phi_4). \tag{4.49}$$

This perturbation is charge-conserving and spin-zero. If it is relevant, then the edge is in a different phase. To find this phase, it is helpful to make the basis change

$$W'^T (K_1' \oplus \sigma_z) W' = K_2' \oplus \sigma_z, \tag{4.50}$$

where

$$K_2' = \begin{pmatrix} 2 & 1 \\ 1 & 4 \end{pmatrix} \tag{4.51}$$

and

$$W' = \begin{pmatrix} 2 & 1 & 0 & -1 \\ 1 & -1 & 0 & -1 \\ 0 & 0 & -1 & 0 \\ -3 & 2 & 0 & 3 \end{pmatrix}. \tag{4.52}$$

Making the basis change $\phi = W'\phi'$, we see that

$$\phi_1 + 7\phi_2 + \phi_3 + 3\phi_4 = \phi_4' - \phi_3'. \tag{4.53}$$

Therefore, the resulting phase is described by (4.51). This is a different phase, as may be seen by noting that the lattice corresponding to Eq. (4.51) is an even lattice while the lattice corresponding to Eq. (4.46) is odd.

The difference between the two edge phases is even more dramatic than in the previous example. One edge phase has gapless fermionic excitations while the other one does not! This example shows that an edge reconstruction can relate a theory with fermionic topological order to one with bosonic topological order. Again, these two edge phases of the $\nu = 8/7$ can be distinguished by the voltage dependence of the current backscattered at a quantum point contact and the tunneling current from a metallic lead. In the $K_1'$ edge phase (4.46), the backscattered current at a QPC is dominated by the tunneling term $\cos(\phi_2^T - \phi_2^B)$; using Eq (4.12) this yields the current-voltage relation

$$I_1^b \propto V^{-5/7}, \tag{4.54}$$

while the single-electron tunneling into a metallic lead is dominated by the tunneling term $\psi^\dagger_{\text{lead}} e^{i\phi_1^T}$, which, using Eq (4.14), yields the familiar linear current-voltage scaling

$$I_1^{\text{tun}} \propto V. \tag{4.55}$$

In the $K_2'$ edge phase (4.51), the backscattered current at a QPC is dominated by the backscattering term $\cos(\phi_2'^T - \phi_2'^B)$, yielding:

$$I_2^b \propto V^{-3/7}. \tag{4.56}$$

The tunneling current from a metallic lead is due to the tunneling of charge-2$e$ objects created by the edge operator $e^{i\phi_1'+4i\phi_2'}$. If we assume that the electrons are fully spin-polarized and $S_z$ is conserved, then the most relevant term that tunnels 2$e$ into the metallic lead is $\psi^\dagger_{\text{lead}}\partial\psi^\dagger_{\text{lead}} e^{i\phi_1'^T+4i\phi_2'^T}$. Using Eq (4.14) the tunneling current is proportional to a very high power of the voltage:

$$I_2^{\text{tun}} \propto V^7. \tag{4.57}$$

Again, although the theories look drastically different, we can show that the bulk $S$ matrices are isomorphic. First, the discriminant group of the $K_1'$ theory is $\mathbb{Z}/7$ whose generator we can take to be the $(0, 4)$ quasiparticle. We label all quasiparticles in this theory as $\psi_j \equiv (0, 4j), j = 0, 1, \ldots, 6$. The $S$ matrix is given by $S_{jj'} = \frac{1}{\sqrt{7}} e^{-\frac{32\pi i}{7} jj'}$. For the other theory given by $K_2'$, the discriminant group is generated by $(0, 1)^T$ and we denote the quasiparticles by $\psi_j'$. The $S$ matrix is given by $S'_{jj'} = \frac{1}{\sqrt{7}} e^{-\frac{4\pi i}{7} jj'}$. Now we

make the following identification:

$$\psi'_j \longleftrightarrow \psi_j. \tag{4.58}$$

The $S$ matrices are then seen to be identical:

$$S_{j,j'} = \frac{1}{\sqrt{7}} e^{-\frac{32\pi i}{7} jj'} = \frac{1}{\sqrt{7}} e^{-\frac{4\pi i}{7} jj'} = S'_{jj'}. \tag{4.59}$$

## 4.4 Edge Phase Transitions

In the previous section, we gave two simple examples of edge phase transitions that can occur between two distinct chiral theories. In this section, we discuss how edge transitions can occur in full generality.

The chiral Luttinger liquid action is stable against all perturbations involving only the gapless fields in the action in Eq. (4.6) (or, equivalently in the integer case, the action in Eq. (4.1)). However, as we have seen in the previous section, strong interactions with gapped excitations can drive a phase transition that occurs purely at the edge. While the bulk is completely unaffected, the edge undergoes a transition into another phase.

On the way to understanding this in more generality, we first consider an integer quantum Hall state. At the edge of such a state, we expect additional gapped excitations that we ordinarily ignore. However, they can interact with gapless excitations. (Under some circumstances, they can even become gapless.[65]) Let us suppose that we have an additional left-moving and and additional right-moving fermion which, together, form a

gapped unprotected excitation. Then additional terms must be considered in the action. Let us first consider the case of an integer quantum Hall edge. The action in Eqs. (4.1) and (4.2) becomes $S_0 + S_1 + S_u$ with

$$S_u = \int dx\, dt \Big( \psi^\dagger_{N+1} \left( i\partial_t + v_{N+1} i\partial_x \right) \psi_{N+1} + \psi^\dagger_{N+2} \left( i\partial_t - v_{N+2} i\partial_x \right) \psi_{N+2} + u \psi^\dagger_{N+1} \psi_{N+2} + v_{I,N+1} \psi^\dagger_I \psi_I \psi^\dagger_{N+1} \psi_{N+1} + v_{I,N+2} \psi^\dagger_I \psi_I \psi^\dagger_{N+2} \psi_{N+2} + h.c. + \mathcal{L}_{N,L} \Big), \quad (4.60)$$

where $\psi_{N+1}$, $\psi_{N+2}$ annihilate right- and left-moving excitations which have an energy gap $u$ for $v_{I,N+1} = v_{I,N+2} = 0$. So long as $v_{I,N+1}$ and $v_{I,N+2}$ are small, this energy gap survives, and we can integrate out $\psi_{N+1}$, $\psi_{N+2}$, thereby recovering the action $S_0 + S_1$ in Eqs. (4.1) and (4.2), but with the couplings renormalized. However, if $v_{I,N+1}$ and $v_{I,N+2}$ are sufficiently large, then some of the other terms in the action, which we have denoted by $\mathcal{L}_{N,L}$ in Eq. (4.60) may become more relevant than $u$. These include terms such as

$$\mathcal{L}_{N,L} = u_I \psi^\dagger_I \psi_{N+2} + \text{h.c.} + \ldots . \quad (4.61)$$

In order to understand these terms better, it is helpful to switch to the bosonic representation, where there is no additional overhead involved in considering the general case of a chiral Abelian state, integer or fractional:

$$S = \int dx\, dt \Big( \frac{1}{4\pi} \left( K \oplus \sigma_z \right)_{IJ} \partial_t \phi^I \partial_x \phi^J - \frac{1}{4\pi} V_{IJ} \partial_x \phi^I \partial_x \phi^J + \sum_{m_I} u_{m_I} \cos\left( m_I \phi^I \right) + \frac{1}{2\pi} \sum_I \epsilon_{\mu\nu} \partial_\mu \phi^I A_\nu \Big). \quad (4.62)$$

Here, $I = 1, 2, \ldots, N+2$; and $(K \oplus \sigma_z)_{IJ}$ is the direct sum of $K$ and $\sigma_z$: $(K \oplus \sigma_z)_{IJ} = K_{IJ}$ for $I = J = 1, 2, \ldots, N$, $(K \oplus \sigma_z)_{IJ} = 1$ for $I = J = N+1$, $(K \oplus \sigma_z)_{IJ} = -1$ for $I = J = N+2$, and $(K \oplus \sigma_z)_{IJ} = 0$ if $I \in \{1, 2, \ldots, N\}$, $J \in \{N+1, N+2\}$ or vice-versa. The interaction matrix has $V_{I,N+1} \equiv v_{I,N+1}$, $V_{I,N+2} \equiv v_{I,N+2}$. The $m^I$s must be integers because the $\phi^I$s are periodic. For instance, $m_I = (0, 0, \ldots, 0, 1, -1)$ corresponds to the mass term $u(\psi^\dagger_{N+1}\psi_{N+2} + \text{h.c.})$ in Eq. (4.60), so $u_{m_I} = u$. In the last term, we are coupling all modes equally to the electromagnetic field, i.e. this term can be written in the form $t_I \epsilon_{\mu\nu}\partial_\mu \phi^I A_\nu$ with $t_I = 1$ for all $I$. This is the natural choice, since we expect additional fermionic excitations to carry electrical charge $e$.

In general, most of the couplings $u_{m_I}$ will be irrelevant at the Gaussian fixed point. An irrelevant coupling cannot open a gap if it is small enough to remain in the basin of attraction of the Gaussian fixed point. However, if we make the coupling large enough, it may be in the basin of attraction of another fixed point and it may open a gap. We will not comment more on this possibility here. However, we can imagine tuning the $V_{IJ}$s so that any given $u_{m_I}$ is relevant. To analyze this possibility, it is helpful to change to the variables $X^a = e^a_I \phi^I$, in terms of which the action takes the form

$$S = \int dx\, dt \Bigg( \frac{1}{4\pi}\eta_{ab}\partial_t X^a \partial_x X^b - \frac{1}{4\pi} v_{ab}\partial_x X^a \partial_x X^b + \sum_{m_I} u_{m_I} \cos\left(m_I f^I_a X^a\right) + \frac{1}{2\pi}\sum_I f^J_a \epsilon_{\mu\nu}\partial_\mu X^a A_\nu. \Bigg) \quad (4.63)$$

$e_I^a$ and $f_a^I$ are bases for the lattice $\Lambda_{N+2}$ and its dual $\Lambda_{N+2}^*$, where the lattice $\Lambda_{N+2}$ corresponds to $K \oplus \sigma_z$. The variables $X^a$ satisfy the periodicity condition $\mathbf{X} \equiv \mathbf{X} + 2\pi\mathbf{y}$ for $\mathbf{y} \in \Lambda_{N+2}$. Note that, since one of the modes is left-moving, the Lorentzian metric $\eta_{ab} = \mathrm{diag}(\mathbf{1}_{N-1}, -1)$ appears in Eq. (4.63).

Since $f_a^I$ is a basis of the dual lattice $\Lambda_{N+2}^*$, the cosine term can also be written in the form

$$\sum_{\mathbf{v} \in \Lambda_{N+2}^*} u_{\mathbf{v}} \cos\left(\mathbf{v} \cdot \mathbf{X}\right).$$

The velocity/interaction matrix is given by $v_{ab} = V_{IJ} f_a^I f_b^J$. Now suppose that the velocity/interaction matrix takes the form

$$v_{ab} = v\, O^c{}_a \delta_{cd} O^d{}_b, \tag{4.64}$$

where $O \in \mathrm{SO}(N+1, 1)$. Then we can make a change of variables to $\tilde{X}^a \equiv O^a{}_b X^b$. We specialize to the case of a single cosine perturbation associated with a particular vector in the dual lattice $\mathbf{v}_0 \equiv p_I \mathbf{f}^I$ which we will make relevant (we have also set $A_\nu = 0$ since it is inessential to the present discussion). Now Eq. (4.63) takes the form

$$S = \frac{1}{4\pi} \int dx\, dt \left( \eta_{ab} \partial_t \tilde{X}^a \partial_x \tilde{X}^b - v \delta_{ab} \partial_x \tilde{X}^a \partial_x \tilde{X}^b + u_{\mathbf{v}_0} \cos\left( p_I f_a^I (O^{-1})^a{}_b \tilde{X}^b \right) \right). \tag{4.65}$$

If this perturbation has equal right and left scaling dimensions (i.e., is spin-zero), then its scaling dimension is simply twice its left scaling dimension with corresponding beta function

$$\frac{du_{\mathbf{v}_0}}{d\ell} = \left(2 - q_{N+2}^2\right) u_{\mathbf{v}_0}, \tag{4.66}$$

where $q_b \equiv p_I f_a^I (O^{-1})^a{}_b$. The transformation $O^{-1}$ can be chosen to be a particular boost in the $(N+2)$-dimensional space $\mathbb{R}^{N+1,1}$. Because $q_a$ is a null vector (i.e., a light-like vector) in this space, by taking the boost in the opposite direction of the "spatial" components of $q_a$, we can "Lorentz contract" them, thereby making $q_{N+2}$ as small as desired. Thus, by taking $v_{ab}$ of the form (4.64) and choosing $O \in \mathrm{SO}(N+1,1)$ so that $q_{N+2}^2 < 2$, we can make this coupling relevant.

When this occurs, two modes, one right-moving and one left-moving, will acquire a gap. We will then be left over with a theory with $N$ gapless right-moving modes. The gapless excitations $\exp(i\mathbf{v}\cdot\mathbf{X})$ of the system must commute with $\mathbf{v}_0 \cdot \mathbf{X}$ and, since the cosine fixes $\mathbf{v}_0 \cdot \mathbf{X}$, any two excitations that differ by $\mathbf{v}_0 \cdot \mathbf{X}$ should be identified. Thus, the resulting low-energy theory will be associated with the lattice $\Gamma$ defined by $\Gamma \equiv \Lambda_\perp / \Lambda_\parallel$, where $\Lambda_\perp, \Lambda_\parallel \subset \Lambda_{N+2}$ are defined by $\Lambda_\perp \equiv \{\mathbf{v} \in \Lambda_{N+2} \,|\, \mathbf{v}\cdot\mathbf{v}_0 = 0\}$ and $\Lambda_\parallel \equiv \{n\mathbf{v}_0 \,|\, n \in \mathbb{Z}\}$. If $\mathbf{g}_I$ is a basis for $\Gamma$, then we can define a K-matrix in this basis, $\tilde{K}_{IJ} = \mathbf{g}_I \cdot \mathbf{g}_J$. The low-energy effective theory for the gapless modes is

$$S \;=\; \int dx\, dt \left( \frac{1}{4\pi} \tilde{K}_{IJ} \partial_t \phi^I \partial_x \phi^J \;-\; \frac{1}{4\pi} \tilde{V}_{IJ} \partial_x \phi^I \partial_x \phi^J \;+\; \frac{1}{2\pi} \tilde{t}_I \epsilon_{\mu\nu} \partial_\mu \phi^I A_\nu \right). \quad (4.67)$$

When $\mathbf{v}_0 = (0, 0, \ldots, 0, 1, -1)$ is the only relevant operator, $\phi^{N+1}$ and $\phi^{N+2}$ are gapped out. Therefore, $\Gamma = \Lambda$ and $\tilde{K}_{IJ} = K_{IJ}$. However, when other operators are present, $\Gamma$ could be a different lattice $\Gamma \ncong \Lambda$, from which it follows that $\tilde{K}_{IJ} \neq K_{IJ}$ (and, $\tilde{K} \neq W^T K W$ for any $W$).

We motivated the enlargement of the theory from $K$ to $K \oplus \sigma_z$ by assuming that an additional pair of gapped counter-propagating fermionic modes comes down in energy and interacts strongly with the gapless edge excitations. This counter-propagating pair of modes can be viewed as a thin strip of $\nu = 1$ integer quantum Hall fluid or, simply, as a fermionic Luttinger liquid. Of course, more than one such pair of modes may interact strongly with the gapless edge excitations, so we should also consider enlarging the K-matrix to $K \oplus \sigma_z \oplus \sigma_z \ldots \oplus \sigma_z$. We can generalize this by imagining that we can add any one-dimensional system to the edge of a quantum Hall state. (This may not be experimentally-relevant to presently observed quantum Hall states, but as a matter of principle, this is something that could be done without affecting the bulk, so we should allow ourselves this freedom.) Any clean, gapless 1D system of fermions is in a Luttinger liquid phase (possibly with some degrees of freedom gapped). Therefore, $K \oplus \sigma_z \oplus \sigma_z \ldots \oplus \sigma_z$ is actually the most general possible form for the edge theory.

One might wonder about the possibility of attaching a thin strip of a fractional quantum Hall state to the edge of the system. Naively, this would seem to be a generalization of our putative most general form $K \oplus \sigma_z \oplus \sigma_z \ldots \oplus \sigma_z$. To illustrate the issue, let us consider a bulk $\nu = 1$ IQH state and place a thin strip of $\nu = 1/9$ FQH state at its edge. The two edges that are in close proximity can be described by the following K-matrix:

$$K = \begin{pmatrix} 1 & 0 \\ 0 & -9 \end{pmatrix}. \tag{4.68}$$

As discussed in Ref. 131, this edge theory can become fully gapped with charge-non-conserving backscattering. Then we are left with the outer chiral edge of the thin strip, which is described by $K = (9)$, which can only bound a topologically ordered $\nu = 1/9$ Laughlin state. The subtlety here is that a thin strip of the fractional quantum Hall state has no two-dimensional bulk and should be considered as a purely one-dimensional system. Fractionalized excitations, characterized by fractional conformal spins only make sense when a true 2D bulk exists. If the width of the strip is small, so that there is no well-defined bulk between them, then we can only allow operators that add an integer number of electrons to the two edges. We cannot add fractional charge since there is no bulk which can absorb compensating charge. Thus the minimal conformal spin of any operator is 1/2. In other words, starting from an one-dimensional interacting electronic system, one cannot change the conformal spin of the electron operators. So attaching a thin strip of FQH state is no different from attaching a trivial pair of modes.

In a bosonic system, we cannot even enlarge our theory by a pair of counter-propagating fermionic modes. We can only enlarge our theory by a Luttinger liquid of bosons or, equivalently, a thin strip of $\sigma_{xy} = \frac{2e^2}{h}$ bosonic integer quantum hall fluid.[131,133,148] Such a system has K-matrix equal to $\sigma_x$, which only has bosonic excitations. Equivalently, bosonic systems must have even $K$-matrices – matrices with only even numbers along the diagonal – because all particles that braid trivially with every other particle must be a boson. Since the enlarged matrix must have the same de-

terminant as the original one because the determinant is the ground state degeneracy of the bulk phase on the torus,[137] we can only enlarge the theory by $\sigma_x$, the minimal even unimodular matrix. Therefore, in the bosonic case, we must enlarge our theory by $K \to K \oplus \sigma_x$.

In the fermionic case, we must allow such an enlargement by $\sigma_x$ as well. We can imagine the fermions forming pairs and these pairs forming a bosonic Luttinger liquid which enlarges $K$ by $\sigma_x$. In fact, it is redundant to consider both $\sigma_z$ and $\sigma_x$: for an odd matrix $K$, $W(K \oplus \sigma_z)W^T = K \oplus \sigma_x$, where

$$W = \begin{pmatrix} 1 & 0 & \cdots & 0 & y_1 & -y_1 \\ 0 & 1 & \cdots & 0 & y_2 & -y_2 \\ \vdots & \vdots & \vdots & \vdots & \vdots & \vdots \\ 0 & 0 & \cdots & 1 & y_N & -y_N \\ 0 & 0 & \cdots & 0 & 1 & -1 \\ x_1 & x_2 & \cdots & x_N & s & 1-s \end{pmatrix} \tag{4.69}$$

Here the vector $\vec{x}$ has an odd length squared, i.e. $\vec{x}^T K \vec{x}$ is odd; by definition of $K$ odd, such an $\vec{x}$ must exist. The vector $\vec{y}$ is defined as $\vec{y} = -K\vec{x}$ and the integer $s$ by $s = \frac{1}{2}(1 - \vec{x}^T K \vec{x})$. Thus $K \oplus \sigma_x$ is $\mathrm{GL}(N+2, \mathbb{Z})$-equivalent to $K \oplus \sigma_z$ and our previous discussion for fermionic systems could be redone entirely with extra modes described by $\sigma_x$. However, if $K$ is even, then $K \oplus \sigma_x$ is not $\mathrm{GL}(N+2, \mathbb{Z})$-equivalent to $K \oplus \sigma_z$.

We remark that although $\sigma_z$ enlargement and $\sigma_x$ enlargement are equivalent for fermionic states when topological properties are concerned, they do make a difference in charge vectors: the appropriate charge vector for the $\sigma_z$ block should be odd and

typically taken to be $(1,1)^T$. However the charge vector for the $\sigma_x$ block must be even and needs to be determined from the similarity transformation.

To summarize, a quantum Hall edge phase described by matrix $K_1$ can undergo a purely edge phase transition to another edge phase with $\mathrm{GL}(N,\mathbb{Z})$-inequivalent $K_2$ (with identical bulk) if there exists $\tilde{W} \in \mathrm{GL}(N+2k,\mathbb{Z})$ such that

$$K_2 \oplus \sigma_x \oplus \ldots \oplus \sigma_x = \tilde{W}^T \left(K_1 \oplus \sigma_x \oplus \ldots \oplus \sigma_x\right) \tilde{W}. \tag{4.70}$$

for some number $k$ of $\sigma_x$s on each side of the equation. In a fermionic system with $K_1$ odd, an edge phase transition can also occur to an even matrix $K_2$ if

$$K_2^{\mathrm{even}} \oplus \sigma_z \oplus \ldots \oplus \sigma_x = \tilde{W}^T \left(K_1^{\mathrm{odd}} \oplus \sigma_x \oplus \ldots \oplus \sigma_x\right) \tilde{W}. \tag{4.71}$$

## 4.5 Stable Equivalence, Genera of Lattices, and the Bulk-Edge Correspondence for Abelian Topological Phases

### 4.5.1 Stable Equivalence and Genera of Lattices

In the previous section, we saw that a bulk Abelian quantum Hall state associated with $K_1$ has more than one different stable chiral edge phase if there exists $\mathrm{GL}(N,\mathbb{Z})$-

inequivalent $K_2$ and $\tilde{W} \in \mathrm{GL}(N+2k, \mathbb{Z})$ such that

$$K_2 \oplus \sigma_x \oplus \ldots \oplus \sigma_x = \tilde{W}^T \left(K_1 \oplus \sigma_x \oplus \ldots \oplus \sigma_x\right) \tilde{W}. \tag{4.72}$$

This is an example of a stable equivalence; we say that $K_1$ and $K_2$ are *stably equivalent* if, for some $n$, there exist signature $(n,n)$ unimodular matrices $L_i$ such that $K_1 \oplus L_1$ and $K_2 \oplus L_2$ are *integrally equivalent*, i.e. are $\mathrm{GL}(N+2n, \mathbb{Z})$-equivalent. If there is a choice of $L_i$s such that both are even, we will say that $K_1$ and $K_2$ are "$\sigma_x$-stably equivalent" since the $L_i$s can be written as direct sums of $\sigma_x$s. We also saw in Eq. 4.71 that when $K_1$ is odd and $K_2$ is even, we will need $L_2$ to be an odd matrix. We will call this "$\sigma_z$-stable equivalence" since $L_2$ must contain a $\sigma_z$ block. We will use $U$ to denote the signature $(1,1)$ even Lorentzian lattice associated with $\sigma_x$. Then $\sigma_x$-stable equivalence can be restated in the language of lattices as follows. Two lattices $\Lambda_1$, $\Lambda_2$ are $\sigma_x$-stably equivalent if $\Lambda_1 \oplus U \cdots \oplus U$, and $\Lambda_2 \oplus U \cdots \oplus U$ are isomorphic lattices. Similarly, $U_z$ will denote the Lorentzian lattice associated with $\sigma_z$. Occasionally, we will abuse notation and use $\sigma_x$ and $\sigma_z$ to refer to the corresponding lattices $U$, $U_z$.

Stable equivalence means that the two $K$-matrices are equivalent after adding "trivial" degrees of freedom – i.e. purely 1D degrees of freedom that do not require any change to the bulk. This is analogous to the notion of stable equivalence of vector bundles, according to which two vector bundles are stably equivalent if and only if isomorphic bundles are obtained upon joining them with trivial bundles.

We now introduce the concept of the *genus* of a lattice or integral quadratic form. Two integral quadratic forms are in the same *genus*[143,149] when they have the same signature and are equivalent over the *p-adic integers* $\mathbb{Z}_p$ for every prime $p$. Loosely speaking, equivalence over $\mathbb{Z}_p$ can be thought of as equivalence modulo arbitrarily high powers of $p$, i.e. in $\mathbb{Z}/p^n$ for every $n$. The importance of genus in the present context stems from the following statement of Conway and Sloane:[143]

*Two integral quadratic forms $K_1$ and $K_2$ are in the same genus if and only if $K_1 \oplus \sigma_x$ and $K_2 \oplus \sigma_x$ are integrally equivalent.*

Proofs of this statement are, however, difficult to pin down in the literature. It follows, for instance, from results in Ref. 149 about a refinement of the genus called the spinor genus. Below, we show how it follows in the even case from results stated by Nikulin.[144] This characterization of the genus is nearly the same as the definition of $\sigma_x$-stable equivalence given in (4.72), except that Eq. (4.72) allows multiple copies which is natural since a physical system may have access to multiple copies of trivial degrees of freedom. Its relevance to our situation follows from the following theorem that we demonstrate below:

*Two $K$-matrices $K_1$ and $K_2$ of the same dimension, signature and type are stably equivalent if and only if $K_1 \oplus \sigma_x$ and $K_2 \oplus \sigma_x$ are integrally equivalent, i.e. only a single copy of $\sigma_x$ is needed in Eq. (4.72).*

Thus any edge phase that can be reached via a phase transition involving multiple sets of trivial 1D bosonic degrees of freedom (described by K-matrix $\sigma_x$) can also be reached through a phase transition involving only a single such set. We demonstrate this by appealing to the following result stated by Nikulin[144] (which we paraphrase but identify by his numbering):

Corollary 1.16.3: *The genus of a lattice is determined by its discriminant group $A$, parity, signature $(r_+, r_-)$, and bilinear form $b$ on the discriminant group.*

Since taking the direct sum with multiple copies of $\sigma_x$ does not change the parity, or bilinear form on the discriminant group, any $K_1$ and $K_2$ that are $\sigma_x$-stably equivalent are in the same genus. The theorem then follows from the statement[143] above that only a single copy of $\sigma_x$ is needed.

In the even case, the theorem follows directly from two other results by Nikulin:[144]

Corollary 1.13.4: *For any even lattice $\Lambda$ with signature $(r_+, r_-)$ and discriminant quadratic form $q$, the lattice $\Lambda \oplus U$ is the only lattice with signature $(r_+ + 1, r_- + 1)$ and quadratic form $q$.*

Theorem 1.11.3: *Two quadratic forms on the discriminant group are isomorphic if and only if their bilinear forms are isomorphic and they have the same signature* (mod 8).

If lattices $\Lambda_1$ and $\Lambda_2$ are in the same genus, they must have the same $(r_+, r_-)$ and bilinear form $b$. According to Theorem 1.11.3, they must have the same quadratic form,

namely $q([\mathbf{x}]) = \frac{1}{2}b([\mathbf{x}],[\mathbf{x}])$, which is well-defined in the case of an even lattice. Then, Corollary 1.13.4 tells us that $\Lambda_1 \oplus U$ is the unique lattice with signature $(r_+ + 1, r_- + 1)$ and quadratic form $q$. Since $\Lambda_2 \oplus U$ has the same signature $(r_+ + 1, r_- + 1)$ and quadratic form $q$, $\Lambda_1 \oplus U \cong \Lambda_2 \oplus U$. Thus, we see that any two even $K$-matrices in the same genus are integrally-equivalent after taking the direct sum with a single copy of $\sigma_x$. Of course, our previous arguments that used Nikulin's Corollary 1.16.3 and the characterization of genus from Conway and Sloane[143] are stronger since they apply to odd matrices.

### 4.5.2 Bulk-Edge Correspondence

Since the quadratic form $q([\vec{u}])$ gives the $T$ and $S$ matrices according to Eqs. (4.23) and (4.25), we can equally-well say that the genus of a lattice is completely determined by the particle types, $T$-matrix, $S$-matrix, and right- and left-central charges. For a bosonic system, the genus completely determines a bulk phase. Conversely, a bulk topological phase almost completely determines a genus: the bulk phase determines $(c_+ - c_-)$ mod 24 while a genus is specified by $(c_+, c_-)$. However, if the topological phase is fully chiral, so that it can have $c_- = 0$, then it fully specifies a family of genera that differ only by adding central charges that are a multiple of 24, i.e. $3k$ copies of the $E_8$ state for some integer $k$ (see Section 4.7.1 for a discussion of this state). Thus, up to innocuous shifts of the central charge by 24, we can say that

*A bulk bosonic topological phase corresponds to a genus of even lattices while its edge phases correspond to the different lattices in this genus.*

The problem of detemining the different stable edge phases that can occur for the same bosonic bulk is then the problem of determining how many distinct lattices there are in a genus.

In the fermionic case, the situation is more complicated. A fermionic topological phase is determined by its particle types, its $S$-matrix, and its central charge (mod 24). It does not have a well-defined $T$-matrix because we can always change the topological twist factor of a particle by $-1$ simply by adding an electron to it. According to the following result of Nikulin, these quantities determine an odd lattice:

Corollary 1.16.6: *Given a finite Abelian group $A$, a bilinear form $b : A \times A \to \mathbb{Q}/\mathbb{Z}$, and two positive numbers $(r_+, r_-)$, then, for sufficiently large $r_+, r_-$, there exists an odd lattice for which $A$ is its discriminant group. $b$ is the bilinear form on the discriminant group, and $(r_+, r_-)$ is its signature.*

Since the $S$-matrix defines a bilinear form on the Abelian group of particle types, this theorem means that the quantities that specify a fermionic Abelian topological phase are compatible with an odd lattice. Clearly, they are also compatible with an entire genus of odd lattices since $\sigma_x$ stable equivalence preserves these quantities. Moreover, by Corollary 1.16.3, there is only a single genus of odd lattices that are compatible with

this bulk fermionic Abelian topological phase. However, Corollary 1.16.3 leaves open the possibility that there is also a genus of even lattices that is compatible with this fermionic bulk phase, a possibility that was realized in one of the examples in Section 4.3. This possibility is discussed in detail in Section 4.6. However, the general result that we can already state, up to shifts of the central charge by 24 is

*A bulk fermionic topological phase corresponds to a genus of odd lattices while its edge phases correspond to the different lattices in this genus and, in some cases (specificed in Section 4.6), to the different lattices in an associated genus of even lattices.*

In principle, one can determine how many lattices there are in a given genus by using the Smith-Siegel-Minkowski mass formula[143] to evaluate the weighted sum

$$\sum_{\Lambda \in g} \frac{1}{|\mathrm{Aut}(\Lambda)|} = m(K) \tag{4.73}$$

over the equivalence classes of lattices in a given genus $g$. Each equivalence class of forms corresponds to a lattice $\Lambda$. The denominator is the order of the automorphism group $\mathrm{Aut}(\Lambda)$ of the lattice $\Lambda$. The right-hand-side is the *mass* of the genus of $K$, which is given by a complicated but explicit formula (see Ref. 143).

Given a K-matrix for a bosonic state, one can compute the size of its automorphism group[3], which gives one term in the sum in (4.73). If this equals the mass formula on the right-hand-side of Eq. (4.73), then it means the genus has only one equivalence class.

[3]For generic K-matrices without any symmetries, the automorphism group often only consists of two elements: $W = \pm I_{N\times N}$.

If not, we know there is more than one equivalence class in the genus. Such a program shows[150] that, in fact, all genera contain more than one equivalence class for $N > 10$, i.e. all chiral Abelian quantum Hall states with central charge $c > 10$ have multiple distinct stable chiral edge phases. For $3 \leq N \leq 10$, there is a finite set of genera with only a single equivalence class;[151] all others have multiple equivalence classes. The examples of $\nu = 16$ analyzed in Ref. 124 and $\nu = 12/23$ that we gave in Section 4.7 are, in fact, the rule. Bosonic chiral Abelian quantum Hall states with a single stable chiral edge phase are the exception, they can only exist for $c \leq 10$ and they have been completely enumerated.[151]

This does not tell us how, given one equivalence class, to find other equivalence classes of $K$-matrices in the same genus. However, one can use the Gauss reduced form[143] to find all quadratic forms of given rank and determinant by brute force. Then we can use the results at the end of previous Section to determine if the resulting forms are in the same genus.

### 4.5.3 Primary Decomposition of Abelian Topological Phases

According to the preceding discussion, two distinct edge phases can terminate the same bulk phase if they are both in the same genus (but not necessarily only if they are in the same genus in the fermionic case). It may be intuitively clear what this means, but it is useful to be more precise about what we mean by "the same bulk phase". In

more physical terms, we would like to be more precise about what it means for two theories to have the same particle types and $S$- and $T$-matrices. In more formal terms, we would like to be more precise about what is meant in Nikulin's Theorem 1.11.3 by isomorphic quadratic forms and bilinear forms. In order to do this, it helps to view an Abelian topological phase in a somewhat more abstract light. When viewed from the perspective of an edge phase or, equivalently, a K-matrix, the bulk phase is determined by the signature $(r_+, r_-)$, together with the bilinear form on the discriminant group $\Lambda^*/\Lambda$ induced by the bilinear form on the dual lattice $\Lambda^*$ determined by $K$. As we have seen, this data uniquely specifies a nondegenerate quadratic form $q\colon \Lambda^*/\Lambda \to \mathbb{Q}/\mathbb{Z}$ on the discriminant group. Therefore, we may view the genus more abstractly in terms of an arbitrary finite Abelian group $A$ and a quadratic form $q\colon A \to \mathbb{Q}/\mathbb{Z}$, making no direct reference to an underlying lattice. We will sometimes call such a quadratic form a *finite* quadratic form to emphasize that its domain is a finite Abelian group. The elements of the group $A$ are the particle types in the bulk Abelian topological phase.

Now suppose we have two bulk theories associated with Abelian groups $A$, $A'$, quadratic forms $q\colon A \to \mathbb{Q}/\mathbb{Z}$, $q'\colon A' \to \mathbb{Q}/\mathbb{Z}$ and chiral central charges $c_-$, $c'_-$. These theories are the same precisely when the chiral central charges satisfy $c_- \equiv c'_- \mod 24$, and when the associated quadratic forms are *isomorphic*. This latter condition means that there exists a group isomorphism $f\colon A' \to A$ such that $q' = q \circ f$. Note that if the quadratic forms are isomorphic then the chiral central charges must be equal (mod 8)

according to the Gauss-Milgram sum. However, the bulk theories are the same only if they satisfy the stricter condition that their central charges are equal modulo 24.

The implications of this become more apparent after observing that any Abelian group factors as a direct sum $A \simeq \oplus_p A_p$ over primes dividing $|A|$, where $A_p \subset A$ is the *p-primary* subgroup of elements with order a power of $p$. Any isomorphism $f\colon A' \to A$ must respect this factorization by decomposing as $f = \oplus_p f_p$, with each $f_p\colon A'_p \to A_p$. Furthermore, every finite quadratic form decomposes into a direct sum $q = \oplus_p q_p$ of *p-primary* forms; we call $q_p$ the *p-part* of $q$. This ultimately leads to a physical interpretation for $p$-adic integral equivalence: if $p$ is odd, two K-matrices are $p$-adically integrally equivalent precisely when the $p$-parts of their associated quadratic forms are isomorphic. Additional subtleties arise when $p = 2$ but, as we will see, these are the reason for the distinction between $\sigma_x$- and $\sigma_z$-equivalence.

The image of a given finite quadratic form $q$ is a finite cyclic subgroup $N_q^{-1}\mathbb{Z}/\mathbb{Z} \subset \mathbb{Q}/\mathbb{Z}$ isomorphic to $\mathbb{Z}/N_q$, where $N_q$ is the *level* of the finite quadratic form $q$. The level is the smallest integer $N$ such that $q$ factors through $\mathbb{Z}/N$, implying that the topological spins of particles in $A_q$ are $N_q$th roots of unity. Because the level of the direct sum of finite quadratic forms is the least common multiple of the levels of the summands, the level of $q = \oplus_p q_p$ is equal to the product $N_q = \prod_p N_{q_p}$ of the levels of the $q_p$. If $p$ is odd, the level of $q_p$ is the order of the largest cyclic subgroup of $A_p$, while it is typically twice as big for $q_2$. Physically, this means that the entire theory uniquely factors into a

tensor product of anyon theories such that the topological spins of the anyons in the $p$th theory are $p$th-power roots of unity. This decomposition lets us express a *local-to-global principle* for finite quadratic forms: $q$ and $q'$ are isomorphic iff $q_p$ and $q'_p$ are for every $p$. Indeed, if one views prime numbers as "points" in an abstract topological space[4], this principle says that $q$ and $q'$ are *globally equivalent* (at all primes) iff they are locally equivalent at each prime dividing $|A|$.

Further information about the prime theories is obtained by decomposing each $A_p$ into a product

$$A_p \simeq \prod_{m=0}^{m_p} (\mathbb{Z}/p^m)^{d_{p^m}} \tag{4.74}$$

of cyclic groups, where $d_{p^0}, \ldots, d_{p^{m_p-1}} \geq 0$ and $d_{p^{m_p}} > 0$. When $p$ is odd, there is a 1-1 correspondence between bilinear and quadratic forms on $A_p$ because multiplication by 2 is invertible in every $\mathbb{Z}/p^m$. Furthermore, given a quadratic form $q_p$ on $A_p$ for odd $p$, we claim there always exists an automorphism $g \in \mathrm{Aut}(A_p)$ that fully diagonalizes $q_p$ relative to a fixed decomposition (4.74) such that

$$q_p \circ g = \bigoplus_m \big( \underbrace{q^+_{p^m} \oplus \ldots \oplus q^+_{p^m} \oplus q^{\pm}_{p^m}}_{d_{p^m} \text{ terms}} \big), \tag{4.75}$$

where

$$q^+_{p^m}(x) = \frac{1}{p^m} 2^{-1} x^2 \bmod \mathbb{Z},$$

[4]This space is known as $\mathrm{Spec}(\mathbb{Z})$. Rational numbers are identified with functions on this space according to their prime factorizations.

$$q^-_{p^m}(x) = \frac{1}{p^m} u_p 2^{-1} x^2 \bmod \mathbb{Z}$$

and $u_p$ is some fixed non-square modulo $p^n$. A dual perspective is that, given $q_p$, it is always possible to choose a decomposition (4.74) of $A_p$ relative to which $q_p$ has the form of the right-hand-side of (4.75). However, not every decomposition will work for a given $q_p$ because $\mathrm{Aut}(A_p)$ can mix the different cyclic factors. For example, $\mathrm{Aut}((\mathbb{Z}/p)^d) \simeq \mathrm{GL}(d, \mathbb{Z}/p)$ mixes the cyclic factors of order $p$. There will also be automorphisms mixing lower-order generators with ones of higher order, such as the automorphism of $\mathbb{Z}/3 \oplus \mathbb{Z}/9 = \langle \alpha_3, \alpha_9 \rangle$ defined on generators by $\alpha_3 \mapsto \alpha_3$ and $\alpha_9 \mapsto \alpha_3 + \alpha_9$. Physically, this means that the anyon theory associated to $A_p$ further decomposes into a tensor product of "cyclic" theories, although now such decompositions are not unique because one can always redefine the particle types via automorphisms of $A_p$.

### 4.5.4 $p$-adic Symbols

Two K-matrices are $p$-adically integrally equivalent iff the diagonalizations of the $p$-parts of their associated finite quadratic forms coincide. The numbers $d_{p^m}$ and the sign of the last form in the $m$th block thus form a complete set of invariants for $p$-adic integral equivalence of K-matrices. This data is encoded into the *$p$-adic symbol*, which is written as $1^{\pm d_{p^0}} p^{\pm d_{p^1}} (p^2)^{\pm d_{p^2}} \cdots$ (terms with $d_{p^m} = 0$ are omitted) and can

be computed using Sage.[152] Two K-matrices are $p$-adically integrally equivalent iff their $p$-adic symbols coincide.

The $p$-adic symbol can be computed more directly by noting that K-matrices are equivalent over the $p$-adic integers when they are equivalent by a *rational* transformation whose determinant and matrix entries do not involve dividing by $p$. Such transformations can be reduced modulo arbitrary powers of $p$ and give rise to automorphisms of the $p$-part $A_p$ of the discriminant group. Given a K-matrix $K$, there always exists a $p$-adically integral transformation $g$ putting $K$ into *$p$-adically block diagonalized*[143] form

$$gKg^T = K_{p^0} \oplus pK_{p^1} \oplus p^2K_{p^2} \oplus \cdots , \tag{4.76}$$

where $\det(K_{p^m})$ is prime to $p$ for every $m$.

A more direct characterization of the genus can now be given: Two K-matrices are in the same genus iff they are related by a *rational* transformation whose determinant and matrix entries are relatively prime to twice the determinant, or rather, to the level $N$ of the associated discriminant forms. Such a transformation suffices to simultaneously $p$-adically block-diagonalize $K$ over the $p$-adic integers for every $p$ dividing twice the determinant, and a similar reduction yields the entire quadratic form on the discriminant group, with some extra complications when $p = 2$. Such a non-integral transformation mapping two edge theories as $g(\Lambda_1) = \Lambda_2$ does not, however induce fractionalization in the bulk since it reduces to an isomorphism between the discriminant groups $\Lambda_1^*/\Lambda_1 \to$

$\Lambda_2^*/\Lambda_2$. For example, the $\nu = 12/11$ K-matrices (4.32) and (4.37) are related by the following rational transformation that divides by 3:

$$\begin{pmatrix} 1 & 0 \\ -1/3 & 1 \end{pmatrix}\begin{pmatrix} 3 & 1 \\ 1 & 4 \end{pmatrix}\begin{pmatrix} 1 & -1/3 \\ 0 & 1 \end{pmatrix} = \begin{pmatrix} 1 & 0 \\ 0 & 11 \end{pmatrix}.$$

One might be tempted to look at this transformation and conclude that one of the particle types on the left-hand-side has undergone fractionalization and divided into 3 partons (due to the $-1/3$ entries in the matrix), thereby leading to the phase on the right-hand-side. But in mod 11 arithmetic, the number 3 is invertible, so no fractionalization has actually occurred.

When $p \neq 2$, the $p$-adic symbol can be directly computed from any such $p$-adic block diagonalization, as the term $(p^m)^{\pm d_{p^m}}$ records the *dimension* $d_{p^m} = \dim(K_{p^m})$ and *sign* $\pm$ of $\det(K_{p^m})$, the latter being given by the *Legendre symbol*

$$\left(\frac{\det(K_{p^m})}{p}\right) = \begin{cases} +1 & \text{if } p \text{ is a square mod } p \\ \\ -1 & \text{if } p \text{ is not a square mod } p. \end{cases}$$

In this case, it is further possible to $p$-adically diagonalize all of the blocks $K_{p^m}$, in which case there exists a $p$-adically integral transformation $g$ that diagonalizes the form $Q(\mathbf{x}) = \frac{1}{2}\mathbf{x}^T K^{-1}\mathbf{x}$ on the dual lattice $\Lambda^*$ such that its reduction modulo $\Lambda$ takes the form (4.75).

When $p = 2$, it is possible that only some of the blocks $K_{2^m}$ in the decomposition (4.76) can be 2-adically diagonalized[143] (we call these blocks *odd*). The remaining *even*

| K-matrix | $p$-adic symbols | quadratic form |
|---|---|---|
| $\left(\begin{smallmatrix}1&0\\0&7\end{smallmatrix}\right)$<br>$\left(\begin{smallmatrix}2&1\\1&4\end{smallmatrix}\right)$ | $1_0^{+2}\ 1^{+1}7^{+1}$<br>$1_{\text{even}}^{+2}\ 1^{+1}7^{+1}$ | $q_7^+$ |
| $\left(\begin{smallmatrix}1&0\\0&11\end{smallmatrix}\right)$<br>$\left(\begin{smallmatrix}3&1\\1&4\end{smallmatrix}\right)$ | $1_4^{-2}\ 1^{+1}11^{+1}$ | $q_{11}^+$ |
| $\left(\begin{smallmatrix}3&0\\0&5\end{smallmatrix}\right)$<br>$\left(\begin{smallmatrix}2&1\\1&8\end{smallmatrix}\right)$ | $1_0^{+2}\ 1^{-1}3^{+1}\ 1^{-1}5^{+1}$<br>$1_{\text{even}}^{+2}\ 1^{-1}3^{+1}\ 1^{-1}5^{+1}$ | $q_3^+ \oplus q_5^+$ |
| $\left(\begin{smallmatrix}2&3\\3&16\end{smallmatrix}\right)$<br>$\left(\begin{smallmatrix}4&1\\1&6\end{smallmatrix}\right)$ | $1_{\text{even}}^{+2}\ 1^{+1}23^{+1}$ | $q_{23}^+$ |
| $K_{A_4}$<br>$5 \oplus \mathbb{I}_3$ | $1_{\text{even}}^{-4}\ 1^{+3}5^{+1}$<br>$1_0^{-4}\ 1^{+3}5^{+1}$ | $q_5^+$ |
| $K_{E_8}$<br>$\mathbb{I}_8$ | $1_{\text{even}}^{+8}$<br>$1_0^{+8}$ | 0 |
| $K_{E_8} \oplus \mathbb{I}_4$<br>$\mathbb{I}_{12}$<br>$K_{D_{12}^+}$ | $1_4^{+12}$ | 0 |
| $\left(\begin{smallmatrix}&2\\2&\end{smallmatrix}\right)$ | $2_{\text{even}}^{+2}$ | $q_{2,2}^+$ |
| $K_{D_4}$ | $1_{\text{even}}^{-2}\,2_{\text{even}}^{-2}$ | $q_{2,2}^-$ |
| $\left(\begin{smallmatrix}4&2\\2&4\end{smallmatrix}\right)$ | $2_{\text{even}}^{-2}\ 1^{+1}3^{+1}$ | $q_{2,2}^- \oplus q_3^+$ |

Figure 4.1: ***p*-adic symbols and discriminant quadratic forms for various K-matrices appearing in this paper.** We begin with the canonical 2-adic symbol in every case, followed by the symbols for each prime dividing the determinant. Each block contains inequivalent-but-stably-equivalent matrices. The last few rows contain K-matrices giving rise to some of the exceptional 2-adic quadratic forms mentioned in the text.

blocks can only be block diagonalized into $2 \times 2$ blocks of the form $\left(\begin{smallmatrix} 2a & b \\ b & 2c \end{smallmatrix}\right)$ with $b$ odd, or rather, some number of copies of $\sigma_x$ and $\left(\begin{smallmatrix} 2 & 1 \\ 1 & 2 \end{smallmatrix}\right)$. As with odd $p$, the 2-adic symbol associated to such a block diagonalization records the dimensions $d_{2^m}$ of the blocks, together with the *signs* of the determinants $\det(K_{2^m})$, which are given by the *Jacobi symbols*

$$\left(\frac{2}{\det(K_{2^m})}\right) = \begin{cases} +1 & \text{if } \det(K_{2^m}) \equiv \pm 1 \bmod 8 \\ -1 & \text{if } \det(K_{2^m}) \equiv \pm 3 \bmod 8 \end{cases}$$

and record whether or not $\det(K_{p^m})$ is a square mod 8. In addition to this data, the 2-adic symbol also records the parities as well as the traces $\mathrm{Tr}K_{2^m}$ mod 8 of the odd blocks. An additional complication is that a given K-matrix can be 2-adically diagonalized in more than one way, and while the dimensions and parities of the blocks will be the same, the signs and traces of the odd blocks – and thus the 2-adic symbols – can be different. While this makes checking 2-adic equivalence more difficult, it is nonetheless possible to define a *canonical* 2-adic symbol[143] that *is* a complete invariant for 2-adic equivalence. We record these canonical 2-adic symbols for many of the K-matrices considered in this paper in Table 4.1.

The reason for the additional complexity when $p = 2$ is because multiplication by 2 is not invertible on the 2-primary part $(\mathbb{Q}/\mathbb{Z})_2$ of $\mathbb{Q}/\mathbb{Z}$. This implies that if $q$ refines a bilinear form on a 2-group then so does $q+\frac{1}{2}$ mod $\mathbb{Z}$, and sometimes these refinements are not isomorphic. For example, there is only one nondegenerate bilinear form $b_2(x, y) =$

$\frac{xy}{2}$ mod $\mathbb{Z}$ on $\mathbb{Z}/2$, with two non-isomorphic quadratic refinements $q_2^{\pm}(x) = \pm\frac{x}{4}$ mod $\mathbb{Z}$. Each of these refinements has level 4 and corresponds respectively to the semion $K = (2)$ and its conjugate $K = (-2)$. These give the $S$ and $T$ matrices

$$S_2 = \frac{1}{\sqrt{2}}\begin{pmatrix} 1 & 1 \\ 1 & -1 \end{pmatrix}, \quad T_2^{\pm} = e^{\mp\frac{2\pi i}{24}}\begin{pmatrix} 1 & \\ & \pm i \end{pmatrix}.$$

On $\mathbb{Z}/2 \times \mathbb{Z}/2$, there are two isomorphism classes of nondegenerate bilinear forms. The first class is represented by

$$(b_2 \oplus b_2)(x, y) = \tfrac{1}{2}(x_1y_1 + x_2y_2) \text{ mod } \mathbb{Z}$$

and has the $S$-matrix

$$S_2 \otimes S_2 = \frac{1}{2}\begin{pmatrix} 1 & 1 & 1 & 1 \\ 1 & -1 & 1 & -1 \\ 1 & 1 & -1 & -1 \\ 1 & -1 & -1 & 1 \end{pmatrix}.$$

All the refinements in this case have level 4 and are given by tensor products of semions. Up to isomorphism, this gives three refinements $q_2^+ \oplus q_2^+$, $q_2^+ \oplus q_2^-$ and $q_2^- \oplus q_2^-$, determined by the K-matrices $\left(\begin{smallmatrix} 2 & \\ & 2 \end{smallmatrix}\right)$, $\left(\begin{smallmatrix} 2 & \\ & -2 \end{smallmatrix}\right)$ and $\left(\begin{smallmatrix} -2 & \\ & -2 \end{smallmatrix}\right)$ with $c_- = 2, 0, -2$ respectively.

The second class of bilinear forms on $\mathbb{Z}/2 \times \mathbb{Z}/2$ contains the single form

$$b_{2,2}(x, y) = \tfrac{1}{2}(x_1y_2 + x_2y_1) \text{ mod } \mathbb{Z}$$

and gives the $S$-matrix

$$S_{2,2} = \frac{1}{2}\begin{pmatrix} 1 & 1 & 1 & 1 \\ 1 & 1 & -1 & -1 \\ 1 & -1 & 1 & -1 \\ 1 & -1 & -1 & 1 \end{pmatrix}.$$

It is refined by two isomorphism classes $q^{\pm}_{2,2}$ of quadratic forms with T-matrices $T^{\pm}_{2,2} = \mathrm{diag}(1, \pm 1, \pm 1, -1)$ (these have level 2, the exception to the rule), up to the usual phase of $-2\pi i c_-/24$. The form $q^{+}_{2,2}$ is given by the K-matrix $\left(\begin{smallmatrix} & 2 \\ 2 & \end{smallmatrix}\right)$ and corresponds to the toric code. The form $q^{-}_{2,2}$ is given by the K-matrix

$$K_{D_4} = \begin{pmatrix} 2 & 0 & 1 & 0 \\ 0 & 2 & -1 & 0 \\ 1 & -1 & 2 & -1 \\ 0 & 0 & -1 & 2 \end{pmatrix}$$

of $\mathrm{SO}(8)_1$, or equivalently, by the restriction of the quadratic form associated to the K-matrix $\left(\begin{smallmatrix} 4 & 2 \\ 2 & 4 \end{smallmatrix}\right)$ to the 2-part of its discriminant group $\mathbb{Z}/2 \times \mathbb{Z}/2 \times \mathbb{Z}/3$. Again, these are distinguished by their signatures, which are 0 and 4 mod 8. The 2-adic diagonalizations of these K-matrices contain examples of even blocks, as illustrated in to even blocks in Table 4.1.

Further complexity arises for higher powers of 2: There are two bilinear forms $b^{\pm}_4$ on $\mathbb{Z}/4$, and four $b^{1,3,5,7}_{2^m}$ on each $\mathbb{Z}/2^m$ when $m \geq 3$. There are also four quadratic forms $q^{1,3,5,7}_{2^m}$ on $\mathbb{Z}/2^m$ for every $m \geq 2$, all with level $2^{m+1}$. Therefore, the bilinear forms $b^{\pm}_4$ have two refinements each, while the rest have unique refinements. On top of all this, even more complexity arises from the fact that factorizations of such forms is not typically unique. It is therefore less straightforward to check equivalence of 2-adic forms. It is nonetheless still possible to define a canonical 2-adic symbol[143] that is a complete invariant for 2-adic equivalence of K-matrices. However, this symbol carries strictly more information than the isomorphism class of the 2-part of the discriminant form because it

knows the parity of $K$. To characterize the even-odd equivalences that we investigate in the next section, the usual 2-adic equivalence is replaced with equivalence of the 2-parts of discriminant forms as in the odd $p$ case above.

The 2-adic symbol contains slightly more information than just the equivalence class of a quadratic form on the discriminant group. This is evident in our even-odd examples, for which all $p$-adic symbols for odd $p$ coincide, with the only difference occurring in the 2-adic symbol. It is however clear that two K-matrices $K_{\text{even}}$ and $K_{\text{odd}}$ of different parities are stably equivalent precisely when either $K_{\text{even}} \oplus 1$ and $K_{\text{odd}} \oplus 1$ are in the same genus, or otherwise, when $K_{\text{even}} \oplus \sigma_z$ and $K_{\text{odd}} \oplus \sigma_z$ are in the same genus. A detailed study of the 2-adic symbols in this context will appear elsewhere.

## 4.6 Stable Equivalence between Odd and Even Matrices: Fermionic Bulk States with Bosonic Edges

We now focus on the case of fermionic systems, which are described by odd $K$-matrices (i.e., matrices that have at least one odd number on the diagonal). We ask: Under what circumstances is such a K-matrix equivalent, upon enlargement by $\sigma_z$ (or $\sigma_x$, since it makes no difference for an odd matrix), to an even K-matrix enlarged by $\sigma_z$:

$$K_{\text{odd}} \oplus \sigma_z = W^T (K_{\text{even}} \oplus \sigma_z) W ? \tag{4.77}$$

This question can be answered using the theory of quadratic refinements.[141,142]

As we have alluded to earlier, the naive definition of a quadratic form on the discriminant group breaks down for odd matrices. To be more concrete, $\frac{1}{2}\vec{u}^2 \pmod 1$ is no longer well-defined on the discriminant group. In order to be well-defined on the discriminant group, shifting $\vec{u}$ by a lattice vector $\boldsymbol{\lambda} \in \Lambda$ must leave $q(\vec{u})$ invariant modulo integers, so that $e^{2\pi i q(\vec{u})}$ in Eq. (4.23) is independent of which representative in $\Lambda^*$ we take for an equivalence class in $A = \Lambda^*/\Lambda$. When $K$ is odd, there are some vectors $\boldsymbol{\lambda}$ in the original lattice $\Lambda$ such that

$$q(\vec{u} + \boldsymbol{\lambda}) \equiv q(\vec{u}) + \frac{1}{2} \bmod 1. \tag{4.78}$$

Physically, such a vector is just an electron ($\boldsymbol{\lambda} \cdot \boldsymbol{\lambda}$ is an odd integer). One can attach an odd number of electrons to any quasiparticle and change the exchange statistics by $-1$. In a sense, the discriminant group should be enlarged to $A \oplus (A + \boldsymbol{\lambda}_{\text{odd}})$: quasiparticles come in doublets composed of particles with opposite fermion parity, and therefore opposite topological twists. The Gauss-Milgram sum over this enlarged set of quasiparticles is identically zero, which is a clear signature that the Abelian topological phase defined by an odd K-matrix is not a TQFT in the usual sense.

While the $T$ matrix is not well-defined for a fermionic theory, the $S$ matrix, which is determined by the discriminant bilinear form $b([\vec{v}], [\vec{v}'])$, makes perfect sense. This is because a full braid of one electron around any other particle does not generate a non-trivial phase.

Given a bilinear form $b$, a systematic approach for defining a quadratic form that is well-defined on the discriminant group comes from the theory of quadratic refinements. The crucial result is that a given bilinear form can *always* be lifted to a quadratic form $q$ on the discriminant group. The precise meaning of "lifting" is that there exists a well-defined discriminant quadratic form such that $b([\vec{v}],[\vec{v}']) = q([\vec{v}+\vec{v}']) - q([\vec{v}]) - q([\vec{v}'])$.[141,142] With $q$, the topological twists are well-defined: $e^{2\pi i q(\vec{u})} = e^{2\pi i q(\vec{u}+\vec{\lambda})}$ for all $\vec{u} \in \Lambda^*$ and $\lambda \in \Lambda$. We will give a constructive proof for the existence of such a $q$, given any odd K-matrix.

Once the existence of such a quadratic form $q([\vec{v}])$ is established, we can evaluate the Gauss-Milgram sum (4.27) and determine $c_-$ mod 8. We then appeal to the following result of Nikulin:[144]

Corollary 1.10.2: *Given an Abelian group $A$, a quadratic form $q$ on $A$, and positive integers $(r_+, r_-)$ that satisfy the Gauss-Milgram sum for $q$, there exists an even lattice with discriminant group $A$, quadratic form $q$ on the discriminant group, and signature $(r_+, r_-)$, provided $r_+ + r_-$ is sufficiently-large.*

Using Corollary 1.10.2, we immediately see that an even lattice characterized by $(A, q, c_- \text{ mod } 8)$ exists, whose Gram matrix is denoted by $K_{\text{even}}$. Recall that the chiral central charge $c_-$ is equal to the signature $\sigma = r_+ - r_-$ of the lattice. Next we show that $K_{\text{even}}$ is $\sigma_z$-stably equivalent to the odd matrix we started with: namely, (4.77) holds for

this $K_{\text{even}}$. Since $K_{\text{even}}$ and $K$ share the same discriminant group and $S$ matrix, they are stably equivalent upon adding unimodular lattices, according to Theorem 1. 1. 9. In other words, there exist unimodular matrices $U$ and $U'$ such that

$$K \oplus U \simeq K_{\text{even}} \oplus U'. \tag{4.79}$$

Apparently $U'$ must be odd. We now add to both sides of the equation the conjugate of $U'$ denoted by $\overline{U'}$:

$$K \oplus (U \oplus \overline{U'}) \simeq K_{\text{even}} \oplus (U' \oplus \overline{U'}). \tag{4.80}$$

On the right-hand side, $U' \otimes \overline{U'}$ is equivalent to $\sigma_z \oplus \sigma_z \oplus \cdots \sigma_z$. On the left-hand side, $U \oplus \overline{U'}$ can be transformed to the direct sum of $\mathbb{I}_n$ where $n = \sigma(U) - \sigma(U') = \sigma(K_{\text{even}}) - \sigma(K)$ and several $\sigma_{z/x}$'s. Here $\mathbb{I}_n$ is the $|n| \times |n|$ identity matrix and when $n$ is negative we take it to be $-\mathbb{I}_{|n|}$. If $n \neq 0 \mod 8$, then $K_{\text{even}}$ has a different chiral central charge as $K$. Therefore we have arrived at the following theorem:

*For any odd $K$ matrix, $K \oplus \mathbb{I}_n$ is $\sigma_z$-stably equivalent to an even $K$-matrix for an appropriate $n$.*

The physical implication is that by adding a certain number of Landau levels the edge phase of a fermionic Abelian topological phase is always stably equivalent to a purely bosonic edge phase which has no electron excitations in its low-energy spectrum.

The possible central charges of the bosonic edge theory are $c_{\text{ferm}} + n + 8m$ for $m \in \mathbb{Z}$. We can consider a fermionic system with an additional $8m + n$ Landau levels, where $m$ is the smallest positive integer such that $8m + n > 0$. Such a fermionic theory has precisely the same discriminant group as the original fermionic theory and, consequently, is associated with precisely the same bosonic system defined by the refinement $q([\vec{u}])$. So even if the original fermionic theory does not have a stable chiral edge phase with only bosonic excitations, there is a closely-related fermionic theory with some extra filled Landau levels which does have a chiral edge phase whose gapless excitations are all bosonic. A simple example of this is given by the $\nu = 1/5$ Laughlin state, which has $K = 5$. The corresponding bosonic state has $c = 4$, so the $\nu = 1/5$ Laughlin state does not have a chiral edge phase whose gapless excitations are all bosonic. However, the central charges do match if, instead, we consider the $\nu = 3 + \frac{1}{5} = 16/5$ state. This state *does* have a bosonic edge phase, with K-matrix

$$K_{A_4} = \begin{pmatrix} 2 & 1 & 0 & 0 \\ 1 & 2 & 1 & 0 \\ 0 & 1 & 2 & 1 \\ 0 & 0 & 1 & 2 \end{pmatrix} \tag{4.81}$$

corresponding to $\mathrm{SU}(5)_1$. (Ordinarily, the Cartan matrix for SU(5) is written with $-1$s off-diagonal, but by a change of basis we can make them equal to $+1$.)

In the following we demonstrate concretely how to obtain a particular discriminant quadratic form $q$, starting from the odd lattice given by $K$. We already know that the naive definition $\frac{1}{2}\vec{u}^2 (\mathrm{mod}\ 1)$ does not qualify as a discriminant quadratic form. In order

to define a quadratic form on the discriminant group, we first define a quadratic function $Q_{\mathbf{w}}(\vec{u})$ according to:

$$Q_{\mathbf{w}}(\vec{u}) = \frac{1}{2}\vec{u}^2 - \frac{1}{2}\vec{u}\cdot\vec{w}, \tag{4.82}$$

for $\vec{w} \in \Lambda^*$. Such a linear shift preserves the relation between the quadratic function ($T$ matrix) and the bilinear form ($S$ matrix):

$$Q_{\mathbf{w}}(\vec{u}+\vec{v}) - Q_{\mathbf{w}}(\vec{u}) - Q_{\mathbf{w}}(\vec{v}) = \vec{u}\cdot\vec{v}. \tag{4.83}$$

(Notice that $\vec{u}\cdot\vec{v}$ is the symmetric bilinear form $b(\vec{u},\vec{v})$ in Stirling's thesis[142]). Notice that at this stage $Q_{\mathbf{w}}$ is not yet a quadratic form on $A$, being just a quadratic function.

If, for any $\boldsymbol{\lambda} \in \Lambda$, $Q_{\mathbf{w}}$ satisfies $Q_{\mathbf{w}}(\vec{u}+\boldsymbol{\lambda}) \equiv Q_{\mathbf{w}}(\vec{u}) \bmod 1$ or, in other words,

$$\boldsymbol{\lambda}\cdot\boldsymbol{\lambda} \equiv \boldsymbol{\lambda}\cdot\vec{w} \bmod 2. \tag{4.84}$$

then we can define the following quadratic form on the discriminant group:

$$q([\vec{u}]) = Q_{\mathbf{w}}(\vec{u}).$$

Expanding $\vec{w}$ in the basis of the dual lattice $\vec{w} = w_I\vec{f}^I$ and expanding $\boldsymbol{\lambda}^I\vec{e}_I$, we find that this condition is satisfied if we take $w_I \equiv K_{II} \bmod 2$. Thus, for a Hall state expressed in the symmetric basis, we may identify $\vec{w}$ with twice the spin vector $s_I = K_{II}/2$.[135,153]

A central result of Ref. 141 is that such a $\vec{w}$ leads to a generalized Gauss-Milgram sum:

$$\frac{1}{\sqrt{|A|}} e^{\frac{2\pi i}{8}\vec{w}^2} \sum_{\vec{u}} e^{2\pi i Q_{\vec{w}}(\vec{u})} = e^{2\pi i\sigma/8}, \tag{4.85}$$

where, in order for the notation to coincide, we have replaced the chiral central charge with the signature $\sigma$ on the right-hand-side of the above equation. Note that the choice of $\vec{w}$ here is not unique. We can check that the modified Gauss-Milgram sum holds for $\vec{w} + 2\boldsymbol{\lambda}^*$ where $\boldsymbol{\lambda}^* \in \Lambda^*$. First note that

$$Q_{\vec{w}+2\boldsymbol{\lambda}^*}(\vec{u}) = \frac{1}{2}\vec{u}^2 - \frac{1}{2}\vec{u}\cdot\vec{w} - \vec{u}\cdot\boldsymbol{\lambda}^* = Q_{\vec{w}}(\vec{u} - \boldsymbol{\lambda}^*) - \frac{1}{2}\boldsymbol{\lambda}^{*2} - \frac{1}{2}\boldsymbol{\lambda}^*\cdot\vec{w}, \tag{4.86}$$

while at the same time

$$(\vec{w} + 2\boldsymbol{\lambda}^*)^2 = \vec{w}^2 + 4\boldsymbol{\lambda}^*\cdot\vec{w} + 4\boldsymbol{\lambda}^{*2}. \tag{4.87}$$

Therefore,

$$e^{\frac{2\pi i}{8}(\vec{w}+2\boldsymbol{\lambda}^*)^2}\sum_{\vec{u}} e^{2\pi i Q_{\vec{w}+2\boldsymbol{\lambda}^*}(\vec{u})} = e^{\frac{2\pi i}{8}\vec{w}^2}\sum_{\vec{u}} e^{2\pi i Q_{\vec{w}}(\vec{u}-\boldsymbol{\lambda}^*)} = e^{2\pi i\sigma/8}. \tag{4.88}$$

One can freely shift $\vec{w}$ by $2\lambda^*$. Consequently, $\vec{w}$ is really an equivalence class in $\Lambda^*/2\Lambda^*$.

In Appendix E, we further prove that such a representative $\vec{w}$ can always be chosen to lie in the original lattice $\Lambda$. We denote such a $\vec{w}$ by $\vec{w}_0$. The advantage of such a choice can be seen from the expression

$$e^{2\pi i Q_{\vec{w}_0}(\vec{u})} = e^{\pi i\vec{u}^2}e^{\pi i\vec{u}\cdot\vec{w}_0}$$

the topological twists. Since $\vec{w}_0$ now lives in $\Lambda$, we have $\vec{u}\cdot\vec{w}_0 \in \mathbb{Z}$ and $e^{\pi i\vec{u}\cdot\vec{w}_0} = \pm 1$. This corroborates our intuition that one can salvage the Gauss-Milgram sum in the case of odd matrices by inserting appropriate signs in the sum.

In addition, we can prove that our quadratic function now defines a finite quadratic form because $Q_{\vec{w}_0}(n\vec{u}) \equiv n^2 Q_{\vec{w}_0}(\vec{u}) \bmod \mathbb{Z}$. To see why this is true, we use the definition of $q$:

$$Q_{\vec{w}_0}(n\vec{u}) = \frac{n^2}{2}\vec{u}^2 - \frac{n}{2}\vec{u}\cdot\vec{w}_0 \equiv \left(\frac{n^2}{2}\vec{u}^2 - \frac{n^2}{2}\vec{u}\cdot\vec{w}_0\right) \bmod \mathbb{Z}. \tag{4.89}$$

The second equality follows from the elementary fact that $n^2 \equiv n \,(\mathrm{mod}\ 2)$ together with $\vec{u}\cdot\vec{w}_0 \in \mathbb{Z}$. Therefore the definition $q([\vec{u}]) = Q_{\vec{w}_0}(\vec{u}) \bmod \mathbb{Z}$ is well-defined.

Having found the discriminant quadratic form $q(\vec{u})$, the generalized Gauss-Milgram sum now can be re-interpreted as the ordinary Gauss-Milgram sum of a bosonic Abelian topological phase. As aforementioned, there exists a lifting to an even lattice with the signature $\sigma' \equiv (\sigma - \vec{w}_0^2) \bmod 8$ where $\sigma$ is the signature of the odd matrix $K$ and thus the number of Landau levels we need to add is $n = -\vec{w}_0^2 \bmod 8$.

Hence, we have the sufficient condition for the existence of an even lattice that is stably equivalent to a given odd lattice: $\sigma' = \sigma$, or $\vec{w}_0^2 \equiv 0 \bmod 8$.

An obvious drawback of this discussion is that it is not constructive (which stems from the non-constructive nature of the proof of Nikulin's theorem[144]): we do not know how to construct uniquely the even matrix corresponding to a given discriminant group, quadratic form $q$, and central charge $c$. The distinct ways of lifting usually result in lattices with different signatures.

## 4.7 Novel Chiral Edge Phases of the Conventional Bulk Fermionic $\nu = 8, 12, \frac{8}{15}, \frac{16}{5}$ states

Now that the general framework has been established, in this section we consider a few experimentally relevant examples and their tunneling signatures.

### 4.7.1 $\nu = 8$

The integer quantum Hall states are the easiest to produce in experiment and are considered to be well understood theoretically. But surprisingly, integer fillings, too, can exhibit edge phase transitions. The smallest integer filling for which this can occur is at $\nu = 8$, because eight is the smallest dimension for which there exist two equivalence classes of unimodular matrices. One class contains the identity matrix, $\mathbb{I}_8$, and the other contains $K_{E_8}$, defined in Appendix F, which is generated by the roots of the Lie algebra of $E_8$. $K_{E_8}$ is an even matrix and hence describes a system whose gapless excitations are all bosonic[124,133] (although if we consider the bosons to be paired fermions, it must contain gapped fermionic excitations.) Yet, counterintuitively, it is stably equivalent to the fermionic $\mathbb{I}_8$; for $W_8$ defined in Appendix F,

$$W_8^T(K_{E_8} \oplus \sigma_z)W_8 = \mathbb{I}_8 \oplus \sigma_z, \tag{4.90}$$

This is an example of the general theory explained in Section 4.6, but it is an extreme case in which both phases have only a single particle type – the trivial particle. The chiral central charges of both phases are equal and so Nikulin's theorem guarantees that the two bulk phases are equivalent (when the bosonic $E_8$ state is understood to be ultimately built out of electrons) and that there is a corresponding edge phase transition between the two chiral theories.

The action describing the $\mathbb{I}_8$ state with an additional left- and right-moving mode is

$$S = \int dx\, dt \left( \frac{1}{4\pi} \left( \mathbb{I}_8 \oplus \sigma_z \right)_{IJ} \partial_t \phi^I \partial_x \phi^J - \frac{1}{4\pi} V_{IJ} \partial_x \phi^I \partial_x \phi^J + \frac{1}{2\pi} \sum_I \epsilon_{\mu\nu} \partial_\mu \phi^I A_\nu \right). \quad (4.91)$$

The charge vector is implicitly $t_I = 1$ for all $I$. As we have shown in previous sections, the basis change $\phi' = W_8 \phi$ makes it straightforward to see that if the perturbation

$$S' = \int dx dt u' \cos\left( \phi'_9 \pm \phi'_{10} \right) \quad (4.92)$$

is the only relevant term, then the two modes $\phi'_9$ and $\phi'_{10}$ would be gapped and the system would effectively be described by $K_{E_8}$.

As in the previous examples, measurements that probe the edge structure can distinguish the two phases of the edge. Consider, first, transport through a QPC that allows tunneling between the two edges of the Hall bar. In the $\nu = 8$ state with $K = \mathbb{I}_8$, the backscattered current will be proportional to the voltage

$$I^b_{\mathbb{I}_8} \propto V \quad (4.93)$$

because the most relevant backscattering operators, $\cos(\phi_I^T - \phi_I^B)$, correspond to the tunneling of electrons. In contrast, when $K = K_{E_8}$, there is no single-electron backscattering term. Instead, the most relevant operator is the backscattering of charge-$2e$ bosons – i.e. of pairs of electrons – from terms like $\cos(\phi_1'^T - \phi_4'^T - \phi_1'^B + \phi_4'^B)$, which yields different current-voltage relation

$$I_{E_8}^b \propto V^3. \tag{4.94}$$

An alternative probe is given by tunneling into the edge from a metallic lead. In the $K = \mathbb{I}_8$ case, the leading contribution is due to electrons tunneling between the lead and the Hall bar from the terms $\psi_{\text{lead}}^\dagger e^{i\phi_I^T}$, yielding

$$I_{\mathbb{I}_8}^{\text{tun}} \propto V. \tag{4.95}$$

However, in the $K_{E_8}$ case there are no fermionic charge-$e$ operators to couple to the electrons tunneling from the lead. Instead, the leading term must involve two electrons from the lead tunneling together into the Hall bar. The amplitude for this event may be so small that there is no detectable current. If the amplitude is detectable, then we consider two cases: if the quantum Hall state is not spin-polarized or if spin is not conserved (e.g. due to spin-orbit interaction), then the leading contribution to the tunneling current is from terms like $\psi_{\text{lead},\downarrow}^\dagger \psi_{\text{lead},\uparrow}^\dagger e^{i\phi_1'^T - i\phi_4'^T}$, which represents two electrons of opposite spin tunneling together into the Hall bar, yielding

$$I_{E_8}^{\text{tun}} \propto V^3. \tag{4.96}$$

If the quantum Hall state is spin-polarized, and tunneling from the lead is spin-conserving, then the pair of electrons that tunnels from the lead must be a spin-polarized $p$-wave pair, corresponding to a tunneling term like $\psi^\dagger_{\text{lead},\downarrow}\partial\psi^\dagger_{\text{lead},\downarrow}e^{i\phi_1'^T - i\phi_4'^T}$ in the Lagrangian, and we instead expect

$$I^{\text{tun}}_{E_8} \propto V^5. \tag{4.97}$$

Another important distinction between the two edge phases is the minimal value of electric charge in the low-energy sector, which can be probed by a shot-noice measurement,[29,30] as was done in the $\nu = 1/3$ fractional quantum Hall state.[31,32] The $\mathbb{I}_8$ phase has gapless electrons, so the minimal charge is just the unit charge $e$. However, the $E_8$ edge phase is bosonic and consequently the minimal charge is at least $2e$ (i.e. a pair of electrons). (Electrons are gapped and, therefore, do not contribute to transport at low temperatures and voltages.) Quantum shot noise, generated by weak-backscattering at the QPC is proportional to the minimal current-carrying charge and the average current. So we expect a shot-noise measurement can also distinguish the two edge phases unambiguously.

### 4.7.2 $\nu = 12$

In dimensions-9, -10, and -11, there exist two unique positive definite unimodular lattices, whose $K$-matrices are (in the usual canonical bases) $\mathbb{I}_{9,10,11}$ or $K_{E_8} \oplus \mathbb{I}_{1,2,3}$. In

each dimension, the two lattices, when enlarged by direct sum with $\sigma_z$, are related by the similarity transformation of the previous section. However in dimension-12, a new lattice appears, $D_{12}^+$, defined in Appendix F. One salient feature of this matrix is that it has an odd element along the diagonal, but it is not equal to 1, which is a symptom of the fact that there are vectors in this lattice that have odd (length)$^2$ but none of them have (length)$^2$=1. The minimum (length)$^2$ is 2. Upon taking the direct sum with $\sigma_z$, the resulting matrix is equivalent to $\mathbb{I}_{12} \oplus \sigma_z$ – and hence to $K_{E_8} \oplus \mathbb{I}_4 \oplus \sigma_z$ using the transformation of the previous section – by the relation $W_{12}^T(K_{D_{12}^+} \oplus \sigma_z)W_{12} = \mathbb{I}_{12} \oplus \sigma_z$, where $W_{12}$ is defined in Appendix F.

Consider the action of the $\nu = 12$ state with two additional counter propagating gapless modes and with the implicit charge vector $t_I = 1$:

$$S = \int dx\, dt \left( \frac{1}{4\pi} \left(\mathbb{I}_{12} \oplus \sigma_z\right)_{IJ} \partial_t \phi^I \partial_x \phi^J - \frac{1}{4\pi} V_{IJ} \partial_x \phi^I \partial_x \phi^J + \frac{1}{2\pi} \sum_I \epsilon_{\mu\nu} \partial_\mu \phi^I A_\nu \right). \quad (4.98)$$

The matrix $W_{12}$ suggests a natural basis change $\phi' = W_{12}\phi$ in which the perturbation

$$S' = \int dx dt u' \cos\left(\phi'_9 \pm \phi'_{10}\right) \quad (4.99)$$

can open a gap, leaving behind an effective theory described by $K_{D_{12}^+}$.

It is difficult to distinguish the $\mathbb{I}_{12}$ edge phase from the $E_8 \oplus \mathbb{I}_4$ phase because both phases have charge-$e$ fermions with scaling dimension-1/2. However, both of these edge phases can be distinguished from the $D_{12}^+$ phase in the manner described for the $\nu = 8$ phases in the previous subsection. At a QPC, the most relevant backscattering terms

will have scaling dimension 1; one example is the term $\cos(\phi_{11}'^T - \phi_{11}'^B)$, which yields the current-voltage relation

$$I^b_{D^+_{12}} \propto V^3. \tag{4.100}$$

This is the same as in the $E_8$ edge phase at $\nu = 8$ because the most-relevant backscattering operator is a charge-$2e$ bosonic operator with scaling dimension 2. There is a charge-$e$ fermionic operator $\exp(i(\phi_2'^T + 2\phi_{12}'^T))$, but it has scaling dimension 3/2. Its contribution to the backscattered current is $\propto V^5$, which is sub-leading compared to the contribution above, although its bare coefficient may be larger. However, if we couple the edge to a metallic lead via $\psi^\dagger_{\text{lead}} \exp(i(\phi_2'^T + 2\phi_{12}'^T))$, single-electron tunneling is the dominant contribution for a spin-polarized edge, yielding

$$I^{\text{tun}}_{D^+_{12}} \propto V^3, \tag{4.101}$$

while pair tunneling via the coupling $\psi^\dagger_{\text{lead}} \partial \psi^\dagger_{\text{lead}} e^{i\phi_{11}'^T}$ gives a sub-leading contribution $\propto V^5$. If the edge is spin-unpolarized, pair tunneling via the coupling $\psi^\dagger_{\text{lead},\uparrow} \psi^\dagger_{\text{lead},\downarrow} e^{i\phi_{11}'^T}$ gives a contribution with the same $V$ dependence as single-electron tunneling.

### 4.7.3 Fractional Quantum Hall States with Multiple Edge Phases

In Section 4.3, we discussed the $\nu = 8/7$ state, which has two possible edge phases. Our second fermionic fractional quantum Hall example is

$$K_1 = \begin{pmatrix} 3 & 0 \\ 0 & 5 \end{pmatrix} \tag{4.102}$$

with $t = (1, 1)^T$. We again assume that a pair of gapped modes interacts with these two modes, and we assume that they are modes of oppositely-charged particles (e.g. holes), so that $t = (1, 1, -1, -1)^T$. Upon enlarging by $\sigma_z$, we find that $K_1 \oplus \sigma_z = W^T (K_2 \oplus \sigma_z) W$, where

$$K_2 = \begin{pmatrix} 2 & 1 \\ 1 & 8 \end{pmatrix} \tag{4.103}$$

and

$$W = \begin{pmatrix} 1 & 3 & 0 & 1 \\ 0 & 3 & 0 & 1 \\ 0 & 0 & 1 & 0 \\ 1 & 8 & 0 & 3 \end{pmatrix}. \tag{4.104}$$

If the following perturbation is relevant, it gaps out a pair of modes:

$$S' = \int dx\, dt\, u' \cos(-3\phi_1 - 5\phi_2 + \phi_3 + 3\phi_4). \tag{4.105}$$

Under the basis change (4.104), $-3\phi_1 - 5\phi_2 + \phi_3 + 3\phi_4 = \phi_3' + \phi_4'$, so the remaining theory has K-matrix (4.103).

In the $K_1$ edge phase (4.102), the backscattered current at a QPC is dominated by the tunneling term $\cos(\phi_2^T - \phi_2^B)$, which yields

$$I_1^b \propto V^{-3/5}, \tag{4.106}$$

while the tunneling current from a metallic lead is dominated by the single-electron tunneling term $\psi_{\text{lead}}^\dagger e^{3i\phi_1^T}$, which yields

$$I_1^{\text{tun}} \propto V^3. \tag{4.107}$$

In the $K_2$ edge phase (4.103), the backscattered current at a QPC is dominated by the tunneling term $\cos(\phi_2'^T - \phi_2'^B)$, yielding

$$I_1^b \propto V^{-11/15}, \tag{4.108}$$

while the tunneling current from a metallic lead is dominated by the pair-tunneling term $\psi_{\text{lead}}^\dagger \partial\psi_{\text{lead}}^\dagger e^{i\phi_1'^T - 7i\phi_2'^T}$, which assumes a spin-polarized edge, and yields

$$I_2^{\text{tun}} \propto V^{11}. \tag{4.109}$$

As we discussed in Section 4.6, the $\nu = 16/5$ state can have two possible edge phases, one with

$$K_1 = \begin{pmatrix} 1 & 0 & 0 & 0 \\ 0 & 1 & 0 & 0 \\ 0 & 0 & 1 & 0 \\ 0 & 0 & 0 & 5 \end{pmatrix}, \tag{4.110}$$

which is essentially the edge of the $\nu = 1/5$ state, together with 3 integer quantum Hall edges. The other possible phase has

$$K_2 = \begin{pmatrix} 2 & 1 & 0 & 0 \\ 1 & 2 & 1 & 0 \\ 0 & 1 & 2 & 1 \\ 0 & 0 & 1 & 2 \end{pmatrix}. \tag{4.111}$$

Upon enlarging by a pair of gapped modes, the two matrices are related by $K_1 \oplus \sigma_z = W^T(K_2 \oplus \sigma_z)W$, where

$$W = \begin{pmatrix} 1 & 0 & 0 & 2 & 0 & -1 \\ -1 & 1 & 0 & -4 & 0 & 2 \\ 1 & -1 & 1 & 6 & 0 & -3 \\ -1 & 1 & -1 & -8 & 1 & 4 \\ 0 & 0 & 0 & 5 & 0 & -2 \\ -1 & 1 & -1 & -10 & 1 & 5 \end{pmatrix} \tag{4.112}$$

If the gapped modes are oppositely charged holes, then the following perturbation carries no charge:

$$S' = \int dxdtu' \cos(-\phi_1 + \phi_2 - \phi_3 - 5\phi_4 + \phi_5 + 3\phi_6) \tag{4.113}$$

If this perturbation is relevant, it will gap out a pair of modes and leave behind an effective theory describe by the K-matrix (4.111),

The two edge phases of the $\nu = 16/5$ state can be distinguished by the voltage dependence of the current backscattered at a quantum point contact and the tunneling current from a metallic lead. In the $K_1$ edge phase, the backscattered current at a QPC is dominated by the quasiparticle backscattering term $\cos(\phi_4^T - \phi_4^B)$, yielding the current-voltage relation

$$I_1^b \propto V^{-3/5}. \tag{4.114}$$

In the $K_2$ edge phase, there are several terms that are equally most-relevant, including, for example $\cos(\phi_1'^T - \phi_1'^B)$, which yield the current-voltage relation

$$I_2^b \propto V^{3/5}. \tag{4.115}$$

Meanwhile, in the $K_1$ edge phase, single-electron tunneling from a metallic lead given by, for example, $\psi_{\text{lead}}^\dagger e^{i\phi_1^T}$, yields the dependence

$$I_1^{\text{tun}} \propto V, \tag{4.116}$$

while in the $K_2$ edge phase there are only pair-tunneling terms; one such term for a spin-polarized edge is $\psi^\dagger_{\text{lead}}\partial\psi^\dagger_{\text{lead}}e^{i\phi_1'^T+i\phi_4'^T}$, which yields

$$I_2^{\text{tun}} \propto V^5. \tag{4.117}$$

We now consider an example of a bosonic fractional quantum Hall state with $\nu = 12/23$,

$$K_1^b = \begin{pmatrix} 2 & 3 \\ 3 & 16 \end{pmatrix} \tag{4.118}$$

and $t = (1,1)^T$. (This is a natural choice of charge vector for bosonic atoms in a rotating trap. For paired electrons in a magnetic field, it would be more natural to have $t = (2,2)^T$) By a construction similar to the one discussed in the fermionic cases of $\nu = 8, 12, 8/7, 8/15$ and the bosonic integer quantum Hall cases of $\nu = 8, 16$, this state has another edge phase described by

$$K_2^b = \begin{pmatrix} 4 & 1 \\ 1 & 6 \end{pmatrix} \tag{4.119}$$

and $t = (1,-1)^T$. As in the previous cases, the two edge phases can be distinguished by transport through a QPC or tunneling from a metallic lead.

## 4.8 Some Remarks on Genera of Lattices and Bulk Topological Phases

The focus in this paper is on the multiple possible gapless edge phases associated with a given bulk topological phase. However, having established that the former correspond to lattices while the latter correspond to genera of lattices (or, possibly, pairs of genera of lattices), we note here that some results on genera of lattices published by Nikulin in Ref. 144 have direct implications for bulk topological phases. We hope to explore these relations more thoroughly in the future.

We begin by noting that the data that determine a genus of lattices is precisely the data that determine a $2+1$-D Abelian topological phase. Recall that the elements of the discriminant group $A$ of a lattice form the particle content of an Abelian topological phase. We can turn this around by noting that the particle content and fusion rules of any Abelian topological phase can be summarized by an Abelian group $A$ whose elements are the particle types in the theory and whose multiplication rules give the fusion rules of the theory. The fusion rules take the form of the multiplication rules of an Abelian group because only one term can appear on the right-hand-side of the fusion rules in an Abelian topological phase. Meanwhile, specifying the $S$-matrix for the topological phase is equivalent to giving a bilinear form on the Abelian group $A$ according to $S_{[\mathbf{v}],[\mathbf{v}']} = \frac{1}{\sqrt{|A|}} e^{-2\pi i b([\mathbf{v}],[\mathbf{v}'])}$. A quadratic form $q$ on the Abelian group $A$ determines

the topological twist factors or, equivalently, the $T$-matrix of an Abelian topological phase according to $\theta_{[\mathbf{v}]} = e^{2\pi i q([\vec{v}])}$. Finally, the signature of the form, the number of positive and negative eigenvalues $r_+$ and $r_-$ of the quadratic form $q$, determines the right and left central charges, according to $c_R = r_+$ and $c_L = r_-$. The chiral central charge $c_- = c_R - c_L$ is given by $c_- = r_+ - r_-$ which, in turn, determines the modular transformation properties of states and, consequently, the partition functions of the bulk theory on closed 3-manifolds (e.g. obtained by cutting a torus out of $S^3$, performing a Dehn twist, and gluing it back in). The signature is determined (mod 8) by the quadratic form $q$, according to the Gauss-Milgram sum:

$$\frac{1}{\sqrt{|A|}} \sum_{a \in A} e^{2\pi i q(a)} = e^{2\pi i c_- /8}$$

We now consider Nikulin's Theorem 1.11.3, given in Section 4.5 and also his result

Proposition 1.11.4: *There are at most* 4 *possible values for the signature* (mod 8) *for the quadratic forms associated with a given bilinear form on the discriminant group.*

Theorem 1.11.3 (given in Section 4.5) states that the $S$-matrix and $r_+ - r_-$ (mod 8) completely and uniquely determine the $T$-matrix, up to relabellings of the particles that leave the theory invariant. In Section 4.6 we show constructively that such a $T$-matrix exists in the fermionic case. Proposition 1.11.4 tells us that, for a given $S$-matrix, there are at most 4 possible values for the signature $r_+ - r_-$ (mod 8) and, therefore, at most

4 possible $T$-matrices. One way to interpret this is that the elements of the $T$-matrix are the square roots of the diagonal elements of the $S$-matrix; therefore, they can be determined, up to signs from the $S$-matrix. There are, at most, four consistent ways of doing this, corresponding to, at most, four possible values of the Gauss-Milgram sum.

Then, Theorem 1.10.2, stated in Section 4.6, tells us that the quadratic form defines an even lattice. Thus, to any fermionic Abelian topological phase, we can associate a bosonic Abelian topological phase with the same particle types, fusion rules, and $S$-matrix. The bosonic phase has a well-defined $T$-matrix, unlike the fermionic phase. In addition, we have:

Theorem 1.3.1: *Two lattices $S_1$ and $S_2$ have isomorphic bilinear forms on their discriminant groups if and only if there exist unimodular lattices $L_1$, $L_2$ such that $S_1 \oplus L_1 \cong S_2 \oplus L_2$.*

In other words, two lattices have isomorphic bilinear forms if they are stably equivalent under direct sum with arbitrary unimodular lattices, i.e. if we are allowed to take direct sums with arbitrary direct sums of $\sigma_x$, $\sigma_z$, 1, and $K_{E_8}$. One example of this is two lattices in the same genus. They have the same parity, signature, and bilinear form and are stably equivalent under direct sum with $\sigma_x$, as required by the theorem. However, we can also consider lattices that are not in the same genus. The example that is relevant to the present discussion is a pair of theories, one of which is fermionic and the other

bosonic. They have the same $S$-matrix but may not have the same chiral central charges. The theorem tells us that the difference can be made up with unimodular theories. But since $\sigma_x$ and $\sigma_z$ do not change the chiral central charge, the unimodular lattices given by the theorem must be hypercubic lattices. (In the fermionic context, the $E_8$ lattice is $\sigma_z$-stably equivalent to the 8-dimensional hypercubic lattice.) In other words, *every fermionic Abelian topological phase is equivalent to a bosonic Abelian topological phase, together with some number of filled Landau levels.*

Finally, we consider Nikulin's Corollary 1.16.3, given in Section 4.5, which states that the genus of a lattice is determined by its parity, signature, and bilinear form on the discriminant group. Recall that the parity of a lattice is even or odd according whether its K-matrix is even or odd. The even case can occur in a purely bosonic system while the odd case necessarily requires "fundamental" fermions, i.e. fermions that braid trivially with respect to all other particles. Therefore, specifying the parity, signature, and bilinear form on an Abelian group $A$ is equivalent to specifying (1) whether or not the phase can occur in a system in which the microscopic constituents are all bosons, (2) the $S$-matrix, and (3) the chiral central charge. (According to the previous theorem, the $T$-matrix is determined by the latter two.) This is sufficient to specify any Abelian topological phase. According to Corollary 1.16.3, these quantities specify a genus of lattices. Thus, given any Abelian topological phase, there is an associated genus of lattices. We can take any lattice in this genus, compute the associated K-matrix (in

some basis) and define a $\mathrm{U}(1)^{r_+ + r_-}$ Chern-Simons theory. A change of basis of the lattice corresponds to a change of variables in the Chern-Simons theory. Different lattices in the same genus correspond to different equivalent $\mathrm{U}(1)^{r_+ + r_-}$ Chern-Simons theories for the same topological phase. Therefore, it follows from Corollary 1.16.3 that *every Abelian topological phase can be represented as a* $\mathrm{U}(1)^N$ *Chern-Simons theory.*

## 4.9 Discussion

A theoretical construction of a bulk quantum Hall state typically suggests a particular edge phase, which we will call $K_1$. The simplest example of this is given by integer quantum Hall states, as we discussed in Sections 4.2 and 4.7. However, there is no reason to believe that the state observed in experiments is in this particular edge phase $K_1$. This is particularly important because the exponents associated with gapless edge excitations, as measured through quantum point contacts, for instance, are among the few ways to identify the topological order of the state.[50,154] In fact, such experiments are virtually the only way to probe the state in the absence of interferometry experiments[33,58,87,94,96,99,155] that could measure quasiparticle braiding properties. Thus, given an edge theory $K_2$ that is deduced from experiments, we need to know if a purely edge phase transition can take the system from $K_1$ to $K_2$ – in other words, whether the edge theory $K_2$ is consistent with the proposed theoretical construction of the bulk state. We would

also like to predict, given an edge theory $K_2$ deduced from experiments, what other edge phases $K_3, K_4, \ldots$ might be reached by tuning parameters at the edge, such as the steepness of the confining potential. In this paper, we have given answers to these two questions.

The exotic edge phases at $\nu = 8, 12$ discussed in this paper may be realized in experiments in a number of materials which display the integer quantum Hall effect. These include Si-MOSFETs,[2] GaAs heterojunctions and quantum wells (see, e.g. Refs. 5, 156 and references therein), InAs quanutm wells,[157] graphene,[158] polar $ZnO/Mg_xZn_{1-x}O$ interfaces.[159] In all of these systems, edge excitations can interact strongly and could be in an $E_8$ phase at $\nu = 8$ or the $D_{12}^+$ phase or the $E_8 \oplus \mathbb{I}_4$ phase at $\nu = 12$. To the best of our knowledge, there are no published studies of the detailed properties of edge excitations at these integer quantum Hall states.

The novel edge phase that we have predicted at $\nu = 16/5$ could occur at the $\nu = 3 + 1/5$ state that has been observed[160] in a 31 million $cm^2/Vs$ mobility GaAs quantum well. This edge phase is dramatically different than the edge of the $\nu = 1/5$ Laughlin state weakly-coupled to 3 filled Landau levels. Meanwhile, a $\nu = 8/15$ state could occur in an unbalanced double-layer system (or, possibly, in a single wide quantum well) with $\nu = 1/3$ and $1/5$ fractional quantum Hall states in the two layers. Even if the bulks of the two layers are very weakly-correlated, the edges may interact strongly, thereby leading to the alternative edge phase that we predict. Finally, if an $\nu = 8/7$ state is

observed, then, as in the two cases mentioned above, it could have an edge phase without gapless fermionic excitations.

We have focussed on the relationship between the $K$-matrices of different edge phases of the same bulk. However, in a quantum Hall state, there is also a $t$-vector, which specifies how the topological phase is coupled to the electromagnetic field. An Abelian topological phase specified by a $K$-matrix splits into several phases with inequivalent $t$-vectors. Therefore, two different $K$-matrices that are stably equivalent may still belong to different phases if the corresponding $t$-vectors are are not related by the appropriate similarity transformation. However, in all of the examples that we have studied, given a $(K, t)$ pair, and a $K'$ stably equivalent to $K$, we were always able to find a $t'$ related to $t$ by the appropriate similarity transformation. Said differently, we were always able to find an edge phase transition driven by a charge-conserving perturbation. It would be interesting to see if there are cases in which there is no charge-conserving phase transition between stably-equivalent $K$, $K'$ so that charge-conservation symmetry presents an obstruction to an edge phase transition between $K$, $K'$.

When a bulk topological phase has two different edge phases, one that supports gapless fermionic excitations and one that doesn't, as is the case in the $\nu = 8$ integer quantum Hall state and the fractional states mentioned in the previous paragraph, then a domain wall at the edge must support a fermionic zero mode. For the sake of concreteness, let us consider the $\nu = 8$ IQH edge. Suppose that the edge of the system lies along

the $x$-axis and the edge is in the conventional phase with $K = \mathbb{I}_8$ for $x < 0$ and the $K_{E_8}$ phase for $x > 0$. The gapless excitations of the edge are fully chiral; let us take their chirality to be such that they are all right-moving. A low-energy fermionic excitation propagating along the edge cannot pass the origin since there are no gapless fermionic excitations in the $E_8$ phase. But since the edge is chiral, it cannot be reflected either. Therefore, there must be a fermionic zero mode at the origin that absorbs it.

We discussed how the quadratic refinement allows us to relate a given fermionic theory to a bosonic one. One example that we considered in detail related $K_1 = \begin{pmatrix} 1 & 0 \\ 0 & 7 \end{pmatrix}$ to $K_2 = \begin{pmatrix} 2 & 1 \\ 1 & 4 \end{pmatrix}$. Both of these states are purely chiral. However, we noted that we are not restricted to relating purely chiral theories; we could have instead considered a transition between the $\nu = 1/7$ Laughlin edge and the non-chiral theory described by $K = \begin{pmatrix} 2 & 1 & 0 \\ 1 & 4 & 0 \\ 0 & 0 & -1 \end{pmatrix}$. This transition does not preserve chirality, but the chiral central charges of the two edge theories are the same. It can be shown that there exist regions in parameter space where the non-chiral theory is stable – for example, if the interaction matrix, that we often write as $V$, is diagonal, then the lowest dimension backscattering operator has dimension equal to 4. Even more tantalizingly, it is also possible to consider the $\nu = 1/3$ Laughlin edge which admits an edge transition to the theory described by $K' = \begin{pmatrix} -2 & -1 \\ -1 & -2 \end{pmatrix} \oplus \mathbb{I}_{3\times 3}$. The upper left block is simply the conjugate or $(-1)$ times the Cartan matrix for $\mathrm{SU}(3)_1$. About the diagonal $V$ matrix point, the lowest dimension backscattering term is marginal; it would be interesting to know if stable regions exist.

The theory of quadratic refinements implies that any fermionic TQFT can be realized as a bosonic one, together with some filled Landau levels, as we discussed as the end of Sec. 4.8. In particular, it suggests the following picture: a system of fermions forms a weakly-paired state in which the phase of the complex pairing function winds $2N$ times around the Fermi surface. The pairs then condense in a bosonic topological phase. The winding of the pairing function gives the additional central charge (and, if the fermions are charged, the same Hall conductance) as $N$ filled Landau levels. The remarkable result that follows from the theory of quadratic refinements is that all Abelian fermionic topological phases can be realized in this way.

In this paper, we have focused exclusively on fully chiral states. However, there are many quantum Hall states that are not fully chiral, such as the $\nu = 2/3$ states. The stable edge phases of such states correspond to lattices of indefinite signature. Once again, bulk phases of bosonic systems correspond to genera of lattices while bulk phases of fermionic systems correspond either to genera of lattices or to pairs of genera – one even and one odd. Single-lattice genera are much more common in the indefinite case than in the definite case.[143] If an $n$-dimensional genus has more than one lattice in it then $4^{[\frac{n}{2}]}d$ is divisible by $k^{\binom{n}{2}}$ for some non-square natural number $k$ satisfying $k \equiv 0$ or $1 \pmod 4$, where $d$ is the determinant of the associated Gram matrix (i.e. the K-matrix). In particular, genera containing multiple equivalence classes of $K$-matrices must have

determinant greater than or equal to 17 if their rank is 2; greater than or equal to 128 if their rank is 3; and $5^{\binom{n}{2}}$ or $2 \cdot 5^{\binom{n}{2}}$ for, respectively, even or odd rank $n \geq 4$.

Quantum Hall states are just one realization of topological phases. Our results apply to other realizations of Abelian topological states as well. In those physical realizations which do not have a conserved U(1) charge (which is electric charge in the quantum Hall case), there will be additional U(1)-violating operators which could tune the edge of a system between different phases.

Although we have, in this paper, focussed on Abelian quantum Hall states, we believe that non-Abelian states can also have multiple chiral edge phases. This will occur when two different edge conformal field theories with the same chiral central charge are associated with the same modular tensor category of the bulk. The physical mechanism underlying the transitions between different edge phases associated with the same bulk is likely to be the same as the one discussed here. In this general case, we will not be able to use results on lattices and quadratic forms to find such one-to-many bulk-edge correspondances. Finding analogous criteria would be useful for interpreting experiments on the $\nu = 5/2$ fractional quantum Hall state.

# Chapter 5

# Future Directions

The experiment described in Chapter 2 is currently in progress. We look forward to seeing the signatures of various fractional edge phases.

We are also curious if the microwave experiment could be carried out in topological insulators to provide evidence of the topological phase, complementary to the conductance plateau. In the topological phase, there would be a single peak because both edge modes have the same velocity under time reversal symmetry; the experiment would measure this velocity. Upon applying a magnetic field, the peaks would split and then disappear.

We would like to extend the results of Chapters 3 and 4 to non-Abelian states. It is clear how to compute the tunneling current and shot noise described in Chapter 3 for the $\nu = 5/2$ state, but the calculation is technically more difficult. However, it

is not immediately clear how to extend the classification scheme of Chapter 4 to non-Abelian states because the $K$-matrix description does not apply. This result could be important regarding the $\nu = 5/2$ state because some existing experiments strive to distinguish candidate states by their tunneling signatures, which could change if the system transitioned to a different edge phase.

Another immediate question that arises from Chapter 4 is how to tune the transition between different edge phases experimentally. In the integer case, this would require a 10-fermion interaction term, which seems intractable. In the fractional case, it might only require a 4-fermion term, which is more feasible. However, there is no experimental precedent for tuning the interactions at the edge in a controlled manner.

There is a lot more to learn. We hope to continue the investigations described in this work and uncover more of the mysteries hidden in quantum Hall edges.

# Appendices

# Appendix A

# Magnetoplasmon lifetime from phonon coupling

Here we calculate the decay rate of the magnetoplasmon edge modes at Laughlin fractions $\nu = 1/m$ by considering their coupling to phonons, following Ref. 161

$$\mathcal{S}_{mp-ph} = \int dt d^3\vec{x} d^3\vec{x}' \rho_{3D}(\vec{x}, t)\mathcal{V}_{ij}(\vec{x} - \vec{x}')\partial_i u_j(\vec{x}', t) \tag{A.1}$$

where the field $\vec{u}$ is the ion displacement field, $\rho_{3D}$ is the 3D charge density, and $\mathcal{V}$ is symmetric in its indices and contains the deformation potential, which is the effect of deformations of the lattice on the local electron density, and the piezoelectric effect, which is the long-ranged electric field caused by lattice distortions, according to (as

discussed, for instance, in Ref 162)

$$\mathcal{V}_{ij}(\vec{x}-\vec{x}') = D\delta(\vec{x}-\vec{x}')\delta_{ij} + eh_{14}V_{ij}(\vec{x}-\vec{x}') \tag{A.2}$$

where $D$ is the deformation potential constant, $h_{14}$ is the piezoelectric coupling constant, and the electric potential generated by a lattice strain satisfies

$$\sum_i q_i V_{ij}(\vec{q}) = \sum_\lambda iM_\lambda(\hat{q})\left(\epsilon^\lambda_{\vec{q}}\right)_j \tag{A.3}$$

where $\epsilon^\lambda_{\vec{q}}$ is the polarization vector for a phonon with polarization $\lambda$ and wave vector $\vec{q}$, $h_{14}$ is a piezoelectric coupling constant and $M_\lambda$ is an anisotropy factor.

We consider here a circular geometry,

$$\rho_{3D}(\vec{x}) = \delta(z)\delta(R-|r|)\rho(s) \tag{A.4}$$

for which the interaction action can be rewritten as

$$S_{mp-ph} = \int \frac{d\omega}{2\pi}\frac{1}{L}\sum_k \int \frac{d^3\vec{q}}{(2\pi)^3}\phi(k,\omega)u_j(\vec{q},-\omega)C_j(k,\vec{q}) \tag{A.5}$$

where

$$C_j(k,\vec{q}) = -q_i k\frac{L}{2\pi}\mathcal{V}_{ij}(\vec{q})e^{in_k\theta_{\vec{q}}}(i)^{n_k}J_{n_k}(\frac{L}{2\pi}q_\parallel) \tag{A.6}$$

and $\theta_{\vec{q}}$ is the azimuthal angle of $\vec{q}$; $q_\parallel$ is the magnitude of the component of $\vec{q}$ that lies in the plane of the droplet; $J_n$ is the $n$th Bessel function of the first kind; and $n_k \equiv kL/2\pi$.

The decay rate of the edge modes is given by the self-energy

$$\Sigma(k,\omega) = -\frac{2\pi i}{Lmk}\int \frac{d^3\vec{q}}{(2\pi)^3}\langle u_i(\vec{q},\omega)u_j(-\vec{q},-\omega)\rangle C_i(k,\vec{q})C_j(-k,-\vec{q}) \tag{A.7}$$

The imaginary part of the self-energy gives us the decay rate of the edge mode. Using the phonon propagator,

$$\langle u_i(\vec{q},\omega)u_j(-\vec{q},-\omega)\rangle = \frac{1}{\rho}\frac{i(\epsilon^{\lambda}_{\vec{q}})_i(\epsilon^{\lambda}_{-\vec{q}})_j}{\omega^2-(v_\lambda q)^2+i\delta} \tag{A.8}$$

where $\rho$ is the mass density of the device, we find the imaginary part of the self-energy,

$$\mathrm{Im}\left[\Sigma(k,\omega)\right] = \frac{kL}{2\pi m\rho}\int\frac{d^3\vec{q}}{(2\pi)^3}\left(J_{n_k}\big(q_\parallel L/2\pi\big)\right)^2\left(D^2q^2+e^2h_{14}^2\sum_\lambda\left(M_\lambda(\hat{q})\right)^2\right)\pi\delta(\omega^2-v_\lambda^2q^2) \tag{A.9}$$

We immediately find the contribution proportional to $D^2$:

$$\mathrm{Im}\left[\Sigma(k,\omega)\right]^D = D^2\frac{k\omega^2}{8\pi m\rho v_l^4} \tag{A.10}$$

To find the piezoelectric contribution requires the anisotropy factors for a 2DEG oriented on the (001) plane of GaAs:[163]

$$\begin{aligned}\big(M_l(q_\parallel,q_\perp)\big)^2 &= \frac{9q_\perp^2q_\parallel^4}{2(q_\perp^2+q_\parallel^2)^3}\\ \big(M_t(q_\parallel,q_\perp)\big)^2 &= \frac{8q_\perp^4q_\parallel^2+q_\parallel^6}{4(q_\perp^2+q_\parallel^2)^3}\end{aligned} \tag{A.11}$$

where $q_\perp$ is the component of $\vec{q}$ perpendicular to the plane of the 2DEG, from which we find,

$$\mathrm{Im}\left[\Sigma(k,\omega)\right]^{pz} = e^2h_{14}^2\frac{k}{8\pi m\rho}\left(\frac{13}{32}\frac{1}{v_t^2}+\frac{9}{32}\frac{1}{v_l^2}\right) \tag{A.12}$$

We now specialize to the parameter values for a GaAs quantum well:[161,164,165] $D = 12\mathrm{eV}$, $h_{14} = 1.2\times10^7\mathrm{V/cm}$, $v_l = 5.14\times10^3\mathrm{m/s}$, $v_t = 3.04\times10^3\mathrm{m/s}$ and $\rho = 5.3\mathrm{g/cm}^3$. For

droplets with $L = 10 - 50\mu$m, these numbers yield

$$\begin{aligned} \mathrm{Im}\left[\Sigma(k,\omega)\right]^{D} &= (\nu n_k^3) \times (.01 - 1.5\mathrm{kHz}) \\ \mathrm{Im}\left[\Sigma(k,\omega)\right]^{pz} &= (\nu n_k) \times (2.8 - 14\mathrm{MHz}) \end{aligned} \tag{A.13}$$

where $n_k = Lk/2\pi$ is the mode number.

# Appendix B

# Correction to absorption peak heights in the presence of a QPC

## B.1 Integer and Laughlin states

To find the first order correction $\delta R(\omega)$ in the presence of $\mathcal{L}_{tun}$ it is helpful to define the retarded Green's function $\chi(s_1, s_2, t) \equiv -i\Theta(t)\langle[\phi(s_1, t), \phi(s_2, 0)]\rangle$ and its Fourier transform $\chi(k_1, k_2, \omega) \equiv \int_0^L ds_1 ds_2 e^{-ik_1 s_1 - ik_2 s_2} \int dt e^{i\omega t}\chi(s_1, s_2, t)$, in terms of which we can write the absorption spectrum using the fluctuation-dissipation theorem

$$R(\omega) = \frac{E^2}{16\pi^2 L^2}\coth\frac{\beta\omega}{2}\sum_{k_1,k_2}(-k_1k_2)y(k_1)y(k_2)\Big(i\chi(-k_1,-k_2,\omega) - i\chi(-k_2,-k_1,-\omega)\Big) \tag{B.1}$$

To find the order $\lambda$ correction to $R(\omega)$ we need to find the order $\lambda$ correction to $\chi$. We do perturbation theory in imaginary time:

$$\begin{aligned}\delta\chi(s_1,s_2,\omega_n) &= \int_0^\beta d\tau d\tau' e^{i\omega_n\tau}\Big(\langle\phi(s_1,\tau)\phi(s_2,0)\mathcal{L}_{tun}(\tau')\rangle_0 - \langle\phi(s_1,\tau)\phi(s_2,0)\rangle_0\langle\mathcal{L}_{tun}(\tau')\rangle_0\Big)\\ &= \int_0^\beta d\tau d\tau' e^{i\omega_n\tau}\Big(\langle\phi(s_1,\tau)(\phi(s_a,\tau')-\phi(s_b,\tau'))\rangle_0\langle\phi(s_2,0)(\phi(s_a,\tau')-\phi(s_b,\tau'))\rangle_0\langle\mathcal{L}_{tun}(\tau')\rangle_0\Big)\\ &= \left(\chi_0(s_1,s_a,\omega_n)-\chi_0(s_1,s_b,\omega_n)\right)\left(\chi_0(s_2,s_a,-\omega_n)-\chi_0(s_2,s_b,-\omega_n)\right)\langle\mathcal{L}_{tun}(0)\rangle_0 \qquad \text{(B.2)}\end{aligned}$$

where all the expectation values are imaginary time ordered and the subscript 0 indicates correlation functions calculated at $\lambda = 0$. We have omitted contributions to a zero frequency peak. The middle equality comes from the identity for quadratic fields $\langle\hat{O}_1\hat{O}_2 e^{i\alpha\hat{O}_3}\rangle = \Big(\langle\hat{O}_1\hat{O}_2\rangle - \alpha^2\langle\hat{O}_1\hat{O}_3\rangle\langle\hat{O}_2\hat{O}_3\rangle\Big)\langle e^{i\alpha\hat{O}_3}\rangle$ and time translational invariance allows us to change the argument of $\mathcal{L}_{tun}$ in the last line. Using the Lagrangian (2.2), we find,

$$\chi_0(s_i,s_j,\omega_n) = -\frac{2\pi}{mL}\sum_{k_j}\frac{1}{k_j}\frac{e^{ik(s_i-s_j)}}{i\omega_n - kv} \qquad \text{(B.3)}$$

From which we can simplify Eq B.2

$$\delta\chi(s_1,s_2,\omega_n) = \frac{4\pi^2}{m^2L^2}\prod_{j=1,2}\left(\sum_{k_j}\frac{e^{ik_js_j}\left(e^{-ik_js_a}-e^{-ik_js_b}\right)}{k_j((-1)^{j+1}(i\omega_n)-k_jv)}\right)\langle\mathcal{L}_{tun}(0)\rangle_0 \qquad \text{(B.4)}$$

and find the order $\lambda$ correction to Eq B.1 by taking $i\omega_n \to \omega + i\eta$,

$$\begin{aligned}\delta R(\omega) = &-\frac{E^2}{4m^2}\coth\frac{\beta\omega}{2}\langle\mathcal{L}_{tun}(0)\rangle_0\frac{1}{L^2}\sum_{k_1,k_2}y(k_1)y(k_2)(e^{ik_1s_a}-e^{ik_1s_b})(e^{ik_2s_a}-e^{ik_2s_b})\\ &\times\frac{2}{v(k_1+k_2)}\left(\frac{\eta(\omega)}{\eta(\omega)^2+(\omega+k_1v)^2}-\frac{\eta(\omega)}{\eta(\omega)^2+(\omega-k_2v)^2}\right) \qquad \text{(B.5)}\end{aligned}$$

There is a subtlety in calculating the expectation value of the tunneling Lagrangian $\langle \mathcal{L}_{tun}(0)\rangle_0$. As mentioned in Sec 2.3.1, electrons acquire a phase $\theta$ upon circling the droplet, so the field $\phi$ is not perfectly periodic. Instead, $\Psi_{el}(s=0) = \Psi_{el}(s=L)e^{i\theta}$, where $\Psi_{el} = e^{im\phi}$ is the electron annihilation operator, from which it follows that $\phi(0) = \phi(L) + \theta/m$. Hence, the mode expansion of $\phi$ includes a zero-mode proportional to $\theta$:

$$\phi(s,t) = -\frac{\theta}{m}\frac{s}{L} + \sqrt{\frac{2\pi}{mL}} \sum_{k=\frac{2\pi n}{L}>0} \frac{1}{\sqrt{k}} \left( e^{ik(s-vt)}\phi_k + e^{-ik(s-vt)}\phi_k^\dagger \right) \tag{B.6}$$

We can regard $\theta$ as a classical variable that commutes with the $\phi_k$, which themselves satisfy $\left[\phi_k, \phi_{k'}^\dagger\right] = \delta_{k,k'}$. The value of $\theta$ is fixed by macroscopic parameters:

$$\theta = 2\pi(\Phi/\Phi_0 + n_{tot}) \tag{B.7}$$

where $\Phi$ is the flux penetrating the droplet, $\Phi_0 = h/e$ is the flux quantum and $n_{tot}$ is the number of charge $e/m$ quasiparticles in the bulk in the Laughlin case (in the integer case, $n_{tot} = 0$.) Consistency with the definition of $\theta$ requires $\arg(\lambda) = -\theta_L/m + \alpha$, where $\alpha$ is independent of magnetic field and quasiparticle number and $\theta_L = 2\pi(\Phi_L/\Phi_0 + n_L)$ is the Aharonov Bohm phase an electron would acquire from circling only the left lobe of the droplet when there is flux $\Phi_L$ piercing the left lobe and $n_L$ quasiparticles inside. Using the mode expansion (B.6), we can now correctly evaluate:

$$\langle \mathcal{L}_{tun}(0)\rangle_0 = |\lambda| 2\cos\left(\arg(\lambda) - \frac{(s_a - s_b)\theta}{Lm}\right) \exp\left[\frac{\pi}{mL}\sum_{k>0}\frac{2}{k}(\cos(k(s_a - s_b)) - 1)\coth\frac{\beta v k}{2}\right] \tag{B.8}$$

## B.2 $\nu = 5/2$

To find the first order correction $\delta R(\omega)$ to the absorption spectrum at $\nu = 5/2$ in the presence of $\mathcal{L}^{52}_{tun}$ we follow the calculation in Appendix B.1 and reach Eq B.5 with $m = 2$ and

$$\langle \mathcal{L}_{tun}(0)\rangle_0 \to \langle \mathcal{L}^{5/2}_{tun}(0)\rangle_0 = \lambda \langle \sigma(s_a,0)\sigma(s_b,0)\rangle \langle e^{i\phi(s_a,0)/2} e^{-i\phi(s_b,0)/2}\rangle + h.c. \tag{B.9}$$

We can find

$$\langle e^{i\phi(s_a,0)/2} e^{-i\phi(s_b,0)/2}\rangle = \exp\left[\frac{\pi}{L}\sum_{k>0}\frac{1}{k}\left(\cos(k(s_a-s_b))-1\right)\coth\frac{\beta v k}{2} - i\frac{\theta_{5/2}}{4}\frac{s_a-s_b}{L}\right] \tag{B.10}$$

where we have used the mode expansion

$$\phi(s,t) = \sqrt{\frac{\pi}{L}}\sum_{k>0}\frac{1}{\sqrt{k}}\left(e^{ik(s-vt)}\phi_k + e^{-ik(s-vt)}\phi_k^\dagger\right) - \frac{\theta_{5/2}}{2}\frac{s}{L} \tag{B.11}$$

where $\theta_{5/2} = 2\pi\left(\Phi/\Phi_0 + n_{tot}/2\right)$ and $n_{tot}$ is the number of $e/4$ quasiparticles in the bulk, to account for the non-periodicity of $\phi$, as described in Appendix B.1. Consistency with the choice of $\theta_{5/2}$ requires $\arg(\lambda) = -\theta_L/4 + \alpha$, where $\alpha$ is the non-Aharonov Bohm contribution to the phase and $\theta_L = 2\pi(\Phi_L/\Phi_0 + n_L)$ is the Aharonov-Bohm phase an electron would acquire from circling the left lobe of the droplet.

We now seek the correlation function $\langle\sigma(s_a)\sigma(s_b)\rangle$. When there are no bulk quasiparticles, the correlation function is given by[166]

$$\langle\sigma(s_a)\sigma(s_b)\rangle_{\text{no qp}} = \frac{e^{-i\pi/16}}{\left(\frac{L}{\pi}\sin\left(\frac{\pi}{L}(s_a-s_b)\right)\right)^{1/8}} \tag{B.12}$$

A quasiparticle in the bulk contributes a branch cut that crosses the perimeter of the droplet at some point $s_j$ for all times. We can think of this branch cut as coming from the creation of a quasiparticle at $s_j$ at a time in the far past and its subsequent annihilation in the far future. Hence, the two point function with one quasiparticle in the bulk is computed by

$$\langle \sigma(s_a,t)\sigma(s_b(t)\rangle_{\text{bulk qp}} = \lim_{T\to\infty} \frac{\langle (\sigma(s_j,T)\sigma(s_a,t)\sigma(s_b,t)\sigma(s_j,-T)\rangle_{\text{no qp}}}{\langle \sigma(s_j,T)\sigma(s_j,-T)\rangle_{\text{no qp}}} \tag{B.13}$$

The numerator and denominator can be calculated using bosonization,[166] specifically, by the method of 167. Additional quasiparticles can be included by adding more pairs to the numerator and denominator. When we do this, we always assume that the pair of $\sigma$ quasiparticles at the QPC are fused to the identity, i.e. there is an energy cost for creating a fermion on the edge. We also assume that the fermion parity of the entire system, consisting of the droplet and the point at infinity, is even. We cite the results for specific cases in earlier sections.

# Appendix C

# Non-equilibrium correlation functions

## C.1 Introduction

Because current flows from one edge of the Hall bar to the other, the system at hand is not in equilibrium. Hence, we rely on the Schwinger-Keldysh formalism[168,169] to calculate correlators: to do this, we double the time contour so that $t$ goes from $-\infty$ to $+\infty$ and back to $-\infty$ again. It is convenient to label the forward and backward moving time paths by a superscript $\mu = \pm$, so that each time $t$ is now labeled by $t^\mu$ and an integral over all times is now $\int_K dt \equiv \int_{-\infty}^{\infty} dt^+ + \int_{\infty}^{-\infty} dt^- = \int_{-\infty}^{\infty} dt^+ - \int_{-\infty}^{\infty} dt^-$. Correlation functions now depend on which side of the contour the times lie on. A

thorough explanation of bosonic correlators is given in Refs 29 and 92. Here we state the result for right- or left-moving bosonic fields $\phi_{R/L}$:

$$\begin{aligned}\langle\phi_{R/L}(t_1^\mu, x_1)\phi_{R/L}(t_2^\nu, x_2)\rangle &\equiv -\ln G^{\mu\nu}_{R/L}(t_1 - t_2, x_1 - x_2) \\ &= -\ln\left(\epsilon + iK^{\mu\nu}(t_1 - t_2)(v_{R/L}(t_1 - t_2) \mp (x_1 - x_2))\right) \quad \text{(C.1)}\end{aligned}$$

where

$$K^{\mu\nu}(t) = \Theta(\mu\nu)\mathrm{sgn}(\mu t) + \Theta(-\mu\nu)\mathrm{sgn}\nu \quad \text{(C.2)}$$

$v_{R/L} > 0$ denotes the velocity of the respective mode and $\epsilon$ is a small positive number. Fermions get an extra minus sign:

$$\langle\psi_{R/L}(t_1^\mu, x_1)\psi^\dagger_{R/L}(t_2^\nu, x_2)\rangle = \frac{K^{\mu\nu}(t_1 - t_2)}{G^{\mu\nu}_{R/L}(t_1 - t_2, x_1 - x_2)} \quad \text{(C.3)}$$

Similarly to the minus sign for fermions, we need to consider the Klein factors for the bosonic tunneling operators when we consider systems with two QPCs, as in Sec 3.2. Without the Klein factors, the tunneling terms in the Lagrangian at $x = 0$ and $x = d$ generically do not commute:

$$\left(e^{iq\phi_T(0)}e^{iq\phi_B(0)}\right)\left(e^{i\Phi(d)}e^{-ir\phi_T(d)}\right) = \left(e^{i\Phi(d)}e^{-ir\phi_T(d)}\right)\left(e^{iq\phi_T(0)}e^{iq\phi_B(0)}\right)e^{i\pi(q_n r_n - q_c r_c)\mathrm{sgn}(d)} \quad \text{(C.4)}$$

(We have bosonized the external lead $\Psi \sim e^{-i\Phi}$ and shown the spatial arguments but suppressed the time arguments.) However, because the product of the pair of operators in each set of parenthesis is bosonic, they are physically required to commute. This

discrepancy is resolved by including Klein factors. The prescription is as follows: to each tunneling quasiparticle or electron operator, we attach a Klein factor $\kappa_{x,T/B/E}$, where the subscript $x = 0, a$ indicates the position at which the tunneling operator acts and $T/B/E$ indicates the edge: top/bottom/external lead. For example: $e^{iq\phi_T(0)} \to \kappa_{0,T}^\dagger e^{iq\phi_T(0)}$. The $\kappa$s then must satisfy the commutation relation:

$$\kappa_{0,T}^\dagger \kappa_{0,B} \kappa_{d,E}^\dagger \kappa_{d,T} = \kappa_{d,E}^\dagger \kappa_{d,T} \kappa_{0,T}^\dagger \kappa_{0,B} e^{-i\pi(q_n r_n - q_c r_c)\mathrm{sgn}(d)} \tag{C.5}$$

In the calculation of any physical quantity, the $\kappa$s will come in pairs $\kappa_{0/d,T}^\dagger \kappa_{0/d,B/E}$. Following Ref 170, it is convenient to bosonize these pairs:

$$\kappa_{0,T}^\dagger \kappa_{0,B} = e^{-i\theta_0}, \quad \kappa_{d,E}^\dagger \kappa_{d,T} = e^{-i\theta_d} \tag{C.6}$$

Using $\mathrm{sgn}(d) = -1$, we find $[\theta_0, \theta_d] = -i\pi(q_n r_n - q_c r_c)$. If $q_c r_c > q_n r_n$ then conventional raising and lowering operators can be defined by $a = \frac{1}{\sqrt{2\pi(q_c r_c - q_n r_n)}}(\theta_0 + i\theta_d)$, where $\langle a^\dagger a \rangle_0 = 0, \langle a a^\dagger \rangle = 1$. This readily yields $\langle \theta_0 \theta_d \rangle = -\langle \theta_d \theta_0 \rangle = i\langle \theta_0 \theta_0 \rangle = i\langle \theta_d \theta_d \rangle = i\frac{\pi}{2}(q_c r_c - q_n r_n)$. (If $q_n r_n > q_c r_c$, the roles of $a$ and $a^\dagger$ are reversed). Finally, since the system is not in equilibrium, we will actually need to use $\langle \theta_0(t_1^\mu)\theta_d(t_2^\nu)\rangle = i\frac{\pi}{2}K^{\mu\nu}(t_1 - t_2)(q_c r_c - q_n r_n)$.

The Klein factors drop out of the leading order current and noise calculations, which only include one QPC, but are important in computing the excess noise and current.

## C.2 Fermionic excess current and noise calculations

Here we show the details of how to find $\Delta I_{tun}$ to leading order as written in Eq (3.13) using the correlators described in Sec C.1. As a warm-up, we calculate the leading order noise and current across a QPC using the Keldysh formalism. Model the current injection at $x = d$ by the tunneling term

$$\mathcal{L}_{tun} = -\lambda e^{-i\omega_0 t}\psi_1^\dagger \cdots \psi_n^\dagger \psi_{n+1} \cdots \psi_{2n}\delta(x-d) + h.c. \tag{C.7}$$

where each of the fermion fields obeys the Lagrangian (3.1) for some chirality that will not be important here. The current operator corresponding to this tunneling term is $I_{tun} = e\frac{d}{dt}N_T = ie[N_T, H] = -ier_c\lambda e^{-i\omega_0 t}\psi_1^\dagger \cdots \psi_n^\dagger \psi_{n+1} \cdots \psi_{2n} + h.c.$, where $N_T$ is the number operator for the charged electron fields on the top edge and $r_c$ is an integer that counts the charged fields. Then the current across the QPC is given to leading order by

$$\begin{aligned}
\langle I_{tun}\rangle_0 &= \langle I_{tun} i\int dt \mathcal{L}_{tun}\rangle \\
&= er_c|\lambda|^2 \int_K dt \prod_{j=1}^{n}\langle\psi_j^\dagger(0^+)\psi_j(t^\mu)\rangle \prod_{j=n+1}^{2n}\langle\psi_j(0^+)\psi_j^\dagger(t^\mu)\rangle e^{-i\omega_0 t} + h.c. \\
&= er_c|\lambda|^2 \int_K \left(\frac{K^{+\mu}(-t)}{G^{+\mu}(-t)}\right)^{2n} (-2i\sin(\omega_0 t)) \\
&= -2ier_c|\lambda|^2 \left(\int_{-\infty}^{\infty} dt \frac{(\mathrm{sgn}(-t))^{2n}}{(\epsilon + i|t|)^{2n}} - \frac{(-1)^{2n}}{(\epsilon+it)^{2n}}\right)\sin(\omega_0 t) \\
&= \frac{2\pi}{\Gamma(2n)} er_c|\lambda|^2(\omega_0)^{2n-1}
\end{aligned} \tag{C.8}$$

where here we have absorbed the velocity into the coupling constants. We have placed the time 0 on the + side of the Keldysh contour (as long as it is fixed, either side is correct) and integrated the time $t$ over both sides. We have suppressed the space index because it does not enter. Notice that in the second to last line, the integrand disappears when $t > 0$, which enforces chirality. This result yields Eqs (3.10) and (3.11).

The noise across the junction $S(t) = \frac{1}{2}\{I_{tun}(t^+), I_{tun}(0^-)\}$ is similarly computed and its Fourier transform $S(\omega)$ is found to be

$$S(\omega) = \frac{1}{2} e r_c I_{tun} \left( |1 - \omega/\omega_0|^{2n-1} + |1 + \omega/\omega_0|^{2n-1} \right) \tag{C.9}$$

which yields the usual relation in the zero-frequency limit $S(\omega = 0) = e r_c I_{tun}$. However, when there are multiple tunneling terms $\mathcal{L}_{tun,k}$ that tunnel different amounts of charge $n_k$, the proportionality of the total current and noise that are measured is lost, and $S(\omega = 0)/I_{tun} = e \left(\sum_k n_k I_{tun,k}\right) / \left(\sum_k I_{tun,k}\right)$.

### C.2.1 Excess current

We now tackle the next order in perturbation theory to find $\Delta I_{tun}$. Using Eqs (3.3), (3.5), and (3.13) and the correlation functions of the previous section yields

$$\begin{aligned} \frac{\Delta I_{tun}}{e|\lambda_2|^2|\Lambda_2|^2} = 2 \int_K dt_1^\mu dt_2^\nu dt_3^\sigma \frac{2i \sin(\omega_0 t_1 + \omega_1(t_3 - t_2))}{\left(G^{+\mu}(-t_1, 0)\right)^2 \left(G^{\nu\sigma}(t_2 - t_3, 0)\right)^2} \\ \times \Big( F_L(0,1,2,3) + F_L(0,3,1,2) \Big) \Big( F_R(0,1,2,3) + F_R(0,3,1,2) \Big) \end{aligned} \tag{C.10}$$

where

$$F_{L/R}(i,j,k,l) = \frac{K^{\mu_i\mu_j}(t_i - t_j)K^{\mu_k\mu_l}(t_k - t_l)}{G^{\mu_i\mu_j}_{L/R}(t_i - t_j, x_i - x_j)G^{\mu_k\mu_l}_{L/R}(t_k - t_l, x_k - x_l)} \tag{C.11}$$

and $t_0 = 0, x_0 = x_1 = 0, x_2 = x_3 = d$. The subscripts $R/L$ have been omitted where there is no $x$ argument. The factor of 2 in front of Eq (C.10) is from another set of terms that occurs in Eq (3.13) which is related by $t_2 \leftrightarrow t_3$.

We now consider each term in Eq (C.10) when the product in the second line is expanded. The term $F_L(0,1,2,3)F_R(0,1,2,3)$ disappears when all parts of the Keldysh contour are summed over (even before integration) because it does not mix times 0 and $t_1$ with $t_2, t_3$. We now consider the term $F_L(0,1,2,3)F_R(0,3,1,2)$, which, when each contribution of the Keldysh contour is added, contributes to the right hand side of Eq (C.10)

$$\begin{aligned}
\Delta I_{tun,12} = &\int_{-\infty}^{0} dt_1 dt_2 dt_3 \frac{4i\sin(\omega_0 t_1 + \omega_1(t_3 - t_2))}{(\epsilon - it_1)^3} \times \\
&\left( \frac{1}{(\mathrm{sgn}(t_2 - t_3)\epsilon + i(t_2 - t_3))^3(\epsilon - i(t_3 - d_R))(\mathrm{sgn}(t_1 - t_2)\epsilon + i(t_1 - t_2 + d_R))} \right. \\
&- \frac{1}{(-\epsilon + i(t_2 - t_3))^3(-\epsilon - i(t_3 - d_R))(\mathrm{sgn}(t_1 - t_2)\epsilon + i(t_1 - t_2 + d_R))} \\
&- \frac{1}{(\epsilon + i(t_2 - t_3))^3(\epsilon - i(t_3 - d_R))(-\epsilon + i(t_1 - t_2 + d_R))} \\
&\left. + \frac{1}{(-\mathrm{sgn}(t_2 - t_3)\epsilon + i(t_2 - t_3))^3(-\epsilon - i(t_3 - d_R))(-\epsilon + i(t_1 - t_2 + d_R))} \right) + h.c. \\
= &\Theta(-d_R)\pi \int_{-\infty}^{\infty} dt_1 dt_3 4i\sin(-\omega_0 t_1 + \omega_1 t_3) \left( \frac{1}{(\epsilon - it_1)^3} + \frac{1}{(\epsilon + it_1)^3} \right) \times
\end{aligned}$$

$$\left(\frac{1}{(\epsilon - it_3)^3(\epsilon - i(t_3 - t_1))} - \frac{1}{(\epsilon + it_3)^3(\epsilon + i(t_3 - t_1))}\right)$$
$$= 8\pi^2\Theta(-d_R)\int_{-\infty}^{\infty} dt_1 \left(\frac{1}{(\epsilon - it_1)^3} + \frac{1}{(\epsilon + it_1)^3}\right) \times$$
$$\left(\frac{-\omega_1 t_1 \cos(\omega_0 t_1) + \sin(\omega_0 t_1)(1 - \frac{1}{2}t_1^2\omega_1^2) - \sin((\omega_0 - \omega_1)t_1)}{t_1^3}\right) \tag{C.12}$$

We have introduced $d_{R/L} = d/v_{R/L}$ and absorbed overall factors of velocity into the tunneling constant. In the first line of Eq (C.12), the integral is only written for $t_i < 0$ because the $t_i > 0$ terms cancel; this is an example of how the Keldysh contour enforces chirality. To get the first equality, we used the expression for a delta-function

$$\lim_{\epsilon \to 0} \frac{\epsilon}{\epsilon^2 + x^2} = \pi\delta(x) \tag{C.13}$$

with some algebraic manipulations. The second equality is from doing the $t_3$ integral exactly. The denominator $1/t_1^3$ in the first line should not be a concern because the limit of the entire term in parenthesis is a constant as $t_1 \to 0$. Consequently, we can push the pole at $t_1 = 0$ to either side of the imaginary axis in order to do the contour integral. This strategy yields

$$\Delta I_{tun,12} = -\frac{2}{15}\pi^3 \left(10\omega_0^2\omega_1^3 - 5\omega_0\omega_1^4 + \omega_1^5\right)\Theta(-d_R) \tag{C.14}$$

We now impose the condition that the neutral fermions are Majorana fermions. This generates an extra term in the 4-point correlation function $\langle\psi_0(0,0)\psi_0(t_1,0)\psi_0(t_2,d)\psi_0(t_3,d)\rangle$ of Eq (C.10) that is equivalent to taking $\omega_1 \to -\omega_1$. Consequently, when the neutral

fermions are Majorana fermions,

$$\Delta I_{tun,12} = \frac{4}{3}\pi^3\omega_0\omega_1^4\Theta(-d_R) \tag{C.15}$$

This yields Eq (3.14) in the main text.

The next term in Eq (C.10) to consider is the term that contains the product $F_L(0,3,1,2)F_R(0,1,2,3)$. By symmetry, this term will yield Eq (C.15) with $d \leftrightarrow -d$. The final term in Eq (C.10) is that which contains $F_L(0,3,1,2)F_R(0,3,1,2)$ and contributes to the right hand side of Eq (C.10),

$$\begin{aligned}
\Delta I_{tun,22} = &\int_{-\infty}^{0} dt_1dt_2dt_3 \frac{4i\sin(\omega_0 t_1 + \omega_1(t_3-t_2))}{(\epsilon - it_1)^2} \\
&\times \Bigg( \frac{(\epsilon - i(t_3+d_L))^{-1}(\mathrm{sgn}(t_1-t_2)\epsilon + i(t_1-t_2-d_L))^{-1}}{(\mathrm{sgn}(t_2-t_3)\epsilon + i(t_2-t_3))^2(\epsilon - i(t_3-d_R))(\mathrm{sgn}(t_1-t_2)\epsilon + i(t_1-t_2+d_R))} \\
&- \frac{(-\epsilon - i(t_3+d_L))^{-1}(\mathrm{sgn}(t_1-t_2)\epsilon + i(t_1-t_2-d_L))^{-1}}{(-\epsilon + i(t_2-t_3))^2(-\epsilon - i(t_3-d_R))(\mathrm{sgn}(t_1-t_2)\epsilon + i(t_1-t_2+d_R))} \\
&- \frac{(\epsilon - i(t_3+d_L))^{-1}(-\epsilon + i(t_1-t_2-d_L))^{-1}}{(\epsilon + i(t_2-t_3))^2(\epsilon - i(t_3-d_R))(-\epsilon + i(t_1-t_2+d_R))} \\
&+ \frac{(-\epsilon - i(t_3+d_L))^{-1}(-\epsilon + i(t_1-t_2-d_L))^{-1}}{(-\mathrm{sgn}(t_2-t_3)\epsilon + i(t_2-t_3))^2(-\epsilon - i(t_3-d_R))(-\epsilon + i(t_1-t_2+d_R))} \Bigg) + h.c. \\
= &\int_{-\infty}^{0} dt_1dt_2dt_3 \frac{4i\sin(\omega_0 t_1 + \omega_1(t_3-t_2))}{(\epsilon - it_1)^2} \left( \frac{1}{-(d_R+d_L)^2} \right) \\
&\times \Bigg( \frac{1}{(\mathrm{sgn}(t_2-t_3)\epsilon + i(t_2-t_3))^2(\epsilon - i(t_3-d_R))(\mathrm{sgn}(t_1-t_2)\epsilon + i(t_1-t_2+d_R))} \\
&- \frac{1}{(-\epsilon + i(t_2-t_3))^2(-\epsilon - i(t_3-d_R))(\mathrm{sgn}(t_1-t_2)\epsilon + i(t_1-t_2+d_R))} \\
&- \frac{1}{(\epsilon + i(t_2-t_3))^2(\epsilon - i(t_3-d_R))(-\epsilon + i(t_1-t_2+d_R))} \\
&+ \frac{1}{(-\mathrm{sgn}(t_2-t_3)\epsilon + i(t_2-t_3))^2(-\epsilon - i(t_3-d_R))(-\epsilon + i(t_1-t_2+d_R))} \Bigg) + h.c.
\end{aligned}$$

$$
\begin{aligned}
&= -\frac{4\pi}{(d_R+d_L)^2}\int_{-\infty}^{\infty} dt_1 dt_2 i\sin(\omega_0 t_1-\omega_1 t_2)\left(\frac{1}{(\epsilon-it_1)^2}-\frac{1}{(\epsilon+it_1)^2}\right)\\
&\times\left(\frac{1}{(\epsilon-it_2)^2(\epsilon-i(t_2+t_1))}+\frac{1}{(\epsilon+it_2)^2(\epsilon+i(t_2+t_1))}\right)\\
&= -\frac{8\pi^2}{(d_R+d_L)^2}\int_{-\infty}^{\infty} dt_2\left(\omega_0\cos(\omega_1 t_2)\left(\frac{1}{(\epsilon-it_2)^3}+\frac{1}{(\epsilon+it_2)^3}\right)\right.\\
&\left.-\sin(\omega_1 t_2)\left(\frac{i}{(\epsilon-it_2)^4}-\frac{i}{(\epsilon+it_2)^4}\right)\right)\\
&= -\frac{8\pi^3}{(d_R+d_L)^2}\left(\omega_0\omega_1^2+\frac{1}{3}\omega_1^3\right) \qquad \text{(C.16)}
\end{aligned}
$$

where we have absorbed overall factors of velocity into the tunneling constant. In the first equality, we have taken $d_{R/L} < 0$ and removed the infinitesimal $\epsilon$'s from terms in the denominator that are not small and approximated their values (specifically, the integral is dominated by $t_3, t_2 \approx d_R < 0$ and $t_1 \approx 0$, so $\pm\epsilon - i(t_3 + d_L) \approx -i(d_R + d_L)$ while $\pm\epsilon + i(t_1 - t_2 - d_L) \approx -i(d_R + d_L)$. By symmetry, we will get the same answer when $d_{R/L} > 0$. The second equality again utilizes the delta-function identity (C.13), along with some algebra. The third equality uses the derivative of the delta-function identity and integration by parts. In the main text, we consider the case where the injected current is far away from the tunneling QPC, so that $|d_R + d_L| \gg 1/\omega_0, 1/\omega_1$, and hence $\Delta I_{tun,22} \ll \Delta I_{tun,12}$. However, $\Delta I_{tun,22}$ is present, and in a future experiment where $d$ is of the same scale as the length scale set by the voltages, we would expect it to have an effect, which is independent of the sign of $a$.

### C.2.2 Excess noise

The excess shot noise is defined by

$$\begin{aligned}\Delta S_{tun}(t) &= \frac{1}{2}\left(\langle\{I_2(t), I_2(0)\}\rangle|_{\Lambda_i} - \langle\{I_2(t), I_2(0)\}\rangle|_{\Lambda_i=0}\right) \\ &= \frac{1}{2}\langle\{I_2(t), I_2(0)\}\left(i\int dt_2\mathcal{L}^2_{inj}\right)\left(i\int dt_3\mathcal{L}^2_{inj}\right)\rangle_0 \end{aligned} \tag{C.17}$$

We will compute $\Delta S_{tun}(\omega) = \int dt e^{i\omega t}\Delta S_{tun}(t)$ using the tunneling terms Eqs (3.3) and (3.5):

$$\begin{aligned}\frac{\Delta S_{tun}(\omega)}{e^2|\lambda_2|^2|\Lambda|^2} = -\int_{-\infty}^{\infty} dt 2\cos(\omega t)\int_K dt_2^\nu dt_3^\sigma \frac{2\cos(\omega_0 t + \omega_1(t_3-t_2))}{(G^{+-}(-t,0))^2(G^{\nu\sigma}(t_2-t_3,0))^2}\times \\ \left(F_L(0,1,2,3)+F_L(0,3,1,2)\right)\left(F_R(0,1,2,3)+F_R(0,3,1,2)\right)\end{aligned} \tag{C.18}$$

The factor of $\frac{1}{2}$ that is in the definition of $S(t)$ is cancelled by a factor of 2 that comes from a different term that takes $t_2 \leftrightarrow t_3$. Eq (C.18) looks very similar to Eq (C.10) so we can provide an abbreviated analysis.

The term that contains the product $F_L(0,1,2,3)F_R(0,1,2,3)$ disappears, as in the excess current calculation. We now consider the term that contains $F_L(0,1,2,3)F_R(0,3,1,2)$, the analogue of $\Delta I_{tun,12}$ defined in the previous section:

$$\begin{aligned}\Delta S_{tun,12}(\omega) = 4\int_{-\infty}^{\infty} dt\cos(\omega t)\int_{-\infty}^{0} dt_2 dt_3 \frac{\cos(\omega_0 t + \omega_1(t_3-t_2))}{(\epsilon+it)^3} \\ \times\left(\frac{1}{(\mathrm{sgn}(t_2-t_3)\epsilon + i(t_2-t_3))^3(\epsilon - i(t_3-d_R))(\epsilon+i(t-t_2+d_R))}\right. \\ \left. - \frac{1}{(-\epsilon+i(t_2-t_3))^3(-\epsilon-i(t_3-d_R))(\epsilon+i(t-t_2+d_R))}\right)\end{aligned}$$

$$
\begin{aligned}
&- \frac{1}{(\epsilon + i(t_2 - t_3))^3(\epsilon - i(t_3 - d_R))(-\epsilon + i(t - t_2 + d_R))} \\
&+ \frac{1}{(-\mathrm{sgn}(t_2 - t_3)\epsilon + i(t_2 - t_3))^3(-\epsilon - i(t_3 - d_R))(-\epsilon + i(t - t_2 + d_R))}\Bigg) \\
&= \Theta(-d_R) 4\pi \int_{-\infty}^{\infty} dt dt_3 \cos(\omega t)\cos(\omega_0 t - \omega_1 t_3)\left(\frac{1}{(\epsilon + it)^3} - \frac{1}{(\epsilon - it)^3}\right) \\
&\times \left(\frac{1}{(\epsilon + it_3)^3(\epsilon - i(t - t_3))} - \frac{1}{(\epsilon - it_3)^3(\epsilon + i(t - t_3))}\right) \\
&= \Theta(-d_R) 8\pi^2 i \int_{-\infty}^{\infty} dt \cos(\omega t)\left(\frac{1}{(\epsilon + it)^3} - \frac{1}{(\epsilon - it)^3}\right)\frac{1}{t^3} \\
&\times \left(\cos(\omega_0 t)(-1 + \frac{1}{2}t^2\omega_1^2) - t\omega_1 \sin(\omega_0 t) + \cos((\omega_0 - \omega_1)t)\right) \\
&\xrightarrow{\omega=0} \Theta(-d_R)\frac{2\pi^3}{15}\left(-|\omega_0|^5 - 10\omega_1^2|\omega_0|^3 + 5\omega_1 \mathrm{sgn}(\omega_0)|\omega_0|^4 + |\omega_0 - \omega_1|^5\right) \\
&\xrightarrow{\omega=0} \begin{cases} \Theta(-d_R)\frac{2\pi^3}{15}|\omega_1|^5 & |\omega_0| \ll |\omega_1| \\ -\Theta(-d_R)\frac{4\pi^3}{3}\omega_0^2|\omega_1|^3\mathrm{sgn}(\omega_0\omega_1) & |\omega_0| \gg |\omega_1| \end{cases}
\end{aligned}
\tag{C.19}
$$

As in the previous section, we have absorbed overall factors of velocity in the coupling constants. To obtain the limits of integration in the first line, we used the fact that the integral is dominated by $t \approx 0$ and $t_2, t_3 \approx d_R$ because of the placement of the poles. The rest of the equalities follow similarly to the excess current calculation in the previous section. The result is that in either the limit $|\omega_0| \gg |\omega_1|$ or $|\omega_1| \gg |\omega_0|$, $|\Delta S_{tun,12}(\omega = 0)| = e|\Delta I_{tun,12}|$, but generically, this proportionality does not hold. If the neutral fermions are Majorana fermions then the extra term in the 4-point correlation function contributes an overall factor of two.

Returning to Eq (C.18), the term containing $F_L(0,3,1,2)F_R(0,1,2,3)$ is the same as $\Delta S_{tun,12}$ with $d \to -d$. The final term is that containing $F_L(0,1,2,3)F_R(0,3,1,2)$. Similarly to the calculation of $\Delta I_{tun,22}$, we compute

$$\begin{aligned}
\Delta S_{tun,22}(\omega) &= 4\int_{-\infty}^{\infty} dt\cos(\omega t)\int_{-\infty}^{0} dt_2 dt_3 \frac{\cos(\omega_0 t+\omega_1(t_3-t_2))}{(\epsilon+it)^2} \\
&\times\Bigg(\frac{(\epsilon-i(t_3+d_L))^{-1}(\epsilon+i(t-t_2-d_L))^{-1}}{(\mathrm{sgn}(t_2-t_3)\epsilon+i(t_2-t_3))^2(\epsilon-i(t_3-d_R))(\epsilon+i(t-t_2+d_R))} \\
&-\frac{(-\epsilon-i(t_3+d_L))^{-1}(\epsilon+i(t-t_2-d_L))^{-1}}{(-\epsilon+i(t_2-t_3))^2(-\epsilon-i(t_3-d_R))(\epsilon+i(t-t_2+d_R))} \\
&-\frac{(\epsilon-i(t_3+d_L))^{-1}(-\epsilon+i(t-t_2-d_L))^{-1}}{(\epsilon+i(t_2-t_3))^2(\epsilon-i(t_3-d_R))(-\epsilon+i(t-t_2+d_R))} \\
&+\frac{(-\epsilon-i(t_3+d_L))^{-1}(-\epsilon+i(t-t_2-d_L))^{-1}}{(-\mathrm{sgn}(t_2-t_3)\epsilon+i(t_2-t_3))^2(-\epsilon-i(t_3-d_R))(-\epsilon+i(t-t_2+d_R))}\Bigg) \\
&= -\frac{4}{(d_R+d_L)^2}\int_{-\infty}^{\infty} dt\cos(\omega t)\int_{-\infty}^{0} dt_2 dt_3 \frac{\cos(\omega_0 t+\omega_1(t_3-t_2))}{(\epsilon+it)^2} \\
&\times\Bigg(\frac{1}{(\mathrm{sgn}(t_2-t_3)\epsilon+i(t_2-t_3))^2(\epsilon-i(t_3-d_R))(\epsilon+i(t-t_2+d_R))} \\
&-\frac{1}{(-\epsilon+i(t_2-t_3))^2(-\epsilon-i(t_3-d_R))(\epsilon+i(t-t_2+d_R))} \\
&-\frac{1}{(\epsilon+i(t_2-t_3))^2(\epsilon-i(t_3-d_R))(-\epsilon+i(t-t_2+d_R))} \\
&+\frac{1}{(-\mathrm{sgn}(t_2-t_3)\epsilon+i(t_2-t_3))^2(-\epsilon-i(t_3-d_R))(-\epsilon+i(t-t_2+d_R))}\Bigg) \\
&= -\frac{4\pi}{(d_R+d_L)^2}\int_{-\infty}^{\infty} dt dt_2\cos(\omega t)\cos(\omega_0 t-\omega_1 t_2)\left(\frac{1}{(\epsilon+it)^2}+\frac{1}{(\epsilon-it)^2}\right) \\
&\times\left(\frac{1}{(\epsilon-it_2)^2(\epsilon-i(t_2+t))}+\frac{1}{(\epsilon+it_2)^2(\epsilon+i(t_2+t))}\right) \\
&= \frac{8\pi^2}{(d_R+d_L)^2}\int_{-\infty}^{\infty} dt\cos(\omega t)\left(\frac{1}{(\epsilon+it)^2}+\frac{1}{(\epsilon-it)^2}\right)\frac{1}{t^2}
\end{aligned}$$

$$
\begin{aligned}
&\times \left(\cos((\omega_0+\omega_1)t) - \cos(\omega_0 t) + t\omega_1 \sin(\omega_0 t)\right) \\
&= \frac{4\pi^3}{3(d_R+d_L)^2}\Big(-\left(|\omega+\omega_0+\omega_1|^3 + |\omega-\omega_0-\omega_1|^3\right) + \left(|\omega+\omega_0|^3 + |\omega-\omega_0|^3\right) \\
&+3\omega_1\left(\frac{|\omega+\omega_0|^2}{\mathrm{sgn}(\omega+\omega_0)} - \frac{|\omega-\omega_0|^2}{\mathrm{sgn}(\omega-\omega_0)}\right)\Big) \\
&\xrightarrow{\omega=0} \frac{8\pi^3}{3(d_R+d_L)^2}\left(-|\omega_0+\omega_1|^3 + |\omega_0|^3 + 3\omega_1 \mathrm{sgn}(\omega_0)|\omega_0|^2\right) \\
&\xrightarrow{\omega=0} \begin{cases} -\frac{8\pi^3}{3(d_R+d_L)^2}|\omega_1|^3 & |\omega_0| \ll |\omega_1| \\ -\frac{8\pi^3}{(d_R+d_L)^2}|\omega_0|\omega_1^2 & |\omega_0| \gg |\omega_1| \end{cases}
\end{aligned}
\tag{C.20}
$$

We have absorbed overall factors of velocity into the coupling constants. We assumed $d < 0$ and since the result is symmetry under $d \to -d$, it holds for $d > 0$ as well.

From these results, we see that in any of the limits $|\omega_0| \gg |\omega_1| \gg 1/d_{R/L}$, $|\omega_1| \gg |\omega_0| \gg 1/d_{R/L}$, $|\omega_0| \ll |\omega_1| \ll 1/d_{R/L}$, or $|\omega_1| \ll |\omega_0| \ll 1/d_{R/L}$, the excess noise and excess current are proportional via $\Delta S_{tun}(\omega = 0) = e\Delta I_{tun}$.

## C.3 Bosonic excess current and noise calculation

Here we will show the details of how to find $\Delta I_{tun}$ to leading order as written in Eq (3.23) using the correlators and Klein factors described in Appendix C.1 and the tunneling terms in Eq (3.16) and (3.17). We first find the leading order current and noise, which follow similarly to the fermion case of the previous section. For the remainder of this section, we will omit the sum over quasiparticles and consider the contribution to

the tunneling noise and current from a single species described by $q = (q_n, q_c)$ tunneling from the top edge at $x = 0$ to a single species $q' = (q'_n, q'_c = q_c)$ at the bottom edge, with amplitude $\lambda$ and a single charge-$e$ species tunneling to the external lead described by $r = (r_n, r_c)$ with tunneling amplitude $\Lambda$.

$$\begin{aligned}
\langle I_{tun}\rangle_0 &= \langle I_{tun} i \int dt \mathcal{L}_{tun}\rangle \\
&= q_c e^* |\lambda|^2 \int_K dt \langle e^{iq_n\phi_{n,T}(0^+)} e^{-iq_n\phi_{n,T}(t^\mu)}\rangle \langle e^{iq_c\phi_{c,T}(0^+)} e^{-iq_c\phi_{c,T}(t^\mu)}\rangle \\
&\quad \langle e^{-iq'_n\phi_{n,B}(0^+)} e^{iq'_n\phi_{n,B}(t^\mu)}\rangle \langle e^{-iq'_c\phi_{c,B}(0^+)} e^{iq'_c\phi_{c,B}(t^\mu)}\rangle e^{-iq_c\omega_0 t} + h.c. \\
&= q_c e^* |\lambda|^2 \int_K dt \frac{-2i\sin(q_c\omega_0 t)}{(\epsilon + iK^{+\mu}(-t)(-t))^{q^2+q'^2}} \\
&= q_c e^* |\lambda|^2 \int_{-\infty}^{0} dt \, (-2i\sin(q_c\omega_0 t)) \left( \frac{1}{(\epsilon - it)^{q^2+q'^2}} - \frac{1}{(\epsilon + it)^{q^2+q'^2}} \right) \\
&= \frac{2\pi q_c e^* |\lambda|^2 \mathrm{sgn}(\omega_0) |q_c\omega_0|^{q^2+q'^2-1}}{\Gamma(q^2+q'^2)}
\end{aligned} \tag{C.21}$$

The generalization from Eq (C.8) for fermions is clear. A similar calculation yields:

$$\langle I_{inj}\rangle_0 = \frac{2\pi e |\Lambda|^2 \mathrm{sgn}(\omega_1) |\omega_1|^{r^2}}{\Gamma(1+r^2)} \tag{C.22}$$

where we have absorbed overall factors of velocity into the coupling constant.

The leading order contribution to the shot noise at the QPC at $x = 0$ is found in the same way, yielding

$$\begin{aligned}
S_{tun}(\omega) &= \frac{\pi |\lambda|^2 (q_c e^*)^2}{\Gamma(q^2+q'^2)} \Big( |\omega + q_c\omega_0|^{q^2+q'^2-1} + |\omega - q_c\omega_0|^{q^2+q'^2-1} \Big) \\
&\xrightarrow{\omega=0} \frac{2\pi |\lambda|^2 (q_c e^*)^2}{\Gamma(q^2+q'^2)} |q_c\omega_0|^{q^2+q'^2-1}
\end{aligned} \tag{C.23}$$

This yields the expected proportionality $S_{tun}(\omega = 0) = q_c e^* I_{tun}$. However, if there are multiple species of tunneling quasiparticles, then the total current and shot noise are a sum over the contributions from all quasiparticles and their proportionality is lost.

### C.3.1 Finite temperature

At finite temperature the correlation functions can be deduced from the zero-temperature correlators by conformal transformation. The result is[171]

$$G^{\mu\nu}(t,x) \to \frac{\sin(\pi T G^{\mu\nu}(t,x))}{\pi T} \tag{C.24}$$

where $T$ indicates the temperature. Consequently, the results of the previous section are modified as follows:

$$\begin{aligned}\langle I_{tun}\rangle_0 &= e^*|\lambda|^2 \int_{-\infty}^{\infty} dt \frac{-2i\sin(q_c\omega_0 t)(\pi T)^{q^2+q'^2}}{(\sin(\pi T(\epsilon - it))^{q^2+q'^2}} \\ &= \frac{e^*|\lambda|^2}{(2\pi T)^{1-q^2-q'^2}} 2i \sin\left(\frac{\pi\left(q^2+q'^2\right)}{2}\right) B\left(1-q^2+q'^2, -\frac{iq_c\omega_0}{2\pi T} + \frac{q^2+q'^2}{2}\right) + h.c.\end{aligned} \tag{C.25}$$

where $B$ is the beta-function $B(x,y) = \Gamma(x)\Gamma(y)/\Gamma(x+y)$. Similarly,

$$\begin{aligned}S_{tun}(\omega = 0) = (e^*)^2|\lambda|^2(2\pi T)^{q^2+q'^2-1} 2\cos\left(\frac{\pi}{2}\left(q^2+q'^2\right)\right) \times \\ \left(B\left(1-q^2+q'^2, -\frac{iq_c\omega_0}{2\pi T} + \frac{q^2+q'^2}{2}\right) + h.c.\right)\end{aligned} \tag{C.26}$$

There will be an additional contribution from interactions between the QPC and the noise in the source current.

### C.3.2 Excess current

We now compute the correction to $\Delta I_{tun}$ from the injected current. This is similar to the calculation in Appendix C.2.1, but more difficult because the bosonized edge allows for fractional exponents. Expanding on the definition of $\Delta I_{tun}$ in Eq (3.23) we find

$$\frac{\Delta I_{tun}}{q_c e^* |\lambda|^2 |\Lambda|^2} = 2 \int_K dt_1^\mu dt_2^\nu dt_3^\sigma \frac{2i \sin(q_c \omega_0 t_1 + \omega_1 (t_3 - t_2))}{(G^{+\mu}(-t_1, 0))^{q^2+q'^2} \left(G^{\nu\sigma}(t_2 - t_3, 0)\right)^{1+r^2}} H_{1R} H_{2L} \quad \text{(C.27)}$$

where

$$\begin{aligned} H_{j,R/L} &= \frac{((-1)^j i)^{q_j r_j \left(K^{+\sigma}(-t_3) + K^{\mu\nu}(t_1 - t_2)\right)}}{((-1)^j i)^{q_j r_j (K^{+\nu}(-t_2) + K^{\mu\sigma}(t_1 - t_3))}} \frac{\left(G^{+\nu}_{R/L}(-t_2, -d)\right)^{q_j r_j} \left(G^{\mu\sigma}_{R/L}(t_1 - t_3, -d)\right)^{q_j r_j}}{\left(G^{+\sigma}_{R/L}(-t_3, -d)\right)^{q_j r_j} \left(G^{\mu\nu}_{R/L}(t_1 - t_2, -d)\right)^{q_j r_j}} \\ &= \frac{(i\epsilon K^{+\nu}(-t_2) - (-t_2 \pm d_{R/L}))^{q_j r_j}}{(i\epsilon K^{+\sigma}(-t_3) - (-t_3 \pm d_{R/L}))^{q_j r_j}} \frac{(i\epsilon K^{\mu\sigma}(t_1 - t_3) - (t_1 - t_3 \pm d_{R/L}))^{q_j r_j}}{(i\epsilon K^{\mu\nu}(t_1 - t_2) - (t_1 - t_2 \pm d_{R/L}))^{q_j r_j}} \end{aligned} \quad \text{(C.28)}$$

the index $j = 1, 2$ corresponds to $n, c$. We have introduced $d_{R/L} = d/v_{R/L}$ and absorbed overall factors of velocity into the coupling constants. The $R/L$ index has been suppressed on the correlation functions that have no spatial argument. The powers of $i$ in $H_{j,R/L}$ keep track of the Klein factors, as discussed in Appendix C.1. When we sum over both sides of the Keldysh contour for the times $t_i$, we see that only times $t_i < 0$ survive; this is another example of the Keldysh method enforcing causality. Hence, the integral (C.27) is dominated by $t_1 \approx 0$, $t_{2,3} \approx d_R < 0$. (As shown in Fig 3.1, we are interested in $d < 0$, although by the symmetry of Eq (C.27), the computation for $d > 0$ will be the same as that for $d < 0$ if we swap $q_n, r_n \leftrightarrow q_c, r_c$.) Consequently, the branch cuts in $H_{2L}$

do not approach zero, so we can take $\epsilon = 0$ in $H_{2L}$, as well as $t_2 = t_3$, and find $H_{2L} = 1$. We cannot make these approximations in $H_{1R}$ because $\epsilon$ will matter when the branch cuts get close to zero. Writing out the sum over all parts of the Keldysh contour with this simplification yields

$$
\begin{aligned}
\frac{\Delta I_{tun}}{q_c e^* |\lambda|^2 |\Lambda|^2} &= 4i \int_{-\infty}^{0} dt_1 dt_2 dt_3 \frac{\sin(q_c \omega_0 t_1 + \omega_1 (t_3 - t_2))}{(\epsilon - i t_1)^{q^2 + q'^2}} \\
&\times \left[ \frac{1}{(\epsilon + i|t_2 - t_3|)^{1+r^2}} \left( \frac{(i\epsilon - (-t_2 + d_R))(i\epsilon \mathrm{sgn}(t_1 - t_3) - (t_1 - t_3 + d_R))}{(i\epsilon - (-t_3 + d_R))(i\epsilon \mathrm{sgn}(t_1 - t_2) - (t_1 - t_2 + d_R))} \right)^{q_n r_n} \right. \\
&- \frac{1}{(\epsilon - i(t_2 - t_3))^{1+r^2}} \left( \frac{(i\epsilon - (-t_2 + d_R))(-i\epsilon - (t_1 - t_3 + d_R))}{(-i\epsilon - (-t_3 + d_R))(i\epsilon \mathrm{sgn}(t_1 - t_2) - (t_1 - t_2 + d_R))} \right)^{q_n r_n} \\
&- \frac{1}{(\epsilon + i(t_2 - t_3))^{1+r^2}} \left( \frac{(-i\epsilon - (-t_2 + d_R))(i\epsilon \mathrm{sgn}(t_1 - t_3) - (t_1 - t_3 + d_R))}{(i\epsilon - (-t_3 + d_R))(-i\epsilon - (t_1 - t_2 + d_R))} \right)^{q_n r_n} \\
&\left. + \frac{1}{(\epsilon - i|t_2 - t_3|)^{1+r^2}} \left( \frac{(-i\epsilon - (-t_2 + d_R))(-i\epsilon - (t_1 - t_3 + d_R))}{(-i\epsilon - (-t_3 + d_R))(-i\epsilon - (t_1 - t_2 + d_R))} \right)^{q_n r_n} \right] + h.c. \\
&= 4i \int_{-\infty}^{0} dt_1 dt_2 dt_3 \sin(q_c \omega_0 t_1 + \omega_1 (t_3 - t_2)) \left( \frac{1}{(\epsilon - i t_1)^{q^2 + q'^2}} - \frac{1}{(\epsilon + i t_1)^{q^2 + q'^2}} \right) \\
&\times \left[ \Theta(t_2 - t_3) \left( \frac{1}{(\epsilon + i(t_2 - t_3))^{1+r^2}} \frac{(i\epsilon - (t_1 - t_3 + d_R))^{q_n r_n}}{(i\epsilon - (-t_3 + d_R))^{q_n r_n}} \right. \right. \\
&- \frac{1}{(\epsilon - i(t_2 - t_3))^{1+r^2}} \frac{(-i\epsilon - (t_1 - t_3 + d_R))^{q_n r_n}}{(-i\epsilon - (-t_3 + d_R))^{q_n r_n}} \Bigg) \\
&\times \left( \frac{(i\epsilon - (-t_2 + d_R))^{q_n r_n}}{(i\epsilon - (t_1 - t_2 + d_R))^{q_n r_n}} - \frac{(-i\epsilon - (-t_2 + d_R))^{q_n r_n}}{(-i\epsilon - (t_1 - t_2 + d_R))^{q_n r_n}} \right) \\
&+ \Theta(t_3 - t_2) \left( \frac{1}{(\epsilon - i(t_2 - t_3))^{1+r^2}} \frac{(i\epsilon - (-t_2 + d_R))^{q_n r_n}}{(i\epsilon - (t_1 - t_2 + d_R))^{q_n r_n}} \right. \\
&- \frac{1}{(\epsilon + i(t_2 - t_3))^{1+r^2}} \frac{(-i\epsilon - (-t_2 + d_R))^{q_n r_n}}{(-i\epsilon - (t_1 - t_2 + d_R))^{q_n r_n}} \Bigg) \\
&\times \left. \left( \frac{(i\epsilon - (t_1 - t_3 + d_R))^{q_n r_n}}{(i\epsilon - (-t_3 + d_R))^{q_n r_n}} - \frac{(-i\epsilon - (t_1 - t_3 + d_R))^{q_n r_n}}{(-i\epsilon - (-t_3 + d_R))^{q_n r_n}} \right) \right]
\end{aligned}
$$

$$
\begin{aligned}
&= 4i \int_{-\infty}^{\infty} dt_1 \int_{-\infty}^{0} dt_2 dt_3 \sin(q_c\omega_0 t_1 + \omega_1(t_3 - t_2))\Theta(t_2 - t_3) \\
&\times 2\mathrm{Im}\left[\frac{1}{(\epsilon + i(t_2 - t_3))^{1+r^2}} \frac{(i\epsilon - (t_1 - t_3 + d_R))^{q_n r_n}}{(i\epsilon - (-t_3 + d_R))^{q_n r_n}}\right] \\
&\times 2\mathrm{Im}\left[\frac{(i\epsilon - (-t_2 + d_R))^{q_n r_n}}{(i\epsilon - (t_1 - t_2 + d_R))^{q_n r_n}}\right] 2\mathrm{Im}\left[\frac{1}{(\epsilon - it_1)^{q^2+q'^2}}\right] \\
&= 4i \int_{-\infty}^{\infty} dt_1 dt_2 dt_3 \sin(q_c\omega_0 t_1 + \omega_1(t_3 - t_2))\Theta(t_2 - t_3) \\
&\times 2\mathrm{Im}\left[\frac{1}{(\epsilon + i(t_2 - t_3))^{1+r^2}} \frac{(i\epsilon - (t_1 - t_3))^{q_n r_n}}{(i\epsilon - (-t_3))^{q_n r_n}}\right] \\
&\times 2\left[\frac{(i\epsilon - (-t_2))^{q_n r_n}}{(i\epsilon - (t_1 - t_2))^{q_n r_n}}\right] 2\mathrm{Im}\left[\frac{1}{(\epsilon - it_1)^{q^2+q'^2}}\right]
\end{aligned}
\tag{C.29}
$$

where again we have absorbed overall factors of velocity into the coupling constant. Notice that we have replaced $\mathrm{sgn}(t_1 - t_{2,3})$ with 1; this should not change the integral since it has little or no contribution when $t_1 < t_{2,3}$. To get the third equality, in the term involving $\Theta(t_3 - t_2)$ we shift $t_{2,3} \to t_{2,3} + t_1$, then take $t_1 \to -t_1$, $t_2 \leftrightarrow t_3$. This procedure produces an extra region of integration, $t_1 > 0$, $0 < t_{2,3} < t_1$, but the integral over this region is negligible. To obtain the fourth equality we shift $t_{2,3} \to t_{2,3} + d_R$ and add another negligible region of integration so that all $t_i$ have the same limits of integration. We have assumed $|d_R| \gg 1/|\omega_0|, 1/|\omega_1|$.

The remaining integral is difficult to do analytically, but by rescaling the variables it is evident that $\Delta I_{tun}$ will be a sum of terms $|\omega_0|^\alpha |\omega_1|^\beta$ where $\alpha + \beta = q^2 + q'^2 + r^2 - 2$. We expect that exponents $\alpha, \beta$ that appear will be independent of the product $q_n r_n$, although the coefficients might be dependent. To make progress on the integral above,

we here consider $q_n r_n = 1$, knowing that it will probably give us the right terms with the wrong coefficients; we have confirmed this intuition by repeating the computation with $q_n r_n = 2$ (not shown). With this simplification,

$$\frac{\Delta I_{tun}}{q_c e^* |\lambda|^2 |\Lambda|^2} = 4\pi \int_{-\infty}^{\infty} dt_1 dt_3 \sin(q_c\omega_0 t_1 + \omega_1(t_3 - t_1)) \left( \frac{t_1}{(\epsilon - it_1)^{q^2+q'^2}} - \frac{t_1}{(\epsilon + it_1)^{q^2+q'^2}} \right) \times \left( \frac{i}{(\epsilon + i(t_1 - t_3))^{r^2}(t_3 + i\epsilon)} + \frac{i}{(\epsilon - i(t_1 - t_3))^{r^2}(t_3 - i\epsilon)} \right) \tag{C.30}$$

We have utilized the delta-function identity (C.13). If we assume $r^2$ is an integer, we can do the integral over $t_3$ as a contour integral, as shown in Eq (C.36)), and then assume analytic continuation to all $n$. The result is

$$\begin{aligned}
\frac{\Delta I_{tun}}{q_c e^* |\lambda|^2 |\Lambda|^2} &= -\mathrm{sgn}(\omega_1) 2\pi \int_{-\infty}^{\infty} dt_1 \left( \frac{t_1}{(\epsilon - it_1)^{q^2+q'^2}} - \frac{t_1}{(\epsilon + it_1)^{q^2+q'^2}} \right) \\
&\times \int_{-\infty}^{\infty} dt_3 \left( \frac{e^{-i\mathrm{sgn}(\omega_1)(q_c\omega_0 t_1 + \omega_1(t_3 - t_1))}}{(\epsilon + i(t_1 - t_3))^{r^2}(t_3 + i\epsilon)} \right) + h.c. \\
&= \mathrm{sgn}(\omega_1) \frac{8\pi^2 (-i)^{r^2-1}}{\Gamma(r^2)} \int_0^{\infty} dt_1 \left( \frac{1}{(\epsilon - it_1)^{q^2+q'^2}} - \frac{1}{(\epsilon + it_1)^{q^2+q'^2}} \right) \\
&\times \frac{(\Gamma(r^2) - \Gamma(r^2, it_1|\omega_1|))\, e^{it_1 \mathrm{sgn}(\omega_1)(\omega_1 - q_c\omega_0)}}{t_1^{r^2-1}} + h.c. \\
&= \mathrm{sgn}(\omega_1) \frac{16\pi^2 (-i)^{r^2-2} \sin(\frac{1}{2}\pi(q^2 + q'^2))}{\Gamma(r^2)} \\
&\times \int_0^{\infty} dt_1 \frac{(\Gamma(r^2) - \Gamma(r^2, it_1|\omega_1|))\, e^{it_1 \mathrm{sgn}(\omega_1)(\omega_1 - q_c\omega_0)}}{t_1^{r^2+q^2+q'^2-1}} + h.c. \\
&= \mathrm{sgn}(\omega_1) 16\pi^2 (i)^{q^2+q'^2} \sin(\frac{1}{2}\pi(q^2 + q'^2)) |q_c\omega_0|^{\Delta} (\mathrm{sgn}(\omega_1\omega_0))^{\Delta} \\
&\times \left( \left(1 - \frac{\omega_1}{q_c\omega_0}\right)^{\Delta} \Gamma(-\Delta) - \sum_{k=0}^{r^2-1} \frac{1}{k!} \left( \frac{\omega_1}{q_c\omega_0} \right)^k \Gamma(-\Delta + k) \right) + h.c.
\end{aligned}$$

$$= \begin{cases} \operatorname{sgn}(\omega_1) 16\pi^2 \sin(\pi(q^2+q'^2))|q_c\omega_0|^{q^2+q'^2-2}|\omega_1|^{r^2} \\ \qquad \times \sum_{k=0}^{\infty} \frac{\Gamma(k-q^2-q'^2+2)}{\Gamma(k+r^2+1)} \left(\frac{\omega_1}{q_c\omega_0}\right)^k, \text{ if } |\omega_0| \gg |\omega_1| \\ \operatorname{sgn}(\omega_1) 16\pi^2 \sin(\pi(q^2+q'^2))|\omega_1|^{\Delta} \left( \sum_{k=0}^{\infty} \frac{\Gamma(k-\Delta)}{\Gamma(k+1)} (-1)^{r^2} \left(\frac{q_c\omega_0}{\omega_1}\right)^k \right. \\ \qquad \left. - \sum_{k=0}^{r^2-1} \frac{\Gamma(1-q^2-q'^2-k)}{\Gamma(r^2-k)} \left|\frac{q_c\omega_0}{\omega_1}\right|^{q^2+q'^2-1+k} \operatorname{sgn}(\omega_0\omega_1)^{k+1} \right), \\ \qquad \text{if } |\omega_1| \gg |\omega_0| \end{cases} \tag{C.31}$$

where we have defined $\Delta = r^2 + q^2 + q'^2 - 2$ and assumed $n \in \mathbb{Z}$. Notice that this reproduces the results of Eq (C.14) in either limiting case.

This calculation gives the contribution to the change in tunneling current from a single species $q = (q_n, q_c)$ tunneling from the top edge of the Hall bar to a species $q' = (q'_n, q'_c)$ on the bottom edge and a single species $r = (r_n, r_c)$ tunneling into the external lead. Physically, quasiparticles with $q_n \to -q_n$ and $r_n \to -r_n$ will also be present and could tunnel from the top edge to a species $q'$ on the bottom edge. From the symmetry of the model, taking $q_n r_n \to -q_n r_n$ is equivalent to taking $\omega_1 \to -\omega_1$ in the computation of $\Delta I_{tun}$. Hence, if the tunneling amplitudes for the two types of quasiparticles with opposite contributions from the neutral mode are equal, then the leading contributions from Eq (C.31) will cancel and the subleading terms will dominate. In this case, $\Delta I_{tun}$ will be even in $\omega_1$ and odd in $\omega_0$.

When $a \to -a$, i.e. the current injection is upstream of the QPC, $q_n r_n \to q_c r_c$ in Eq (C.29). At first, this transformation seems inconsequential – after all, we argued that this exponent only changes the final answer by an overall pre-factor – but it becomes important when regarding the symmetry considerations of the previous paragraph. Namely, when $a > 0$, Eq (C.29) is invariant under $q_n \to -q_n$. Consequently, when the contributions from quasiparticles with $q = (q_n, q_c)$ and $(-q_n, q_c)$ are added, $\Delta I_{tun}$ doubles, in contrast to the case when $d < 0$ and terms odd in $\omega_1$ disappear. If $q^2 > 1/2$, the leading term in $\Delta I_{tun}$ is odd in $\omega_1$; hence, when $a > 0$, $\Delta I_{tun}$ is larger by a power of $\text{Max}\left(\frac{\omega_0}{\omega_1}, \frac{\omega_1}{\omega_0}\right)$ than when $d < 0$. This agrees with the intuition that there should be a larger change in tunneling current when the injection is upstream of the QPC than when it is downstream.

### C.3.3 Excess noise

Using Eq (3.16) and (3.17), the excess noise is given by

$$\begin{aligned}\Delta S_{tun}(t) &= \frac{1}{2}\left(\langle\{I_{tun}(t), I_{tun}(0)\}\rangle|_{\Lambda} - \langle\{I_{tun}(t), I_{tun}(0)\}\rangle|_{\Lambda=0}\right) \\ &= \frac{1}{2}\langle\{I_{tun}(t), I_{tun}(0)\}\left(i\int dt_2 \mathcal{L}_{inj}\right)\left(i\int dt_3 \mathcal{L}_{inj}\right)\rangle_0 \end{aligned} \tag{C.32}$$

Here we seek $\Delta S_{tun}(\omega) = \int dt e^{i\omega t}\Delta S_{tun}(t)$. The correlation functions and Klein factors of Appendix C.1 yield the contribution from a single pair of quasiparticle species described

by $m = (q_n, q_c), n = (r_n, r_c)$,

$$\frac{\Delta S_{tun}}{(q_c e^*)^2|\lambda|^2|\Lambda|^2} = -\int_{-\infty}^{\infty} dt 2\cos(\omega t)\int_K dt_2^\nu dt_3^\sigma \frac{2\cos(q_c\omega_0 t + \omega_1(t_3-t_2))H_{1R}H_{2L}}{G^{+-}(-t_1,0))^{q^2+q'^2}(G^{\nu\sigma}(t_2-t_3))^{1+r^2}} \tag{C.33}$$

where $H_{iR/L}$ are defined with $\mu = -$. The similarity to Eq (C.27) is clear. Following the manipulations of Eq (C.29),

$$\begin{aligned}\frac{\Delta S_{tun}(\omega)}{(q_c e^*)^2|\lambda|^2|\Lambda|^2} &= -4\int_{-\infty}^{\infty} dt dt_2 dt_3 \cos(\omega t)\cos(q_c\omega_0 t + \omega_1(t_3-t_2))\Theta(t_2-t_3) \\ &\times 2\mathrm{Re}\left[\frac{1}{(\epsilon - it)^{q^2+q'^2}}\right] 2\mathrm{Im}\left[\frac{(i\epsilon-(-t_2))^{q_n r_n}}{(i\epsilon-(t-t_2))^{q_n r_n}}\right] \\ &\times 2\mathrm{Im}\left[\frac{1}{(\epsilon+i(t_2-t_3))^{1+r^2}}\frac{(i\epsilon-(t-t_3))^{q_n r_n}}{(i\epsilon-(-t_3))^{q_n r_n}}\right]\end{aligned} \tag{C.34}$$

We have again absorbed overall factors of velocity into the coupling constants. We now make the simplifying assumption that $q_n r_n = 1$; as in the current case, we have separately checked that when $q_n r_n = 2$, the only change is a pre-factor (which is the same pre-factor as in the current case). Note that in this case, though, the transformation $q_n r_n \to -q_n r_n$ is equivalent to $\omega_0 \to -\omega_0$. Under this assumption,

$$\begin{aligned}\frac{\Delta S_{tun}(\omega)}{(q_c e^*)^2|\lambda|^2|\Lambda|^2} &= 4\pi i\int_{-\infty}^{\infty} dt dt_3 \cos(\omega t)\cos(q_c\omega_0 t + \omega_1(t_3-t))\left(\frac{t}{(\epsilon-it)^{q^2+q'^2}} + \frac{t}{(\epsilon+it)^{q^2+q'^2}}\right) \\ &\times\left(\frac{i}{(\epsilon+i(t-t_3))^{r^2}(t_3+i\epsilon)} + \frac{i}{(\epsilon-i(t-t_3))^{r^2}(t_3-i\epsilon)}\right) \\ &= -2\pi\int_{-\infty}^{\infty} dt dt_3 \cos(\omega t) 2\mathrm{Re}\left[\frac{t}{(\epsilon-it)^{q^2+q'^2}}\right] 2\mathrm{Re}\left[\frac{e^{-i\mathrm{sgn}(\omega_1)(q_c\omega_0 t+\omega_1(t_3-t)}}{(\epsilon+i(t-t_3))^{r^2}(t_3+i\epsilon)}\right] \\ &= \frac{8\pi^2(-i)^{r^2-1}}{\Gamma(r^2)}\int_0^{\infty} dt\cos(\omega t)\left(\frac{1}{(\epsilon-it)^{q^2+q'^2}} + \frac{1}{(\epsilon+it)^{q^2+q'^2}}\right)\end{aligned}$$

$$
\begin{aligned}
&\times \frac{\left(\left(\Gamma(r^2)-\Gamma(r^2,it|\omega_1|)\right)e^{it(|\omega_1|-q_c\omega_0\mathrm{sgn}(\omega_1))}\right.}{t^{r^2-1}} + h.c. \\
&= \frac{16\pi^2(-i)^{r^2-1}\cos(\frac{\pi}{2}\left(q^2+q'^2\right))}{\Gamma(r^2)} \\
&\times \int_0^\infty dt\cos(\omega t)\frac{\left(\left(\Gamma(r^2)-\Gamma(r^2,it|\omega_1|)\right)e^{it(|\omega_1|-q_c\omega_0\mathrm{sgn}(\omega_1))}\right.}{t^{q^2+q'^2+r^2-1}} + h.c. \\
&\xrightarrow{\omega\to 0} \begin{cases}
\mathrm{sgn}(\omega_1\omega_0)16\pi^2\sin(\pi(q^2+q'^2))|q_c\omega_0|^{q^2+q'^2-2}|\omega_1|^{r^2} \\
\qquad \sum_{k=0}^{\infty}\frac{\Gamma(k-q^2-q'^2+2)}{\Gamma(k+r^2+1)}\left(\frac{\omega_1}{q_c\omega_0}\right)^k, \text{ if } |\omega_0|\gg|\omega_1| \\
-16\pi^2\sin(\pi(q^2+q'^2))|\omega_1|^{\Delta}\left(\sum_{k=0}^{\infty}\frac{\Gamma(k-\Delta)}{\Gamma(k+1)}(-1)^{r^2}\left(\frac{q_c\omega_0}{\omega_1}\right)^k\right. \\
\qquad \left.-\sum_{k=0}^{r^2-1}\frac{\Gamma(1-q^2-q'^2-k)}{\Gamma(r^2-k)}\left|\frac{q_c\omega_0}{\omega_1}\right|^{q^2+q'^2-1+k}\mathrm{sgn}(\omega_0\omega_1)^{k+1}\right), \\
\qquad \text{if } |\omega_1|\gg|\omega_0|
\end{cases}
\end{aligned}
\tag{C.35}
$$

We have utilized the delta-function identity Eq (C.13) and the integral Eq (C.36), taken $n \in \mathbb{Z}$ and defined $\Delta = r^2 + q^2 + q'^2 - 2$. The excess noise from a single species $q = (q_n, q_c)$ on the top edge tunneling across the QPC to a species $q' = (q'_n, q'_c)$ on the bottom edge and a species $r = (r_n, r_c)$ tunneling from the external lead is proportional to the contribution to the excess current from the same species. When quasiparticles with $q_n \to -q_n$ and $r_n \to -r_n$ are also present and tunnel with equal amplitudes, their contribution to the noise will be given by Eq (C.35) with $\omega_0 \to -\omega_0$.

Now consider the case of $d > 0$. Similar to the discussion at the end of the previous section, when $d > 0$, $q_n r_n \to q_c r_c$ in Eq C.34. Consequently, when $d > 0$ and the contributions to the excess noise from quasiparticles with $(\pm q_n, q_c)$ are added together, the excess noise doubles. This is in contrast to the $d < 0$ case when the terms odd in $\omega_0$ drop out. Thus, when $|\omega_0| \gg |\omega_1|$ or when $q^2 < 1/2$ and $|\omega_1| \gg |\omega_0|$, the excess noise will increase by a factor of Max $\left(\frac{\omega_0}{\omega_1}, \frac{\omega_1}{\omega_0}\right)$ when $d > 0$.

### C.3.4 A useful integral

$$
\begin{aligned}
&\int_{-\infty}^{\infty} dt_3 \frac{e^{-i(\omega_0 \mathrm{sgn}(\omega_1) - |\omega_1|)t_1 - i|\omega_1|t_3}}{(t_3 - t_1 + i\epsilon)^{r^2}(t_3 + i\epsilon)} \\
&\qquad = -2\pi i \left( \frac{e^{-i(\omega_0 \mathrm{sgn}(\omega_1) - |\omega_1|)t_1}}{(-t_1)^{r^2}} + \sum_{k=0}^{r^2-1} \frac{(-1)^{r^2-1-k}(-i|\omega_1|)^k e^{-i\omega_0 \mathrm{sgn}(\omega_1)t_1}}{k!\, t_1^{r^2-k}} \right) \\
&\qquad = -2\pi i \left( \sum_{k=0}^{\infty} \frac{(-1)^{r^2} (i|\omega_1|)^k}{k!\, t_1^{r^2-k}} + \sum_{k=0}^{r^2-1} \frac{(-1)^{r^2-1} (i|\omega_1|)^k}{k!\, t_1^{r^2-k}} \right) e^{-i\omega_0 \mathrm{sgn}(\omega_1)t_1} \\
&\qquad = -2\pi i \sum_{k=r^2}^{\infty} \frac{(-1)^{r^2} (i|\omega_1|)^k}{k!\, t_1^{r^2-k}} e^{-i\omega_0 \mathrm{sgn}(\omega_1)t_1} \\
&\qquad = -2\pi (-i)^{r^2} \sum_{k=0}^{\infty} \frac{(i)^{k+1} |\omega_1|^{k+r^2}}{(k+r^2)!} t_1^k e^{-i\omega_0 \mathrm{sgn}(\omega_1)t_1} \\
&\qquad = -\frac{2\pi i (-1)^{r^2}}{\Gamma(r^2) t_1^{r^2}} \left( \Gamma(r^2) - \Gamma(r^2, it_1|\omega_1|) \right) e^{it_1(|\omega_1| - \omega_0 \mathrm{sgn}(\omega_1))}
\end{aligned}
\tag{C.36}
$$

where $\Gamma(r^2, x)$ is the incomplete gamma function. The last equality gives the result for $n \notin \mathbb{Z}$ by analytic continuation.

### C.3.5 Specific results for $r^2 = 2, q^2 = 2/3$

As discussed in the text, the $\nu = 2/3$ edge is expected to be described by $r^2 = 2, q^2 = 2/3$. Using these values, we can do the integrals in Eqs (C.31) and (C.35) exactly (bear in mind that we expect these integrals to be correct up to a constant of proportionality, since we have assumed $q_n r_n = 1$, which does not correctly describe the state, but should not be expected to change the scaling):

$$\Delta I_{tun} = \frac{e}{3}|\lambda|^2|\Lambda|^2\frac{16\pi^3}{\Gamma(7/3)}\mathrm{sgn}(\omega_1)\left(-|q_c\omega_0 - \omega_1|^{4/3} - \frac{4}{3}\omega_1\mathrm{sgn}(\omega_0)|q_c\omega_0|^{1/3} + |q_c\omega_0|^{4/3}\right) \tag{C.37}$$

$$\Delta S_{tun} = \left(\frac{e}{3}\right)^2|\lambda|^2|\Lambda|^2\frac{16\pi^3}{\Gamma(7/3)}\left(\frac{|q_c\omega_0 - \omega_1|^{4/3}}{\mathrm{sgn}(1 - q_c\omega_0\omega_1)} - \frac{4}{3}|\omega_1||q_c\omega_0|^{1/3} + \mathrm{sgn}(\omega_0\omega_1)|q_c\omega_0|^{4/3}\right) \tag{C.38}$$

where $q_c\omega_0 = eV_0/3$. When we assume that quasiparticles with $q_n \to -q_n$ and $r_n \to -r_n$ tunnel with equal amplitudes, we obtain Eqs (3.32) and (3.33) in the main text.

# Appendix D

# Gauss-Smith Normal Form Example

We now apply the method described in Section 4.5 to the $\mathrm{SO}(8)_1$ theory, which is given by the following $K$ matrix:

$$K = \begin{pmatrix} 2 & 0 & 1 & 0 \\ 0 & 2 & -1 & 0 \\ 1 & -1 & 2 & -1 \\ 0 & 0 & -1 & 2 \end{pmatrix} \tag{D.1}$$

It is not clear, simply by inspection, what vectors correspond to generators of the fusion group.

The Gauss-Smith normal form is

$$D = \begin{pmatrix} 1 & 0 & 0 & 0 \\ 0 & 1 & 0 & 0 \\ 0 & 0 & 2 & 0 \\ 0 & 0 & 0 & 2 \end{pmatrix} \tag{D.2}$$

Hence, the fusion group of the theory is $\mathbb{Z}/2 \times \mathbb{Z}/2$.

and the Q matrix

$$Q = \begin{pmatrix} 2 & 0 & 1 & 0 \\ 3 & 1 & 0 & 1 \\ 2 & 0 & 0 & 1 \\ 1 & 0 & 0 & 0 \end{pmatrix} \tag{D.3}$$

So the fusion group is generated by the two quasiparticles corresponding to $(2, 0, 0, 1)$ and $(1, 0, 0, 0)$. We can then compute the $S$, $T$ matrices and the result agrees with what is known (all nontrivial quasiparticles are fermions and they have semionic mutual braiding statistics with each other).

Another useful piece of information from the Smith normal form is that the discriminant group for a $2 \times 2$ K-matrix

$$K = \begin{pmatrix} a & b \\ b & c \end{pmatrix} \tag{D.4}$$

with $\gcd(a, b, c) = 1$ and $d = |ac - b^2|$ is $\mathbb{Z}/d$. More generally, it is $\mathbb{Z}/f \times \mathbb{Z}/(d/f)$ when $\gcd(a, b, c) = f$.

# Appendix E

# Existence proof for shift vector in the generalized Gauss-Milgram sum

Here we show that $\vec{w} \in \Lambda$ exists such that $\boldsymbol{\lambda} \cdot \boldsymbol{\lambda} \equiv \boldsymbol{\lambda} \cdot \vec{w} \bmod 2$ for all $\boldsymbol{\lambda} \in \Lambda$. As discussed in Sec 4.6, the existence of such a vector is necessary to write a generalized Gauss-Milgram sum for fermions. We begin by showing that for any K-matrix, there exists a set of integers $w_J$ such that

$$K_{II} \equiv \sum_{J=1}^{N} K_{IJ} w_J \bmod 2, \text{ for all } I \tag{E.1}$$

where $N$ is the dimension of the K-matrix.

Assume the K-matrix has $M \leq N$ rows that are linearly independent mod 2; denote these rows $R_1, ...R_M$ and define the set $R = \{R_i\}$. The linear independence of the $R_i$

implies that Eq (E.1) is satisfied for these rows, i.e., there exists a set of integers $(w_0)_J$ satisfying

$$K_{II} \equiv \sum_{J=1}^{N} K_{IJ}(w_0)_J \bmod 2, \text{ for all } I \in R \tag{E.2}$$

For a row $I \notin R$, the elements of the $I^{\text{th}}$ row in $K$ can be written as a linear combination of the rows in $R$:

$$K_{IJ} \equiv \sum_{R_i \in R} c_{IR_i} K_{R_i J} \bmod 2, \text{ for } I \notin B \tag{E.3}$$

where the $c_{IR_i} \in \{0, 1\}$ are coefficients. It follows that for $I \notin R$:

$$\begin{aligned} K_{II} &\equiv \sum_{R_i \in R} c_{IR_i} K_{R_i I} \equiv \sum_{R_i \in R} c_{IR_i} K_{IR_i} \\ &\equiv \sum_{R_i, R_j \in R} c_{IR_i} c_{IR_j} K_{R_i R_j} \equiv \sum_{R_i \in R} c_{IR_i}^2 K_{R_i R_i} \\ &\equiv \sum_{R_i \in R} c_{IR_i} K_{R_i R_i} \bmod 2 \end{aligned} \tag{E.4}$$

Furthermore, for $I \notin R$

$$\begin{aligned} \sum_{J=1}^{N} K_{IJ}(w_0)_J &\equiv \sum_{J=1}^{N} \sum_{R_i \in R} c_{IR_i} K_{R_i J}(w_0)_J \\ &\equiv \sum_{R_i \in R} c_{IR_i} K_{R_i R_i} \bmod 2 \end{aligned} \tag{E.5}$$

Hence, for $I \notin R$, $K_{II} \equiv \sum_{J=1}^{N} K_{IJ}(w_0)_J \bmod 2$. Since this equation already holds for $I \in R$, we have shown that $w_0$ is a solution to Eq (E.1).

It follows that for any choice of $\boldsymbol{\lambda} = \lambda_J \vec{e}_J \in \Lambda$,

$$\boldsymbol{\lambda} \cdot \boldsymbol{\lambda} = \sum_{I,J=1}^{N} \lambda_I \lambda_J K_{IJ} \equiv \sum_{I=1}^{N} \lambda_I K_{II}$$

$$\equiv \sum_{I=1}^{N} \lambda_I \sum_{J=1}^{N} K_{IJ}(w_0)_J \equiv \boldsymbol{\lambda} \cdot \boldsymbol{w}_0 \bmod 2 \tag{E.6}$$

where $\vec{w}_0 = (w_0)_J \vec{e}_J$ is a vector in $\Lambda$.

# Appendix F

# Relevant large matrices

Here we define matrices referred to in 4.7:

$$K_{E_8} = \begin{pmatrix} 2 & -1 & 0 & 0 & 0 & 0 & 0 & 0 \\ -1 & 2 & -1 & 0 & 0 & 0 & -1 & 0 \\ 0 & -1 & 2 & -1 & 0 & 0 & 0 & 0 \\ 0 & 0 & -1 & 2 & -1 & 0 & 0 & 0 \\ 0 & 0 & 0 & -1 & 2 & -1 & 0 & 0 \\ 0 & 0 & 0 & 0 & -1 & 2 & 0 & 0 \\ 0 & -1 & 0 & 0 & 0 & 0 & 2 & -1 \\ 0 & 0 & 0 & 0 & 0 & 0 & -1 & 2 \end{pmatrix} \tag{F.1}$$

$$W_8 = \begin{pmatrix} -5 & -5 & -5 & 5 & 5 & 5 & 5 & 5 & 8 & 16 \\ -10 & -10 & -10 & 9 & 9 & 9 & 9 & 9 & 15 & 30 \\ -8 & -8 & -8 & 8 & 7 & 7 & 7 & 7 & 12 & 24 \\ -6 & -6 & -6 & 6 & 6 & 5 & 5 & 5 & 9 & 18 \\ -4 & -4 & -4 & 4 & 4 & 4 & 3 & 3 & 6 & 12 \\ -2 & -2 & -2 & 2 & 2 & 2 & 2 & 1 & 3 & 6 \\ -7 & -7 & -6 & 6 & 6 & 6 & 6 & 6 & 10 & 20 \\ -4 & -3 & -3 & 3 & 3 & 3 & 3 & 3 & 5 & 10 \\ 1 & 1 & 1 & -1 & -1 & -1 & -1 & -1 & -3 & -4 \\ -2 & -2 & -2 & 2 & 2 & 2 & 2 & 2 & 4 & 7 \end{pmatrix} \tag{F.2}$$

$$K_{D_{12}^+} = \begin{pmatrix} 2 & 0 & 1 & 0 & 0 & 0 & 0 & 0 & 0 & 0 & 0 & -1 \\ 0 & 2 & -1 & 0 & 0 & 0 & 0 & 0 & 0 & 0 & 0 & 0 \\ 1 & -1 & 2 & -1 & 0 & 0 & 0 & 0 & 0 & 0 & 0 & 0 \\ 0 & 0 & -1 & 2 & -1 & 0 & 0 & 0 & 0 & 0 & 0 & 0 \\ 0 & 0 & 0 & -1 & 2 & -1 & 0 & 0 & 0 & 0 & 0 & 0 \\ 0 & 0 & 0 & 0 & -1 & 2 & -1 & 0 & 0 & 0 & 0 & 0 \\ 0 & 0 & 0 & 0 & 0 & -1 & 2 & -1 & 0 & 0 & 0 & 0 \\ 0 & 0 & 0 & 0 & 0 & 0 & -1 & 2 & -1 & 0 & 0 & 0 \\ 0 & 0 & 0 & 0 & 0 & 0 & 0 & -1 & 2 & -1 & 0 & 0 \\ 0 & 0 & 0 & 0 & 0 & 0 & 0 & 0 & -1 & 2 & -1 & 0 \\ 0 & 0 & 0 & 0 & 0 & 0 & 0 & 0 & 0 & -1 & 2 & 0 \\ -1 & 0 & 0 & 0 & 0 & 0 & 0 & 0 & 0 & 0 & 0 & 3 \end{pmatrix} \tag{F.3}$$

$$W_{12} = \begin{pmatrix} 11 & 6 & 6 & -6 & -6 & -6 & -6 & -6 & -6 & -6 & -6 & -6 & 0 & 22 \\ -9 & -4 & -5 & 5 & 5 & 5 & 5 & 5 & 5 & 5 & 5 & 5 & 0 & 18 \\ -18 & -9 & -9 & 10 & 10 & 10 & 10 & 10 & 10 & 10 & 10 & 10 & 0 & 36 \\ -16 & -8 & -8 & 8 & 9 & 9 & 9 & 9 & 9 & 9 & 9 & 9 & 0 & 32 \\ -14 & -7 & -7 & 7 & 7 & 8 & 8 & 8 & 8 & 8 & 8 & 8 & 0 & 28 \\ -12 & -6 & -6 & 6 & 6 & 6 & 7 & 7 & 7 & 7 & 7 & 7 & 0 & 24 \\ -10 & -5 & -5 & 5 & 5 & 5 & 5 & 6 & 6 & 6 & 6 & 6 & 0 & 20 \\ -8 & -4 & -4 & 4 & 4 & 4 & 4 & 4 & 5 & 5 & 5 & 5 & 0 & 16 \\ -6 & -3 & -3 & 3 & 3 & 3 & 3 & 3 & 3 & 4 & 4 & 4 & 0 & 12 \\ -4 & -2 & -2 & 2 & 2 & 2 & 2 & 2 & 2 & 2 & 3 & 3 & 0 & 8 \\ -2 & -1 & -1 & 1 & 1 & 1 & 1 & 1 & 1 & 1 & 1 & 2 & 0 & 4 \\ 3 & 2 & 2 & -2 & -2 & -2 & -2 & -2 & -2 & -2 & -2 & -2 & 0 & -7 \\ 0 & 0 & 0 & 0 & 0 & 0 & 0 & 0 & 0 & 0 & 0 & 0 & 1 & 0 \\ 2 & 1 & 1 & -1 & -1 & -1 & -1 & -1 & -1 & -1 & -1 & -1 & 0 & -4 \end{pmatrix} \tag{F.4}$$

# Bibliography

# Bibliography


[1] Klaus von Klitzing. 25 years of quantum Hall effect. In Benoît Douçot, Vincent Pasquier, and Vincent Rivasseau, editors, *The Quantum Hall Effect: Poincaré Seminar 2004*, volume 45 of *Progress in Mathematical Physics*, chapter 1, pages 1–22. Birkhäuser, 2005.

[2] K. von Klitzing, G. Dorda, and M. Pepper. New method for high-accuracy determination of the fine-structure constant based on quantized Hall resistance. *Phys. Rev. Lett.*, 45:494–497, Aug 1980.

[3] Steven Girvin. The quantum Hall effect: Novel excitations and broken symmetries. In A. Comtet, T. Jolicoeur, S. S. Ouvry, and F. David, editors, *Topological Aspects of Low Dimensional Systems*, chapter 1, pages 53–175. Springer-Verlag, 1999.

[4] Allan MacDonald. Introduction to the Physics of the Quantum Hall Regime. *arXiv:cond-mat/9410047*, October 1994.

[5] Richard E. Prange and Steven M. Girvin, editors. *The Quantum Hall Effect*. Springer, 1989.

[6] D. C. Tsui, H. L. Stormer, and A. C. Gossard. Two-dimensional magnetotransport in the extreme quantum limit. *Phys. Rev. Lett.*, 48:1559–62, 1982.

[7] R. Willett, J. P. Eisenstein, H. L. Störmer, D. C. Tsui, A. C. Gossard, and J. H. English. Observation of an even-denominator quantum number in the fractional quantum Hall effect. *Phys. Rev. Lett.*, 59:1776–1779, Oct 1987.

[8] Katrine Rasmussen and Christian J. S. Olsen. Measuring fractional quantum Hall effect. Master's thesis, University of Copenhagen, 2013.

[9] B. I. Halperin. Quantized Hall conductance, current-carrying edge states, and the existence of extended states in a two-dimensional disordered potential. *Phys. Rev. B*, 25:2185–2190, Feb 1982.

[10] R. B. Laughlin. Quantized Hall conductivity in two dimensions. *Phys. Rev. B*, 23(10):5632–5633, May 1981.

[11] R. B. Laughlin. Anomalous quantum Hall effect: An incompressible quantum fluid with fractionally excitations. *Phys. Rev. Lett.*, 50:1395, 1983.

[12] R. B. Laughlin. Quantized motion of three two-dimensional electrons in a strong magnetic field. *Phys. Rev. B*, 27:3383–3389, Mar 1983.

[13] F. D. M. Haldane. Fractional quantization of the Hall effect: A hierarchy of incompressible quantum fluid states. *Phys. Rev. Lett.*, 51:605–608, 1983.

[14] Daniel Arovas, J. R. Schrieffer, and Frank Wilczek. Fractional statistics and the quantum Hall effect. *Phys. Rev. Lett.*, 53:722–723, 1984.

[15] Chetan Nayak. Quantum condensed matter physics – lecture notes. Unpublished, November 2004.

[16] M. Milovanović and N. Read. Edge excitations of paired fractional quantum Hall states. *Phys. Rev. B*, 53:13559–13582, May 1996.

[17] B. I. Halperin. Statistics of quasiparticles and the hierarchy of fractional quantized Hall states. *Phys. Rev. Lett.*, 52(18):1583–6, 1984.

[18] J. K. Jain. Composite-fermion approach for the fractional quantum Hall effect. *Phys. Rev. Lett.*, 63:199–202, Jul 1989.

[19] N. Read. Excitation structure of the hierarchy scheme in the fractional quantum Hall effect. *Phys. Rev. Lett.*, 65:1502–1505, Sep 1990.

[20] B. I. Halperin. Theory of the quantized Hall conductance. *Helv. Phys. Acta*, 56:75, 1983.

[21] M. Greiter, X. G. Wen, and F. Wilczek. Paired Hall state at half filling. *Physical Review Letters*, 66(24):3205–3208, June 1991.

[22] M. Greiter, X. G. Wen, and F. Wilczek. Paired Hall states. *Nucl. Phys. B*, 374(3):567–614, 1992.

[23] M. Greiter and F. Wilczek. Heuristic principle for quantized Hall states. *Modern Physics Letters B*, 4(16):1063–1069, June 1990.

[24] G. Moore and N. Read. Nonabelions in the fractional quantum Hall effect. *Nucl. Phys. B*, 360(2-3):362–96, 1991.

[25] Shou Cheng Zhang. The Chern-Simons-Landau-Ginzburg theory of the fractional quantum Hall effect. *International Journal of Modern Physics B*, 06(01):25–58, 1992.

[26] S. C. Zhang, T. H. Hansson, and S. Kivelson. Effective-field-theory model for the fractional quantum Hall effect. *Phys. Rev. Lett.*, 62(1):82–5, 1989.

[27] Xiao-Gang Wen. Theory of the edge states in fractional quantum Hall effects. *Int. J. Mod. Phys.*, B6:1711, 1992.

[28] C. L. Kane and Matthew P. A. Fisher. Impurity scattering and transport of fractional quantum Hall edge states. *Phys. Rev. B*, 51:13449, 1995.

[29] C. de C. Chamon, D. E. Freed, and X. G. Wen. Tunneling and quantum noise in one-dimensional luttinger liquids. *Phys. Rev. B*, 51(4):2363–2379, 1995.

[30] C. L. Kane and Matthew P. A. Fisher. Nonequilibrium noise and fractional charge in the quantum Hall effect. *Phys. Rev. Lett.*, 72:724, 1994.

[31] R. de Picciotto, M. Reznikov, M. Heiblum, V. Umansky, G. Bunin, and D. Mahalu. Direct observation of a fractional charge. *Nature*, 389:162, 1997.

[32] L. Saminadayar, D. C. Glattli, Y. Jin, and B. Etienne. Observation of the e/3 fractionally charged laughlin quasiparticle. *Phys. Rev. Lett.*, 79:2526, 1997.

[33] C. de C. Chamon, D. E. Freed, S. A. Kivelson, S. L. Sondhi, and X. G. Wen. Two point-contact interferometer for quantum Hall systems. *Phys. Rev. B*, 55:2331, 1997.

[34] F. E. Camino, Wei Zhou, and V. J. Goldman. Realization of a Laughlin quasiparticle interferometer: Observation of fractional statistics. *Phys. Rev. B.*, 72:075342, 2005.

[35] F. E. Camino, W. Zhou, and V. J. Goldman. Aharonov-Bohm electron interferometer in the integer quantum Hall regime. *Phys. Rev. B*, 72:155313, Oct 2005.

[36] Yiming Zhang, D. T. McClure, E. M. Levenson-Falk, C. M. Marcus, L. N. Pfeiffer, and K. W. West. Distinct signatures for coulomb blockade and aharonov-bohm interference in electronic fabry-perot interferometers. *Phys. Rev. B*, 79:241304, 2009.

[37] Nissim Ofek, Aveek Bid, Moty Heiblum, Ady Stern, Vladimir Umansky, and Diana Mahalu. Role of interactions in an electronic fabry–perot interferometer operating in the quantum hall effect regime. *Proceedings of the National Academy of Sciences*, 107(12):5276–5281, 2010.

[38] H Choi, P Jiang, MD Godfrey, W Kang, SH Simon, LN Pfeiffer, KW West, and KW Baldwin. Aharonov–bohm-like oscillations in fabry–perot interferometers. *New Journal of Physics*, 13(5):055007, 2011.

[39] X. G. Wen. Electrodynamical properties of gapless edge excitations in the fractional quantum Hall states. *Phys Rev Lett*, 64:2206, 1990.

[40] A. H. MacDonald. Edge states in the fractional-quantum-Hall-effect regime. *Phys. Rev. Lett.*, 64:220, 1990.

[41] M. D. Johnson and A. H. MacDonald. Composite edges in the $\nu = 2/3$ fractional quantum Hall effect. *Phys. Rev. Lett.*, 67:2060, 1991.

[42] R. C. Ashoori, H. L. Stormer, L. N. Pfeiffer, K. W. Baldwin, and K. West. Edge magnetoplasmons in the time domain. *Phys. Rev. B*, 45:3894, 1992.

[43] C. L. Kane, Matthew P. A. Fisher, and J. Polchinski. Randomness at the edge: Theory of quantum Hall transport at filling $\nu = 2/3$. *Phys. Rev. Lett.*, 72:4129, 1994.

[44] Aveek Bid, N. Ofek, M. Heiblum, V. Umansky, and D. Mahalu. Shot noise and charge at the 2/3 composite fractional quantum Hall state. *Phys. Rev. Lett.*, 103:236802, 2009.

[45] Vivek Venkatachalam, Sean Hart, Loren Pfeiffer, Ken West, and Amir Yacoby. Local thermometry of neutral modes on the quantum Hall edge. *Nat. Phys.*, 8:676, 2012.

[46] Aveek Bid, N. Ofek, H. Inoue, M. Heiblum, C. L. Kane, V. Umansky, and D. Mahalu. Observation of neutral modes in the fractional quantum Hall regime. *Nature*, 466:585, 2010.

[47] H. Inoue, A. Grivnin, Y. Ronen, M. Heiblum, V. Umansky, and D. Mahalu. Proliferation of neutral modes in fractional quantum Hall states. *Nature Communications*, 5:4067, 2014.

[48] J.M. Leinaas and J. Myrheim. On the theory of identical particles. *Il Nuovo Cimento B Series 11*, 37(1):1–23, 1977.

[49] Frank Wilczek. Magnetic flux, angular momentum, and statistics. *Phys. Rev. Lett.*, 48:1144–1146, Apr 1982.

[50] C. Nayak, S. H. Simon, A. Stern, M. Freedman, and S. Das Sarma. Non-abelian anyons and topological quantum computation. *Rev. Mod. Phys.*, 80(3):1083, 2008.

[51] C. Nayak and F. Wilczek. $2n$-quasihole states realize $2^{n-1}$-dimensional spinor braiding statistics in paired quantum Hall states. *Nucl. Phys. B*, 479(3):529–53, 1996. cond-mat/9605145.

[52] Xiao-Gang Wen. Topological order and edge structure of $\nu$=1/2 quantum hall state. *Phys. Rev. Lett.*, 70:355–358, Jan 1993.

[53] Sung-Sik Lee, Shinsei Ryu, Chetan Nayak, and Matthew P. A. Fisher. Particle-hole symmetry and the $\nu = \frac{5}{2}$ quantum Hall state. *Phys. Rev. Lett.*, 99(23):236807, Dec 2007.

[54] Michael Levin, Bertrand I. Halperin, and Bernd Rosenow. Particle-hole symmetry and the pfaffian state. *Phys. Rev. Lett.*, 99(23):236806, Dec 2007.

[55] Iuliana P. Radu, J. B. Miller, C. M. Marcus, M. A. Kastner, L. N. Pfeiffer, and K. W. West. Quasi-particle properties from tunneling in the $\nu = 5/2$ fractional quantum Hall state. *Science*, 320:902, 2008.

[56] M. Dolev, M. Heiblum, V. Umansky, A. Stern, and D. Mahalu. Observation of a quarter of an electron charge at the $\nu = 5/2$ quantum Hall state. *Nature*, 452:829, 2008.

[57] Vivek Venkatachalam, Amir Yacoby, Loren Pfeiffer, and Ken West. Local charge of the $\nu = 5/2$ fractional quantum Hall state. *Nature*, 469:185, 2011.

[58] Ady Stern and Bertrand I. Halperin. Proposed experiments to probe the non-Abelian $\nu = 5/2$ quantum Hall state. *Phys. Rev. Lett.*, 96(1):016802, 2006.

[59] Parsa Bonderson, Alexei Kitaev, and Kirill Shtengel. Detecting non-Abelian statistics in the $\nu = 5/2$ fractional quantum Hall state. *Phys. Rev. Lett.*, 96(1):016803, 2006.

[60] RL Willett, C Nayak, K Shtengel, LN Pfeiffer, and KW West. Magnetic-field-tuned Aharonov-Bohm oscillations and evidence for non-Abelian anyons at $\nu$= 5/2. *Physical Review Letters*, 111(18):186401, 2013.

[61] Kiryl Pakrouski, Michael R. Peterson, Thierry Jolicoeur, Vito W. Scarola, Chetan Nayak, and Matthias Troyer. Phase diagram of the $\nu = 5/2$ fractional quantum Hall effect: Effects of Landau-level mixing and nonzero width. *Phys. Rev. X*, 5:021004, Apr 2015.

[62] C. W. J. Beenakker. Edge channels for the fractional quantum hall effect. *Phys. Rev. Lett.*, 64:216–219, Jan 1990.

[63] A.M. Chang. A unified transport theory for the integral and fractional quantum hall effects: Phase boundaries, edge currents, and transmission/reflection probabilities. *Solid State Communications*, 74(9):871 – 876, 1990.

[64] D. B. Chklovskii, B. I. Shklovskii, and L. I. Glazman. Electrostatics of edge channels. *Phys. Rev. B*, 46:4026–4034, Aug 1992.

[65] C. de C. Chamon and X. G. Wen. Sharp and smooth boundaries of quantum Hall liquids. *Phys. Rev. B*, 49:8227–8241, Mar 1994.

[66] M. Kac. Can one hear the shape of a drum? *Am. Math. Mon.*, 73:1, 1966.

[67] C. Gordon, D. Webb, and S. Wolpert. One cannot hear the shape of a drum. *Bull. Am. Math. Soc.*, 27:134, 1992.

[68] S. J. Allen, Jr., H. L. Störmer, and J. C. M. Hwang. Dimensional resonance of the two-dimensional electron gas in selectively doped GaAs/AlGaAs heterostructures. *Phys. Rev. B*, 28(8):4875, 1983.

[69] V. I. Talyanskii, I. E. Batov, B. K. Medvedev, J. Kotthaus, M. Wassermeier, A. Wixforth, J. Weimann, W. Schlapp, and H. Nikel. Spectrum of low-frequency edge magnetoplasmon waves under conditions of quantum Hall effect. *JETP Letters*, 50(4):221, 1989.

[70] V. I. Talyanskii, M. Wassermeier, A. Wixforth, J. Oshinowo, J. P. Kotthaus, I. E. Batov, G. Weimann, H. Nickel, and W. Schlapp. Edge magnetoplasmons in the quantum Hall effect regime. *Surface Science*, 229:40, 1989.

[71] M. Wassermeier, J. Oshinowo, J. P. Kotthaus, A. H. MacDonald, C. T. Foxon, and J. J. Harris. Edge magnetoplasmons in the fractional quantum Hall effect regime. *Phys Rev B*, 41(14):10287, 1990.

[72] E. Y. Andrei, D. C. Glattli, F. I. B. Williams, and M. Heiblum. Low frequency collective excitations in the quantum Hall system. *Surface Science*, 196:501, 1988.

[73] I. Grodnensky, D. Heitmann, and K. von Klitzing. Nonlocal dispersion of edge magnetoplasma excitations in a two-dimensional electron system. *Phys Rev Lett*, 67(8):1019, 1991.

[74] V. I. Talyanskii, M. Y. Simmons, J. E. F. Frost, M. Pepper, D. A. Ritchie, A. C. Churchill, and G. A. C. Jones. Experimental investigation of the damping of low-frequency edge magnetoplasmons in GaAs-$Al_xGa_{1-x}$ heterostructures. *Phys Rev B*, 50(3):1582, 1994. and references within.

[75] IV Kukushkin, JH Smet, VA Kovalskii, SI Gubarev, K Von Klitzing, and W Wegscheider. Spectrum of one-dimensional plasmons in a single stripe of two-dimensional electrons. *Physical Review B*, 72(16):161317, 2005.

[76] D. V. Smetnev, V. M. Muravev, I. V. Andreev, and I. V. Kukushkin. Study of edge magnetoplasma excitations in two-dimensional electron systems with various edge depletion profiles. *JETP Lett*, 94:137, 2011.

[77] V. A. Volkov, D. V. Galchenkov, L. A. Galchenkov, I. M. Grodnenskii, O. R. Matov, and S. A. Mikhailov. Edge magnetoplasmons under conditions of the quantum Hall effect. *JETP Letters*, 44(11):655–659, 1986.

[78] Alexander L. Fetter. Magnetoplasmons in a two-dimensional electron fluid: disk geometry. *Phys. Rev. B*, 33:5221, 1986.

[79] H. Kamata, T. Ota, K. Muraki, and T. Fujisawa. Voltage-controlled group velocity of edge magnetoplasmon in the quantum Hall regime. *Phys. Rev. B*, 81:085329, 2010.

[80] N. Kumada, H. Kamata, and T. Fujisawa. Edge magnetoplasmon transport in gated and ungated quantum Hall systems. *Phys Rev B*, 84:045314, 2011.

[81] B. Zhitenev, R. J. Haug, K. von Klitzing, and K. Eberl. Experimental determination of the dispersion of edge magnetoplasmons confined in edge channels. *Phys Rev B*, 49:7809, 1994.

[82] G. Ernst, N. B. Zhitenev, R. J. Haug, and K. von Klitzing. Dynamic excitations of fractional quantum Hall edge channels. *Phys Rev Lett*, 79:3748, 1997.

[83] V. J. Goldman and B. Su. Resonant tunneling in the quantum Hall regime: Measurement of fractional charge. *Science*, 267:1010, 1995.

[84] Jens Martin, Shahal Ilani, Basile Verdene, Jurgen Smet, Vladimir Umansky, Diana Mahalu, Dieter Schuh, Gerhard Abstreiter, and Amir Yacoby. Localization of fractionally charged quasi-particles. *Science*, 305:980, 2004.

[85] D. T. McClure, W. Chang, C. M. Marcus, L. N. Pfeiffer, and K. W. West. Fabry-perot interferometry with fractional charges. *Phys. Rev. Lett.*, 108:256804, 2012.

[86] F. E. Camino, Wei Zhou, and V. J. Goldman. e/3 Laughlin quasiparticle primary-filling $\nu = 1/3$ interferometer. *Phys. Rev. Lett.*, 98:076805, 2007.

[87] R. L. Willett, L. N. Pfeiffer, and K. W. West. Measurement of filling factor 5/2 quasiparticle interference with observation of charge $e/4$ and $e/2$ period oscillations. *Proceedings of the National Academy of Sciences (USA)*, 106(22):8853–8858, 2009.

[88] S. Kivelson and M. Rocek. Consequences of gauge-invariance for fractionally charged quasiparticles. *Phys. Lett. B*, 156(1-2):85–88, 1985.

[89] N. Read. Order parameter and Ginzburg-Landau theory for the fractional quantum Hall effect. *Phys. Rev. Lett.*, 62(1):86–9, 1989.

[90] D. T. McClure, Yiming Zhang, B. Rosenow, E. M. Levenson-Falk, C. M. Marcus, L. N. Pfeiffer, and K. W. West. Edge-state velocity and coherence in a quantum Hall fabry-perot interferometer. *Phys. Rev. Lett*, 103:206806, 2009.

[91] X. G. Wen. Chiral luttinger liquid and the edge excitations in the fractional quantum Hall states. *Phys. Rev. B*, 41:12838, 1990.

[92] C. de C. Chamon, D. E. Freed, and X. G. Wen. Nonequilibrium quantum noise in chiral luttinger liquids. *Phys. Rev. B*, 53(7):4034–4053, 1996.

[93] Zi-Xiang Hu, E. H. Rezayi, Xin Wan, and Kun Yang. Edge-mode velocities and thermal coherence of quantum Hall interferometers. *Phys. Rev. B*, 80:235330, 2009.

[94] E. Fradkin, C. Nayak, A. Tsvelik, and F. Wilczek. A Chern-Simons effective field theory for the Pfaffian quantum Hall state. *Nucl. Phys. B*, 516(3):704–18, 1998. cond-mat/9711087.

[95] Sankar Das Sarma, Michael Freedman, and Chetan Nayak. Topologically protected qubits from a possible non-Abelian fractional quantum Hall state. *Phys. Rev. Lett.*, 94(16):166802, Apr 2005.

[96] Parsa Bonderson, Kirill Shtengel, and J. K. Slingerland. Probing non-abelian statistics with quasiparticle interferometry. *Phys. Rev. Lett.*, 97:016401, 2006.

[97] Sanghun An, P Jiang, H Choi, W Kang, SH Simon, LN Pfeiffer, KW West, and KW Baldwin. Braiding of abelian and non-abelian anyons in the fractional quantum Hall effect. *arXiv preprint arXiv:1112.3400*, 2011.

[98] Ping V. Lin, F. E. Camino, and V. J. Goldman. Electron interferometry in the quantum Hall regime: Aharonov-Bohm effect of interacting electrons. *Phys. Rev. B*, 80:125310, 2009.

[99] R. L. Willett, L. N. Pfeiffer, and K. W. West. Alternation and interchange of e/4 and e/2 period interference oscillations consistent with filling factor 5/2 non-abelian quasiparticles. *Phys. Rev. B*, 82:205301, 2010.

[100] Parsa Bonderson, Victor Gurarie, and Chetan Nayak. Plasma analogy and non-abelian statistics for ising-type quantum Hall states. *Phys. Rev. B*, 83(7):075303, Feb 2011.

[101] Parsa Bonderson, Kirill Shtengel, and J. K. Slingerland. Interferometry of non-abelian anyons. *Annals Phys.*, 323:2709, 2008.

[102] Waheb Bishara, Parsa Bonderson, Chetan Nayak, Kirill Shtengel, and J. K. Slingerland. Interferometric signature of non-abelian anyons. *Phys. Rev. B*, 80:155303, 2009.

[103] Waheb Bishara and Chetan Nayak. Odd-even crossover in a non-abelian $\nu = 5/2$ interferometer. *Phys. Rev. B*, 80:155304, 2009.

[104] Waheb Bishara and Chetan Nayak. Edge states and interferometers in the pfaffian and anti-pfaffian states. *Phys. Rev. B*, 77:165302, 2008.

[105] P. Fendley, A. W. W. Ludwig, and H. Saleur. Exact nonequilibrium dc shot noise in luttinger liquids and fractional quantum Hall devices. *Phys. Rev. Lett.*, 75:2196, 1995.

[106] M. Reznikov, R. de Picciotto, T. G. Griffiths, M. Heiblum, and V. Umansky. Observation of quasiparticles with one-fifth of an electron's charge. *Nature*, 399:238, 1999.

[107] T. G. Griffiths, E. Comforti, M. Heiblum, A. Stern, and V. Umansky. Evolution of quasiparticle charge in the fractional quantum Hall regime. *Phys. Rev. Lett.*, 85:3918, 2000.

[108] E. Comforti, Y. C. Chung, M. Heiblum, V. Umansky, and D. Mahalu. Bunching of fractionally charged quasiparticles tunneling through high-potential barriers. *Nature*, 416:515, 2002.

[109] M. Dolev, Y. Gross, R. Sabo, I. Gurman, M. Heiblum, V. Umansky, and D. Mahalu. Characterizing neutral modes of fractional states in the second landau level. *Phys. Rev. Lett.*, 107:036805, 2011.

[110] Yarun Gross, Merav Dolev, Moty Heiblum, Vladimir Umansky, and Diana Mahalu. Upstream neutral modes in the fractional quantum Hall regime: heat waves or coherent dipoles. *Phys. Rev. Lett.*, 108:226801, 2012.

[111] H. Inoue, A. Grivnin, N. Ofek, I. Neder, M. Heiblum, V. Umansky, and D. Mahalu. Charge fractionalization in the integer quantum Hall effect. *Phys. Rev. Lett.*, 112:166801, 2014.

[112] B. Rosenow and B. Halperin. Nonuniversal behavior of scattering between fractional quantum Hall edges. *Phys. Rev. Lett.*, 88:096404, 2002.

[113] B. Trauzettel, P. Roche, D. C. Glattli, and H. Saleur. Effect of interactions on the noise of chiral luttinger liquid systems. *Phys. Rev. B*, 70:233301, 2004.

[114] Olaf Smits, JK Slingerland, and Steven H Simon. Non-equilibrium noise in the (non-) abelian fractional quantum Hall effect. *arXiv:1401.4581*, 2014.

[115] D. E. Feldman and Feifei Li. Charge-statistics separation and probing non-abelian states. *Phys. Rev. B*, 78:161304, 2008.

[116] Eytan Grosfeld and Sourin Das. Probing the neutral edge modes in transport across a point contact via thermal effects in the read-rezayi non-abelian quantum Hall states. *Phys. Rev. Lett.*, 102:106403, 2009.

[117] So Takei and Bernd Rosenow. Neutral mode heat transport and fractional quantum Hall shot noise. *Phys. Rev. B*, 84:235316, 2011.

[118] O. Shtanko, K. Snizhko, and V. Cheianov. Non-equilibrium noise in transport across a tunneling contact between $\nu = 2/3$ fractional quantum Hall edges. *Phys. Rev. B*, 89:125104, 2014.

[119] C. L. Kane and Matthew P. A. Fisher. Transmission through barriers and resonant tunneling in an interacting one-dimensional electron gas. *Phys Rev B*, 46:15233, 1992.

[120] C. L. Kane and Matthew P. A. Fisher. Transport in a one-channel luttinger liquid. *Phys Rev Lett*, 68:1220, 1992.

[121] I. Gurman, R. Sabo, M. Heiblum, V. Umansky, and D. Mahalu. Extracting net current from an upstream neutral mode in the fractional quantum Hall regime. *Nat. Commun.*, 3:1289, 2012.

[122] Giovanni Viola, Sourin Das, Eytan Grosfeld, and Ady Stern. Thermoelectric probe for neutral edge modes in the fractional quantum Hall regime. *Phys. Rev. Lett*, 109:146801, 2012.

[123] X. G. Wen. Gapless boundary excitations in the quantum Hall states and in the chiral spin states. *Phys. Rev. B*, 43:11025–11036, May 1991.

[124] Eugeniu Plamadeala, Michael Mulligan, and Chetan Nayak. Short-range entangled bosonic states with chiral edge modes and $t$ duality of heterotic strings. *Phys. Rev. B*, 88:045131, Jul 2013.

[125] Alexei Kitaev. Toward topological classification of phases with short-range entanglement, October 2011.

[126] Jean-Pierre Serre. *A Course in Arithmetic*. Springer, 1973.

[127] J. Milnor and D. Husemoller. *Symmetric Bilinear Forms*. Springer-Verlag, 1973.

[128] Paul H. Ginsparg. Comment on Toroidal Compactification of Heterotic Superstrings. *Phys. Rev. D*, 35:648, 1987.

[129] F. D. M. Haldane. Stability of chiral luttinger liquids and abelian quantum Hall states. *Phys. Rev. Lett.*, 74:2090–2093, Mar 1995.

[130] Hsien-Chung Kao, Chia-Hung Chang, and Xiao-Gang Wen. Binding transition in quantum Hall edge states. *Phys. Rev. Lett.*, 83:5563–5566, 1999.

[131] Michael Levin. Protected edge modes without symmetry. *Phys. Rev. X*, 3:021009, May 2013.

[132] Yuan-Ming Lu and Ashvin Vishwanath. Classification and properties of symmetry enriched topological phases: A Chern-Simons approach with applications to z2 spin liquids. *arXiv:1302.2634*, 2013.

[133] Yuan-Ming Lu and Ashvin Vishwanath. Theory and classification of interacting integer topological phases in two dimensions: A Chern-Simons approach. *Phys. Rev. B*, 86:125119, Sep 2012.

[134] Shmuel Elitzur, Gregory W. Moore, Adam Schwimmer, and Nathan Seiberg. Remarks on the Canonical Quantization of the Chern-Simons-Witten Theory. *Nucl. Phys. B*, 326:108, 1989.

[135] X. G. Wen and A. Zee. Shift and spin vector: New topological quantum numbers for the Hall fluids. *Phys. Rev. Lett.*, 69:953–956, Aug 1992.

[136] J. Frohlich and A. Zee. Large scale physics of the quantum Hall fluid. *Nucl. Phys. B*, 364, 1991.

[137] X. G. Wen and A. Zee. Classification of Abelian quantum Hall states and matrix formulation of topological fluids. *Phys. Rev. B*, 46(4):2290–301, 1992.

[138] Jürg Fröhlich, Urban M. Studer, and Emmanuel Thiran. An ade-o classification of minimal incompressible quantum Hall fluids. In Mark Fannes, Christian Maes, and Andrè Verbeure, editors, *On Three Levels*, volume 324 of *NATO ASI Series*, pages 225–232. Springer US, 1994.

[139] Jurg Frohlich and Emmanuel Thiran. Integral quadratic forms, Kac-Moody algebras, and fractional quantum Hall effect. An ADE-O classification. *Journal of Statistical Physics*, 76:209, 1994.

[140] Jurg Frohlich, Chamseddine A.H., F. Gabbiani, T. Kerler, C. King, P.A. Marchetti, U.M. Studer, and E. Thiran. The fractional quantum Hall effect, Chern-Simons theory, and integral lattices. *Proc. of ICM.*, 94, 1995.

[141] Dmitry Belov and Gregory W. Moore. Classification of abelian spin Chern-Simons theories. *arXiv:hep-th/0505235*, 2005.

[142] S. D. Stirling. *Abelian Chern-Simons theory with toral gauge group, modular tensor categories, and group categories*. PhD thesis, The University of Texas at Austin, 2008. arXiv:0807.2857.

[143] John Conway and Neil J. A. Sloane. *Sphere Packings, Lattices and Groups*. Springer, 3rd edition, 1998.

[144] V. V. Nikulin. Integral symmetric bilinear forms and some of their applications. *Math. USSR Izv.*, 14:103, 1980.

[145] E. Witten. Quantum field theory and the jones polynomial. *Comm. Math. Phys.*, 121:351, 1989.

[146] A. Kitaev. Anyons in an exactly solved model and beyond. *Ann. Phys.*, 321:2 – 111, 2006.

[147] H. Cohen. *A Course in Computational Algebraic Number Theory*. Springer, New York, 1996.

[148] T. Senthil and Michael Levin. Integer quantum Hall effect for bosons. *Phys. Rev. Lett.*, 110:046801, Jan 2013.

[149] J. W. S. Cassels. *Rational Quadratic Forms*. Academic Press, London, 1978.

[150] G.L. Watson. Transformations of a quadratic form which do not increase the class-number. *Proc. London Math. Soc.*, 12:577587, 1962.

[151] D. Lorch and M. Kirschmer. Single-Class Genera of Positive Integral Lattices. *LMS Journal of Computation and Mathematics*, 16:172–186, 2013.

[152] W.A. Stein et al. *Sage Mathematics Software (Version 5.12)*. The Sage Development Team, 2013. `http://www.sagemath.org`.

[153] Xiao-Gang Wen. Modular transformation and bosonic/fermionic topological orders in abelian fractional quantum Hall states. *arXiv:1212.5121*, 2012.

[154] X. G. Wen. Topological orders in rigid states. *Int. J. Mod. Phys. B*, 4(2):239–71, 1990.

[155] R. L. Willett, L. N. Pfeiffer, and K. W. West, 2013. unpublished.

[156] S. Das Sarma and A. Pinczuk, editors. *Perspectives in quantum Hall effects : novel quantum liquids in low-dimensional semiconductor structures*. Wiley, New York, 1997.

[157] S. Brosiga, K. Ensslin, B. Brar, M. Thomas, and H. Kroemer. Landau and spin levels in inas quantum wells resolved with in-plane and parallel magnetic fields. *Physica B*, 256-258:239–242, 1998.

[158] A. F. Young, C. R. Dean, L. Wang, H. Ren, P. Cadden-Zimansky, K. Watanabe, T. Taniguchi, J. Hone, K. L. Shepard, and P. Kim. Spin and valley quantum Hall ferromagnetism in graphene. *Nature Physics*, 8:550–556, July 2012.

[159] A. Tsukazaki, A. Ohtomo, T. Kita, Y. Ohno, H. Ohno, and M. Kawasaki. Quantum Hall Effect in Polar Oxide Heterostructures. *Science*, 315:1388–, March 2007.

[160] J. P. Eisenstein, K. B. Cooper, L. N. Pfeiffer, and K. W. West. Insulating and fractional quantum Hall states in the first excited Landau level. *Phys. Rev. Lett.*, 88(7):076801, 2002.

[161] U. Zülicke, Robert Bluhm, V. A. Kostelecký, and A. H. MacDonald. Edge-magnetoplasmon wave-packet revivals in the quantum-Hall effect. *Phys. Rev. B*, 55:9800–9816, 1997.

[162] G. D. Mahan. *Many-Particle Physics*. Plenum, New York, 1990.

[163] P. J. Price. Two-dimensional electron transport in semiconductor layers. I. phonon scattering. *Annals of Physics*, 133(2):217–239, 1981.

[164] S. K. Lyo. Low-temperature phonon-drag thermoelectric power in heterojunctions. *Phys. Rev. B*, 38:6345–6347, 1988.

[165] T. Kawamura and S. Das Sarma. Phonon-scattering-limited electron mobilities in $Al_xGa_{1-x}As$/GaAs heterojunctions. *Phys. Rev. B*, 45:3612–3627, 1992.

[166] Philippe Francesco, Pierre Mathieu, and David Senechal. *Conformal Field Theory*. Springer, 1996.

[167] Paul Fendley, Matthew P. A. Fisher, and Chetan Nayak. Edge states and tunneling of non-abelian quasiparticles in the $\nu = 5/2$ quantum Hall state and $p + ip$ superconductors. *Phys. Rev. B*, 75:045317, 2007.

[168] J. Schwinger. Brownian motion of a quantum oscillator. *J. Math. Phys.*, 2:407, 1961.

[169] L. V. Keldysh. Diagram technique for nonequilibrium processes. *Sov. Phys. JETP*, 20:1018, 1965.

[170] R. Guyon, P. Devillard, T. Martin, and I. Safi. Klein factors in multiple fractional quantum Hall edge tunneling. *Phys Rev B*, 65:153304, 2002.

[171] Xiao-Gang Wen. Edge transport properties of the fractional quantum Hall states and weak-impurity scattering of a one-dimensional charge-density wave. *Phys. Rev. B*, 44:5708, 1991.